Closed loop digital control of electrohydraulic systems

Whiting, Ian Martin

Award date:
1987

Awarding institution:
University of Bath

CLOSED LOOP DIGITAL CONTROL OF ELECTROHYDRAULIC SYSTEMS

Submitted by
IAN MARTIN WHITING
for the degree of Ph.D.
of the University of Bath
1987

Copyright

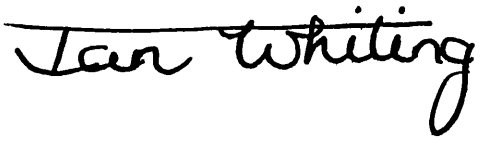

ProQuest LLC
789 East Eisenhower Parkway
P.O. Box 1346
Ann Arbor, MI 48106-1346

SUMMARY

The material presented in this thesis is the result of an investigation into the use of digital closed loop control techniques in electrohydraulic systems. The work was motivated by an awareness of the increasing use of electronics in electrohydraulic systems, and in particular the potential offered by microprocessor control. Throughout the research, the objective was to seek methods whereby microprocessors could be best used to improve the performance and flexibility of electrohydraulic systems whilst reducing the hardware complexity.

The use of microprocessors for closed loop control has in the past been one of the least exploited applications in electrohydraulic systems. However the research has shown that, used in this way, the strategic placing of the microprocessor at the heart of the system can be very beneficial.

The most significant advantages were obtained by the use of the on-line modelling concept to enhance the basic digital controller. Here, the closed loop control signals occurring during plant operation are used in a model of the plant to provide on-line estimates of other unmeasured signals or parameters which occur. These are then used to enhance the control system. Two areas of application have been investigated.

In the first application, digital control and the on-line modelling concept were applied as part of a new electrohydraulic flow control valve design. Although the only measured feedback signal was of the flow throttling element position, the on-line estimation of flow rate and pressure enabled the same minimal valve hardware to be used for pressure control, flow rate control, or throttling element position control. Additionally, on-line digital readout of the estimated signals gave useful visual information about the valve condition.

In the second application, digital control was applied to improve the dynamics of an oscillatory electrohydraulic position control system. On-line modelling was used to generate the controller dynamic compensation necessary to produce a good closed loop dynamic performance. The microprocessor was particularly useful for producing nonlinear control laws to correct for the servosystem nonlinearities.

The most sophisticated form of modelling used was that of on-line identification, where the current plant transfer function is derived from the plant input/output control signals. This was of particular value as the effect of time variable nonlinearities on the plant transfer function could be rapidly identified. On-line identification applied to the servosystem enabled full automation of the control law design stage, requiring no plant data input from the designer. The concept was also used in an adaptive control scheme, enabling Self-Tuning of the controller to maintain a specified dynamic performance in the face of unknown time variable nonlinearities.

ACKNOWLEDGEMENTS

My sincerest appreciation and gratitude are extended to the following:

Dr N.D. Vaughan, for his guidance, encouragement and most valuable advice in supervision. Professor D.E. Bowns and the staff of the Fluid Power Centre, for the provision of facilities and a conducive working environment.

Dowty Group Services (DGS) Ltd., Dowty Hydraulic Units (DHU) Ltd., and the University of Bath, for financial support. Mr A.R. Davies and Mr D.W. Parker of DHU, for their guidance and encouragement, and Mr R. Jennings of DGS for his administrative support.

Postgraduate friends in the schools of Mechanical and Electrical Engineering for practical assistance and useful suggestions. But most of all to Joyce and the children for their enduring support and patience.

IAN WHITING

CONTENTS

1. INTRODUCTION

1.1 Microprocessor Control of Electrohydraulic Systems 1
1.2 Electrohydraulic Servosystems 4
1.3 Electrohydraulic Control Valves 5
1.4 Thesis Layout 6

2. ELECTROHYDRAULIC FLOW CONTROL

2.1 Introduction 8
2.2 Electromechanical Conversion 9
2.3 Valve Servomechanisms 12
2.4 Flow Metering Devices 13
2.5 Feedback Mechanisms 15
2.6 Survey Conclusions 17
2.7 Microprocessor Integrated Flow Control Valve Concept 18
2.8 Digital Pilot Valve Interface 20
2.9 Concluding Remarks 23

3. DIGITAL CONTROL OF ELECTROHYDRAULIC SYSTEMS

3.1 Introduction 24
3.2 The Darkstar Microcomputer 25
3.3 Classical Versus Modern Control Theory 26
3.4 Control Loop Nomenclature and Implementation 28
3.5 Servosystem Simulation Network 31
3.6 Continuous to Discrete Plant Model Transformations 32
3.7 Comparison of Transformation Methods 34
3.8 Sample Period Selection 36

4. POLE PLACEMENT CONTROLLER DESIGN

4.1 Introduction 38
4.2 Controller Synthesis Methods and Constraints 38
4.3 Root Locus Performance Specification 42
4.4 Controller Coefficient Derivation 43
4.5 Controller Design and Implementation 45

4.6 Integral Action Control 46

5. MICROPROCESSOR INTEGRATED FLOW CONTROL VALVE

5.1 Introduction 48
5.2 Valve Hardware Design and Test Rig Layout 48
5.3 Valve Dynamic Modelling 51
5.4 Integral Action Controller Design 54
5.5 Steady State Characteristics and Modelling 56
5.6 Closed Loop Pressure and Flow Control 59
5.7 Further Application of New Valve Concept 62

6. DIGITAL VALVE INTERFACE

6.1 Introduction 64
6.2 Valve Hardware Design and Test Rig Layout 64
6.3 Pilot Valve Switching Characteristics 66
6.4 Pulse Width Modulated Pressure Control 69
6.5 Closed Loop Control 72
6.6 Conclusions and Recommendations 76

7. ELECTROHYDRAULIC SERVOSYSTEM CONTROL

7.1 Introduction 78
7.2 Electrohydraulic Position Control System Test Rig 79
7.3 Servosystem Modelling 81
7.4 Digital Closed Loop Servosystem Control 84
7.5 Plant Inherent Nonlinearities - Inverse Filter Design 88
7.6 Plant Time Variable Nonlinearities 90
7.7 Integral Action Control 91
7.8 Closed Loop Frequency Response 93
7.9 General Discussion 93

8. SERVOSYSTEM IDENTIFICATION

8.1 Introduction 96
8.2 Identification Methods 97
8.3 Recursive Least-Squares (RLS) Identification 99
8.4 Application to Third Order Servosystem Model 103
8.5 Identification of Electrical Simulation Network 105

8.6 Nonlinear Servosystem Identification 106
8.7 Servosystem Identification Robustness 110
8.8 Forgetting Factor Switching Strategy 111
8.9 RLS Identification Parameter Convergence Speed 113

9. SERVOSYSTEM AUTOMATIC CONTROLLER DESIGN AND SELF-TUNING CONTROL
9.1 Introduction 114
9.2 Automatic Controller Design and Self-Tuning Control Algorithm 114
9.3 Adaptive Control Methods 117
9.4 STC Implementation Speed Improvements 120
9.5 STC Robustness 122
9.6 Servosystem Automatic Controller Design 125
9.7 Servosystem Self-Tuning Control 127
9.8 Servosystem STC Robustness 129
9.9 Concluding Remarks and Recommendations 130

10. CONCLUSIONS
10.1 General Closed Loop Digital Control 132
10.2 Application to New Valve Concept 133
10.3 Application to Servosystem 134

REFERENCES

APPENDICES
1 - Electrohydraulic Servosystem Small Perturbation Model 151
2 - Pole/Zero Mapping Rules 158
3 - Steady State Gain Theorem 159
4 - Proportional Flow Control Valve Small Perturbation Model 161
5 - RLS Identification Equations 165

FIGURES

2.1 Flow Control Valve Functional Elements
2.2 Electromagnetic Conversion Devices
2.3 Typical Solenoid Characteristics
2.4 Hydraulic Bridge Circuit
2.5 Typical Hydromechanical Servosystems
2.6 Poppet Valve
2.7 Four Port Directional Poppet Valve
2.8 Poppet Position Control - The Valvistor
2.9 Dynamic Flow Meter
2.10 New Flow Control Valve Concept
2.11 Two Port Flow Control Valve Using a Flow Meter
2.12 Pulse Width Modulation
2.13 Digital Pressure Control Valve

3.1 The Darkstar Microcomputer System
3.2 Darkstar System Layout
3.3 State Feedback Controller
3.4 Classical Controller
3.5 Discrete Block Diagram
3.6 Basic Controller Flow Chart
3.7 Electrical Simulation Network
3.8 Frequency Response of Sampled Plant - Effect of Sampling
3.9 Frequency Response of Pole/Zero Mapping Models - Effect of Sampling
3.10 Darkstar Algorithm Closed Loop Bandwidth

4.1 Z Plane Root Locus Diagram
4.2 Simulator Step Responses Showing Effect of Closed Loop Poles

5.1 New Flow Control Valve Concept
5.2 Valve Assembly Drawing - Scale 1:1
5.3 Parts List for Fig 5.2
5.4 Test Rig Layout
5.5 Overall Valve Open Loop Frequency Response
5.6 Pilot Valve Frequency Response for Different Load Conditions

5.7 Valve Closed Loop Block Diagram
5.8 Overall Valve Uncompensated Step Response
5.9 Overall Valve Uncompensated Closed Loop Frequency Response
5.10 Overall Valve Compensated Step Response
5.11 Overall Valve Compensated Closed Loop Frequency Response
5.12 Poppet Flow Characteristics
5.13 Poppet Free Body Diagram
5.14 Poppet Force Characteristics
5.15 Pilot Valve Characteristic
5.16 Valve Controller Flow Chart
5.17 Servo Pressure Control Mode
5.18 Main Pressure Control Mode
5.19 Flow Control Mode
5.20 Four Port Flow Control Poppet Valve
5.21 Two Port and Four Port Poppet Valve Hardware
5.22 Three Port Flow Control Spool Valve

6.1 PWM Driven Flow Control Valve
6.2 Digital Pilot Valve Assembly Drawing - Scale 2:1
6.3 Parts List for Fig 6.2
6.4 Test Rig Layout
6.5 Solenoid 12V Switching Transients
6.6 Solenoid Force Characteristic
6.7 PWM Valve Drive Circuit Diagram
6.8 Overdrive Switching Transients
6.9 Low Power PWM Valve Drive Circuit Diagram
6.10 S6840 Timer Set Up for PWM
6.11 Ball Valve PWM Current and Pressure Waveforms
6.12 Demodulated PWM pressure Waveforms
6.13 PWM Pilot Valve Characteristic
6.14 PWM Pilot Valve Frequency Response
6.15 Overall PWM Valve Open Loop Frequency Response
6.16 PWM Valve Closed Loop Block Diagram
6.17 Overall PWM Valve Step Responses
6.18 Overall PWM Valve Closed Loop Frequency Responses
6.19 Ball Valve Seat and Pin Wear

7.1 Electrohydraulic Servosystem Schematic
7.2 Test Rig Layout
7.3 Test Rig Data
7.4 Electrohydraulic Servosystem Test Rig
7.5 Cylinder/Valve Flow Gain Showing Dual Gain Characteristic
7.6 Uncompensated Step Response - Analogue Controller
7.7 Change of Resonant Frequency with Load Position
7.8 Open Loop Frequency Response
7.9 Uncompensated Step Response - Dead Volume Added
7.10 Uncompensated Step Response - Effect of Sampling
7.11 Step Response Before and After Compensation
7.12 Root Locus Plots Before and After Compensation
7.13 Compensated Root Locus Plot - Plant at Design Point
7.14 Compensated Step Response - Effect of Step Amplitude
7.15 Inverse Filter Design
7.16 Null Point Eliminator
7.17 Null Point Dither Signal
7.18 Step Response With Inverse Filter Implemented
7.19 Inverse Filter Flow Chart
7.20 Fixed Controller Step Response - Dead Volume Switched In
7.21 Fixed Controller Root Locus - Dead Volume Switched In
7.22 Fixed Controller Step Response - Supply Pressure Changes
7.23 Fixed Controller Root Locus - 150 bar Supply Pressure
7.24 Integral Action Controller Step Response
7.25 Integral Action Control of Step Disturbance
7.26 Integral Action Control System Root Locus
7.27 Fixed Integral Controller Step Response - Supply Pressure Changes
7.28 Uncompensated Closed Loop Frequency Response
7.29 Compensated Closed Loop Frequency Response

8.1 Recursive Least-Squares Identification Schematic
8.2 RLS Identification Algorithm Flow Chart
8.3 Frequency Response of Sampled Plant - Effect of Sampling
8.4 RLS Identification of Sampled Plant Using Pole/Zero Mapping
8.5 Servosystem RLS Identification Schematic
8.6 RLS Identification of Directional Nonlinearity

8.7 RLS Identification of Supply Pressure Changes
8.8 Uncompensated Step Response - Supply Pressure Changes
8.9 RLS Identification of Simulated Change in Load Inertia
8.10 Uncompensated Step Response - Effect of Inverse Filter
8.11 RLS Identification With and Without Inverse Filter Added
8.12 Parameter Estimate Fluctuation at 0.99 Forgetting Factor
8.13 Parameter Estimate Fluctuation at 0.96 Forgetting Factor
8.14 Parameter Estimate Decay at 0.996 Forgetting Factor
8.15 Parameter Estimate Decay at 0.98 Forgetting Factor
8.16 Action of Forgetting Factor Switching Strategy
8.17 Parameter Estimation - Effect of Signal Dynamics
8.18 Parameter Estimate Convergence at 0.996 Forgetting Factor
8.19 Parameter Estimate Convergence at 0.98 Forgetting Factor

9.1 Self-Tuning Control Schematic
9.2 STC Algorithm Implementation
9.3 Model Reference Adaptive Control Schematic
9.4 RLS Identification Before and After Controller Implementation
9.5 Controller Switching in Transient
9.6 Error Signal Before and After Controller Compensation
9.7 STC During a Step Change in Supply Pressure
9.8 STC During a Simulated Step Change in Load Inertia
9.9 STC During an Increase in Demanded Step Amplitude
9.10 Effect of Low Forgetting Factor on STC Step Response
9.11 STC When Sluggish Root Positions are Selected
9.12 STC During a Low Frequency Sinusoidal Demand Signal
9.13 STC During a High Frequency Sinusoidal Demand Signal

A1.1 Electrohydraulic Servosystem Plant Model
A1.2 Block Diagram Representation
A3.1 Digital Controller Block Diagram
A4.1 Flow Control Valve Plant Model
A4.2 Detailed Block Diagram
A4.3 Reduced Order Block Diagram

NOTATION

The two applications of closed loop digital control studied in this thesis each give rise to a set of equations used in their physical modelling. Additionally, since in both cases the digital controller structure and general equations are the same, this gives rise to a set of discrete general controller equations which are relevant in both applications. The notation for the equations presented in this thesis is thus presented in the three mentioned categories. This is followed by a listing of the abbreviated terms which occur in the thesis.

GENERAL DIGITAL CONTROL NOTATION

a_i	i th coefficient of the discrete plant model
b	s plane transfer function root position
$e(k)$	Controller output (drive) signal at the k th sample instant
$er(k)$	Input to inverse filter before saturation limiting
$\hat{e}(k)$	Part calculation of drive signal
f_i	i th coefficient of the forward path controller filter
g_i	i th coefficient of the feedback path controller filter
k	k th sample instant
n	Plant model order
n_c	Controller order
s	Laplace transformation variable/operator
$u(k)$	Controller demand signal at k th sample instant
$y(k)$	Controller feedback signal at k th sample instant
$\hat{y}(k)$	Estimated feedback signal at k th sample instant
$y_d(k)$	Difference between k th and $(k-1)$th feedback signal
z	Z transformation variable/operator

$\underline{A}(k)$	Parameter estimate vector
$A_D(z)$	Plant model denominator polynomial
$A_N(z)$	Plant model numerator polynomial
$\underline{C}(k)$	Covariance matrix of plant/model errors
$F(z)$	Controller forward path filter polynomial
$G(z)$	Controller feedback path controller filter

G_{ss}	Steady sate gain
$H(z)$	Discrete transfer function
K	Forward path gain
K_a	Acceleration feedback gain
K_v	Velocity feedback gain
K_f	Position feedback gain
N_T	Asymptotic convergence time constant - Number of sample periods
$\underline{P}(k)$	Covariance matrix of input/output information
R	Sinusoidal signal amplitude
T	Time constant
T_c	Parameter convergence time constant
$T(z)$	Desired characteristic equation polynomial
$\underline{X}(k)$	Information vector

α	Forgetting factor
ζ	Damping ratio
τ	Sample period
ϕ	Phase lag
ω	Frequency
ω_n	Natural frequency
$\Delta\tau$	Time error between controller input and output

FLOW CONTROL VALVE NOTATION

Variable names appearing here in upper case may be used in lower case during the text to represent a small change in the variable.

A	Poppet flow area
A_p	Poppet servo pressure area
C_a	Armature damping coefficient
C_p	Poppet damping coefficient
C_{suf}	Small perturbation flow gains
C_q	Discharge coefficient
D	Poppet seat Diameter
D_n	Pilot valve seat diameter
F_b	Bernoulli flow force

F_m	Solenoid armature magnetic force
F_s	Servo valve flow force on armature
I	Pilot valve drive current
K_a	Pilot valve force versus current gain
K_q	Flow rate model gain
K_s	Armature force versus pressure gain
M_a	Armature mass
M_p	Poppet mass
M_1	Poppet force model coefficient
M_2	Poppet force model coefficient
P	Poppet main flow pressure
P_d	Poppet pressure - between poppet and damping restrictor
P_s	Servo pressure - between pilot valve and damping restrictor
Q	Poppet main flow rate
Q_c	Overall pilot flow rate from supply
Q_n	Pilot valve nozzle flow rate
Q_d	Flow rate through damping restrictor
R_p	Main flow pressure ratio
V	Flow velocity
V_y	Poppet feedback voltage signal at microcomputer interface
V_c	SMR output voltage signal at microcomputer interface
V_d	Trapped volume between poppet and damping restrictor
V_s	Trapped volume between pilot valve and damping restrictor
X	Armature position
Y	Poppet position
β	Oil bulk modulus
γ	Poppet cone angle
ρ	Oil density

ELECTROHYDRAULIC SERVOSYSTEM NOTATION

Variable names appearing here in upper case may be used in lower case during the text to represent a small change in the variable.

A_a	Cylinder piston annulus area

A_p	Cylinder full piston area
C	Load damping
C_{sat}	Small perturbation flow gains
F	Load force
I	Servovalve current
K_f	Load velocity versus applied force gain
K_g	Numerator gain
K_i	Servovalve spool position versus current gain
K_s	Orifice flow gain
L	Cylinder stroke
L_a	Length of annulus cylinder area
L_p	Length of full cylinder area
M	Load mass
P_a	Pressure in annulus area cylinder volume
P_p	Pressure in full area cylinder volume
P_s	Supply pressure
Q_a	Flow rate into/from annulus area cylinder volume
Q_p	Flow rate into/from full area cylinder volume
R_G	Directional gain ratio
R_P	Directional damping ratio
T	Compressibility time constant
V	Piston velocity
V_a	Annulus area cylinder volume
V_p	Full area cylinder volume
X	Servovalve spool position
Y	Load position
β	Oil bulk modulus
ρ	Oil density
ΔP	Orifice pressure drop

ABBREVIATIONS

A/D	Analogue to Digital (converter)
BCPL	Basic Combined Programming Language
CE	Characteristic Equation

D/A	Digital to Analogue (converter)
FET	Field Effect Transistor
I/O	Input/Output
LHS	Left Hand Side
LVDT	Linear Variable Differential Transformer
MRAC	Model Reference Adaptive Control
PID	Proportional plus Integral plus Derivative
PRBS	Pseudo Random Binary Signal
PWM	Pulse Width Modulation
RLS	Recursive Least-Squares (identification)
RHS	Right Hand Side
SMR	Signal Modulation Ratio
STC	Self-Tuning Control
VDU	Visual Display Unit

1. INTRODUCTION

1.1 Microprocessor Control of Electrohydraulic Systems

101 Recent advances in electrohydraulic and microelectronic technologies have been a catalyst for a large increase in the research and development of electrohydraulic systems. Consequently the latest generation of electrohydraulic devices have improved performance and flexibility, and are more cost effective than their predecessors. Whilst the integration of microprocessors into electrohydraulic devices has been a major contributor to these advances, in many cases the potential offered by the microprocessor is not utilised to the full. For example, one of the most beneficial uses of the microprocessor is as a closed loop controller, however to date the exploitation of digital closed loop techniques in electrohydraulic systems has been very limited.

102 The work presented in this thesis is intended to show by application how closed loop microprocessor control can be used to best advantage in electrohydraulic systems. The work divides naturally into three parts: first, the development of general algorithms suitable for electrohydraulic systems; secondly, the application of digital control in a new control valve concept; and thirdly, application to an electrohydraulic position servosystem. An introduction to each of these three areas of work forms the remainder of this chapter.

103 The first commercially marketed microprocessor systems were released in 1971, and since that time the hardware requirement for such devices has been reduced, highly complex systems now being available on a single chip. The increased facilities and greater speed of processing offered, has revolutionised the design and application of electronic and electromechanical devices in many engineering disciplines. The field of electrohydraulic engineering is no exception, and there are many cases reported of the use of microprocessors in electrohydraulic systems [1.2]. The principal reasons for incorporating microprocessors into electrohydraulic systems can be summarised as follows:

(a) Complex logical and arithmetic functions can be executed on-line repeatedly and precisely, which would otherwise be unattainable at reasonable cost.

(b) Changes in these functions can be programmed at will, with no hardware alterations and the minimum of inconvenience.

(c) The same microprocessor controlled electrohydraulic system can be made to behave in many different ways, simply by changing the microprocessor program. Thus hardware can be standardised and costs reduced.

104 Whilst (a), (b) and (c) above are all commendable characteristics of microprocessor control, these advantages must be offset against the expense of incorporating the microprocessor. In some applications microprocessors have been used simply to replace an analogue control system, and here the microprocessor is used merely as a fashionable gimmick, providing no real improvement. The successful cost effective use of microprocessor control depends on the experience and imagination of the design engineer to recognise where and how the microprocessor should be applied.

105 There are several recognised ways of using microprocessors in electrohydraulic systems [3], ranging from data logging and monitoring which have no direct action in the system, up to adaptive closed loop control which can alter on-line both the steady state and dynamic system performance. In the past, the use of microprocessors in closed loop control systems has been limited largely to the generation of demand signals, and any servo loops have been closed using conventional analogue methods. The quantising and sampling effect of digital control, and insufficient processing speed have discouraged the use of the microprocessor as a closed loop controller. However with the release of 16-bit processors operating at higher clock rates and with more powerful instruction sets, closed loop control is now feasible in many cases.

106 Closed loop control is potentially the most powerful use of the microprocessor in electrohydraulic systems since it is placed at the very heart of the system, having control of dynamic and steady state performance in addition to generating the demand signal. The control algorithm is usually derived from a model of the electrohydraulic plant, either explicitly or implicitly specified in the algorithm software. The model can be made to run in real time, in parallel with the actual system to be controlled. Obtaining an adequate model is usually the most difficult part, but once perfected the information derived from the model can be used to

control the electrohydraulic system in a variety of ways. For example, a number of cases have been reported where the desired feedback parameter of a closed loop system could not be measured directly, and a microprocessor was used to derive these parameters internally from other more easily measured feedback signals [4,5]. Where control of closed loop dynamics is required, the internally specified model must be a fully dynamic representation of the plant. The dynamic information generated can then be used to modify the loop feedback and forward path signals. There is growing evidence of the success of these methods in electrohydraulic servosystem control [6,7].

107 Perhaps the ultimate concept in the dynamic control of closed loop electrohydraulic systems is adaptive control. In the event of a time variable plant nonlinearity occurring, the microprocessor automatically corrects the controller to maintain any desired dynamic performance. Over the years a very large proportion of the control literature has been devoted to this subject. Surveys have shown that in the main the work presented has been academic in nature [8]. The limited number of practical applications reported have been restricted largely to process plants, having very slow dynamics compared with servosystems [9,10]. The availability of more sophisticated microprocessor systems has made closed loop adaptive control of electrohydraulic systems feasible, and a small number of cases of the successful application of adaptive control have recently been reported [11,12].

108 The eventual acceptance of the microprocessor controller in electrohydraulic systems is dependent on the development of advanced control techniques, so that the full potential of the microprocessor can be exploited. For this reason the work presented in this thesis is concerned with the development and application of microprocessor implemented closed loop techniques for electrohydraulic systems. Two areas of application have been studied, both of which demonstrate the advantages of microprocessor control. First, digital closed loop control is applied as part of a newly devised electrohydraulic flow control valve concept, and is shown to improve the valve versatility whilst reducing its complexity. Secondly, closed loop adaptive control is applied to an electrohydraulic servosystem to simplify the controller design problem and compensate for plant nonlinearities. The background to both the new electrohydraulic valve concept and electrohydraulic servosystem control, is described in the following two sections.

1.2 Electrohydraulic Servosystems

109 Electrohydraulic servosystems combine the enormous power transfer capabilities of hydraulic actuation with the flexibility and precision of electronic control. In every case this is achieved by a flow control device which determines the direction and magnitude of hydraulic flow in proportion to an electrical drive signal. Typically a servovalve would be used for this purpose. The accuracy and response of the closed loop system depends directly on the characteristics of the servovalve and the type of controller used in producing the valve drive signal.

110 Electrohydraulic servovalves were first developed in the 1950's for aerospace applications where dynamic performance and steady state accuracy were important. Very soon after that, industrial versions of the same valves were developed for high precision industrial applications. By the early 1960's a large variety of designs were available [13], most of them based on variants of the well known torque motor construction, used in either single or two stage designs. Time has shown the superiority of a small number of these devices, and at the present day the market is dominated by the two stage double nozzle flapper design.

111 The relatively new proportional valve technology poses an alternative to servovalves only in lower performance applications. Where absolute precision and superior dynamic performance are required the servovalve remains unrivaled, thus for many years the valve element in electrohydraulic servosystems has remained unchanged.

112 In addition to the servovalve the performance of a closed loop system is influenced by the design of the closed loop controller. Almost without exception controllers are based on the use of analogue amplifier circuits, the absolute minimum controller being a simple summing junction. Very often the controller has a degree of flexibility for changing gains in the forward path and feedback paths, and where necessary dynamic compensation such as lead/lag or PID networks are used. Typically, the controller gains would be chosen to give good control at the worst operating conditions seen by the plant. Away from the worst condition the controller would yield a less than optimal response. With a fixed coefficient linear controller, plant nonlinearities are thus handled by accepting less than the desired performance. Sometimes, in very nonlinear systems, a fixed coefficient controller is

unable to produce a satisfactory overall performance and it is necessary to consider nonlinear control laws. However in an analogue system this can be difficult to implement. Analogue controllers are also limited in the type of control action which can be implemented. For example, if the feedback compensation requires derivative action, the noise problems associated with electronic differentiating networks may force the use of velocity and acceleration transducers [14]. Thus adding both to the cost and complexity of the controller.

113 If electrohydraulic systems are not to loose more ground to their all-electrical counterparts, then it is essential that these problems be overcome, and new solutions be found which improve performance whilst reducing costs [15]. Closed loop control using a microprocessor provides a solution to these problems since nonlinear controllers can be easily constructed, and derivative signals can be calculated inside the microprocessor and used in place of derivative feedback transducers.

114 In this thesis, general algorithms are developed based on the plant modelling principle, which are able to generate the necessary compensating feedback signals and also cope with plant nonlinearities. Additionally an on-line identification method is developed which allows automatic controller design and adaptive control to be implemented. The function of the algorithms was tested by application to a particularly nonlinear electrohydraulic position control system which exhibited undesirable oscillatory dynamics.

1.3 Electrohydraulic Control Valves

115 In recent years a bewildering number of new flow control valve designs have become available, and the best choice of valve to meet a specific application has become far from obvious. Prior to the late 1970's the choice in electrohydraulic valves was limited but clearly defined. On one hand was the crude and sluggish but inexpensive directional solenoid operated valve, and on the other, the very expensive but dynamically responsive flow control servovalve. For on/off control the engineer would select the former, and for modulated directional control, the latter. The introduction of 'proportional' control valves has helped to fill the gap between these two extremes. The characteristics of proportional valves range from high grade directional valves to low grade servovalves and they generally have the advantage of being less expensive than servovalves and less sensitive to

contamination [16]. The reduction of cost is achieved at the expense of the dynamic and steady state characteristics, however in many lower performance servosystem applications proportional valves can give adequate control.

116 The impetus behind the development of proportional valves has been the availability of advanced electronic interfacing and new techniques in electrohydraulic conversion [17]. Most commercially available proportional valves are based on the so called proportional solenoid, which can be designed to give a change of force linearly related to the solenoid current. However, whilst these valves are gaining acceptance amongst engineers, researchers are creating the next generation of proportional valves. The objectives being as always, to reduce cost whilst improving versatility reliability and performance. A more recent criterion is to make valves which are easily interfaced with microprocessor systems, and a number of researchers have developed so called 'digital' control valves for this purpose [18,19,20,21]. Several avenues have been explored using anything from stepper motors to high speed ball valves.

117 The research presented in this thesis had the same objectives, but arrived at a solution by different means. Simplifications in hardware and improvements in versatility were obtained by including a microprocessor as an integral part of the valve design, used as a closed loop controller. An on-line model of the valve, running in parallel with it, enabled the derivation of the valve flows and pressures from the position feedback and drive signal. Any one of these values could then be used to close the loop. Thus by electronic signalling the valve could be changed to control either pressure or flow, whilst not directly measuring either of these quantities. A further hardware simplification was made by incorporating an on/off pilot stage in the valve, controlled using pulse width modulated drive signals.

1.4 Thesis Layout

118 The work presented in this thesis is devoted to the development and application of microprocessor implemented closed loop control techniques for electrohydraulic systems. The thesis is divided into three sections, one covering the theoretical aspects of digital control, another covering application of the techniques to the new flow control valve concept, and the third, application to an electrohydraulic position control system.

119 The theoretical sections cover all aspects of the algorithms developed, starting from the fundamental effects of sampling, and finishing up with the development of adaptive control algorithms. The algorithms developed have been tested using linear analogue models of the electrohydraulic systems to which they later were applied. Rather than lump all the theory together, it has been broken up into separate chapters, each being presented prior to description of application of the theory in the thesis. The theoretical chapters are numbers 3,4,8 and 9.

120 The application of closed loop microprocessor control techniques in a new flow control valve design has implications in the design of the valve hardware itself. A valve was specially designed to demonstrate the new concept. Thus in addition to the digital control aspects, a significant portion of the research has been devoted to the study of flow control valve design concepts, and this forms Chapter 2 of the thesis. The concepts outlined in the survey lead to the fundamental principles of the new flow control valve design. The valve hardware design used during the research is presented in Chapter 5. This chapter also covers the method of modelling the valve, and the implementation of the model inside the microprocessor to enable four different modes of flow control. The new valve concept demonstrates how closed loop control can be used to improve performance and flexibility whilst reducing the hardware costs. The valve design is further simplified in chapter 6, where the use of a pulse width modulated pilot valve is investigated.

121 In the second application studied, the on-line modelling technique is used to demonstrate how microprocessor control can be used to improve the closed loop dynamic performance of an electrohydraulic servosystem. The concepts are investigated by application to a rectilinear position control system driving a large inertia load having low damping. The resulting low frequency, lightly damped oscillations which occur in such systems are difficult to eliminate, and consequently limit the system closed loop bandwidth. In Chapter 7 the rig details and linear modelling of the servosystem is considered. The use of a fixed coefficient digital controller to improve the closed loop response is demonstrated, and the effect of nonlinearities in the servosystem investigated. Chapters 8 and 9 are devoted to the development of the Recursive Least Squares identification technique, for use both in automatic controller design and Self-Tuning adaptive control. The application of on-line identification and adaptive control to the electrohydraulic servosystem is presented and the advantages and disadvantages of the techniques demonstrated.

2. ELECTROHYDRAULIC FLOW CONTROL

2.1 Introduction

201 The study of the application of closed loop digital control in electrohydraulic valve design was initiated with a survey of electrohydraulic conversion techniques. This was considered essential since the valve hardware itself plays an important part in obtaining the full advantages of microprocessor control. The term 'flow control valve' used widely throughout this chapter, refers to any electrohydraulic valve able to continuously modulate the level of flow rate. In this chapter the fundamental elements of flow control valve designs are surveyed, and this is followed by more detailed discussion of the most promising concepts and devices. The chapter culminates in the development of a new flow control valve concept, which combines the simplest of hardware with the logical and arithmetic powers of microprocessor control.

202 For the purposes of the discussion, four functional elements which make up a flow control valve have been identified, and these will be considered in turn. Each of the functional parts and their relationships is shown in Fig 2.1. They are, firstly, the electromechanical conversion device, in which the valve input signal is processed and by some means translated into a mechanical effect. Secondly the hydromechanical servomechanism, whereby the mechanical effect is applied to change the position of the flow metering element. Thirdly is the flow metering element itself, and lastly the feedback mechanism.

203 In the following four sections from 2.2 to 2.5 each of the above mentioned devices is considered in turn, and the most promising techniques in each category identified. The survey is concluded in section 2.6, and this leads to the new flow control valve concept, presented in section 2.7. The further simplification of the hardware by the application of digital demodulation principles is discussed in section 2.8, and in conclusion a digital on/off pulse width modulated interface is proposed for the new valve concept.

2.2 Electromechanical Conversion

204 The electromechanical conversion element of a valve comprises two parts, the signal processing stage, which modifies and amplifies the input signal, and the conversion device itself by which the mechanical effect is achieved. Ideally the converting device should have a linear input/output relationship having minimal hysteresis, have good dynamic characteristics, and require the minimum of processing of the drive signal.

205 There are only a small number of physical phenomena whereby practical electromechanical conversion can take place. The most widely used is electromagnetism, however the electrorheological and piezoelectric effects provide feasible alternatives.

206 The electrorheological phenomena has radical implications in the design of hydraulic systems. Conceptually, the electrorheological flow control valve would be a solid state device, employing very high potential electrostatic fields applied across the fluid passing through the valve. Changing the field strength effectively causes local changes in the fluid viscosity, and hence rate of flow through the fixed valve flow path. Using four such valves in a wheatstone bridge arrangement it is possible to control the motion of an actuator [22].

207 However, the electrorheological effect is best suited to the solution of problems which rely essentially on the viscosity of fluids for their operation, for example fluid couplings and variable dampers [23]. The very high frequency response of electrorheological devices also makes them ideally suited for use in high frequency vibrator applications [24]. Although electrorheological valves give some control over the flow of fluid, they offer nothing like the precision and wide range of flow control expected of electrohydraulic valves. Thus it is difficult to conceive that the electrorheological effect will ever provide a feasible alternative to conventional valve technology.

208 Piezoelectric materials have less radical implications in valve design. The effect is created by applying large electrostatic fields across thin pieces of piezoelectric material. Typically, field strengths of about 1.0 kV/mm are required, giving corresponding material strains of the order of 0.0005. These extremely small

movements are amplified either by using large stacks of thinly cut material, or by the transverse strain of a piezoelectric bimorph [25]. In one application [26], where a piezoelectric bimorph flapper was used instead of a conventional servovalve flapper, test results showed that due to poor hysteresis, the valve could only be made to work accurately using pulse width modulation (PWM) drive signals. Driven in this way the valve gave a performance comparable with more conventional servovalves. Although piezoelectric devices can be less expensive to construct, hysteresis, thermal distortions, large drive voltages and the large dimensions required to obtain appreciable movements, have discouraged their use in valve design.

209 Almost all commercially available electrohydraulic valves employ electromagnetic principles in the converting element, the most commonly used devices being shown in Fig 2.2. The torque motor, shown in Fig 2.2(a), is the conversion element most often used in servovalves. It has a linear torque versus current characteristic and due to the absence of sliding surfaces has very low mechanical hysteresis. The torque is generated by the interaction of the permanent magnet flux and the current controlled electromagnetic coil flux. Unfortunately torque motors are complex and delicately balanced devices which require great care in construction if null shift problems are to be avoided. Thus manufacturing and assembly procedures for torque motors tend to be specialised, making them both expensive and difficult to service in the field.

210 Until the 1970's torque motor driven servovalves were used for almost all proportional flow control applications. However this changed with the introduction of the much simpler proportional solenoid device (Fig 2.2(b)). The proportional solenoid was developed directly from the on/off solenoid concept and looks very similar in construction. The difference in performance however is quite marked. Fig 2.3(a) shows typical force versus armature position characteristics for an on/off solenoid. The changing air gap gives a very nonlinear characteristic making it difficult to control intermediate armature positions. This is especially so in the high force, small air gap region of the stroke. By comparison the proportional solenoid characteristics Fig 2.3(b), have a linear working range independent of stroke, where the generated force is proportional only to the applied current. The linear characteristic is obtained by careful design of the magnetic circuit, including the positioning of a nonmagnetic ring in the flux path (Fig 2.2(b)). This effectively

gives a constant circuit reluctance irrespective of the armature position [27]. The armature is located and moves inside the pressure tube, thus special care is taken with the armature bearing surfaces and concentricity to ensure that hysteresis is minimised [28]. Compared to the torque motor the proportional solenoid is much simpler in construction, is very robust, is less sensitive to contamination, and can be serviced in the field.

211 In every respect, proportional solenoids are generally considerably larger than torque motors, and this has consequences in both the electronic drive design and in their dynamic performance. Typically, a proportional solenoid drive would supply 1 A of current compared with 5 mA for a torque motor driven from the same voltage level. Dynamically, the proportional solenoid valve has a relatively poor response, due electrically to the large inductance of the solenoid, and mechanically to the large inertia and low accelerating forces of the armature [29]. The proportional solenoid is a unidirectional device and must rely on either springs or hydraulic counteracting forces on the return stroke. In situations where bidirectional movement is required, as for a spool valve, two proportional solenoids are often used, one for positive motion and the other for negative motion.

212 The moving coil force motor, shown in Fig 2.2(c), has an advantage in this latter respect in that it is a bidirectional device. The electromechanical conversion occurs by placing current carrying conductors in a constant transverse magnetic field. The permanent magnetic field is generated in a substantial radial air gap in which the coil windings operate. A correspondingly large permanent magnet circuit is required, however the bulk of the magnetic components can be minimised using high coercivity materials such as Samarium Cobalt. Besides bidirectionality, force motors also have the advantage of a naturally linear relationship between the driving current and force output, thus no special linearising techniques are required at the design stage. Also the device does not suffer from saturation, responding to large overdriving currents, and thus improving the dynamic response and reducing stiction sensitivity. Electromagnetically, the force motor can have a superior dynamic performance compared with proportional solenoids, since the main magnetic field is of constant flux and the coil inductance is small. The same is true mechanically since both the bobbin and coil inertia's are relatively small. The bobbin can be mounted such that their are no sliding parts and this helps to reduce hysteresis effects [30].

213 Whilst the force motor is superior in many ways to the proportional solenoid it has not been widely used in the past. However the development of new less expensive magnetic materials should make these devices more popular in the future.

2.3 Valve Servomechanisms

214 The valve servomechanism is used to transmit the mechanical converter output to the flow metering device (Fig 2.1). In single stage valve designs the servomechanism is very simply a connecting link between the conversion element and metering device. The simplicity of single stage devices is very attractive, and leads to inexpensive and robust valve designs, however study of these devices has shown that they often have poor dynamic and static characteristics, requiring elaborate spool shaping to eliminate flow forces [31]. Good characteristics require the generation of high forces from the servomechanism, both to accelerate the metering device during transients, and to minimise the effects of flow and stiction forces which can cause positional error and hysteresis. In single stage devices these requirements can only be met by having high powered conversion devices. However, potential improvement in dynamics caused by increasing the available forces is often lost because of the increased inertia of the device. A comparison of the various electromagnetic conversion devices in this context showed that the moving coil force motor gives the best solution for larger single stage designs [32].

215 The deficiencies of single stage actuation are overcome by the use of an intermediate hydromechanical servomechanism in a two stage valve construction. The advantage is obtained by using the potential of readily available high pressure hydraulic fluid to amplify the electromechanical converter forces prior to application to the flow metering element. There are a number of methods of achieving this end, but all of them are based on various arrangements of the hydraulic bridge circuit. A common arrangement is shown in figure 2.4. In one arm, flow passes through restrictors 1 and 2, which controls the pressure at port A, and in the other flow passes through restrictors 3 and 4 controlling the pressure at port B. In the most general arrangement the electromechanical converter has independent control over all four orifices to control the pressure in A and B. Often the restrictors are controlled such that as the pressure increases in one port, it decreases in the other. This differential pressure is applied to move the metering element.

216 Some mechanical arrangements of the servomechanism are shown in Fig 2.5, for example, Fig 2.5(a) shows one arm of a bridge circuit of nozzle/flapper construction, where restrictors 1 and 2 correspond to those in Fig 2.4. Restrictor 1 is fixed, and either a rotary or rectilinear output conversion device can be used to vary restrictor 2 and hence the servo pressure. This single sided arrangement is often used in proportional solenoid valve designs, and its success depends on the careful matching of the two restrictors. A two sided arrangement based on the torque motor conversion device is often used in the first stage of servovalve designs [13].

217 The servovalve nozzle/flapper arrangement though small in size is used to control high pressures, and thus gives a very high force amplification whilst maintaining good dynamic characteristics. The flow orifices are typically around 0.4 mm diameter and are prone to clogging with contaminant, thus good oil filtration, typically 5 to 10 micron, is required. If nozzle blockage does occur, a hard over situation results which in many situations could have catastrophic consequencies. The jet pipe amplifier, shown in Fig 2.5(b), is an alternative circuit construction which provides some improvement. Instead of a flapper the torque motor drives a jet pipe which diverts the jet flow preferentially, either to line A or B, the pressure recovery on each side depending on the jet pipe position. This arrangement is fail-safe in the event of a jet pipe blockage and is reputed to have a number of other advantages over the nozzle/flapper arrangement [33]. Finally, Fig 2.5(c) shows a two armed construction using a spool type first stage. For a given spool lap condition the electromechanical conversion device determines all four restrictor flow areas depending on the applied drive current. Spool type pilot stages with rectangular ports provide very high hydromechanical force amplification and good linearity, but suffer from stiction on the spool faces thus needing good oil filtration and careful machining.

2.4 Flow Metering Devices

218 The spool construction of Fig 2.5(c) is also the basis of the main stage flow metering device of most four way valves, and is used because of its compactness, high power amplification and linearity. However good results are only obtained by precision manufacture, which is necessary to reduce leakage and achieve linearity about the null point. The former parameter is dependent on having very tight diametral tolerances since there is no positive seating, and the latter on precise axial

location between the various metering edges. Usually it is necessary to match the spool and sleeve in a temperature controlled environment. All of these manufacturing complexities make the spool/sleeve assembly a large factor in the overall valve cost. There are a number of alternatives which can be used as the metering element in multiple flow path control valves. The use of plates has been tried, and it has been shown that due to the metering edges being exposed and flat the manufacturing costs can be reduced [34]. However, pressure balancing of the plate is necessary if large stiction forces are to be eliminated. In practice plate valves are not widely used in electrohydraulic control valve designs.

219 Both of the metering element designs so far mentioned have been of multiple flow path single element construction, however significant advantages can be obtained using an independent element for each metering edge. Such a construction can easily be made using poppet valves. The poppet is also a positive seating device having a long engagement length between the poppet land and cartridge (Fig 2.6), thus good performance is achieved around the null point, and leakage from the back face of the poppet into the flow chamber is low. Consequently, compared with a spool the diametral manufacturing tolerances of the poppet can be slackened, and since also there are no axial land alignment problems the poppet is a relatively inexpensive device to manufacture. The poppet valve is also reputed to be less contaminant sensitive.

220 In its basic form the poppet valve is a two port metering element, however multiple flow-path valves can easily be constructed using individual elements. For example a four port valve can be constructed from four poppets to control the direction of motion of a cylinder drive, as shown in Fig 2.7. Each of the cylinder ports is served by two poppets, one to connect the high pressure port and one the return port. Poppet switching is controlled by small on/off electrohydraulic pilot valves, individually energised. The complete independence of control of each metering element produces some interesting switching possibilities. For example, the four valves of Fig 2.7 give a total of sixteen poppet switching combinations. The co-ordination of the switching modes is an ideal task for microprocessor logic. Even further the switching times of each metering element can be synchronised, for example, to reduce pressure transients during switching [35]. In some cases it has been found that poppet valves used in this way give faster response, smoother operation,and greater efficiency than spool valves [36].

221 The use of poppets in the construction of flow modulating control valves is more difficult as the lift of each poppet must be controlled independently. The problem is made additionally complicated as the poppet, unlike a spool, is a very load sensitive device, responsive to the changes in flow and pressure which occur. If the flow forces are minimised by careful valve construction then the poppet valve becomes sensitive to flow pressure only. This is the basis of many two stage pressure control valves, where the poppet servo pressure is set by a pilot valve, and the main flow pressure rises to a corresponding level, maintaining the poppet in equilibrium. Again, lift control of the four poppets is an ideal task for microprocessor control, and it will be shown later that the load sensitive characteristic of poppet valves can also be used to advantage by the microprocessor.

222 A recent innovation in poppet lift control is the so called 'Valvistor', shown diagrammatically in Fig 2.8 [37]. The poppet face has a small slot which allows a small amount of main stage flow to pass through to the servo side of the poppet. This forms one variable restrictor in a bridge circuit. The other variable restrictor shown in Fig 2.8 is controlled either manually, or by a pilot valve. Increasing the area of this restrictor causes a drop in poppet servo pressure, thus the poppet starts to open, increasing the flow through the slot in its land until the servo pressure force is again in equilibrium with the main flow poppet forces. Hence equilibrium is reached with the poppet in a new position proportional to the change in area of the controlled restrictor.

2.5 Feedback Mechanisms

223 The final link completing the valve design is the feedback mechanism (see Fig 2.1), which can be mechanical, hydromechanical or electrical in nature, and is present in one form or another in every control valve design [38]. Indeed feedback is often inherent in the design of the various functional elements already discussed. For example the valve drive may have current feedback, or the conversion device and servomechanism could be a proportional solenoid using pressure feedback to balance the armature forces. However, here the discussion centres around the overall feedback of the valve output used to close the loop between the first and second stages, which for a flow control valve could mean feedback of pressure, flow rate or flow metering area.

224 The most easily measured and hence widely used feedback is that of metering element position, from which the flow area can be inferred. If the pressure drop across the flow area is constant, this signal also gives an indication of flow rate. In servovalves, where the valve pressure drop is often high compared with the load pressure fluctuations, the corresponding variations in flow are small, and in any case if the valve is used in a closed loop system, slight variations in gain caused by pressure fluctuations are not significant. However in proportional valves, large percentage changes in pressure drop often occur, having a significant effect on the flow rate. In open loop applications, for which proportional valves are often used, this may not be acceptable. One solution is to put a pressure drop regulator either in parallel or series with the valve to maintain a constant pressure drop across the flow metering element.

225 The dynamic measurement of flow suitable for feedback cannot be achieved using conventional flow metering devices, ie positive displacement or turbine meters, since their dynamic performance is inadequate. However, a number of alternative devices having higher dynamic performance have been designed [39]. All of them are based on the same principle, and an example is shown in Fig 2.9. The flow through the valve is also made to pass through a specially constructed poppet. By careful selection of the spring, and shaping of the poppet flow area versus lift characteristic, the poppet position can be made to change linearly with flow [40]. The dynamics of this device are sufficiently fast for use as a transducer in flow control valve designs, and in practice it has been found to work well.

226 There are two places where feedback can occur in a valve design, these are shown in Fig 2.1. Mechanical or hydromechanical feedback to the converter/servomechanism interface has in the past been the most widely used method. For example, in a servovalve a feedback wire is often used to transmit a force feedback of spool position to the torque motor flapper, and this balances out the torque motor deflection when the correct spool position is reached. The necessity of mechanical interconnections used in this type of feedback imposes definite restrictions on the layout and packaging of the valve design. Greater flexibility in design packaging is obtained using electrical feedback devices, no restrictions being imposed on the physical relationship between the first and second stages. The expanding use of electronics and microprocessors in electrohydraulic systems has led to a corresponding increase in the use of electrical feedback devices,

since the electronic controller offers a great deal of flexibility in the design and adjustment of the closed loop dynamic performance.

2.6 Survey Conclusions

227 The valve functional elements briefly surveyed in the previous sections are the basic building blocks of any valve design, the choice of which influences its cost and performance. The survey has shown that the latest advances in valve design have been largely in the electrically interfaced components, ie the conversion and feedback elements. Servomechanism and flow metering devices have remained unchanged for many years. However in the light of developments in the electrically interfaced components, these devices must be reconsidered as they may be more appropriate in new valve designs. For example, whereas in the past four way control implied the use of a spool, it is now often found that the poppet valve gives greater performance and flexibility.

228 It is probable that any further developments will continue the trend already set, incorporating even more advanced electromechanical interfacing into valve designs. In electromechanical conversion devices, as pointed out by the survey, there are very few practical conversion principles which can be utilised, and it is probable that future designs will centre around the more efficient and cost effective use of conventional electromagnetic principles. This involves not only the mechanical hardware of the conversion device, but also the design of the drive electronics, and the control methods utilised. In this area there has also been great efforts to design interfaces which would enable easy connection to microprocessors.

229 The rapid growth of microprocessor technology offers great potential for the enhancement of electrohydraulic valves. The possibility of incorporating a microprocessor as an integral part, rather than a peripheral device, in a new valve design, was the starting point of the work presented in this thesis, the aims being to reduce costs and improve flexibility without loss of performance. Two areas of research have been identified and investigated: first, the use of a microprocessor closed loop controller to maximise the performance and flexibility advantages offered using electrical feedback; and secondly, the improvement and simplification of electromechanical conversion by the utilisation of pulse width modulated (PWM) control signals. Both of these concepts will be introduced in the following

sections.

2.7 Microprocessor Integrated Flow Control Valve Concept

230 The use of electrical feedback in valve design in conjunction with an electronic controller, gives an increased degree of flexibility compared to hydromechanical feedback. For example some manufacturers use PID closed loop controllers, in which each of the three terms can be varied to optimise the valve dynamic performance. However, although these terms can be used to shape the valve step and frequency responses, the corresponding rise time and bandwidth is limited by the elements used in the valve construction. In proportional valve designs the maximum closed loop bandwidth is typically around 10 to 20 Hz. Dynamics in this bandwidth are slow enough to enable the beneficial use of a microprocessor to close the loop. The microprocessor gives greater freedom and flexibility in shaping the valve dynamic response, and additionally allows the execution of complex control algorithms which would not be possible using an analogue controller.

231 The benefit of the microprocessor in closed loop control is obtained when an on-line model of the valve being controlled is implemented in parallel with it, as was described in paragraphs 106 and 117. Conceptually, the model is designed to calculate in real time the pressures and flows which occur in the real valve, this information then being used either as an indication of the valve condition or used as an alternative feedback.

232 The valve model must be calculated using only the normal operating control signals, ie the valve drive and position feedback signals. If any other information is required in calculating the full set of valve operating parameters, the inclusion of another transducer to obtain this information will add to the complexity of the valve and may make its cost prohibitive. This constraint has strong implications in the choice of valve hardware. A conventional spool type valve for example, is not ideal for modelling purposes, since the spool position (ie the feedback parameter), is load pressure insensitive, and the spool pressure drop can not be calculated from this nor from the drive signal. Calculation of the flow through the valve would require the undesirable inclusion of a pressure transducer in addition to the spool position feedback transducer.

233 The requirements of this modelling constraint are met however by using a simple poppet valve as the flow metering element. It can be shown that the flow rate through a poppet flow area is predominantly a function of two variables, the poppet lift and the servo pressure applied to the back face of the poppet [31]. If the servo pressure is applied to move the poppet by the use of a proportional electrohydraulic pressure control valve, then the controlled servo pressure is a function of the applied drive current. Thus using this signal and the poppet position feedback signal, it is feasible to calculate all of the pressures and flows occurring within the valve. The accuracy of control obtained using indirectly calculated feedback parameters will depend on the behaviour of unmodelled effects such as hysteresis and temperature drift, and it is necessary to ensure that these effects are minimised in the valve design.

234 A schematic of the proposed new flow control valve concept is shown in Fig 2.10. The pressure control pilot valve forms one controllable restrictor in a bridge circuit, the other restrictor being fixed and matched to suit the pilot valve. Increasing the current in the pilot valve reduces the nozzle flow area thereby increasing the servo pressure. The increase in pressure causes the poppet to close until it reaches either a new equilibrium position or the valve seat. The microprocessor is used to close the loop, operating on two external signals (the demand and feedback signals), to produce the appropriate drive signal for the pressure control valve. The drive and feedback signals, e and y, are used in the model to calculate the valve pressures and flows, and Fig 2.10 shows that any one of these estimated parameters can be used for feedback. In the diagram the flow rate control mode is shown selected. In this mode the valve is thus automatically correcting for any changes in load pressure which may occur. The blocks F and G in the forward path and feedback path respectively, are microprocessor implemented dynamic transfer functions, used to tune the valve closed loop dynamics.

235 The reduction in valve hardware resulting from the use of microprocessor control is best illustrated by comparison with other, already existing, two port flow control valve designs. Without the microprocessor the poppet flow cannot be derived indirectly, and must be measured using an extra transducer. The hardware required for doing this was discussed in paragraph 225 and shown in Fig 2.9. The output of such a device can be used as feedback either hydromechanically to the

pilot stage or electrically to an electronic controller [39,40]. The latter version is shown conceptually in Fig 2.11. The feedback signal is measured electrically from the position of the flow feedback poppet, and compared with a demand signal input to the controller. This generates an input to a closed loop position control system around the main flow control poppet, the lift of which is controlled to maintain the demanded flow. Thus it can be clearly seen that the microprocessor solution can give significant savings in valve hardware.

236 Another advantage of the new valve concept is the flexibility offered by the microprocessor. In executing the valve model, the servo pressure, poppet lift, main flow pressure and flow rate signals are calculated. Any one of these can be used for feedback at any time simply by indicating the change of feedback mode electronically to the microprocessor. This ability could be valuable in some industrial processes where at different times in an operating cycle, both flow and pressure control is required.

2.8 Digital Pilot Valve Interface

237 In recent years many researchers have sought to reduce the complexity of the electromechanical conversion element, both to enable simplified interfacing to microprocessors and to gain some performance or cost advantage [41,42]. Rather than looking for new conversion methods the trend has been to use existing principles but arranged in simple ways, or driven by novel control signals [20,43]. Often these valves are termed 'digital valves', but this is a loose term which tends to be used to describe anything that is not strictly analogue in control.

238 There are three commonly used so called 'digital valve' concepts. These are: first, parallel input valves, in which each of the data bus lines of a microprocessor are used to control a correspondingly sized on/off logic valve. Secondly, stepper motor driven valves, which are considered digital because of their discrete stepping characteristic; and thirdly, pulse width modulation (PWM) driven valves, which are considered to be digital because there are only two operating states - on or off.

239 Only the first mentioned principle is truly digital in the same sense as the microprocessor, since here the flow changes in a binary fashion as signalled by the microprocessor bus lines. However valves designed on this principle are very bulky

[42], for example, an 8-bit processor would require eight different valves, the largest valve having a flow area one hundred and twenty eight times that of the smallest valve. The smallest valve would be minute, being difficult to construct, and the largest valve would probably have to be of two stage design to obtain a reasonable dynamic response. All of these factors make such a valve impractical for general use.

240 The stepper motor is a unique electromechanical converting device, both in that it effectively has a built in position feedback, and in that the output is rotational instead of rectilinear. Hence the most effective and direct use of a stepper motor is in application to rotary metering devices, and both plate and spool type elements have been tried [44,45]. More widely the stepper motor has been coupled via a rotary to rectilinear transmission, such as a screw thread or cam, great care being taken to eliminate backlash [46]. Used as a single stage device, the high force requirement leads to large motors with poor dynamic performance [47]. This problem has been overcome by the design of two stage valves, using a smaller motor and hydromechanical amplification. However in such valves the simplification in design or cost saving is not so apparent [48].

241 Valves designed using pulse width modulation (PWM) signals, are easily interfaced to microprocessors, but more importantly give significant simplifications in the valve design. The principle of PWM is shown in Fig 2.12. The PWM signal is on/off in nature at a high and constant frequency, but the period of on to off time is varied, (compare Fig 2.12(a) and 2.12(b)). This signal is then passed through a demodulating element, for example a restrictor orifice, which has a bandwidth considerably less than that of the PWM frequency. When the PWM signal is switched on and off the output of the demodulating element aims first to full signal and then to zero. However, the switching frequency is so high that the output never reaches the extremes of its range, and takes up a mean position proportional to the mean value of the PWM signal over a number of cycles. This mean value is the proportion of on-time in a complete PWM cycle, known as the 'Signal Modulation Ratio' (SMR).

242 The simplicity in valve design comes about by choosing the correct place of demodulation within the valve. There are a number of possibilities, and these are

best seen by considering again Fig 2.1. At low PWM frequencies, demodulation could be made to take place downstream of the valve in the system being controlled, and in this case the entire valve could be made from on/off elements, making it very inexpensive and robust [18,49]. However in some applications the relatively low frequency high amplitude pulsations in the system may not be desirable.

243 Hydraulic demodulation within the valve can be made to occur by increasing the frequency of the signal, and placing a demodulating restrictor between the servomechanism and the flow metering device. Using this arrangement, the entire first stage can be constructed from simple on/off components. Attempts to eliminate the power dissipation through the restrictor by using fluid inertia effects for demodulation have shown that unacceptably long lengths of fluid are required, accompanied by very high PWM frequencies [50,51].

244 Demodulation of the PWM signal can also be achieved by increasing the frequency even further, and using the inertia effects of the converter moving parts, or the dynamics of the electronic drive circuit. For example, in a proportional solenoid, either the armature inertia or the solenoid circuit time constant could be used to demodulate the signal. However, here the pilot stage would still need to be of proportional construction, and the only advantage gained would be a reduction of hysteresis caused by PWM dither of the armature.

245 In the new valve concept shown in Fig 2.10, the most expensive item is the pressure control valve, which comprises both the electromechanical converter and the servomechanism. Thus to simplify this part of the valve, the PWM principle described in paragraph 243 can be applied and is shown schematically in Fig 2.13. Instead of a proportional pressure control valve, a three port on/off solenoid activated ball valve is used to set the pressure to either high or low levels depending on the PWM signal. This pulsating pressure signal is then passed through a demodulating restrictor so that the mean pressure level seen on the back face of the poppet is proportional to the signal modulation ratio (SMR). The pilot valve then provides the same function as the proportional valve previously described, whilst being simpler in construction.

2.9 Concluding Remarks

246 The two concepts of sections 2.7 and 2.8 can be amalgamated together to make a control valve which is inexpensive, robust, contaminant insensitive and very flexible in application. Such an overall concept is shown in Fig 6.1. However, the use of closed loop microprocessor control and PWM as described in sections 2.7 and 2.8 are two separate areas of research and are treated as such in this thesis.

247 Before the software design and the valve hardware can be discussed, it is necessary for the reader to be aware of the principles and implications of digital closed loop control applied to electrohydraulic systems. Thus the presentation of the valve design and test results is delayed until Chapter 5. Chapter 3 is devoted to discussion of digital control concepts applied to electrohydraulic systems, and Chapter 4 to the development of a Pole Placement controller design technique.

Fig 2·1

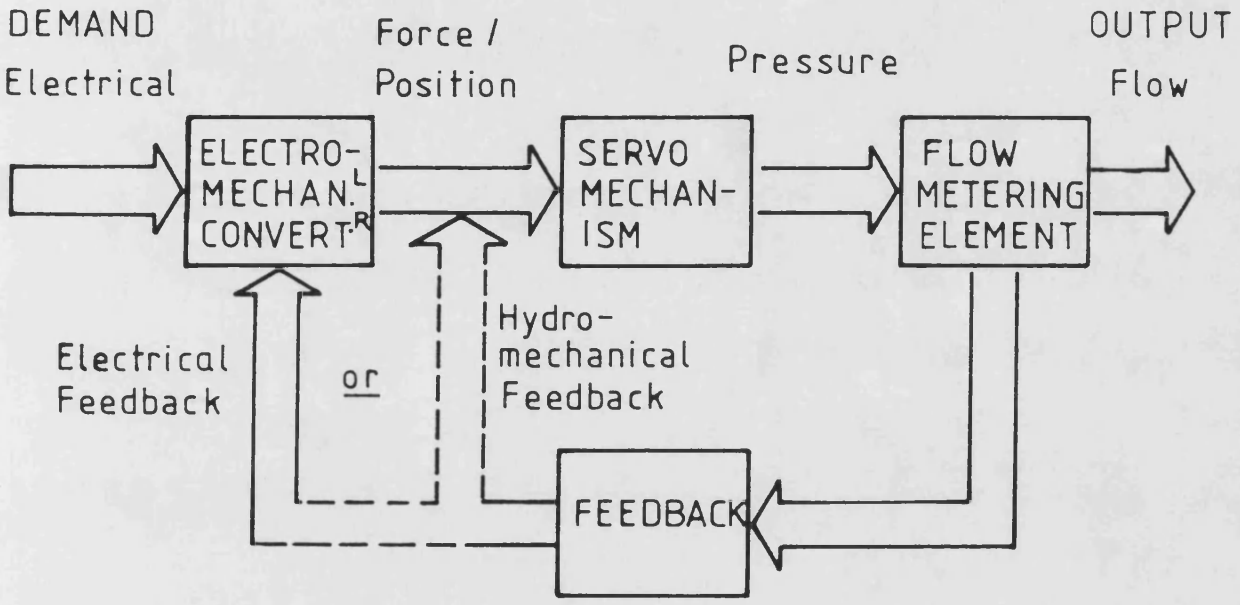

2·1 FLOW CONTROL VALVE FUNCTIONAL ELEMENTS.

Fig 2·2

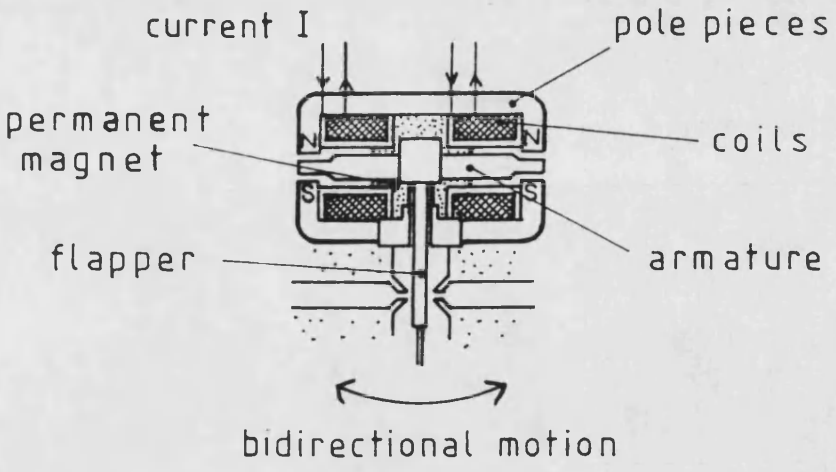

(a) TORQUE MOTOR

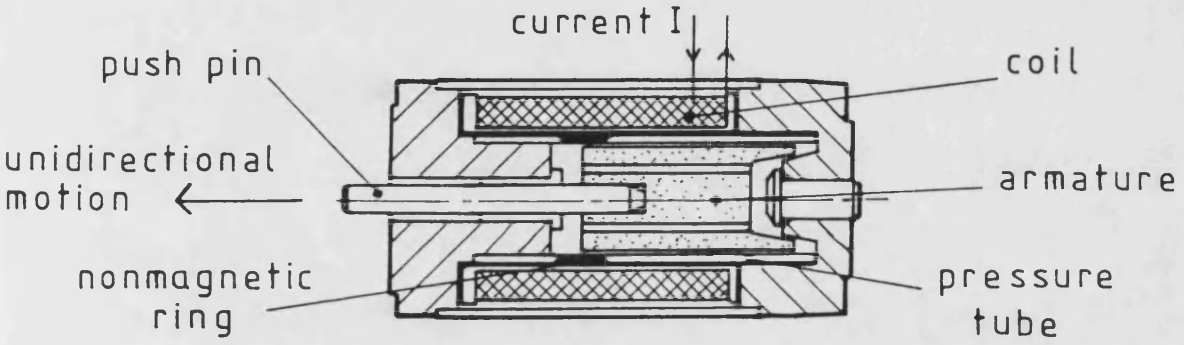

(b) PROPORTIONAL SOLENOID

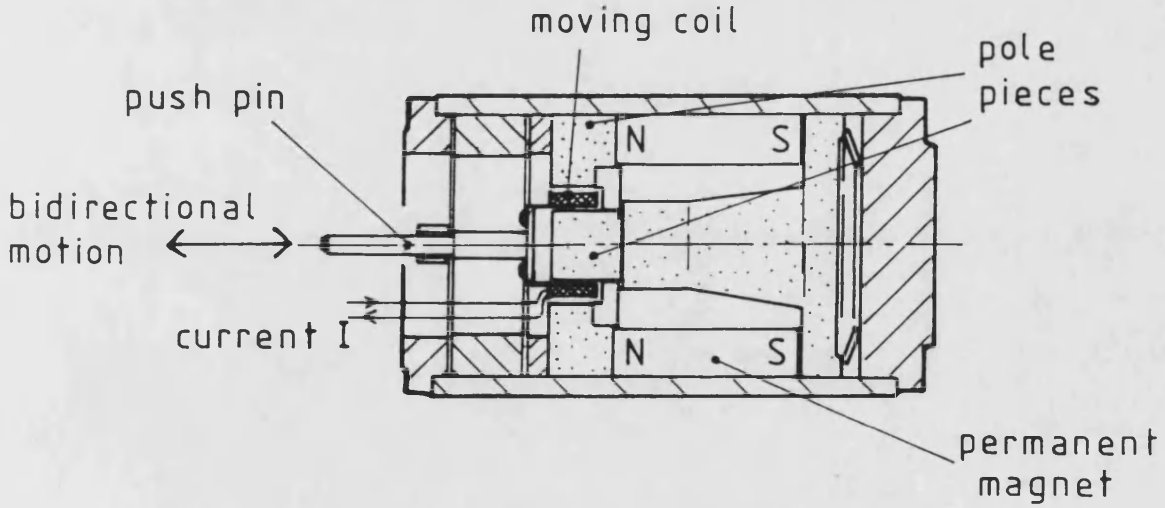

(c) FORCE MOTOR

2·2 ELECTROMAGNETIC CONVERSION DEVICES

Fig 2·3

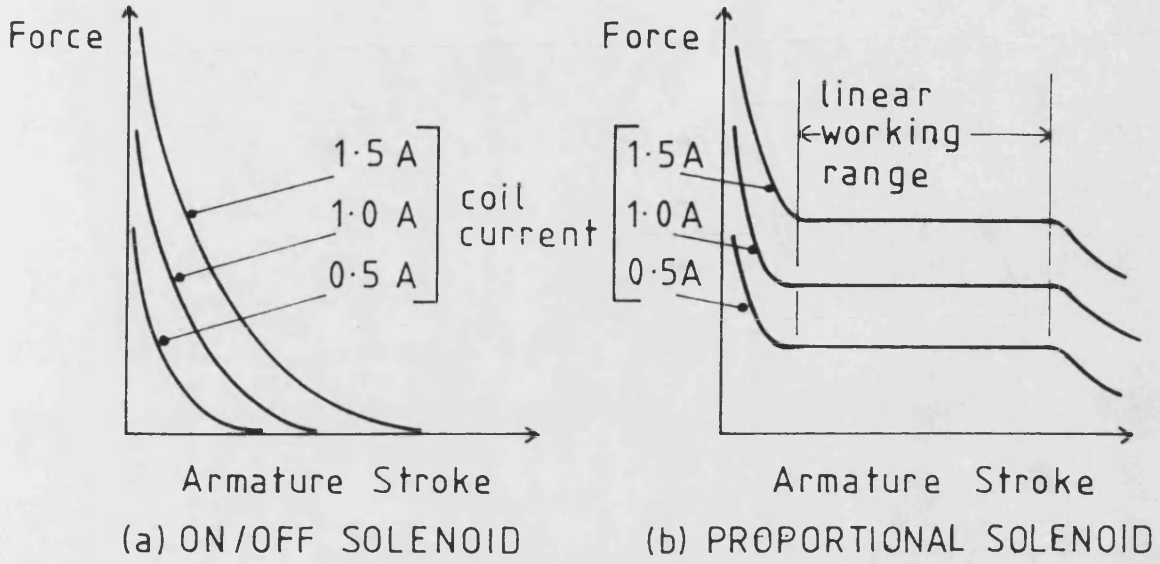

2·3 TYPICAL SOLENOID CHARACTERISTICS

Fig 2·4

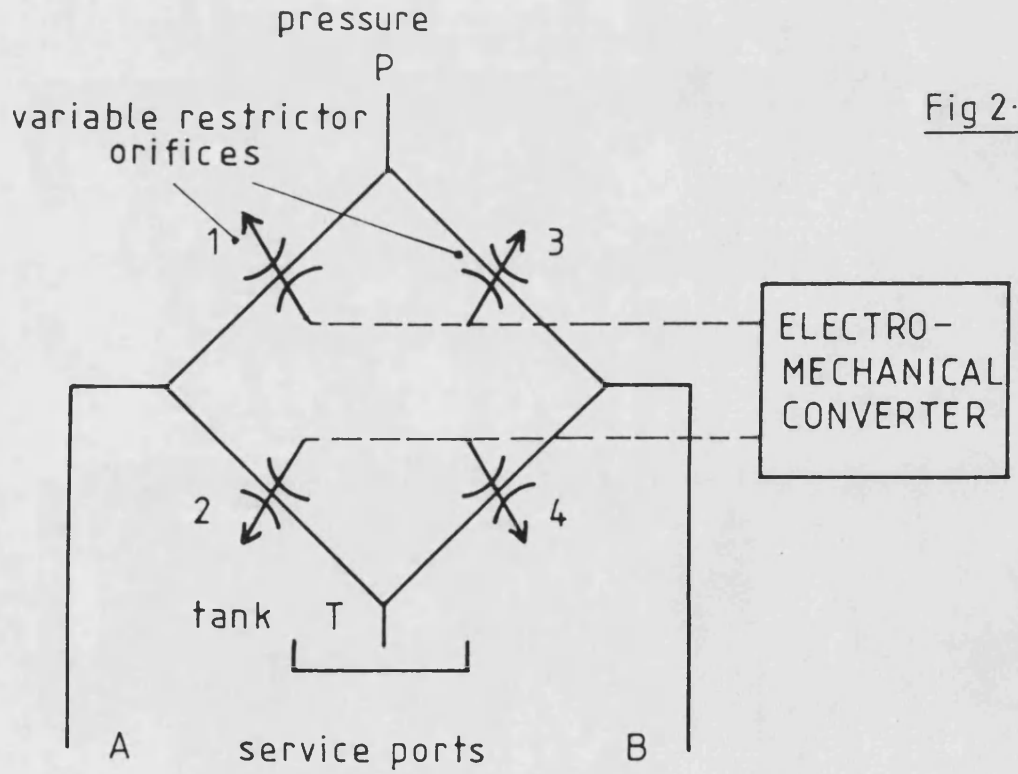

2·4 HYDRAULIC BRIDGE CIRCUIT

Fig 2·5

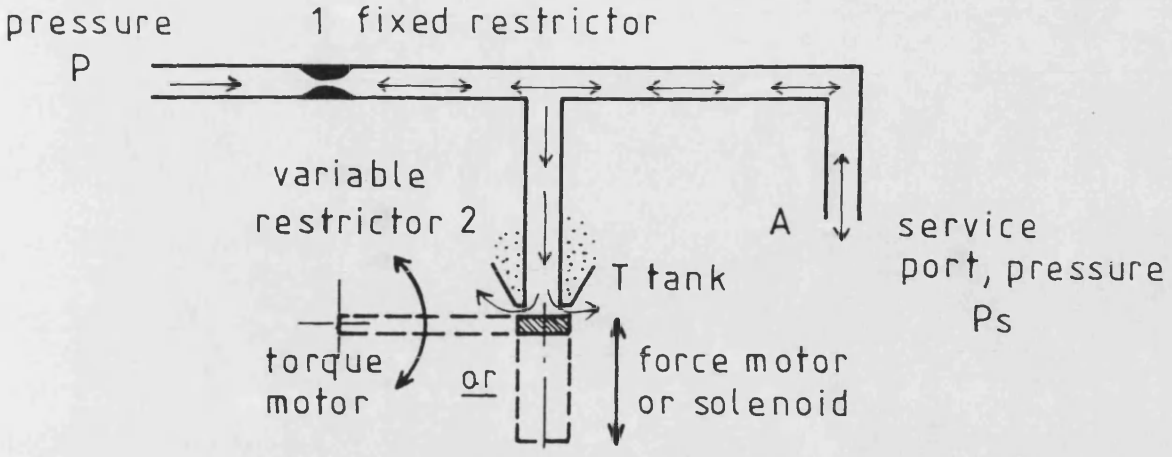

(a) NOZZLE/FLAPPER BRIDGE

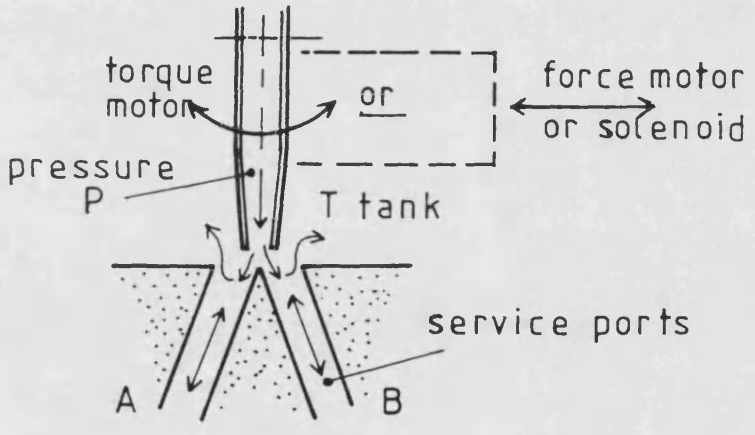

(b) JET PIPE SERVO

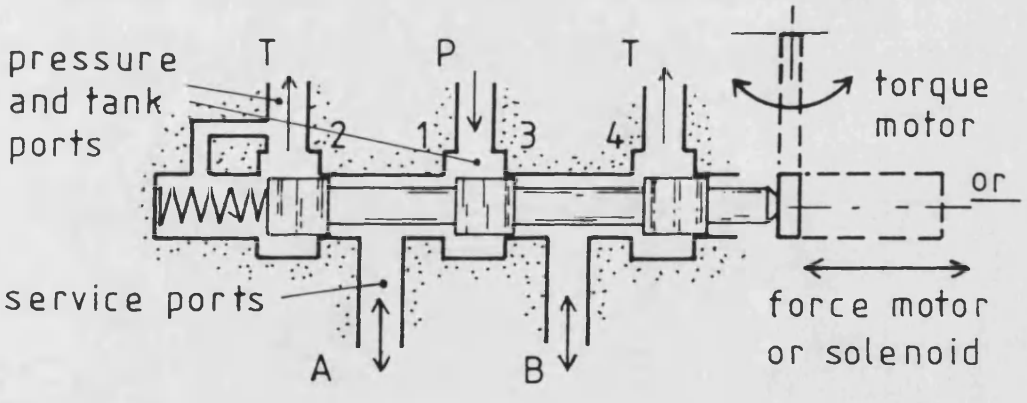

(c) FOUR WAY SPOOL BRIDGE

2·5 TYPICAL HYDROMECHANICAL SERVO SYSTEMS

Fig 2·6

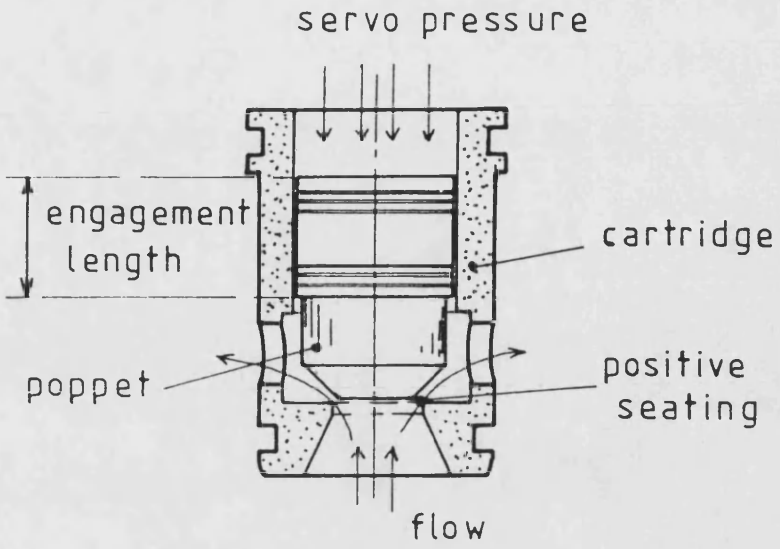

2·6 POPPET VALVE

Fig 2·7

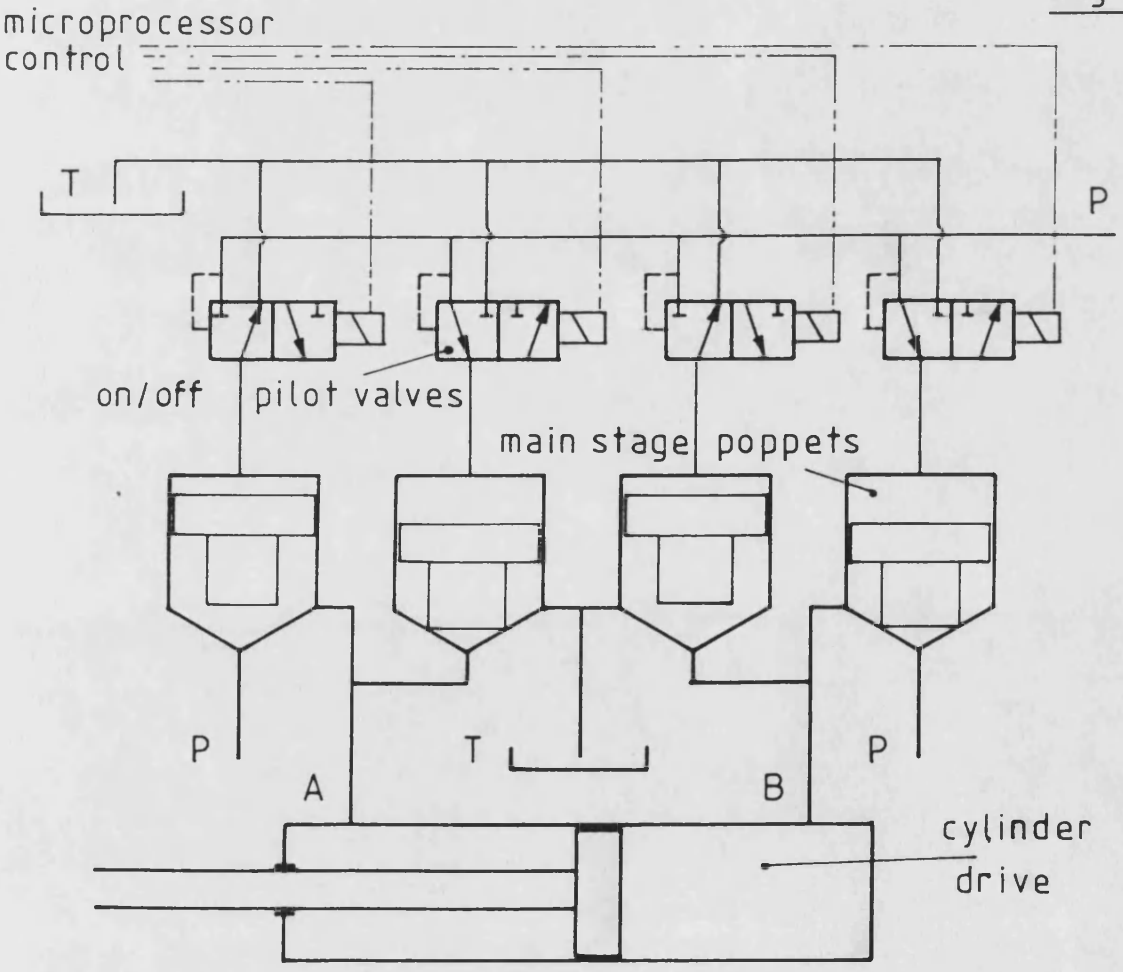

2·7 FOUR PORT DIRECTIONAL POPPET VALVE

Fig 2·8

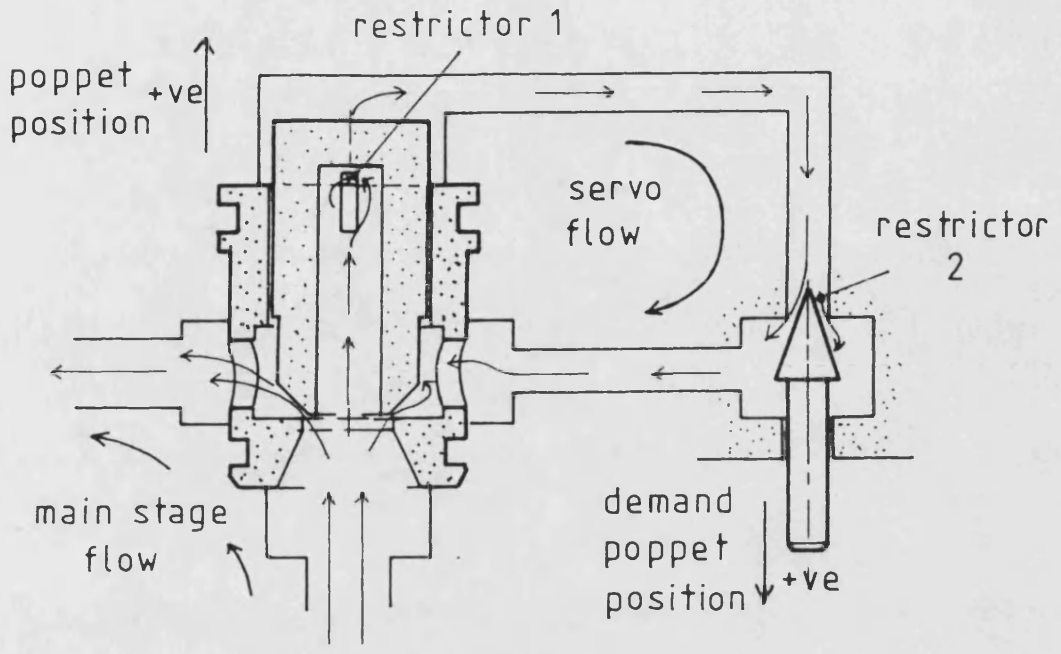

2·8 POPPET POSITION CONTROL ~ THE VALVISTOR

Fig 2·9

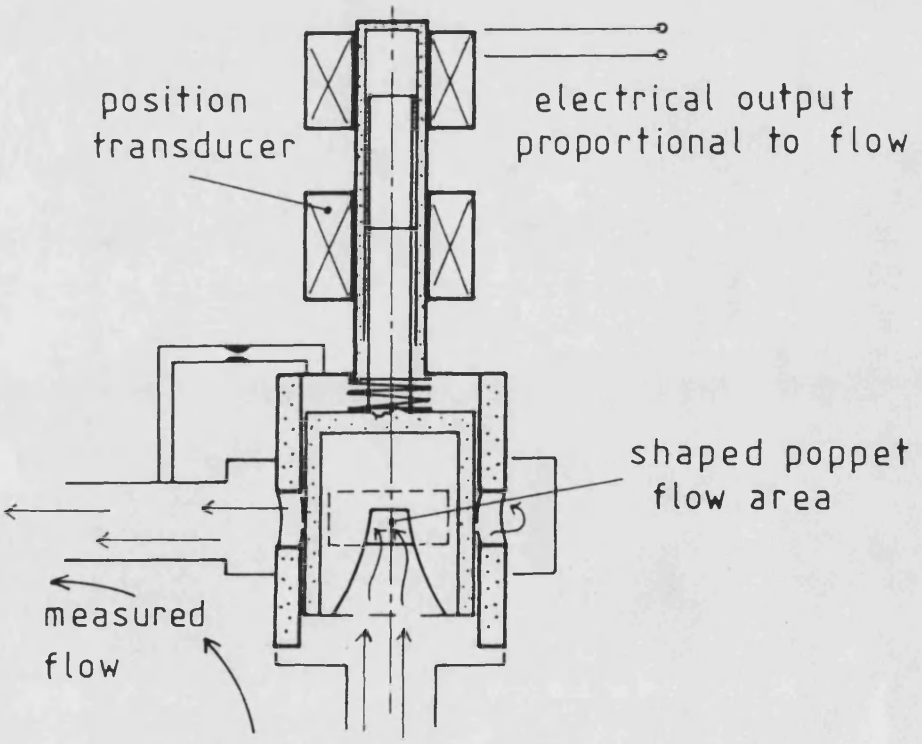

2·9 DYNAMIC FLOW METER

Fig 2·10

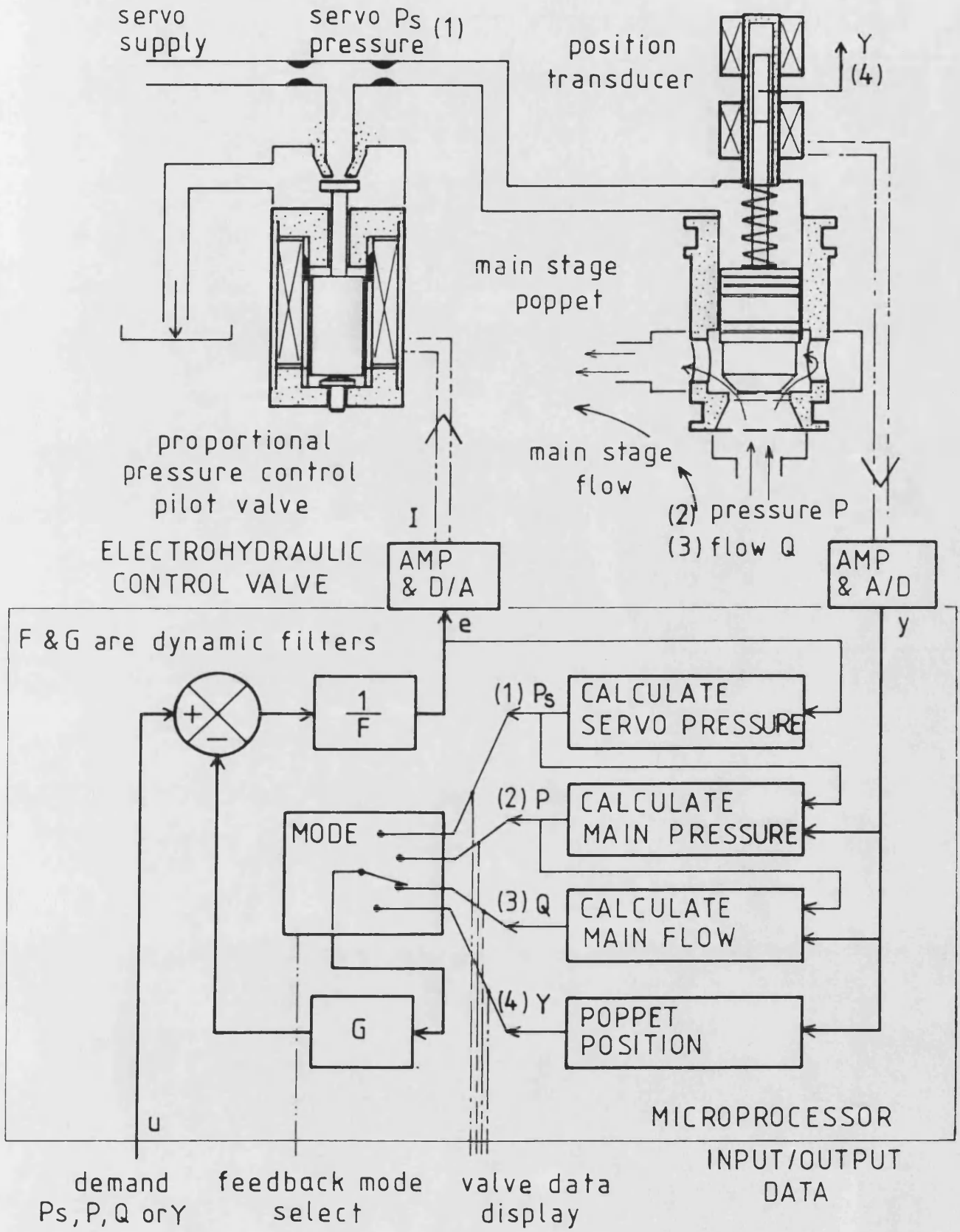

2·10 NEW FLOW CONTROL VALVE CONCEPT

Fig 2·11

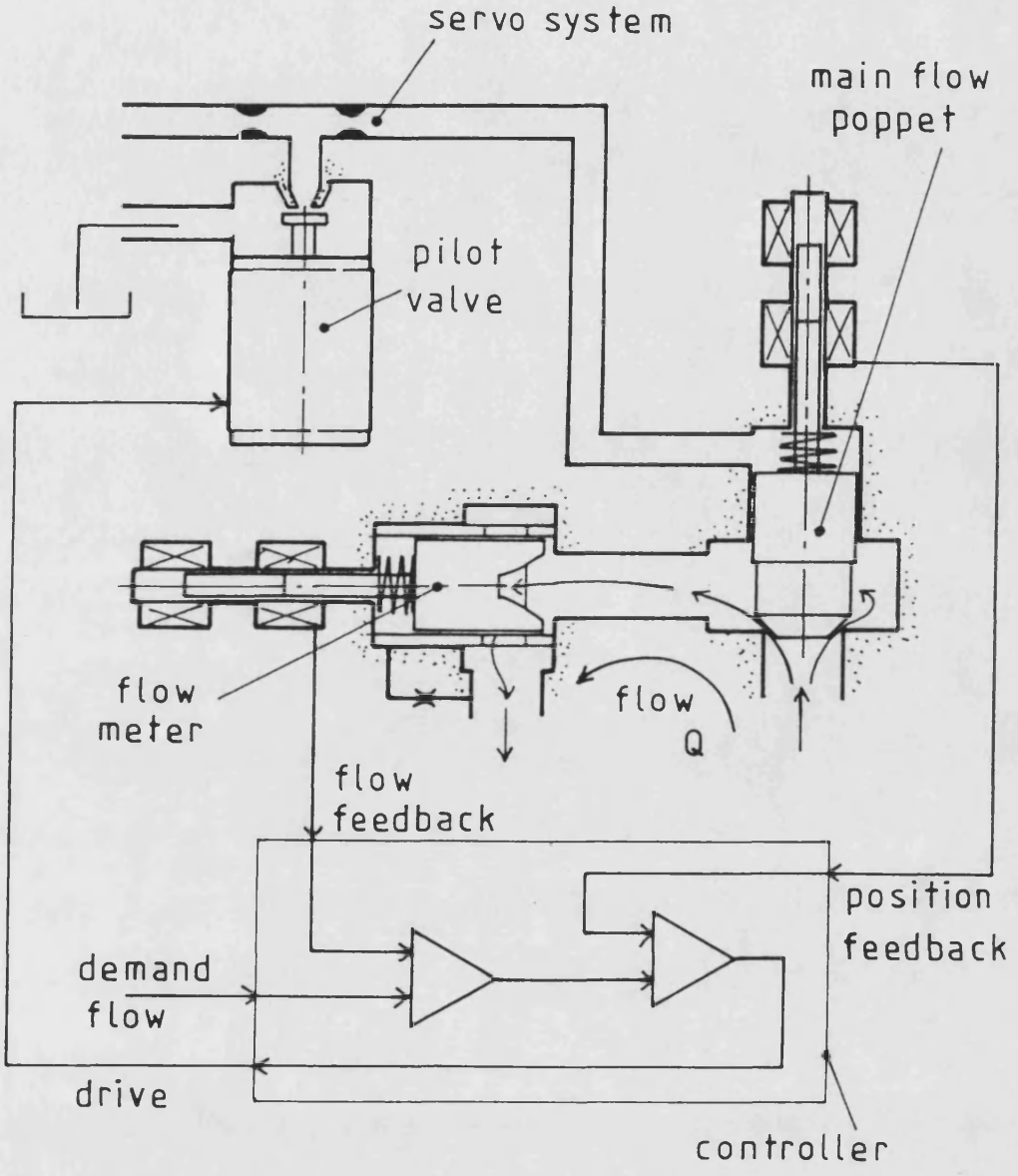

2·11 TWO PORT FLOW CONTROL VALVE USING A FLOW METER

Fig 2·12

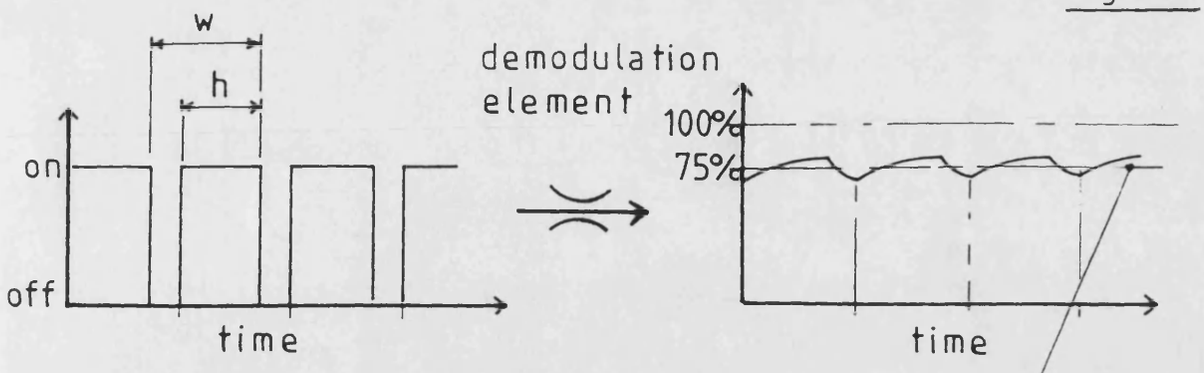

(a) SIGNAL MODULATION RATIO 0·75

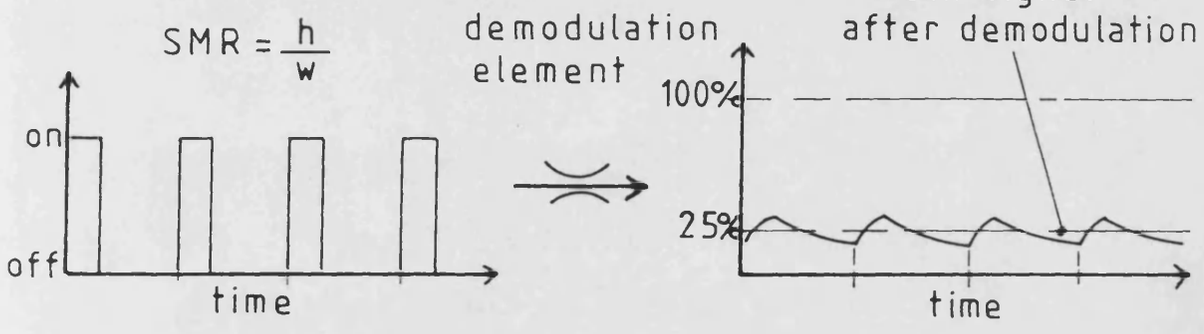

(b) SIGNAL MODULATION RATIO 0·25

2·12 PULSE WIDTH MODULATION

Fig 2·13

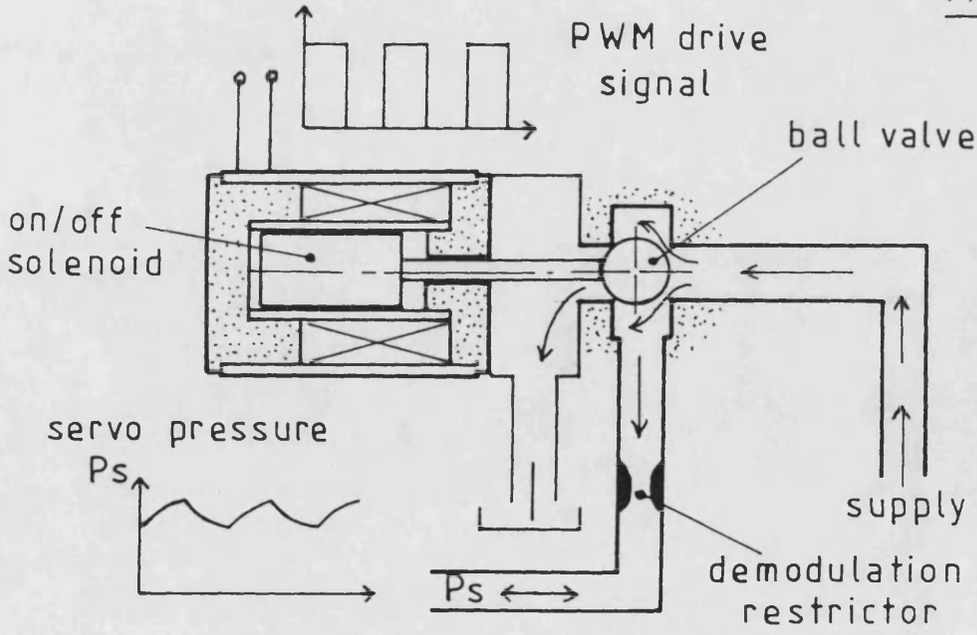

2·13 DIGITAL PRESSURE CONTROL VALVE

3. DIGITAL CONTROL OF ELECTROHYDRAULIC SYSTEMS

3.1 Introduction

301 Design techniques for digital control systems are numerous and varied. Often it is difficult to establish which technique is best suited to a specific application. This chapter considers some of the alternative approaches to digital controller design, and focuses on the techniques used during the research. Also the effects and implications of introducing digital control are discussed.

302 The Darkstar microcomputer system, used to develop and execute all of the algorithms presented in this thesis is introduced in section 3.2. The fundamental mathematical approaches to controller design are discussed in section 3.3, and for single input/output electrohydraulic servosystem control, the classical methods using discrete transfer functions are favoured. A general block diagram structure suitable for representation of the great majority of digital servosystems is proposed, and the block diagram nomenclature used throughout the thesis defined. Section 3.4 also discusses the method of implementing the control law. To assist in algorithm development, and observe the effects of digital closed loop control in an ideal situation, an electrical dynamic simulation network was used, and is presented in section 3.5.

303 The discrete classical controller design approach requires a discrete transfer function representation of the electrohydraulic plant, and various methods of producing this model are discussed in section 3.6. The Pole/Zero Mapping method, chosen because of its simplicity in application and accuracy of representation, was used throughout the course of the research. Slow sampling is often necessary in digital servosystem control so that the maximum time for algorithm processing is achieved. In section 3.7 the effect of slow sampling on the electrohydraulic plant and the accuracy of the Pole/Zero Mapping model is investigated. Finally the implications of sample period restrictions on the application of microprocessor closed loop control is discussed, and demonstrated by consideration of the Darkstar processing performance during the course of the research.

3.2 The Darkstar Microcomputer

304 For research purposes a fully equipped development microcomputer known as 'Darkstar' was used, both for algorithm development, data processing, and for execution of the control algorithms. The Darkstar is a general purpose machine, built at the University of Bath, the system consisting of a central processing card supplemented by a number of peripheral cards, all of which are mounted in a double height card frame. The card frame system gives flexibility to add cards as required to meet a specific application, and is mounted along with two 5.25 inch floppy disc drives and a peripheral display panel in a sturdy laboratory proof cabinet, as can be seen from Fig 3.1.

305 The Darkstar layout used during the research is shown in Fig 3.2. At the heart of the system is the central processor, built around a 68000 microprocessor and driven from an 8 MHz clock. For data processing purposes 500 K of temporary memory was added, along with a colour graphics facility. The system user interacts with the system via the VDU and keyboard, and permanent data storage is provided by the two double density double sided disc drives. Although designed principally for one user, a facility is provided which enables the support of one other user on a time sharing basis. Electrohydraulic systems were interfaced via a purpose built input/output card carrying eight 12 bit A/D converters, prefiltered by two pole antialiasing filters, and four 12 bit D/A converters. For both input and output, the conversion gains were set to give, 0 binary corresponding to -10.24 V, and 4095 binary to +10.24 V, giving 200 binary steps per volt. The generation of PWM signals was achieved using a programable multi-timer chip.

306 The operating system for the Darkstar is 'Tripos'. This is a multi-tasking operating system, which allows many jobs to take place simultaneously, giving the user the power to create and suspend tasks at will [52]. Three programming languages are supported on the machine, these are 68000 assembler language, BCPL (Basic Combined Programming Language), and Fortran. Although assembler potentially generates the most efficient code, it is very time consuming to program, and for this reason it was only used for the software implemented floating point arithmetic routines, and the input/output device routines. Fortran on the other hand, being a high level language offers ease of programming, but in this case at least, results in a considerably less efficient object code. BCPL is an intermediate

level language which offers a good compromise between these two extremes, giving ease of programming and efficient code [53]. Thus BCPL was used for all of the programs developed during the research. All arithmetic operations were carried out to 32-bit accuracy, and where possible integer arithmetic was used, although if required floating point functions were also available.

3.3 Classical Versus Modern Control Theory

307 The increasing use of microprocessors in control systems, both for analysis synthesis and on-line control, has been paralleled by an increasing number of available implementation techniques. The literature in the field is colossal, and often does not make clear what are the benefits and shortcomings of each technique, or for what applications they are best suited. Very often the end results are the same even though the approaches may be quite different. There are two fundamentally different approaches to controller design which can be applied in either the continuous or discrete domains, these are the so called 'modern' and 'classical' methods. Additionally, in digital electrohydraulic servosystems, where both digital and continuous systems are combined, the question arises; should the electrohydraulic plant be modelled using continuous or discrete equations? This problem will be discussed first.

308 In an analogue control system, both the plant and controller are continuous devices and can often be described mathematically using ordinary differential equations. If the controller is then made digital, the tendency is to use the same continuous domain electrohydraulic plant equations, design the controller as if it also were continuous, and then simply translate it to discrete form for implementation [54]. This technique is known as 'emulation', and has been used successfully in electrohydraulic systems. However its success depends on the use of high sample frequencies so that the distorting effects of sampling can be ignored and the system effectively considered to be continuous [55]. Unfortunately, fast sampling, ie short sample periods, reduces the time available per sample period for processing, and particularly in fast electrohydraulic systems, this proves to be a critical factor limiting the application of digital control [56].

309 Improvements can be made either by having a faster but more expensive microprocessor system, or more attractively using discrete design techniques which

allow reliable controller design using longer sample periods. It has been found that by considering the drive signal D/A and feedback signal A/D converters as part of the electrohydraulic plant, then the plant and thus the closed loop system can be considered to be entirely digital in nature. The resulting discrete equations are no more complicated, and with experience the designer can develop the same physical interpretation of them as he would for continuous equations. The problem of sample period distortions is automatically taken into account, and the controller can be designed with ease based on discrete performance criteria. This approach was used in every case during the research presented in this thesis, and was found to work well for slow sampling.

310 The modern approach to controller design uses a state-space representation, where the linear equations are broken down into first order equations and arranged in matrix form. If the plant to be controlled is of order n, then the feedback of n states is sufficient to enable complete control of the system dynamics. Thus for example, in a third order electrohydraulic position control system, the additional feedback of velocity and acceleration at the correct gain levels would allow control of the closed loop rise time natural frequency and damping ratio. Analogue systems using velocity and acceleration transducers in this way have been shown to work well [57].

311 In digital control systems similar state-space techniques can be used. However, here the microprocessor gives the additional advantage that the velocity and acceleration signal can be obtained indirectly by calculation, thereby eliminating the need for additional transducers. A schematic for a third order system is shown in Fig 3.3. The electrohydraulic plant could be a servovalve driving a cylinder, the cylinder piston position being indicated by a transducer and fed back to the microprocessor. Inside the microprocessor is a model of the plant known as an observer or estimator. The estimator is an on-line model which is made to run in parallel with the real plant, and is supplied with the same drive signal e. The plant/model output error is minimised by a separate estimator feedback of the output error signal $(y-\hat{y})$. The estimator is thus a closed loop system the dynamics of which must be chosen by the control system designer [55]. If the estimated position feedback state $\hat{y}$ is accurately following the plant output, as it should be, then any other required state can be calculated with an accuracy depending on the plant modelling errors of the estimator. Thus it is seen that velocity and

acceleration can be calculated and used as feedback along with the measured position signal. The feedback gains, K_v, K_a, and K_f, must be specially chosen to give the correct closed loop dynamics.

312 Control of the system by classical techniques is based on the use of transfer function representations both of the plant and controller. In the discrete domain the z operator is used, which provides a function similar to that of the Laplace operator s, in the continuous domain. However, whereas the s operator associated with a time dependent variable represents its derivative, the operator z^{-1} represents a one sample period delay in the associated variable [58]. Using z plane transfer function representations of the appropriate controller, closed loop control similar to that obtained using the structure of Fig 3.3 can be achieved. The classical controller structure is shown in Fig 3.4. The measured feedback signal is simply passed through a dynamic filter G, and compared with the demand signal u. The resulting error signal is passed through the forward path filter F, and output to the electrohydraulic plant. The coefficients of the F and G filters must be selected to give the correct closed loop dynamic performance.

313 In a comparison of the two approaches, the neat mathematical structure of modern control theory makes it a natural choice for computer implementation, since it is both versatile and provides a unified representation of equations. In control work the one clear advantage of modern methods is in handling multivariable systems, for which classical methods are not appropriate. However for single input/output systems, such as are considered in this thesis, the modern method which requires an on-line model of the plant and the calculation of feedback states, appears to be more lengthy to implement compared to transform methods. In the classical approach the plant model is represented by a number of transfer function coefficients from which the controller coefficients are calculated prior to operation. The controller implementation is then simply the update of a recursive equation. For these reasons the classical approach has been adopted for all of the research presented in this thesis.

3.4 Control Loop Nomenclature and Implementation.

314 Both the analysis and synthesis stages of control system design were carried out in every case using discrete transfer functions. For this purpose some unification in

block diagram representation is useful. The term 'electrohydraulic plant', previously used rather loosely, is here defined to mean the electrohydraulic components of the control system, including the feedback transducer and A/D sampler on the plant output side, and the D/A converter (ie the sample and hold circuit), on the input side of the plant. Thus the plant is considered to be a digital system in its own right, having digital input e, and digital output y. This is shown with the rest of the control system nomenclature in Fig 3.5, and should be compared with Fig 3.4. As discussed in the previous section F, and G, are the discrete filter transfer functions, the coefficients of which determine the closed loop performance of the system. For reasons discussed in chapter 4, the general transfer functions of these filters are:

$$F(z) = f_1 + f_2 z^{-1} + f_3 z^{-2} \quad \ldots\ldots \tag{3.1}$$

$$G(z) = g_1 + g_2 z^{-1} + g_3 z^{-2} \quad \ldots\ldots \tag{3.2}$$

Where: z^{-1} is the backward shift operator. f_1, f_2, f_3 ..... , are the polynomial coefficients of the F transfer function. g_1, g_2, g_3 ..... , are the polynomial coefficients of the G transfer function.

315 In order that the F and G polynomial coefficients can be calculated, a linear discrete transfer function of the electrohydraulic system is required. In practice this could be achieved by fitting a linear model to the plant frequency response plot. The resulting equation is described generally using the following notation:

$$\frac{y}{e}(z) = \frac{A_N(z)}{A_D(z)} \tag{3.3}$$

Where: A_N and A_D, like F and G, are polynomials in the backward shift operator z^{-1}. Using this notation, from Fig 3.5, the closed loop transfer function is :

$$\frac{y}{u}(z) = \frac{A_N(z)}{F(z)A_D(z) + G(z)A_N(z)} \tag{3.4}$$

316 It can be seen that the choice of the F and G polynomial coefficients influences the characteristic equation, and hence the closed loop performance of the system. The calculation of these coefficients to meet a certain requirement is discussed in

Chapter 4. Here the F and G coefficient values are assumed known, and the discussion centres on the microprocessor implementation of the controller. The controller equation is, from Fig 3.5:

$$e(k)F(z) = u(k) - y(k)G(z) \tag{3.5}$$

For microprocessor implementation it must be expressed as a recursive equation:

$$e(k)(f_1 + f_2 z^{-1} + f_3 z^{-2} \ldots\ldots) = u(k) - y(k)(g_1 + g_2 z^{-1} + g_3 z^{-2} \ldots\ldots) \tag{3.6}$$

If k, is the current time instant, then $k-1$, is the previous sample time instant, and using the backward shift property of z^{-1}, equation 3.6 becomes:

$$f_1 e(k) + f_2 e(k-1) + f_3 e(k-2) \ldots\ldots = u(k) - g_1 y(k) - g_2 y(k-1) - g_3 y(k-2) \ldots\ldots$$

Which rearranged becomes:

$$e(k) = \frac{u(k) - g_1 y(k) - g_2 y(k-1) - g_3 y(k-2) \ldots\ldots}{f_1} - \frac{f_2 e(k-1) + f_3 e(k-2) \ldots\ldots}{f_1} \tag{3.7}$$

317 Equation 3.7 is the recursive filter representation of the controller. The programming of this simple equation is all that is necessary for its implementation. The equation states that the current output $e(k)$, is a function of both the current demand and feedback signals, $u(k)$ and $y(k)$, and previous drive and feedback signals. In practice it is impossible to implement this perfectly because some time is required to read $u(k)$ and $y(k)$ and do the calculation of equation 3.7, then $e(k)$ can be output delayed by a time $\Delta\tau$. However rather than introduce a whole step delay in the RHS of equation 3.7, which would give plenty of time for processing but reduce the stability margins, the algorithm is structured to minimise the time $\Delta\tau$.

318 As shown in Fig 3.6, $e(k)$ in equation 3.7 is calculated in two stages every sample period. The previous information part of equation 3.7 is:

$$\hat{e}(k) = -\frac{g_2 y(k-1)+g_3 y(k-2) \ \ldots\ldots + f_2 e(k-1)+f_3 e(k-2) \ \ldots\ldots}{f_1} \tag{3.8}$$

and is calculated during the course of the sample period whilst awaiting the next clock interrupt. At the start of the next sample period, the present signal values $u(k)$ and $y(k)$ are read and $e(k)$ is quickly calculated using:

$$e(k) = \frac{u(k)-g_1 y(k)}{f_1} + \hat{e}(k) \tag{3.9}$$

Thus $\Delta\tau$ is kept small. In practice it was found that this error could be disregarded provided long sample periods were used compared with the delay period.

319 There are a number of additional tasks in association with the controller implementation which must be carried out. For example in Fig 3.6, after the control output $e(k)$, has occurred, the previous values in the recursive filter must be updated. Also prior to executing $e(k)$, it is essential to ensure that the control signal is not outside of the saturation limits of the valve drive or the range of the D/A converter. Another useful feature for development purposes and included in all of the algorithms developed is the keyboard interrupt which allows the operator to suspend control and select any other programmed task. Apart from these standard features, all of the remaining processing time in the sample period can be used for any other desired purpose. This period has been termed throughout the thesis as the 'auxiliary processing time'.

3.5 Servosystem Simulation Network

320 Prior to the execution of a control algorithm on a real electrohydraulic system, it is essential that it be fully verified and tested. All of the algorithms developed during the course of the research were first tested using analogue filter networks to simulate the electrohydraulic plant. This method of testing was chosen for three reasons: first, the good linearity of the electrical simulation networks allows the linear controller designs to be tested using ideal plant. Thus the effects of the linear controller design can be observed with the minimum of interference from nonlinearities which are in abundance in a real electrohydraulic plant. Secondly, the simulation transfer function parameters can be changed simply by altering the values of variable resistances in the circuit; and thirdly, the use of an analogue

plant simulation means that the developed algorithm can be transferred, unadjusted, to the real situation.

321 The electrical simulation network design is shown in Fig 3.7. It consists of an integrating filter, a first order filter, and a second order oscillatory filter. Each is provided with variable resistors giving a wide range of dynamic control over all of the parameters, and a patch area enabling a variety of transfer functions to be built up. For example, a transfer function representative of many electrohydraulic plants can be built up using the integrating and second order networks, giving the equation:

$$\frac{y}{e}(s) = \frac{K\omega_n^2}{s(s^2+2\zeta\omega_n s+\omega_n^2)} \qquad (3.10)$$

322 Physically, the second order oscillatory transfer function in equation 3.10 often arises because of the mass spring effect of the load inertia and oil compressibility. For example, such an effect is dominant in electrohydraulic cylinder drives where a long stroke cylinder is used to position a large inertia load. Often the components of the cylinder drive and load system provide very low damping, and are thus very oscillatory [59]. The derivation of equation 3.10 for an electrohydraulic cylinder drive forms part of Appendix 1, and the equation is used extensively in later chapters. In the present discussion, the equation is taken as an example whereby some of the effects of sampling and continuous to discrete model transformation methods can be observed.

3.6 Continuous to Discrete Plant Model Transformations

323 In paragraphs 308 and 309 it was pointed out that the complete digital control system would be considered using discrete transfer functions, both for analysis and synthesis. The coefficients of the discrete control law transfer functions, equations 3.1 and 3.2, must be derived from the discrete plant model, equation 3.3, to give the required closed loop transfer function, equation 3.4. However so far in the discussion, the only plant model described is the s plane model of equation 3.10, thus methods of converting this model to the discrete domain must be considered.

324 There are a number of methods available for converting from the s plane to the z plane [55,60], the conversion being obtained with varying degrees of accuracy depending on the plant being modelled and the sample period. In the case of a digital electrohydraulic servosystem, the plant input, ie drive signal, is via a Sample and Hold circuit, where the current output signal is maintained constant until the next sample instant commences. This process is modelled exactly by the the Hold Equivalence conversion method [55]. The resulting discrete transfer function is an exact representation of the plant provided the continuous transfer function is also exact. Using this method, the continuous transfer function, equation 3.10, becomes:

$$\frac{y}{e}(z)_{HE} = \frac{a_1 z^{-1} + a_2 z^{-2} + a_3 z^{-3}}{(1 - z^{-1})(1 - a_4 z^{-1} - a_5 z^{-2})} \qquad (3.11)$$

The above equation is a special case of the general third order transfer function, where the root at $z = -1$, corresponding to integral action, is declared as a factor of the denominator polynomial. Comparing the general equation with the integral action equation, the latter yields one less 'a' coefficient, which helps to reduce the complexity of the control law design and implementation. The five 'a' coefficients are related to the three s plane coefficients of equation 3.10 by exponential and trigonometric functions, the values of which can be found from a set of z transform tables [58].

325 Whilst providing an accurate discrete transfer function, the method gives a large number of numerator coefficients compared to the s plane model. Analysis has shown [61], that the transformation of infinite s plane zeros (ie numerator root positions), generally yields very fast and potentially unstable finite z plane zeros, ie outside of the unit circle. The presence of these zeros is no problem, provided that in the controller design they do not appear as a root of the closed loop characteristic equation [58]. The relatively small contribution of the zeros dynamically, except at very high frequencies, means significant approximation of them can be made whilst maintaining a good model accuracy. This is the basis of some of the other methods of conversion.

326 The simplest model numerator polynomial is given by the Backward Difference Integration method which reduces the polynomial to a single coefficient and infinite roots [55]. This is similar to the continuous model of equation 3.10. All of the transformed coefficients can be calculated simply by making the substitution:

$$s = \frac{z-1}{\tau} \tag{3.12}$$

in the s plane plant model. Although attractive from this point of view, the Backward Difference method when applied to equation 3.10, was found to give poor matching of the frequency response characteristic due to modelling errors, and to be unsuitable for use in controller design.

327 A simple transform method which proved to be good enough for use in controller design was found to be the Pole/Zero Mapping method [55]. Here the poles and zeros of the s plane model are simply replaced by z plane poles and zeros using the transform equation:

$$z = e^{\tau s} \tag{3.13}$$

Thus for example the factor $(s+b)$, becomes, $(z-e^{-\tau b})$. The full set of rules for the Pole/Zero Mapping method is presented in Appendix 2. Application of these rules to equation 3.10 gives the discrete transfer function:

$$\frac{y}{e}(z)_{PZ} = \frac{a_1(1+z^{-1})^2 z^{-1}}{(1-z^{-1})(1-a_2 z^{-1}-a_3 z^{-2})} \tag{3.14}$$

Here, only three 'a' coefficients are used, and the zeros are fixed. The small number of coefficients given by this method reduces the amount of calculation required in controller design and implementation, and later will be shown to greatly increase the implementation speed of an on-line identification algorithm. The Pole/Zero Mapping method was used throughout the research presented in this thesis. A comparison of the Pole/Zero Mapping and Hold Equivalence transformation methods forms the next section.

3.7 Comparison of Transformation Methods

328 The transfer functions produced by the exact Hold Equivalence method and the approximate Pole/Zero Mapping method, have been compared at different sample periods in the frequency domain. The simulation network was set up to model equation 3.10, with the chosen model parameters:

$K = 5.4$ /s $\quad \zeta = 0.172 \quad \omega_n = 4.1$ Hz

The plant transfer function was first derived from frequency response tests whilst running at a very high sample period producing a nominally continuous plant, and the resulting s plane transfer function is shown by the heavily lined curves in both Fig 3.8 and 3.9. The continuous plant transfer function was transformed to the z plane for a number of different sample period lengths as shown below:

Sample Period (ms)	Sample Frequency (Hz)
25	40
40	25
55	18.1
70	14.3

329 The frequency plot of Fig 3.8 shows the response using the exact Hold Equivalence transformation of the s plane model, and demonstrates the effect of sampling on the plant transfer function. It can be seen that for longer sample periods, the amplitude ratio at higher frequencies are attenuated. This is a good feature of sampling as undesirable higher frequency dynamics such as noise are naturally suppressed [62]. However the phase plots show a significant increase in phase lag for longer sample periods, especially at higher frequencies. It can be shown from the sample and hold equation:

$$\frac{y}{e}(s)_{SH} = \frac{1-e^{-\tau s}}{s} \tag{3.15}$$

that the phase lag is about half of a sample period, and this can be verified from Fig 3.8.

330 The same continuous plant frequency plot, but using the approximate Pole/Zero Mapping method to obtain the discrete transformation plots are shown in Fig 3.9. At each sample period, the plot should ideally be the same as for Fig 3.8, any errors observed being a result of the simplified model zero arrangement of equation 3.14 compared with 3.11. Comparison of the frequency plots Fig 3.8 and 3.9 shows good agreement between the phase curves, but that the amplitude ratio is increasingly in

error at the higher frequencies, especially if slow sampling is used. For example, sampling every 70 ms, it can be seen that at the resonant peak the error is about -2.5 dB. The over attenuation of the amplitude ratio at higher frequencies is a direct consequence of the two zeros at $z = -1$, of equation 3.14. Analysis of the numerator transfer function, shows that the amplitude ratio tends to minus infinity at the aliasing frequency, ie when $z = -1$. This forces the frequency plot to descend very rapidly at frequencies approaching the aliasing frequency. The effect is thus naturally accentuated by increasing the sample period length since this brings the aliasing frequency further into the lower frequency range. During the research it was found that the Pole/Zero Mapping method could be used with success for sample frequencies as low as five times the plant resonant frequency, in this case corresponding to a sample period of about 50 ms.

3.8 Sample Period Selection

331 The limitation on the sample period length introduced in the previous section is just one of many constraints limiting the choice of sample period. The absolute lower limit on sample frequency is determined by the onset of aliasing. The sampling frequency must be chosen sufficiently high so that noise and system dynamics, if aliased in the lower frequencies, will not be detrimental to the control system. Most electrohydraulic systems are fortunately low pass in nature, and aliasing problems do not occur. In cases where antialiasing filters are required, their dynamics ought to be considered as part of the plant transfer function at the controller synthesis stage, otherwise detrimental modelling errors may occur. In all except one case, antialiasing filters were not used during the course of the research.

332 In practice the chosen sample period is considerably shorter than the aliasing sample period. This is necessary to meet the tracking and disturbance rejection requirements of the closed loop system and to ensure the stability of the controller design [58,63].

333 During the research it was found that as a rule of thumb, adequate control could be achieved by sampling at around 5 to 10 times the required closed loop bandwidth. Sampling at frequencies lower than this gave rough looking and inconsistent step responses. In oscillatory systems as described by equation 3.10, it was found that good closed loop control could be achieved whilst sampling at a

frequency as low as 5 times the damped natural frequency.

334 The implications of the sample period length in the application of microprocessor closed loop control are far reaching. In order that the extra cost incurred by introducing a microprocessor controller be offset, it must provide some advantage over an analogue controller, and the potential of doing this depends on having sufficient processing time each sample period. The processing time can be split into two parts as indicated in Fig 3.6, these are first and most essentially, the controller implementation time, and second the auxiliary processing time, which can be used to enhance the basic controller. The wider the desired closed loop bandwidth of the system, the shorter the sample period becomes. Consequently in faster systems, a shorter time is available for auxiliary processing, and the microprocessor becomes less cost effective.

335 The processing power of the Darkstar microcomputer system used during the research is typical of many of the recent generation of 16-bit machines now available, and thus can be used to give a rough guide as to what can be achieved at present. The approximate minimum sample period for a variety of algorithms used during the research is shown in Fig 3.10. A sample period of 8 times the closed loop system bandwidth has been assumed, with algorithms written in BCPL. It can be seen that the very simplest of controllers, ie a simple summing junction, takes about 0.5 ms to implement, thus the maximum system bandwidth that can be controlled, is about 250 Hz. For higher order linear controllers the maximum system bandwidth falls rapidly. For example a third order plant controller, ie equation 3.9, is restricted to 80 Hz maximum bandwidth. The need for additional processing time reduces the bandwidth even further. For example, a very basic steady state model for the new proportional valve concept, required just over 4 ms of auxiliary processing time for its implementation. This gave a bandwidth of about 25 Hz which fortunately is acceptable compared to conventional proportional valves. The third order adaptive controller presented in Chapter 7, required nearly 14 ms of auxiliary processing time, corresponding to a closed loop bandwidth of only 8 Hz. Thus it is seen that the most effective applications of microprocessor closed loop control are at present limited to low bandwidth systems. However this situation should improve as faster low cost processor systems are developed and become available.

Fig 3·1

3·1 THE DARKSTAR MICROCOMPUTER SYSTEM

Fig 3·2

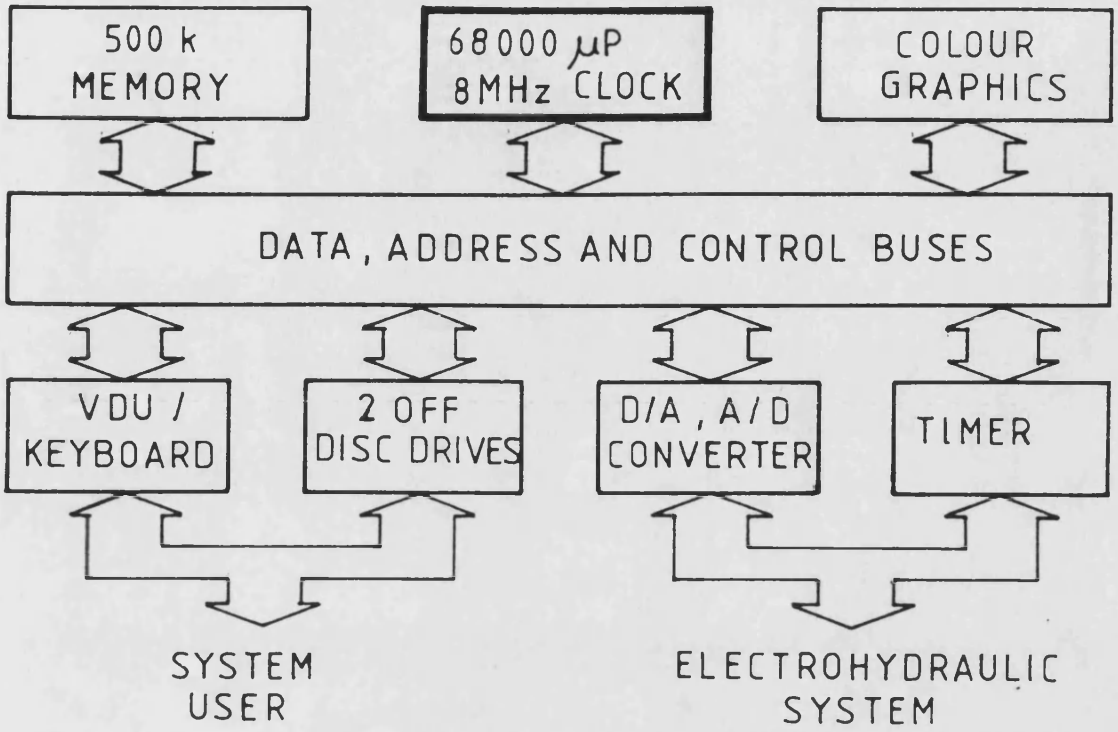

3·2 DARKSTAR SYSTEM LAYOUT

Fig 3·3

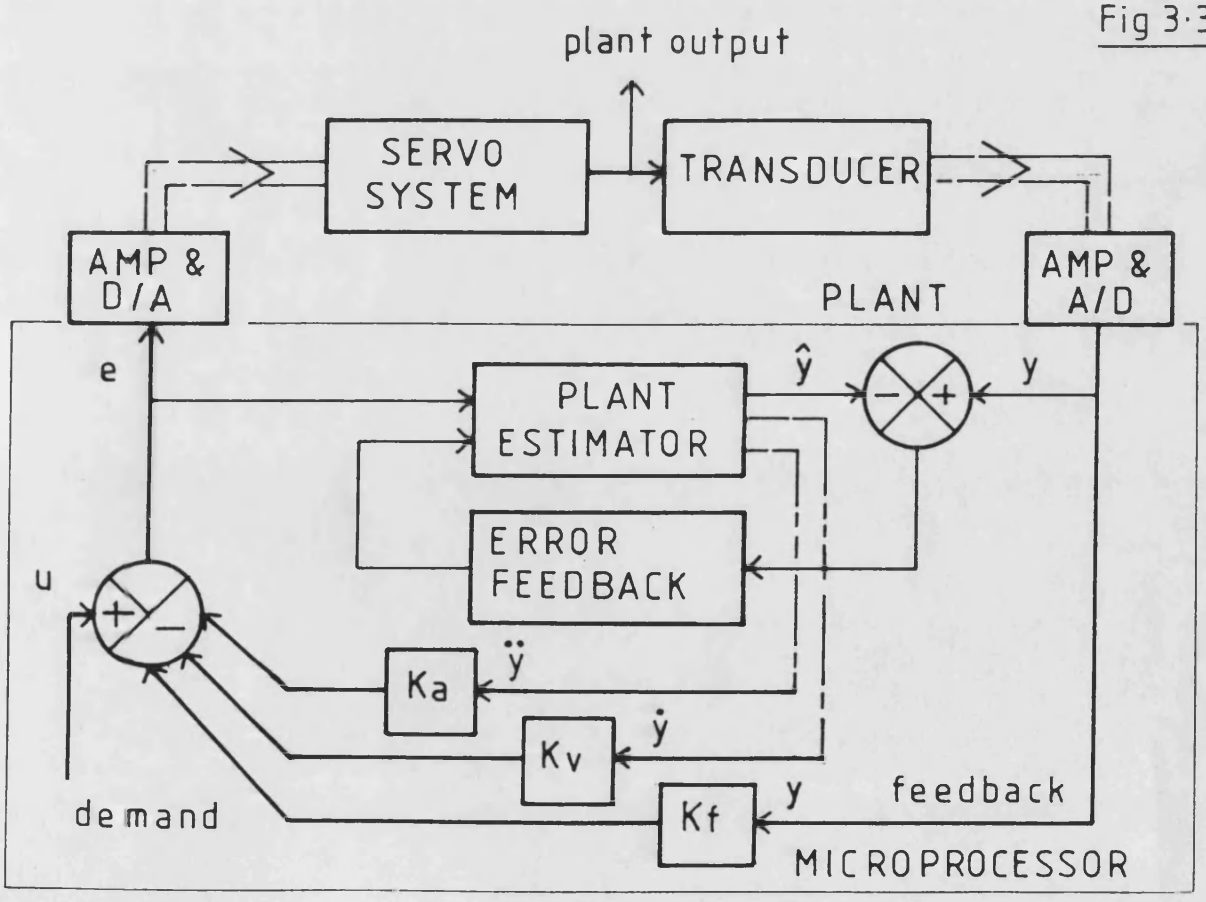

3·3 STATE FEEDBACK CONTROLLER

Fig 3·4

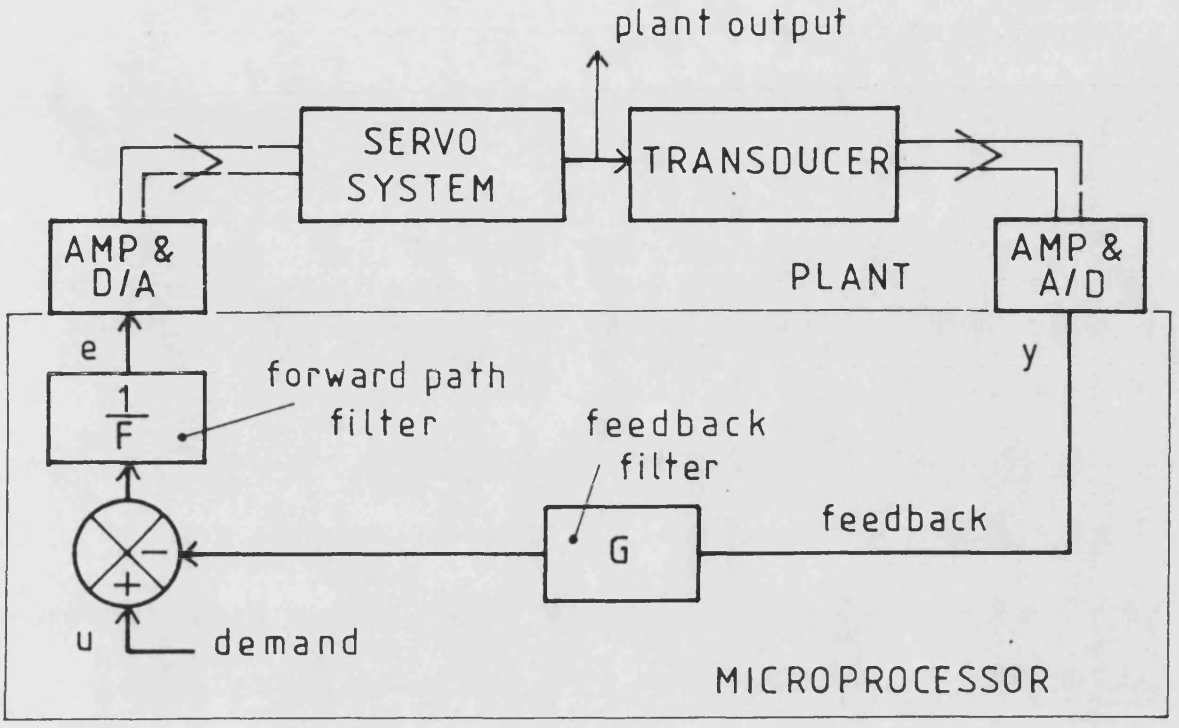

3·4 CLASSICAL CONTROLLER

Fig 3·5

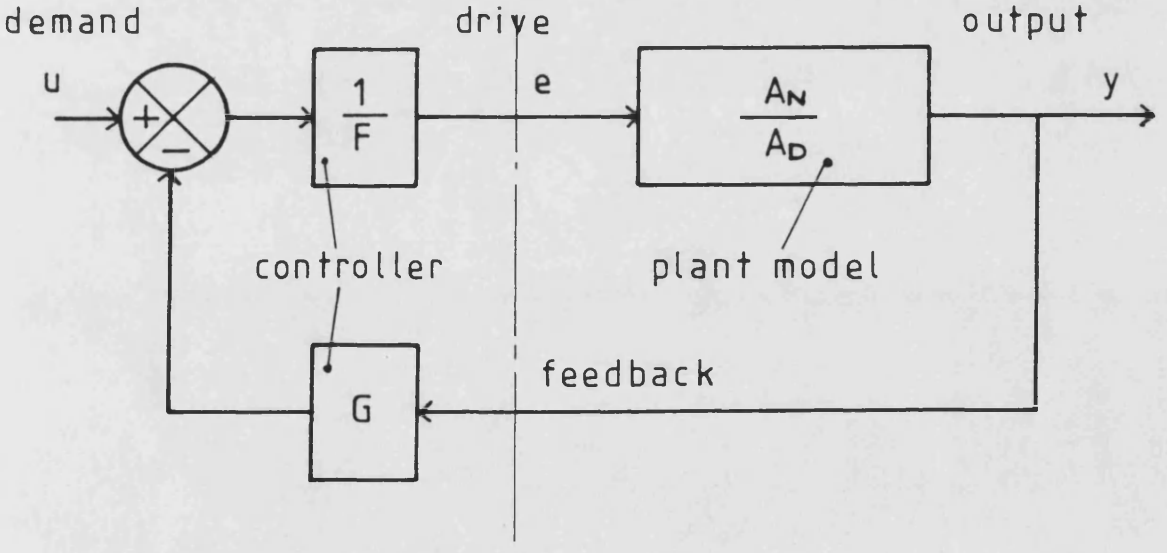

3·5 DISCRETE BLOCK DIAGRAM

Fig 3·6

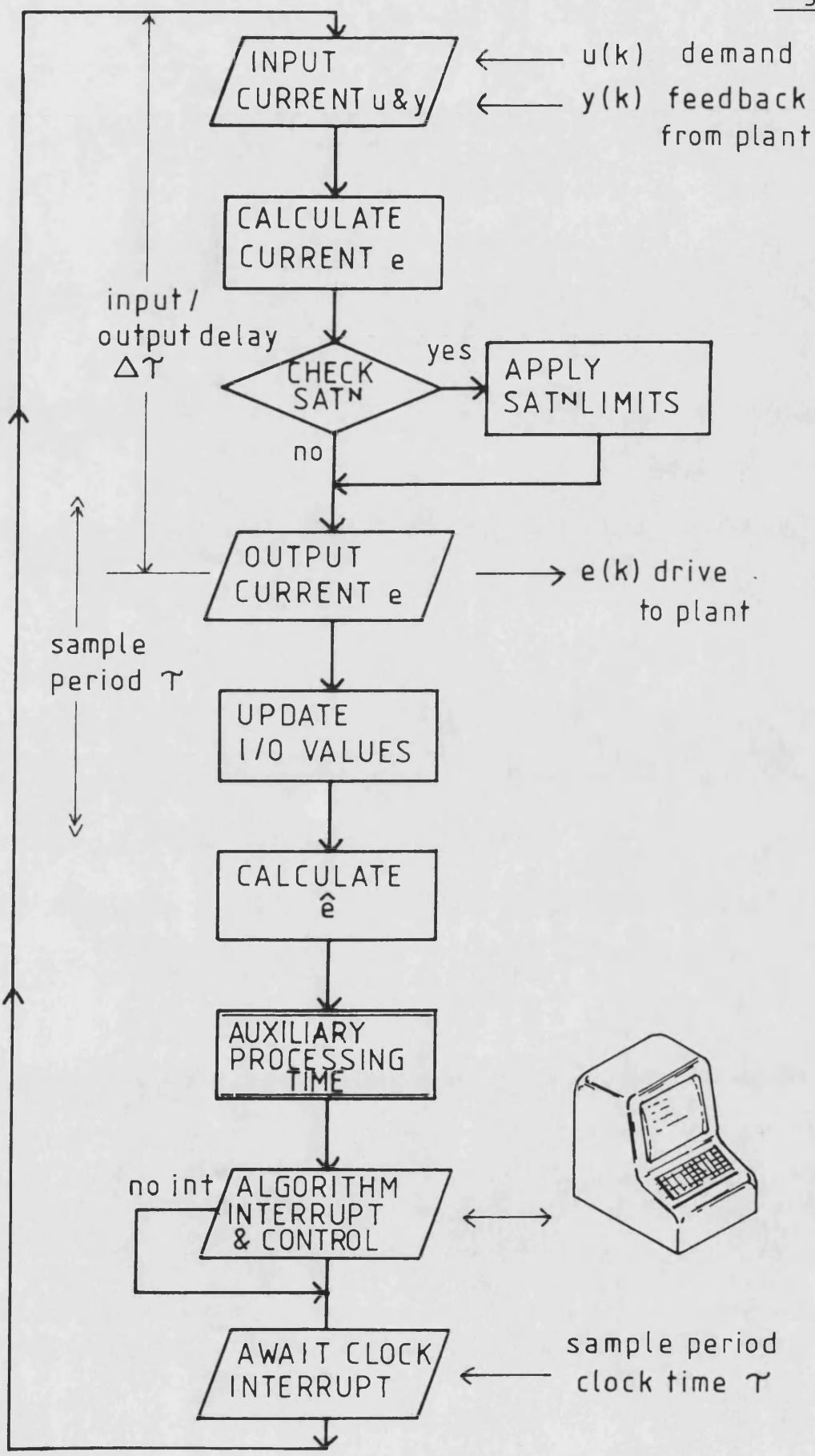

3·6 BASIC CONTROLLER FLOW CHART

Fig 3·7

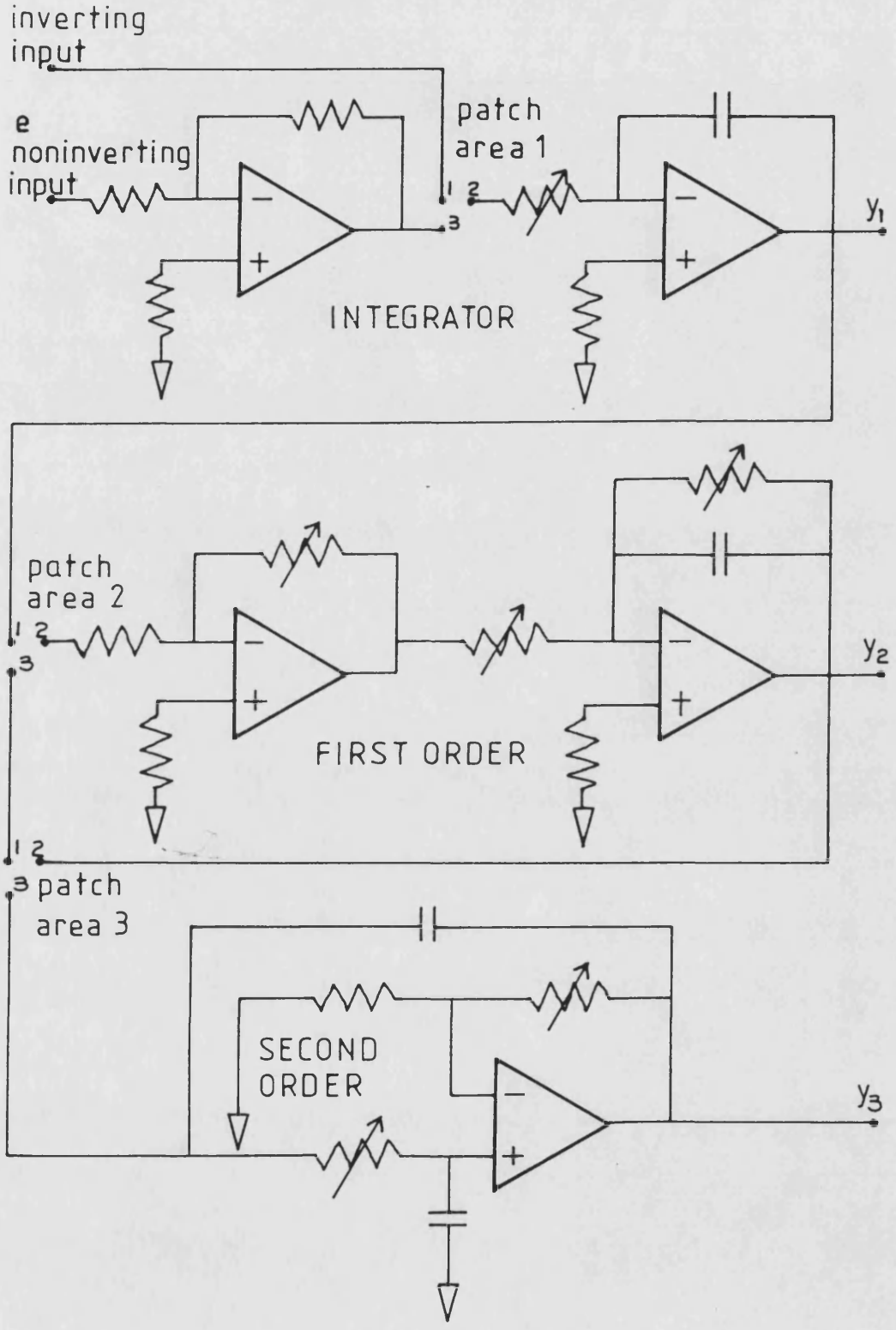

3·7 ELECTRICAL SIMULATION NETWORK

Fig 3·8

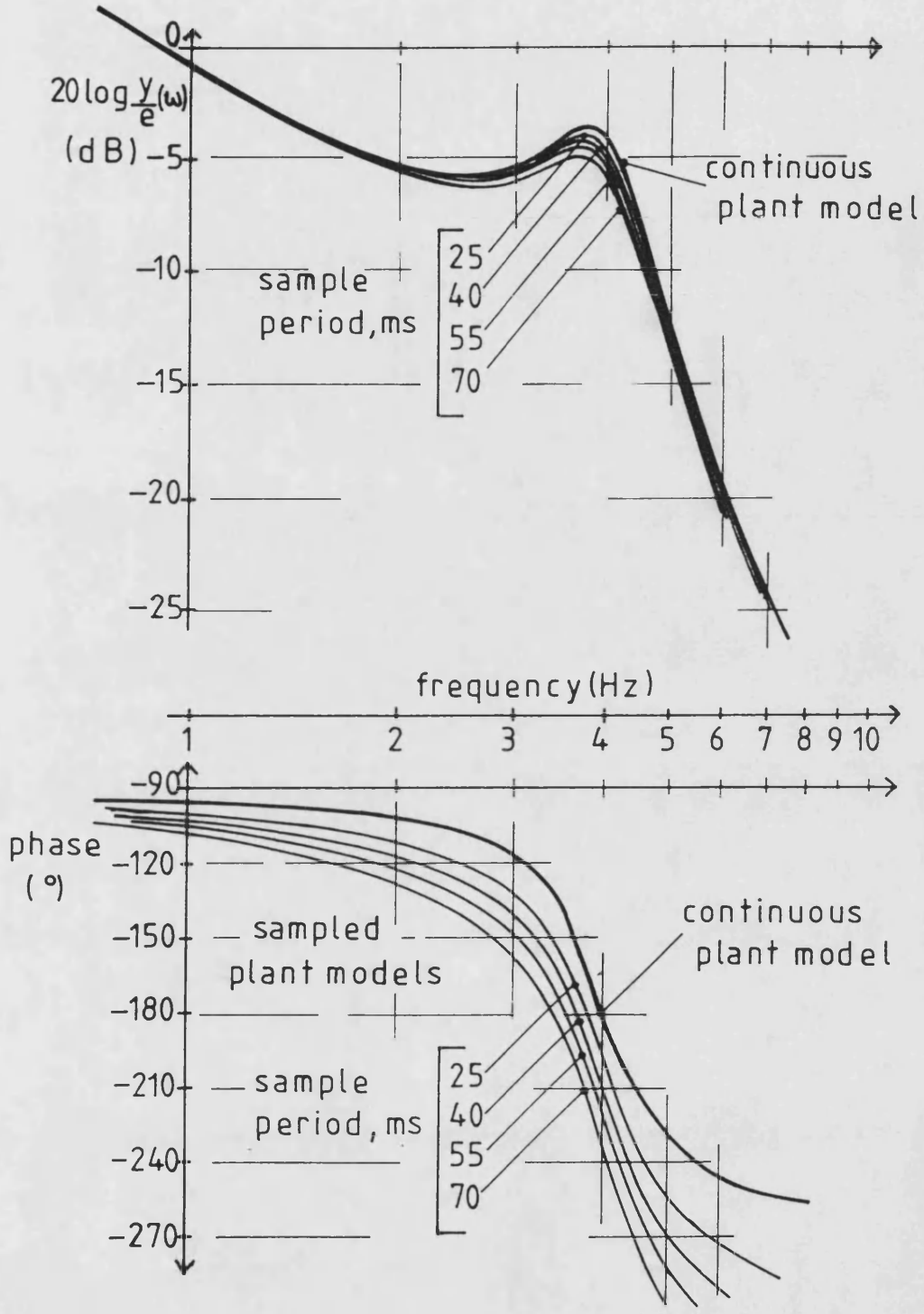

3·8 FREQUENCY RESPONSE OF SAMPLED PLANT ~ EFFECT OF SAMPLING

Fig 3·9

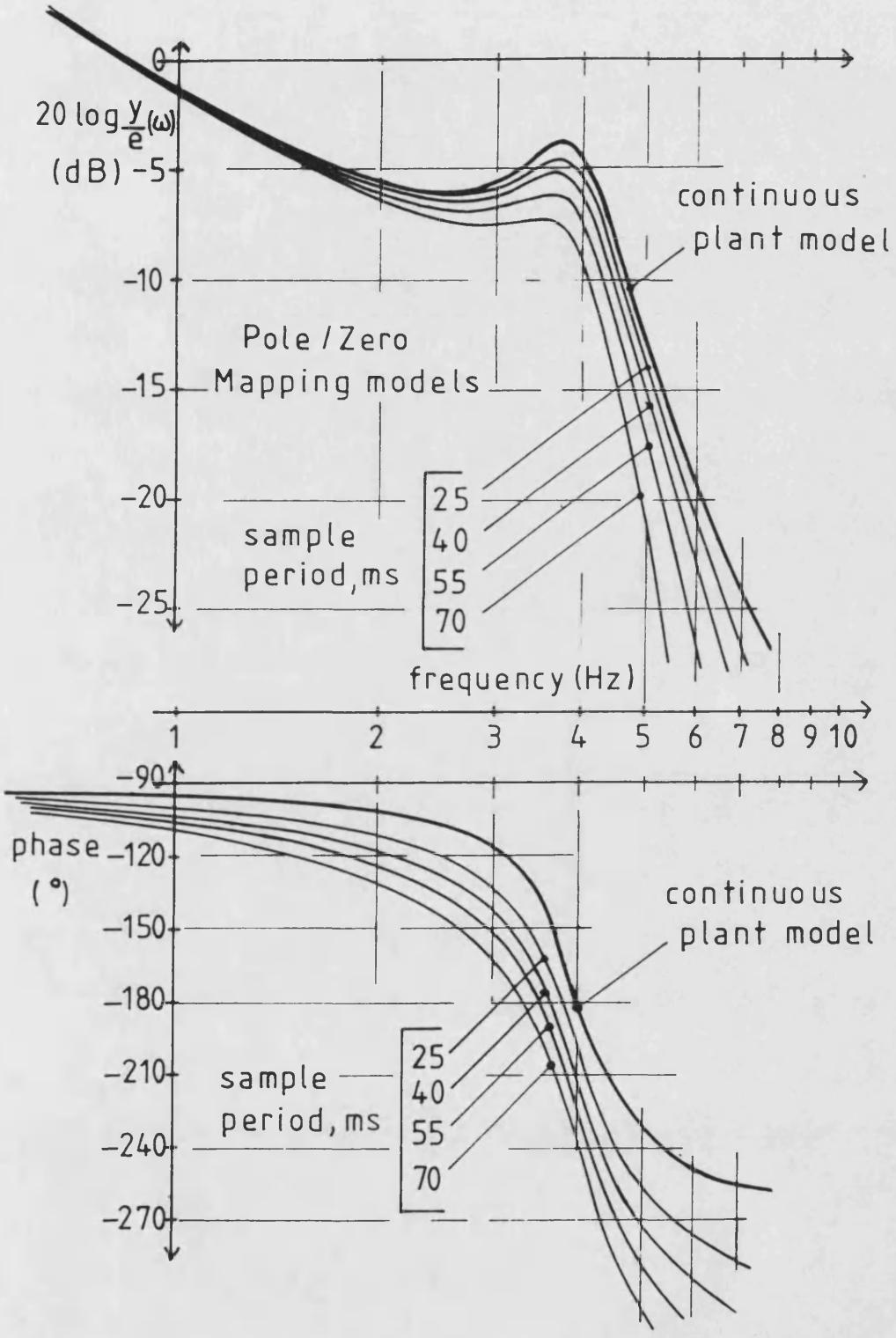

3·9 FREQUENCY RESPONSE OF POLE/ZERO MAPPING MODELS ~ EFFECT OF SAMPLING

Fig 3·10

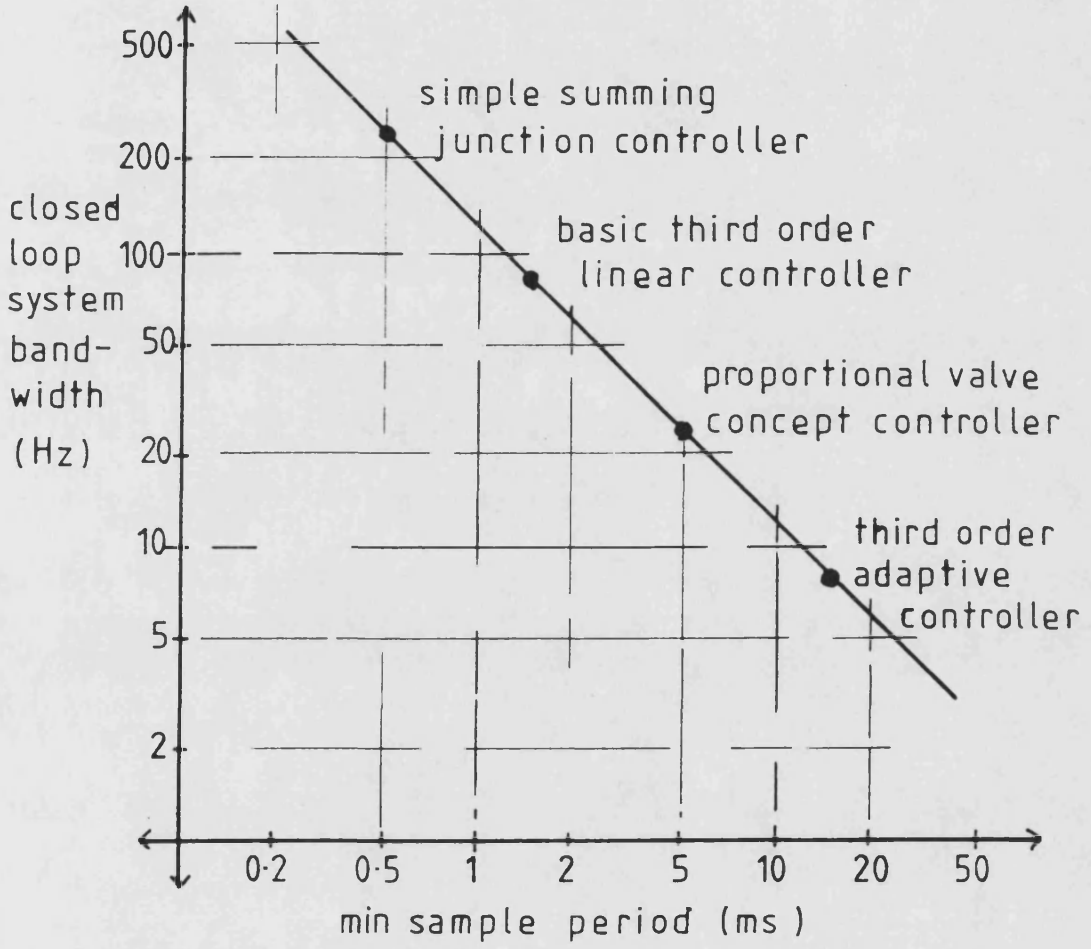

3·10 DARKSTAR ALGORITHM CLOSED LOOP BANDWIDTH

4. POLE PLACEMENT CONTROLLER DESIGN

4.1 Introduction

401 Controller design can be divided into two stages: the analysis stage, where useful information about the plant to be controlled is obtained, and the synthesis stage, where the control law is designed from this information to meet a certain specified closed loop performance. The analysis stage was discussed in section 3.6, the end result being a discrete linear transfer function model of the plant. In this chapter, the subject is the synthesis stage, and both the method of calculating the control law, and specifying the desired performance are discussed.

402 In section 4.2 Pole Placement is chosen in preference to optimal control methods of controller synthesis, and the design constraints dictating the general form of the controller are outlined. The method of choosing the desired closed loop performance using the z plane root locus diagram is the subject of section 4.3, and the appropriate controller design equations for control of a third order system are derived in section 4.4. The technique is tested by application to the electrical simulation network and the effects of changing the desired performance are investigated. Finally in section 4.6 the Pole Placement method is extended to include integral action control.

4.2 Controller Synthesis Methods and Constraints

403 There are two commonly used methods of controller synthesis, these are: the Pole Placement [58], and Optimal design methods [55]. Both methods have the same end result, but whilst the latter can be expressed in terms of pole positions the approach is very different.

404 Using optimal control criteria, an auxiliary cost function is introduced which consists of weighted values of system output, the control signal, and the demand signal. The objective is to calculate the control law which minimises the chosen cost function. Control over the closed loop system response is achieved by adjustment of the cost function weightings. However the relationship between the cost function weightings and the resulting closed loop response is not straight forward and their choice is often made by trial and error [64]. The Optimal synthesis

method is particularly well suited to multivariable problems using modern control methods.

405 In single input/output servo problems, such as are studied in this thesis, an alternative and often more appropriate method is the Pole Placement synthesis technique. Here, advantage is taken of the fact that the pole positions of the closed loop transfer function, ie the roots of the closed loop characteristic equation, determine the nature of the system dynamics and gives the designer an immediate knowledge as to the likely response of the system. The Pole Placement synthesis method, as the name implies, seeks simply to shift the poles to more desirable positions specified by the designer, and this is achieved by the implementation of appropriate controller F and G polynomials. The structure of the controller was presented without explanation in section 3.4, and is the result of a number of imposed constraints which will now be discussed.

406 The constraints on the control law arise from the nature of the servosystem plant model and the requirements of the desired closed loop transfer function. With reference to Fig 3.5, the closed loop transfer function expressed in terms of the controller and plant model polynomials is equated to some desired transfer function:

$$\frac{y}{u}(z) = \frac{A_N(z)}{F(z)A_D(z)+G(z)A_N(z)} = \frac{A_N(z)}{f_1 T(z)} \qquad (4.1)$$

Where T, is the desired characteristic equation polynomial.

407 It can be seen that only the poles of the transfer function are changed, the zeros remaining intact. If it is necessary to change the zeros of the system, then a more general control law is required, having a numerator controller polynomial filtering the demand signal [58]. This filter would enable new zeros to be introduced. However as can be seen from equation 4.1, the old zeros of the polynomial A_N can only be removed by cancellation, ie by including these roots as factors in the desired characteristic equation, T. This procedure is acceptable only for stable zeros well inside the unit circle. If this condition cannot be met then cancellation can lead to an unstable closed loop response. In situations such as this, it is best to leave the zeros unaltered as expressed in equation 4.1 [58,61].

408 In the case of electrohydraulic servosystems, often they are modelled in the continuous domain using transfer functions having all the zeros at infinity, for example the third order equation 3.10 has three infinite zeros. When these zeros are transformed into the discrete domain they tend to be finite and of fast dynamics, being located close to or outside of the unit circle [61]. Thus in these situations, it is both unwise and unnecessary to cancel zeros or to introduce new ones, and equation 4.1 can be used generally in electrohydraulic servosystem design. In practice the Pole/Zero Mapping transform method used during the research approximates the transformation of the s plane infinite zero root positions by assuming them to be fixed at $z = -1$ (see section 3.6). The numerator of both the closed loop and the plant model transfer functions can thus be written:

$$A_N(z) = a_1(1+z^{-1})^{n-1}z^{-1} \tag{4.2}$$

Where n is the order of the plant transfer function, and a_1, is the only numerator polynomial coefficient.

409 In servosystem control problems the plant very often has integral action, for example in a cylinder drive the integral of flow rate gives a corresponding displacement of the piston. This is seen in the plant transfer function by a pole at $s = 0$ in the continuous domain, and a pole at $z = 1$ in the discrete domain, giving the general denominator polynomial:

$$A_D(z) = (1-z^{-1})(1-a_2z^{-1}-a_3z^{-2} \ \ldots\ldots \ a_n z^{n-1}) \tag{4.3}$$

410 The desired characteristic equation polynomial in equation 4.1 is written generally as :

$$T(z) = 1+t_1z^{-1}+t_2z^{-2}+t_3z^{-3} \ \ldots\ldots \tag{4.4}$$

The coefficients t_1, t_2, t_3 ..... are specified by the designer to give a desired dynamic performance. In equation 4.1 the T polynomial is multiplied by the controller coefficient f_1, this is so that the coefficient of the zeroth order of z^{-1} in the denominator polynomials of the LHS and RHS of the equation are the same.

411 Equation 4.1 is constrained to give unity steady state gain, a constraint which determines the value of the coefficient f_1. The derivation of f_1 is obtained by putting $z = 1$ into the polynomials of equation 4.1. (see Appendix 3). Now since from equation 4.3, A_D is zero at $z = 1$, equation 4.1 can be rewritten as:

$$\frac{y}{u}(1) = \frac{1}{G(1)} = \frac{A_N(1)}{f_1 T(1)} = 1 \tag{4.5}$$

Also examination of equations 4.2 and 4.4 shows that:

$$A_N(1) = a_1 2^{n-1} \tag{4.6}$$

$$T(1) = 1+t_1+t_2+t_3 \ldots\ldots \tag{4.7}$$

Thus substituting into equation 4.5 we get that:

$$f_1 = \frac{a_1 2^{n-1}}{1+t_1+t_2+t_3 \ldots\ldots} \tag{4.8}$$

Hence the controller coefficient f_1, to achieve unity steady state gain, can be found easily from knowledge of the plant model numerator coefficient, and the desired performance polynomial coefficients. Similarly, it can be shown from equations 3.2 and 4.5 that for unity steady state gain:

$$g_1+g_2+g_3 \ldots\ldots = 1 \tag{4.9}$$

412 Now that A_N, A_D, T and f_1 are known,the rest of the controller coefficients can be calculated by solving equation 4.1, ie:

$$F(z)A_D(z)+G(z)A_N(z) = f_1 T(z) \tag{4.10}$$

The equation 4.10 results in a set of linear simultaneous equations in the coefficients of the F and G polynomials, which can be solved straightforwardly using matrix methods. A solution assuming the third order plant model equation 3.14, is given in section 4.4, but first the problem of how to choose the T polynomial is discussed.

4.3 Root Locus Performance Specification

413 The root positions of the characteristic equation polynomial T', must be chosen by the designer to specify the desired dynamic performance. However, it is not immediately obvious what the effect of the choice of root positions will be in terms of bandwidth, overshoot or rise time. The problem is made more difficult as the physical effect of the root positions are dependent on the sample period. One way of deriving the root positions is to choose them first in the continuous domain, for example, select the desired time constant, damping ratio and natural frequency, and then use one of the s to z transform techniques (see section 3.6), to convert the roots to the discrete domain. However in practice the distorting effect of slow sampling on the s to z transformation was found to give poor agreement between the desired and actual performance.

414 Although not quite so intuitive as working in the continuous domain, a similar approach can be taken using the z plane root locus diagram marked up as shown in Fig 4.1. The curves marked on the diagram give the z plane root positions for various constant s plane parameters. For example, the lines which emerge radially at the unit circle correspond to various natural frequencies ω_n, in the continuous domain, and the lines radiating from $z = 1$ correspond to various levels of damping ratio ζ. It can be seen from Fig 4.1 that moving outwards towards the unit circle corresponds to a decrease in damping, and moving from right to left increases the natural frequency. A similar guide has also been marked for first order lags, where along the real axis it can be seen that moving from the right towards the origin causes a reduction in time constant, and hence an improvement in the system rise time. Since every characteristic equation can be factored into real roots and/or complex pairs, the curves of Fig 4.1 enables the selection of complex high order transfer functions.

415 A guide to the limit of the root positions that can be demanded was given in section 3.8 in terms of the minimum sample frequency to achieve a desired system bandwidth. This can easily be interpreted as z plane root positions. For example, taking a very slow sampling period of say four times the desired bandwidth, then for a first order system, the equation:

$$z = e^{\tau s} \tag{4.11}$$

with: $s = -\frac{1}{T}$ and $\frac{\tau}{T} = \frac{1}{4}$

where τ is the sample period and T is the lag time constant, gives $z = 0.78$. Real roots much less than this should be used with care by the designer, as this corresponds to sampling less than four times the desired bandwidth. Similarly limits on the natural frequency can be set, beyond which the designer should not work. In practice sampling too slowly was found to cause rough looking inconsistent step responses and in the worst cases caused the onset of the rippling phenomena [65]. This can be observed as high frequency intersample oscillations of the drive signal. In electrohydraulic servosystems this phenomena can cause unnecessary wear of the valve components, and undesirable pressure fluctuations in the system.

416 A very useful guide to selecting the roots of the T polynomial is given by first calculating the roots of the uncompensated closed loop system, ie assuming a unity gain summing junction controller. On the basis of the uncompensated characteristic equation root positions, the designer can move the roots to new positions and observe the changes in the plant closed loop step response which occur.

417 The question also arises as to how many roots, ie what order, should be chosen for the T polynomial. Bearing in mind that the exact shape of the closed loop frequency response is not important beyond achieving a good bandwidth, it is not necessary to choose large numbers of root positions. This simply complicates matters. Generally it was found that good results were obtained by choosing a characteristic equation of the same order as that for the uncompensated closed loop system model. Thus for example in the case of the third order transfer function of equation 3.14, three closed loop roots would be chosen, one real root and a complex pair. The root positions being selected by the designer from the root locus diagram.

4.4 Controller Coefficient Derivation

418 The solution of equation 4.10 to obtain the controller coefficients is best illustrated by an example, and the plant model of equation 3.14 is used for this purpose:

$$\frac{y}{e}(z) = \frac{a_1(1+z^{-1})^2 z^{-1}}{(1-z^{-1})(1-a_2 z^{-1}-a_3 z^{-2})} \qquad (4.12)$$

A third order T polynomial is chosen:

$$T(z) = 1+t_1 z^{-1}+t_2 z^{-2}+t_3 z^{-3} \qquad (4.13)$$

and for this particular case equation 4.10 becomes:

$$(f_1+f_2 z^{-1}+f_3 z^{-2})(1-z^{-1})(1-a_2 z^{-1}-a_3 z^{-2})+$$
$$(g_1+g_2 z^{-1}+g_3 z^{-2})a_1(1+z^{-1})^2 z^{-1} =$$
$$f_1(1+t_1 z^{-1}+t_2 z^{-2}+t_3 z^{-3}) \qquad (4.14)$$

419 The choice of the number of F and G polynomial coefficients, ie the controller order, depends on the orders of the chosen plant model and the desired closed loop transfer function. The order of the controller n_c, must be chosen such that the number of controller coefficients generated is just sufficient to enable a unique solution of equation 4.14. Generally the required order is one less than the plant order, ie:

$$n_c = n-1 \qquad (4.15)$$

Where n_c, is the order of the controller and n, is the order of the plant. Thus as shown in equation 4.14, for the third order plant model and desired transfer function, the controller is of order two, yielding six coefficients. From the LHS of equation 4.14 it can be seen that the closed loop transfer function is really of fifth order, since terms in z^{-5} occur. Thus the third order desired transfer function is obtained by calculating a special case of the 'f' and 'g' coefficients such that the coefficients of orders four and five of the closed loop characteristic equation are set to zero.

420 A set of linear simultaneous equations is obtained by equating the coefficients of powers of z^{-1} on each side of equation 4.14, as shown in equation 4.16 below:

$$\begin{bmatrix} -(1+a_2) & 1 & 0 & 1 & 0 & 0 \\ (a_2-a_3) & -(1+a_2) & 1 & 2 & 1 & 0 \\ a_3 & (a_2-a_3) & -(1+a_2) & 1 & 2 & 1 \\ 0 & a_3 & (a_2-a_3) & 0 & 1 & 2 \\ 0 & 0 & a_3 & 0 & 0 & 1 \\ 0 & 0 & 0 & 1 & 1 & 1 \end{bmatrix} \begin{bmatrix} f_1 \\ f_2 \\ f_3 \\ g_1 a_1 \\ g_2 a_1 \\ g_3 a_1 \end{bmatrix} = \begin{bmatrix} f_1 t_1 \\ f_1 t_2 \\ f_3 t_3 \\ 0 \\ 0 \\ a_1 \end{bmatrix} \qquad (4.16)$$

The sixth equation arises from the unity steady state gain constraint of equation 4.9. The controller coefficient f_1, on the RHS of the equation is already known from equation 4.8, and thus the matrix can be immediately reduced to a five by five. Further reduction and the rapid solution of equation 4.16 is made easier by making use of the zero elements which occur in the matrix.

4.5 Controller Design and Implementation

421 The described method of controller design and implementation was demonstrated on the simulation network using the same plant parameters as presented in section 3.7, ie a third order integral action plant having s plane model parameters:

$K = 5.4\ /s \quad \zeta = 0.172 \quad \omega_n = 4.1$ Hz

The results of these tests are here reproduced to show the effect of changing the closed loop characteristic equation root positions. A sample period of 40 ms was chosen, and the Pole/Zero Mapping method gave equation 4.12 with 'a' coefficient values:

$a_1 = 0.0433 \quad a_2 = 0.8840 \quad a_3 = -0.7015$

The plant frequency plot for these values can be seen in Fig 3.9. The measured uncompensated closed loop step response corresponding to these 'a' coefficients is shown in Fig 4.2(a), together with the calculated closed loop root positions. The pair of conjugate roots, if plotted on the root locus diagram of Fig 4.1, correspond to a closed loop damping ratio of about 0.1, which agrees well with the observed very oscillatory step response.

422 The calculated closed loop root positions were used as a guide to aid in

improving the closed loop performance. For example, Fig 4.2(b) shows what happens when the imaginary parts of the complex pair of roots were moved from 0.75 to 0.65, the measured step response shows less oscillation, as would be expected from Fig 4.1. In the next stage the rise time of the system was improved by making the real root smaller. This is shown in Fig 4.2(c) where the effect on the step response of moving the root from 0.78 to 0.65 can be seen. Finally the closed loop oscillations were removed entirely, as shown in Fig 4.2(d), by selecting 0.4 for the imaginary term. Further attempted increase in rise time by moving the roots even further to the left, resulted in inconsistent step responses and the onset of ringing in the controller [65], as described in paragraph 415. This problem is a consequence of having very few samples during the rise and settling periods, and can be overcome by increasing the sample frequency.

4.6 Integral Action Control

423 In some electrohydraulic servosystems, significant external disturbances occur which create undesirable steady state output errors between the demanded and actual positions. This can be eliminated by introducing integral control action upstream of the disturbance in the control loop. A very common method in both analogue and digital controllers is to use PID control. However this type of control, being in the forward path only, is less flexible than the Pole Placement method presented, and limits the positioning of the characteristic equation roots. The Pole Placement method can easily be extended to include integral action. Instead of the controller F polynomial as in equation 3.1, an extra root at $z = 1$ is added,thus:

$$F(z) = (1-z^{-1})(f_1+f_2z^{-1}+f_3z^{-2} \ldots\ldots) \qquad (4.17)$$

The introduction of integral action provides an extra constraint in equation 4.14, requiring that the order of both the F and G polynomials be increased by one. Thus for the third order plant, a third order controller is required corresponding to seven coefficients. Generally, for integral action control, the controller order is the same as the plant order, ie:

$$n_c = n \qquad (4.18)$$

The controller coefficients are calculated by the solution of a matrix equation

similar to equation 4.16. The integral action constraint increases the matrix order by one, making the calculation processing time slightly longer. The effects of integral action Pole Placement control on real electrohydraulic systems is presented in sections 5.4 and 7.7.

Fig 4·1

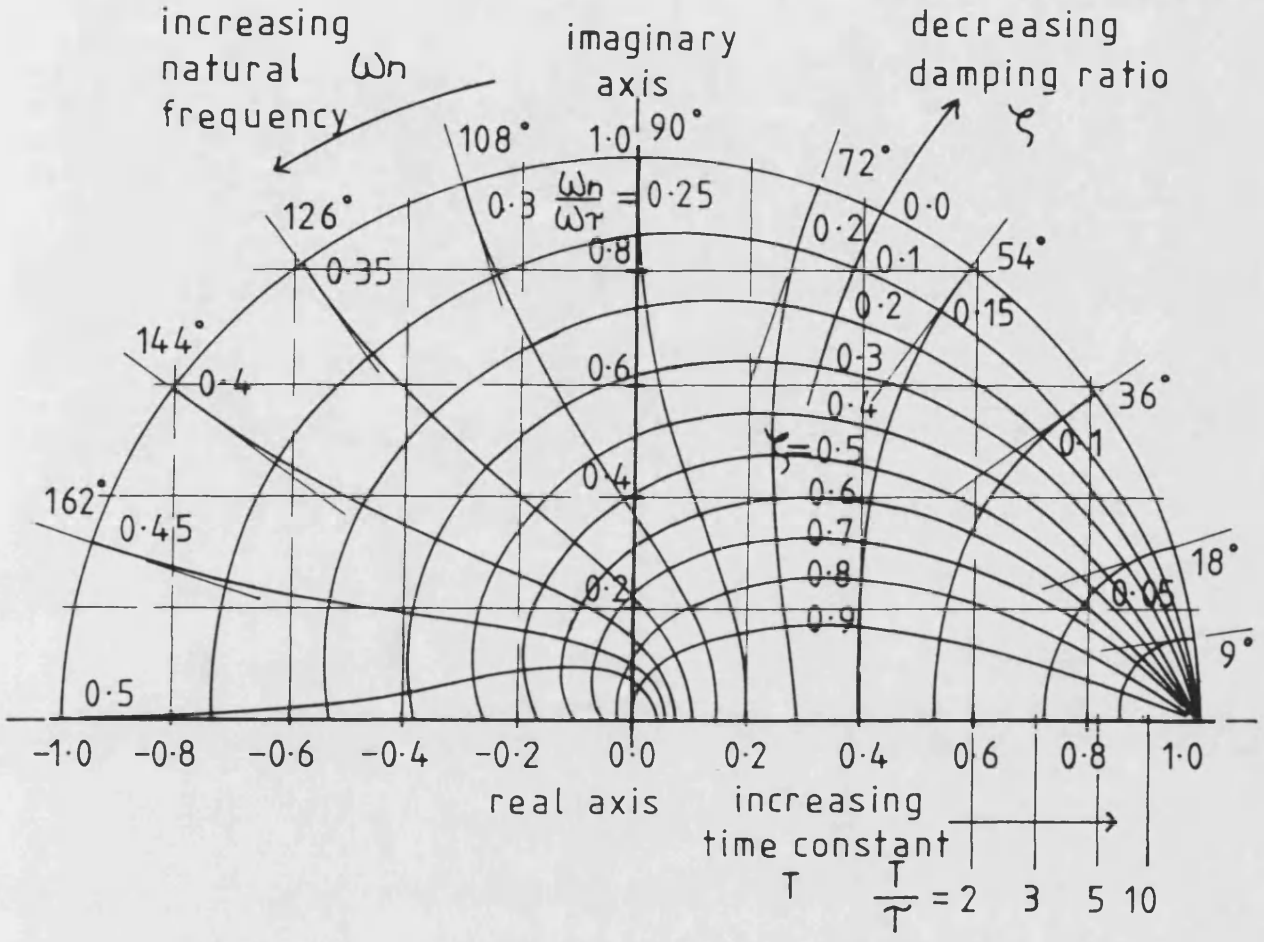

4·1 Z PLANE ROOT LOCUS DIAGRAM

Fig 4·2

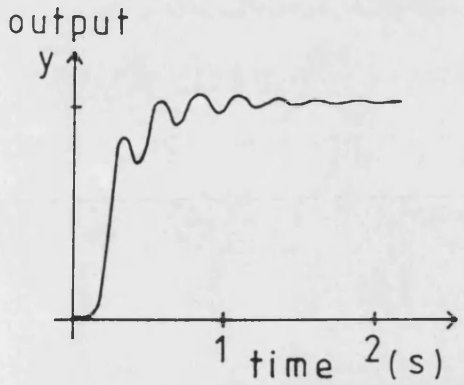

root positions

z = 0·78,
0·53 +/- j 0·75

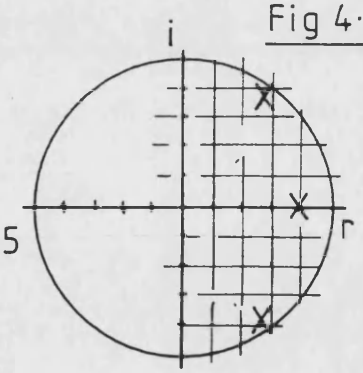

(a) UNCOMPENSATED STEP RESPONSE

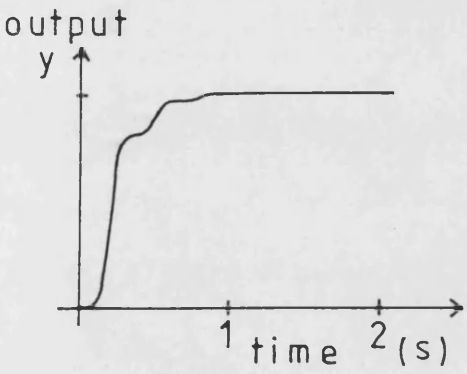

root positions

z = 0·78,
0·53 +/- j 0·65

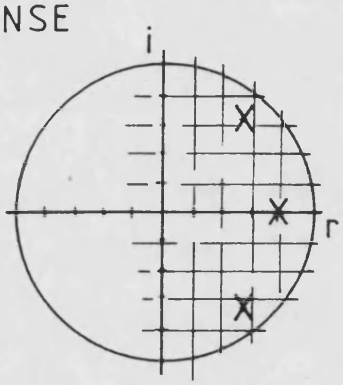

(b) NEW COMPLEX ROOT POSITIONS

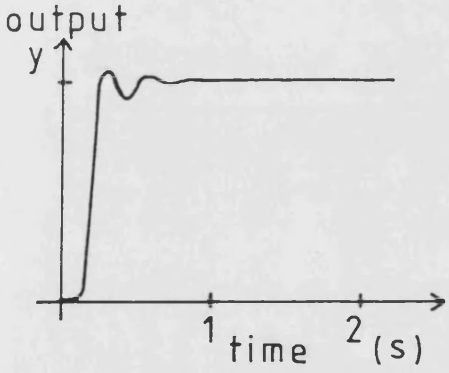

root positions

z = 0·65
0·53 +/- j 0·65

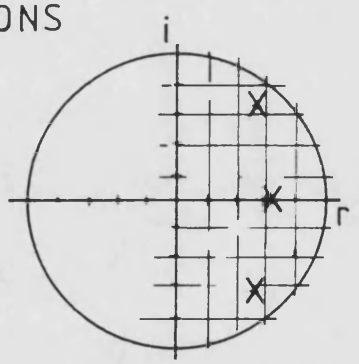

(c) NEW REAL ROOT POSITION

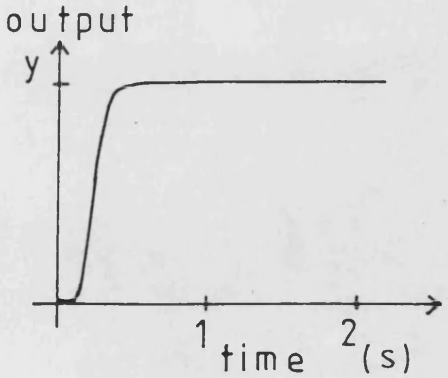

root positions

z = 0·65
0·53 +/- j 0·4

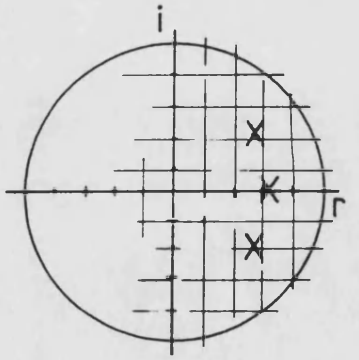

(d) FINAL ROOT POSITIONS

4·2 SIMULATOR STEP RESPONSES SHOWING EFFECT OF CLOSED LOOP POLES

5. MICROPROCESSOR INTEGRATED FLOW CONTROL VALVE.

5.1 Introduction

501 Recent advances in flow control valve design were surveyed in Chapter 2, and this lead to the presentation of a new flow control valve concept in section 2.7 which makes use of closed loop microprocessor control. The basic theory required to calculate and implement controller algorithms was presented in Chapters 3 and 4, and in this chapter its application to the new valve concept is demonstrated.

502 In section 5.2, the detailed design of the valve is discussed, and the test rig layout presented. An investigation into the valve dynamic characteristics in section 5.3 leads to a simple s plane, second order model. The model is compared with measured frequency response characteristics, from which the model parameters used in the controller design are derived. In section 5.4 the s plane model is converted to the discrete domain using the Pole/Zero Mapping method, and a Pole Placement integral action controller designed. The performance of the controller in practice is demonstrated by measured step and frequency response plots.

503 The integral action controller was used to control the valve metering element position whilst its steady state characteristics were investigated. The results of the investigation are compared with theory in section 5.5, from which an on-line model suitable for closed loop control is derived. The success of the model used in the closed loop controller is shown in section 5.6 where various control modes are demonstrated. Finally, the new valve concept is shown to have application in four port valve designs using both poppet and spool constructions.

5.2 Valve Hardware Design and Test Rig Layout

504 A schematic of the control valve design discussed in Chapter 2 is reproduced in Fig 5.1, and its intended function will be briefly summarised here. The valve divides naturally into two parts, the electrohydraulic hardware, and the microprocessor controller. The valve hardware is deliberately designed to be of simple construction using conventional hydraulic components, the advantages of the valve being obtained entirely from the control methods employed, which are based

on an on-line model of the valve. (For this reason, emphasis was placed on designing a valve which could be accurately modelled in software.) The microprocessor controller calculates from the model on-line estimates of the flow rates and pressures which occur in the valve. Any one of these parameters can then be selected for use as feedback, giving control of that parameter without any direct measurement. The use of the microprocessor both reduces the mechanical hardware requirements thereby reducing the cost, and increases the flexibility and potential application of the valve, (see section 2.7).

505 The flow throttling device is a 16 mm diameter outward flowing poppet valve of 2:1 area ratio, chosen because of its contamination insensitivity, positive seating and most importantly, its sensitivity to flow pressure variations, (see paragraphs 232 and 233). By means of the model the poppet can be controlled to set either a demanded upstream pressure P, or flow Q, as alternatives to the more conventional poppet position control. An LVDT position transducer, used for poppet position measurement, is the only direct feedback used. The poppet lift is restricted to a maximum of 2 mm, and movement within this range is controlled by the first stage proportional pressure control valve. Servo pressure P_s, can be controlled from near 0 bar up to 150 bar [66], and is used in closed loop to balance the poppet forces in equilibrium at the desired poppet position, the appropriate valve drive signal being generated by the microprocessor.

506 The valve hardware was designed to demonstrate the principles of the new valve concept whilst minimising the amount of detailed design and manufacture required. Thus where possible, commercially available components were used. A full size sectional engineering assembly drawing of the valve is shown in Fig 5.2, and a corresponding parts list for the most important components of the valve in Fig 5.3. The part numbers relating the two figures are indicated thus, '( )', in the following text. All of the valve components are mounted on, or in, a specially constructed development valve block (1). This also carries additional drillings and tappings to make hydraulic connections to the various components, and to provide transducer mounting points. The pressure control pilot valve (2), is cut away in the sectional drawing but its position is indicated by the dotted lines. The valve is face mounted onto the block (1), and the supply and return lines provided through drillings in the block. This is also true of the servo pressure line connecting the back face of the poppet (4). The servo and damping restrictors (3), and (5), are

drilled plugs which screw directly into the valve block flow passages.

507 The poppet and cartridge (4), and (12), are mounted in a suitably machined bore in the valve block, and axial movement of the cartridge is prevented by the cover cap (7). Screwed into the cover cap is a high pressure LVDT position transducer (6), the core of which is connected to an extension rod (8), which locates deep inside the back face of the poppet. Contact with the poppet is maintained by the preload spring (9). Both the spring preload and the maximum poppet lift are set by spacers (10), and (11), respectively.

508 The poppet, cartridge and spring assembly are proprietary items [67]. The poppet was selected to have a two to one area ratio between the back face diameter and the valve seat diameter, so that a maximum main flow pressure of twice the available servo supply pressure could be controlled. Additionally, the seating face of this type of poppet is a long faced cone, having an included angle of about sixty degrees, this gives a consistent flow path through the poppet over a wide range of poppet lift, thus providing a well behaved easily modelled Bernoulli flow force characteristic [31,68]. The poppet lift was restricted to about 2 mm maximum, a range over which the flow, in theory at least, always adheres to the poppet cone face.

509 Although in a digital system a digital position transducer would have been preferable for interfacing purposes, this was not available at the time of research and an LVDT was used instead (6) [69]. The device was driven from an external 5 kHz oscillator, and the measurement signal was demodulated internally giving a DC output. This signal was then further amplified to give 0 to 10 V range over the 2 mm poppet lift.

510 The correct sizing of the servo restrictor (3), was essential to obtain the full range of servo pressure since the pilot valve is limited to a maximum flow of 3 L/min. On the one hand a high pilot stage gain demands a large diameter restrictor, giving rapid movement of the poppet, and on the other hand the diameter must be kept small so that at low pressures, when the pilot valve is fully open, a low minimum pressure can be achieved. The restrictor was chosen to be 0.65 mm diameter, giving a minimum servo pressure of around 10 bar. The damping restrictor (5), was also chosen to be 0.65 mm diameter, and this was found to

provide adequate valve damping.

511 All of the test results presented in this chapter were carried out using a hand operated needle valve to change the flow conditions upstream of the poppet, and this is shown in the test rig layout diagram of Fig 5.4. The hydraulic supply was from a ring main, the return flow being returned direct to tank by a separate line to eliminate the effect of ring main back pressure variations. The ring main components are omitted from Fig 5.4 for clarity, and a constant pressure supply to the rig can be assumed.

512 All of the electrical amplification and signal processing cards, whether for test purposes or as part of the closed loop system, were mounted in a central card frame, from which data display and plotting using a digital storage oscilloscope was possible. The three pressure signals P, Ps, Pd, were measured using piezoresistive transducers, giving accurate static and dynamic measurement. The signal processing stand also housed a frequency response analyser for sinusoidal dynamic testing. The flow rate from the valve was measured using a positive displacement flow meter over the range 20 to 200 L/min, and for flows below 20 L/min, flow rate was recorded simply by measuring the time taken to fill a calibrated volume.

5.3 Valve Dynamic Modelling

513 The first step in designing software for the valve was to obtain a satisfactory closed loop position control of the poppet, so that the static characteristics could be examined. This was achieved by implementing a fixed coefficient Pole Placement controller, the design of which is discussed in this section. A sample period of 5 ms was chosen as a compromise between the processing time required for auxiliary processing, and the required valve closed loop bandwidth. The rule of thumb suggested in paragraph 333 indicates possible bandwidths between 20 to 40 Hz, which is better than for many conventional proportional valves. In the calculation of the controller coefficients it is essential to have a dynamic model of the valve, and this was obtained by the use of theoretical modelling and frequency response testing.

514 A measured frequency response plot of the plant, relating the poppet output position signal y, to the pilot valve drive signal e, is shown in Fig 5.5. The plot was obtained whilst sampling at a very high frequency, and can be assumed to represent the continuous domain valve transfer function. Since the D/A and A/D converters have the same gain, then the frequency plot of Fig 5.5, although derived from the analogue output and input respectively of these devices, is representative of what is actually seen digitally inside the microprocessor and no gain adjustment is required. The undesirable influence of flow forces and pressure fluctuations in obtaining Fig 5.5 were removed by shutting off the return line so that irrespective of the poppet movement the main flow pressure P, remained constant. Thus Fig 5.5 is representative of the valve dynamics alone, and can be used directly for controller design.

515 The frequency plot of Fig 5.5 descends at -20 dB/decade at low frequencies, indicating the presence of integral action in the plant. At high frequencies, say from 40 to 100 Hz, the slope is about -40 dB/decade suggesting that the valve dynamics are predominantly second order. The phase information backs this up to some extent in that the 18 Hz break point also corresponds to a phase shift of 135^0. However at higher frequencies the phase lag becomes excessive for a second order system.

516 A model of the valve has been obtained by analysis of the valve physical equations. This is shown in Appendix 4, using the small perturbation method to linearise the equations. If the inertia of the moving parts and oil compressibility is included, a sixth order model results, as shown in Fig A4.2. However for controller design purposes, the use of such a high order model unnecessarily increases the controller complexity, whilst adding very little improvement in dynamic performance. A second order transfer function, comparable to that suggested by the plot of Fig 5.5, can be achieved by neglecting the secondary effects of inertia and oil compressibility.

517 The effect of making these assumptions on the model is considered in section A4.2 of the appendix and leads to the reduced block diagram of Fig A4.3, from which by further reduction a second order equation can be obtained, ie:

$$\frac{y}{i}(s) = -\frac{K}{s(1+Ts)} \tag{5.1}$$

where:

$$K = \frac{K_a C_d}{K_s A_p}, \quad T = \frac{C_a C_t}{K_s C_{na}} \tag{5.2}$$

In this transfer function the poppet is modelled as a flow integrator, and the pilot valve as a first order lag. The latter has been verified by frequency response tests on the pilot valve under various conditions as shown in Fig 5.6.

518 The pressure control pilot valve dynamic characteristics are seen to be very sensitive to the type of load being driven by the valve. For example, with no damping restrictor present, and no movement of the poppet, the pressure is being controlled in a large dead volume behind the back face of the poppet (see fig 5.2). As shown by Fig 5.6, this leads to a high frequency resonance at about 65 Hz and is a consequence of interaction between the valve and the compressibility of the dead volume. Inclusion of the damping restrictor, but still with no poppet movement, cuts down the effect of compressibility and gives the second curve in Fig 5.6, showing a less peaky response but still a high bandwidth. The final frequency plot shows what happens when the poppet is allowed to move, as would be the case in reality. Here the bandwidth is much reduced, the -3 dB point being at about 25 Hz. Although the characteristic can be modelled approximately as a first order lag, there is a pronounced depression at about 8 Hz which cannot be accounted for by linear theory. This depression is also seen in Fig 5.5 to influence the overall open loop dynamic performance, causing a depression to occur around the lag break point.

519 The depression in Fig 5.6 is thought to be a consequence of the nonlinear damping orifice flow characteristic. Calculation of the small perturbation flow gain C_d, in equation 5.2, shows that for small perturbations the pressure drop across the restrictor tends to zero and the flow gain to infinity, corresponding to no effective restriction at zero pressure drop. As the restrictor pressure drop is increased C_d becomes smaller. During frequency response testing, variations in the restrictor pressure drop occurred both with time and frequency, thus it is not surprising that the plot shows nonlinear characteristics.

520 In spite of this discrepancy, the second order model of equation 5.1 gives a reasonable linear representation of the valve frequency plot shown in Fig 5.5. Fitting equation 5.1 to the frequency plot by considering the break point to be at 18 Hz gives the valve model:

$$\frac{y}{e}(s) = -\frac{470.0}{s(1+0.0088s)} \tag{5.3}$$

The use of this model in designing an appropriate controller is discussed in the following section.

5.4 Integral Action Controller Design

521 The s plane model equation 5.3 must be converted to the z plane in order that the Pole Placement method described in Chapter 4 can be applied. The conversion is achieved using the Pole/Zero Mapping method (see Appendix 2), giving the general model:

$$\frac{y}{e}(z) = -\frac{a_1(1+z^{-1})z^{-1}}{(1-z^{-1})(1-a_2z^{-1})} \tag{5.4}$$

Where $a_2 = e^{-\frac{\tau}{T}}$, and a_1 must be calculated to give the same gain as equation 5.3 for low frequencies. The values of the 'a' coefficients of the discrete model, assuming a sample period of 5 ms, and the gain and time constant values of equation 5.3, gives: $a_1 = 0.512$, and $a_2 = 0.566$. Thus the discrete plant model is:

$$\frac{y}{e}(z) = -\frac{0.512(1+z^{-1})z^{-1}}{(1-z^{-1})(1-0.566z^{-1})} \tag{5.5}$$

522 The controller is designed from this model using the Pole Placement equations presented in Chapter 4. An integral action controller is necessary to eliminate the steady state error caused by the main flow pressure disturbance P, acting on the poppet. Since the valve model equation 5.5 is of second order, then from equation 4.18 the controller polynomials are also of second order. Additionally a second order closed loop desired model must be specified, ie the T polynomial roots. The resulting closed loop block diagram is shown in Fig 5.7. The controller polynomials are:

$$F(z) = (1-z^{-1})(f_1+f_2z^{-1}) \tag{5.6}$$

$$G(z) = g_1+g_2z^{-1}+g_3z^{-2} \tag{5.7}$$

and for the desired characteristic equation:

$$T(z) = 1+t_1z^{-1}+t_2z^{-2} \tag{5.8}$$

the roots of which can be specified either as two real roots or as a complex pair.

523 By equating the desired characteristic equation polynomial, T, with that derived from Fig 5.7, a set of simultaneous equations similar to those of equation 4.16 can be derived and the corresponding 'f' and 'g' coefficients calculated. An example of this procedure showing the effects of changing the root positions was given in section 4.5, and here only the results of the calculation are noted. Assistance in selecting the best T polynomial was given by calculating the uncompensated closed loop transfer function, ie implementing a summing junction controller. A unity gain controller was found to give an unstable closed loop performance, thus a reduced forward path gain of 0.6 was chosen. Using the 'a' coefficient values in equation 5.5, the resulting uncompensated closed loop root positions were z = 0.602 +/- j0.714. Plotting this pair of roots on the root locus diagram of Fig 4.1 gives an approximate damping ratio of 0.1, and a natural frequency of 30 Hz, which corresponds well with the measured step response shown in Fig 5.8. The uncompensated closed loop frequency plot shown in Fig 5.9 was obtained by further reducing the forward path gain to 0.4, thereby cutting down excessively high amplitudes of oscillation during the frequency response test. At this gain the damped natural frequency is seen to be reduced, but the response is still unacceptably oscillatory.

524 Experimentation with the desired root positions of the T polynomial showed that good integral action control could be achieved by demanding roots at z = 0.63 +/- j0.1, corresponding to a forward path gain slightly less than 0.6 and very heavy damping (see Fig 4.1). A typical closed loop step response with this controller design implemented is shown in Fig 5.10, and it is seen that the oscillations are damped down but are not eliminated as would be expected with these selected root positions. The remaining oscillation could be a consequence of the nonlinear effect

of the damping restrictor discussed in paragraph 519, however since the worst peak to peak oscillation is less than 0.1 mm, this is considered satisfactory. The frequency response plot corresponding to this step response is shown in Fig 5.11, and compared to the uncompensated plot, Fig 5.9, it is seen that the resonant peak is reduced to within acceptable limits. The -3 dB bandwidth occurs at about 25 Hz and the 90^0 lag point at about 12 Hz.

5.5 Steady State Characteristics and Modelling

525 Implementation of the linear controller designed in the previous section took about 1 ms, thus leaving 4 ms for any auxiliary processing requirements. During this period an on-line model of the valve was executed and used to calculate pressures and flow within the valve. This restriction on processing time limited the valve modelling to very simple steady state equations. Three such equations were required to describe fully the valve behaviour. These being: first, the pilot valve pressure versus current characteristic; secondly, the poppet force balance equation; and thirdly, the poppet flow characteristic (see Fig 5.1). In the following paragraphs the method of modelling each of these equations is described.

526 The poppet valve was designed to give a linear flow versus opening characteristic at constant pressure drop, and to behave according to the orifice equation. For this reason the poppet lift was restricted to 2 mm, so that the valve seat provided the dominant flow restriction even when fully open. The flow area versus lift nonlinearity caused by the conical face of the poppet is very slight, and thus was not included in the model. The measured flow characteristics for different poppet pressure drops are shown in Fig 5.12, and can be modelled well by the general equation:

$$Q = K_q Y \sqrt{R_p} \text{ L/min} \tag{5.9}$$

where R_p, is the pressure ratio of P measured in bar compared to 100 bar, ie $P/100$, and Y, is the poppet lift in mm. K_q is the flow gain, and is found by fitting a straight line to the P = 100 bar case in Fig 5.12, giving the equation:

$$Q = \left| \frac{700}{5} \right| Y \sqrt{R_p} \text{ L/min} \tag{5.10}$$

The fit of this model at other pressures can be seen by calculation of the slopes for the 50 and 150 bar cases. The corresponding straight lines drawn in Fig 5.12 show that the orifice equation model gives a good fit over a wide pressure range.

527 Modelling of the poppet forces is necessary so that the poppet main flow pressure P, can be calculated in terms of the servo pressure and the poppet lift. The Bernoulli flow force acting on the poppet has a significant effect and must be included in the calculation. A free body diagram showing the steady state forces included in the model is shown in Fig 5.13 from which the following equation can be written:

$$P - \frac{2F_b}{A_p} = 2P_s + P_c \tag{5.11}$$

where F_b is the Bernoulli flow force. The constant spring preload force is represented in terms of the poppet cracking pressure P_c, ie the pressure required to crack open the poppet with zero return line and servo pressures. The rate of the spring is very low and is neglected.

528 Assuming the flow travels up the conical face of the poppet, the Bernoulli flow force caused by the acceleration of the flow through the valve flow area is:

$$F_b = \dot{m}V\cos(\gamma) \tag{5.12}$$

where velocity through area, $V = \sqrt{\frac{2P}{\rho}}$ and mass flow rate, $\dot{m} = \rho Q$

Thus since:

volume flow rate, $Q = C_q A \sqrt{\frac{2P}{\rho}}$

and flow area, $A = \pi Y [D - Y\sin(\gamma)\cos(\gamma)]\sin(\gamma)$ (5.13)

Then substituting into equation 5.12 gives:

$$F_b = 2C_q P \pi Y [D - Y\sin(\gamma)\cos(\gamma)]\sin(\gamma)\cos(\gamma) \tag{5.14}$$

529 Substituting equation 5.14 into the LHS of equation 5.11 shows that the factors of the LHS are P, and a second order polynomial in Y. Thus the flow force and pressure force terms of equation 5.11 can be combined to give the equation:

$$P(1+M_1Y+M_2Y^2) = 2P_s+P_c$$

or:

$$P = \frac{2P_s+P_c}{1+M_1Y+M_2Y^2} \text{ bar} \qquad (5.15)$$

where pressure is in bar, and poppet lift in mm. The 'M' coefficients were derived experimentally as described in the following paragraph.

530 The effect of the Bernoulli flow force was observed experimentally by holding the poppet servo pressure constant and gradually opening up the poppet. This was achieved using the upstream manually operated needle valve (see Fig 5.4). The results of such a test are shown in Fig 5.14 where servo pressures of 23, 48 and 73 bars were chosen, giving poppet cracking pressures of 50, 100 and 150 bar respectively. It can be seen that for large poppet openings, when the flow through the valve is high, the same servo pressure can support higher main flow pressures. This is because the Bernoulli forces closing the valve effectively supplement the servo pressure force. Equation 5.15 is fitted to this data by choosing the appropriate values of the 'M' coefficients and cracking pressure, giving the model equation:

$$P = \frac{2P_s+4}{1-0.3Y+0.03Y^2} \text{ bar} \qquad (5.16)$$

The model curves corresponding to the test points are shown by the continuous lines in Fig 5.14, and are seen to fit the experimental data with reasonable accuracy.

531 The poppet force balance equation, 5.16, demands that both the poppet lift and servo pressure be known in order that the main flow pressure can be calculated. The servo pressure P_s, set by the pilot valve should ideally be proportional to the valve drive signal e, and have zero hysteresis. Since the drive signal is generated by the microprocessor then the corresponding servo pressure can be calculated from a

model of the pilot valve characteristic. In practice ideal characteristics cannot be obtained, but nonlinearities in the characteristic, provided they are consistent, do not present a problem as they can be modelled in the control algorithm. The modelling of hysteresis effects is difficult, thus a pilot valve with a good hysteresis characteristic was chosen and dither was applied.

532 The pressure characteristic of the pilot valve is shown by the chain dotted lines in Fig 5.15, and it can be seen that with 50 Hz dither applied, the hysteresis band is at worst only 3 or 4 bars which was considered acceptable. Also some nonlinearity in the characteristic at low and high pressure can be observed, and must be taken into account in the model. For implementation purposes the servo pressure was modelled in terms of the microprocessor digital signal e, ie before D/A conversion. The characteristic is divided into three parts to which first and second order polynomial curves are fitted.

For e in the range $600 < e < 1400$:

$$P_s = 0.0935e - 14.5 \text{ bar} \tag{5.17}$$

For e in the range $150 < e \leqslant 600$:

$$P_s = 59.3\times10^{-6}e^2 + 0.0268e + 4.17 \text{ bar} \tag{5.18}$$

and for e in the range $1400 \leqslant e \leqslant 1850$:

$$P_s = -29.6\times10^{-6}e^2 + 0.172e - 66.3 \text{ bar} \tag{5.19}$$

The modelled valve characteristic is the continuous line in Fig 5.15.

533 The equations 5.10, and 5.16 to 5.19 were implemented by the microprocessor to generate on-line estimates of the servo pressure and the poppet flow and pressure from the valve drive and feedback signals. The use of these estimated signals in closed loop control of the valve is discussed in the following section.

537 The next stage in Fig 5.16 is to use the auxiliary processing time to calculate the model parameters, the values can then be output to an external display unit which provides useful on-line information about the valve operating condition. Every sample period the algorithm checks to see if a keyboard interrupt has occurred, and if this is the case then a number of functions can be selected. Otherwise it awaits the next clock interrupt and returns to the start of the algorithm. For the test program, the keyboard interrupt was used either to enable the feedback mode to be changed, or to display the calculated valve data. An emergency stop function was also provided. If the valve was being used in a real situation, then it would be undesirable to have to halt the valve operation to change the feedback mode. Instead of testing for a keyboard interrupt, the algorithm could be designed to read specific memory locations, the contents of which could be changed externally using direct memory access. The demand signal would probably be input externally from a separate microcomputer system.

538 The servo pressure control mode is demonstrated in Fig 5.17 where the measured servo pressure is plotted against the demanded servo pressure. By comparison with Fig 5.15, it can be seen that the model has been used to linearise the pilot valve nonlinear pressure characteristic. The hysteresis band at worst is only 4 bar. This mode of operation uses only the valve drive signal in the model calculation, and is really a simple forward path gain filter rather than a feedback filter. The feedback concept is only used for compatibility with the other modes. The use of the valve for main flow pressure control is demonstrated in Fig 5.18. Three levels of demanded pressure have been set, 50, 100 and 150 bar. The test was carried out by gradually opening up the test rig needle valve which throttles the constant pressure supply line (see Fig 5.4). As the needle valve is opened up, the flow increases and the control valve pressure P_c is maintained at the desired level by opening up the poppet. Also plotted in Fig 5.18 are the constant servo pressure curves of Fig 5.14 for the same cracking pressures. Thus it is demonstrated that the valve model has compensated for the Bernoulli flow forces, maintaining a constant pressure irrespective of flow rate. The inaccuracies in Fig 5.18 are a consequence of inevitable modelling errors.

539 To improve the steady state valve accuracy more complex models and higher performance valve hardware with less hysteresis in the pilot stage would be required. Even then there is no way that secondary effects such as changing oil

properties or temperature drift could easily be taken into account. For example, the pressure control pilot valve used is quoted as having a 2 % temperature drift for a 20 deg.C rise in temperature [66], the resulting errors could only be corrected by on-line measurement of the temperature and inclusion of this effect in the valve model. These factors are also problems which exist in more conventional valve designs. In spite of the modelling errors, the combined valve hardware and control algorithm gave a pressure control accuracy better than +/- 5 bar over the 150 bar range, and this is considered adequate for many applications.

540 When the valve is used in the flow control mode, the square root of pressure is used in the orifice equation calculation, and thus any errors in pressure estimation are halved. Thus greater accuracy can be expected in the flow control mode of operation. The characteristics obtained using the flow feedback mode are shown in Fig 5.19. The test was carried out in a similar manner to that described in paragraph 538, but in this case as the needle valve was opened up thereby attempting to increase the flow, the control valve closed down the poppet lift maintaining the demanded flow rate. The flow rate and poppet lifts were measured at various points and plotted against the square root of pressure factor R_p. This is shown in Fig 5.19 for demanded flows of 25, 50 and 100 L/min. Over the range of poppet opening indicated in Fig 5.19(a), only very small errors between the demanded and the actual flow were detected.

541 For comparison purposes the flow characteristic for the same test but with a constant lift, set to give the correct flow at 100 bar, is also plotted on Fig 5.19(a), thus demonstrating the pressure compensation of the valve in maintaining the correct flow. The lower graph Fig 5.19(b), shows how the poppet lift changes during constant flow control. According to the orifice equation, the poppet lift should change as the inverse of the square root of pressure. The straight lines drawn on the graph pass through the test points and thus indicate good agreement of the measured results with theory.

5.7 Further Application of New Valve Concept

542 The use of microprocessor closed loop control has served two purposes in the new valve concept. First, the use of estimated feedback signals has reduced the amount of valve hardware, thus simplifying the valve construction and cost.

Secondly, the ability to change the mode of control and the valve closed loop dynamics adds a large degree of flexibility, broadening the application of the same simple hardware.

543 The basic two way valve concept used in this research can be used as an element in the design of other flow control valves. For example Fig 5.20 shows a schematic for a four port flow control valve built from poppet valves. As discussed in section 2.4, the use of four poppets instead of a spool gives greater flexibility because each flow metering area can be operated independently, giving sixteen different switching selections. In the arrangement shown in Fig 5.20, the four directional poppets are each activated by three port on/off pilot valves, connecting the poppet back face either to low or high pressure.

544 A photograph of both the two port flow control valve and a four port directional control valve is shown in Fig 5.21. The same poppet and cartridge construction as described in paragraphs 507 and 508 was used in both valve designs. The four port directional valve is made to control flow proportionally by connecting its return lines to the new microprocessor operated flow control valve (see Fig 5.20). The overall system then works as a meter out device, the supply line being fully open and the return flow being throttled to control either pressure or flow depending on the selected feedback mode. A preliminary study of the four port valve is complete, and its use in proportional control is the subject of further investigation [70].

545 The poppet valve as a flow metering device has been ideal for the new flow control valve concept, since it is a load sensitive device amenable to on-line modelling. Spool valves on the other hand are normally insensitive to load pressures, and thus are not amenable to modelling (see section 2.7). However, they can be made load sensitive by applying the load pressure directly to one end of the spool as shown in Fig 5.22. The schematic shows in principle how the same microprocessor control techniques can be applied to a three port spool valve. On one end of the spool the servo pressure from the pressure control valve is applied, and on the other end the cylinder port B pressure is applied. Thus in the equilibrium position the pilot valve drive signal gives an indication of the servo pressure and hence the presure in port B. Thus since the spool position is known from the feedback transducer, the flow rate in port B can be calculated and hence controlled.

Fig 5·1

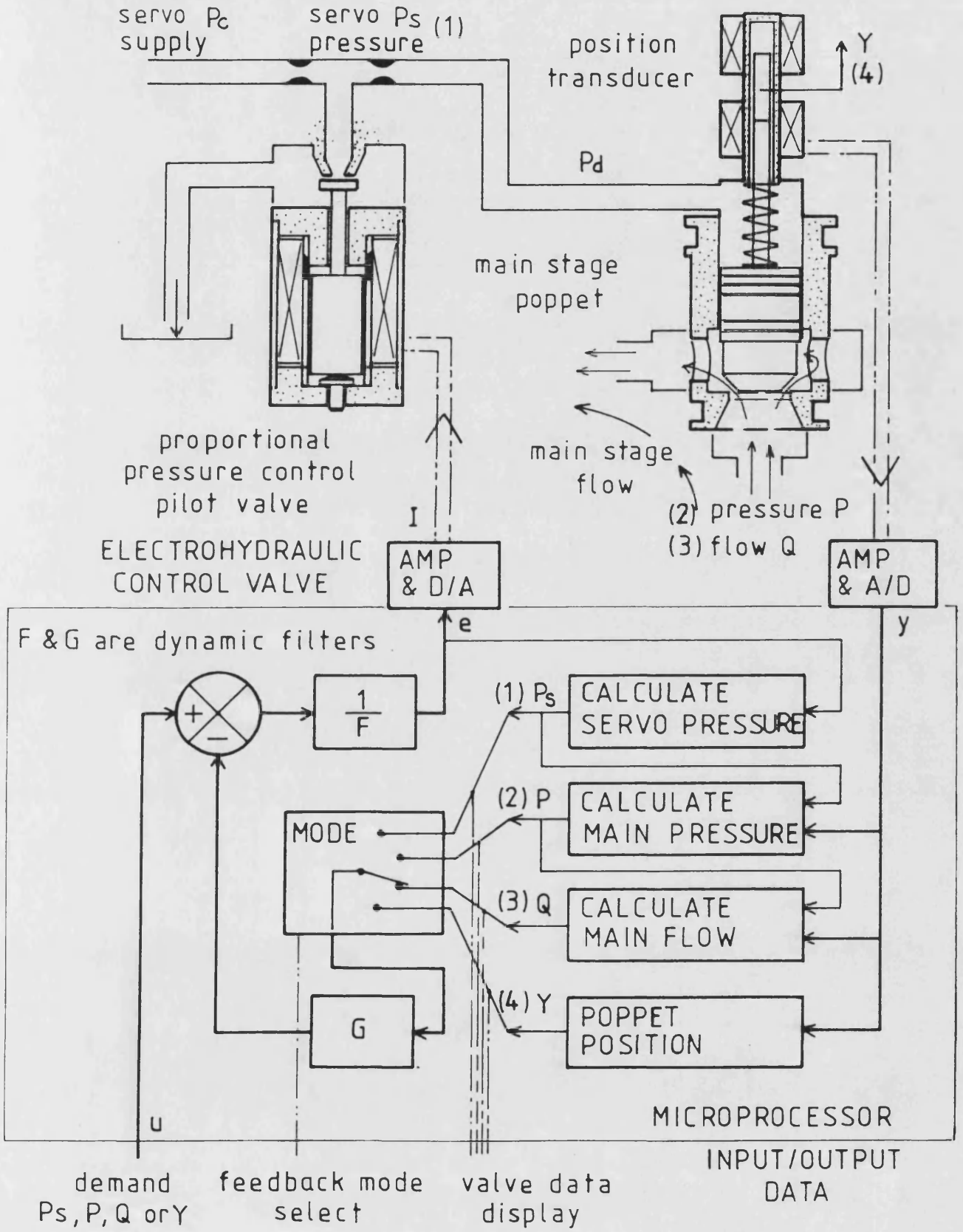

5·1 NEW FLOW CONTROL VALVE CONCEPT

Fig 5·2

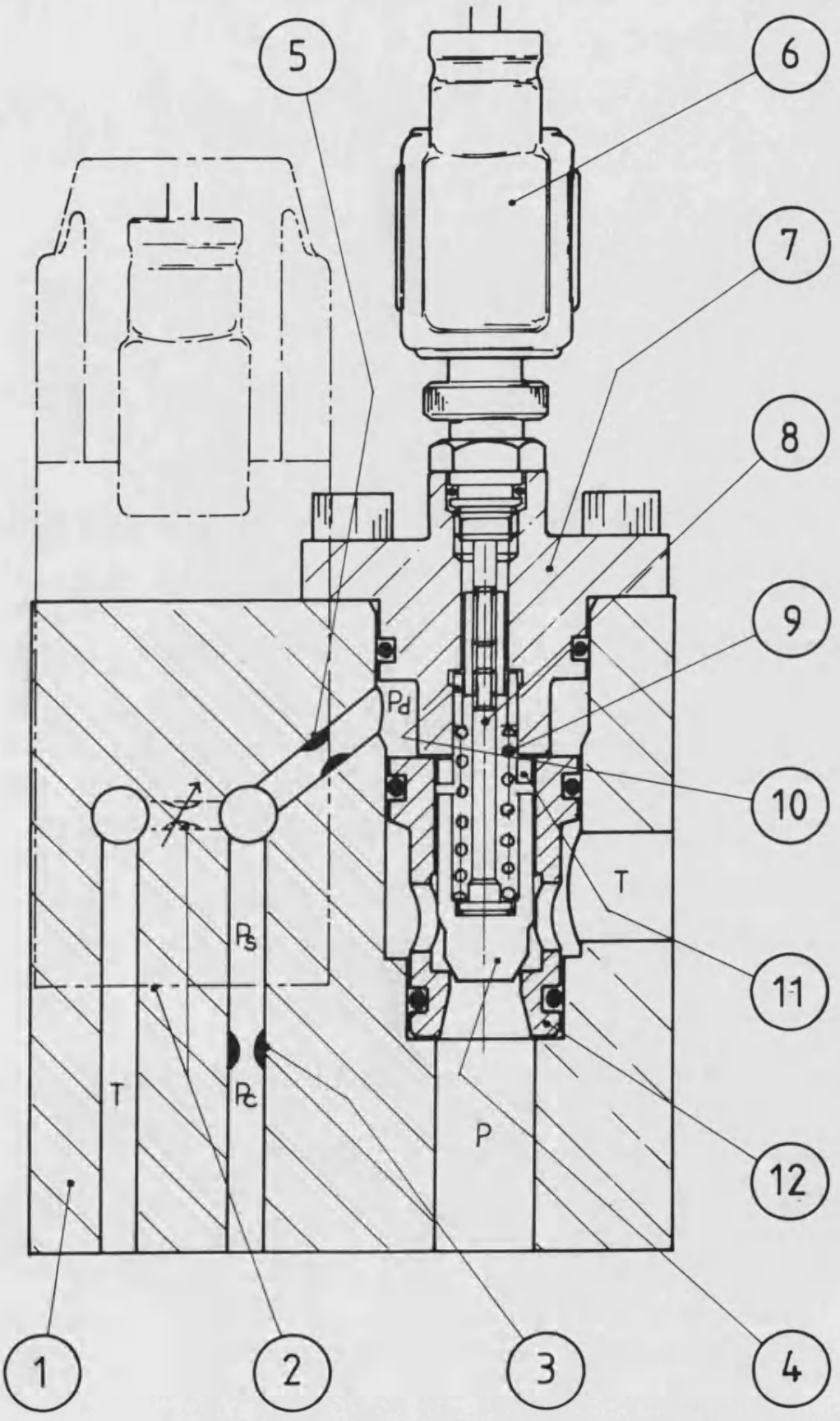

5·2 VALVE ASSEMBLY DRAWING ~ SCALE 1:1

Fig 5·3

PART N°	NAME	COMMENTS
1	VALVE BLOCK	
2	PRESSURE CONTROL VALVE	ref [66] 150 bar max
3	SERVO RESTRICTOR	diameter 0·65 mm
4	POPPET	ref [67], 2:1 area ratio diameter 16 mm
5	DAMPING RESTRICTOR	diameter 0·65 mm
6	POSITION TRANSDUCER	ref [69]
7	COVER CAP	
8	EXTENSION ROD	
9	PRELOAD SPRING	ref [67]
10	PRELOAD SPACER	cracking pressure 4 bar
11	LIFT SPACER	poppet lift 2mm max
12	CARTRIDGE	ref [67]

5·3 PARTS LIST FOR FIG 5·2

Fig 5·4

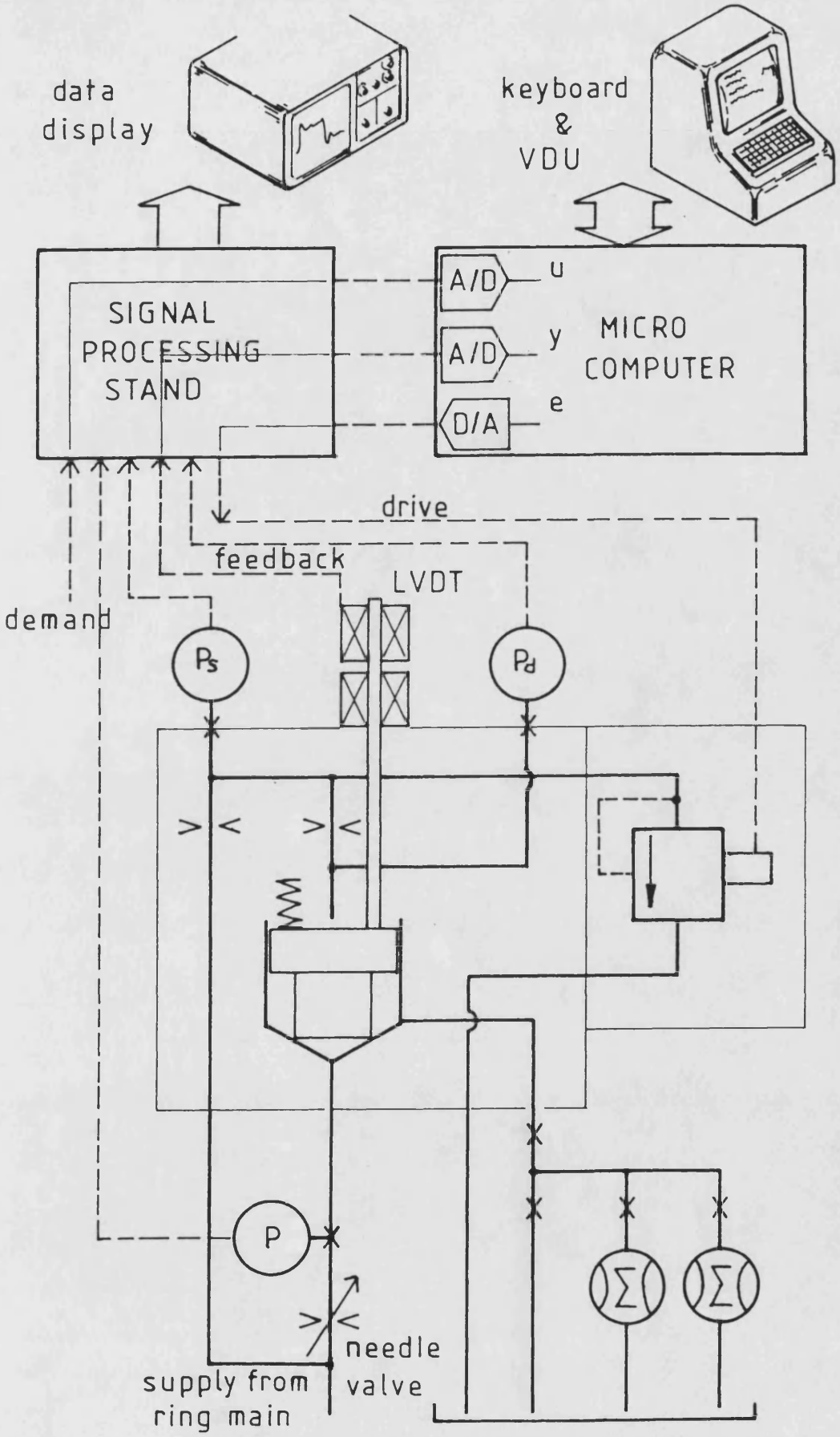

5·4 TEST RIG LAYOUT

Fig 5·5

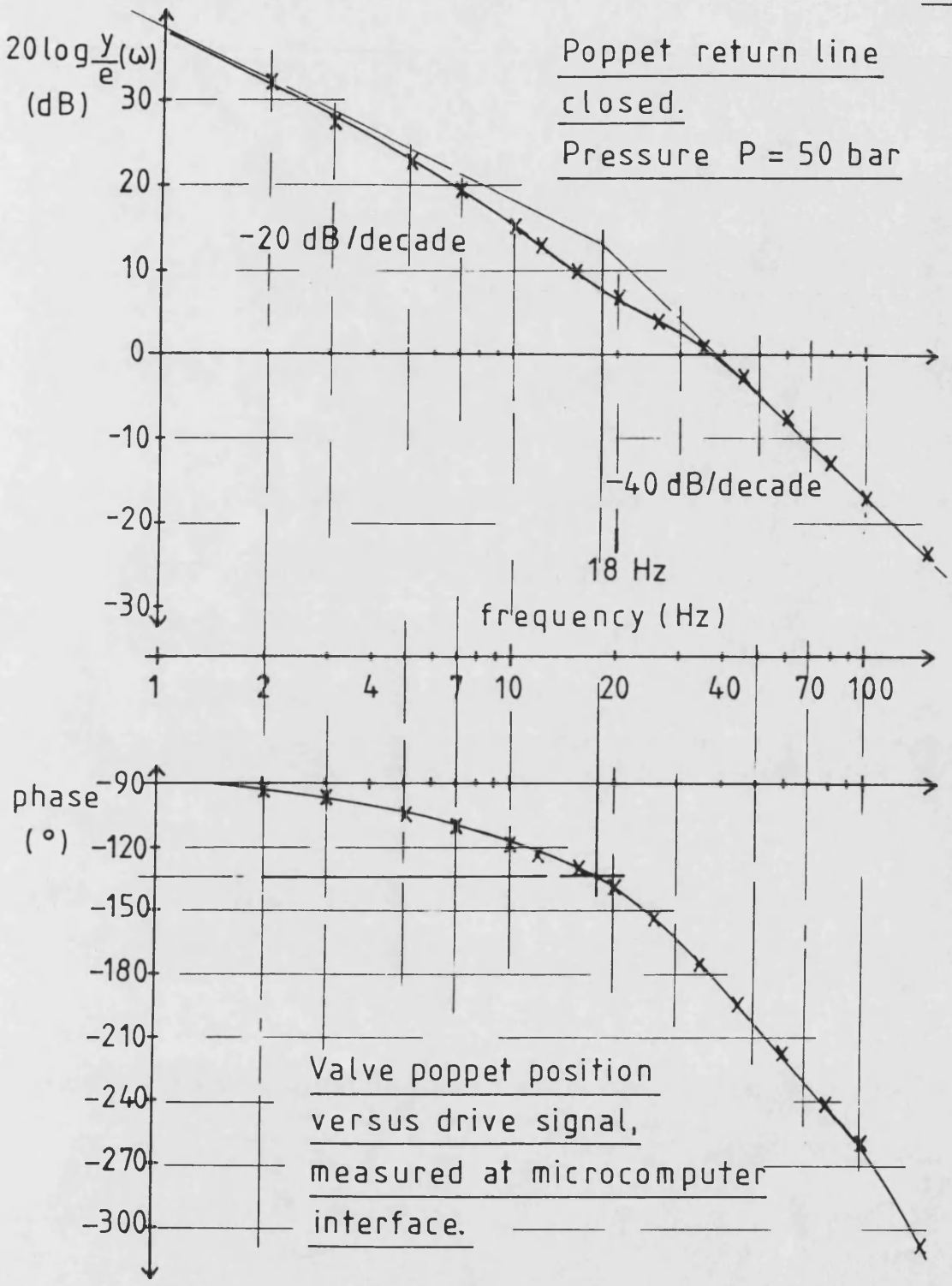

5·5 OVERALL VALVE OPEN LOOP FREQUENCY RESPONSE

Fig 5·6

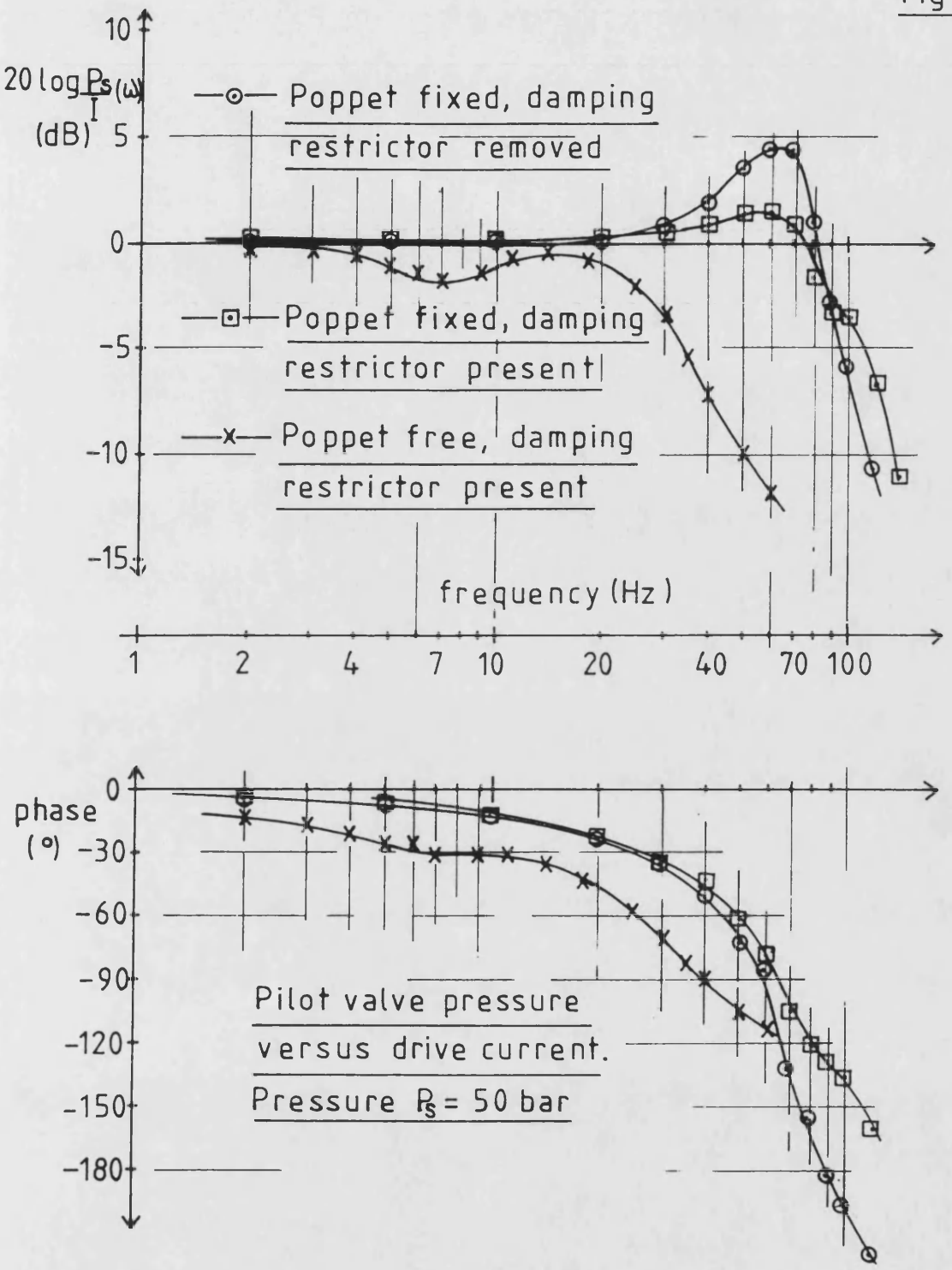

5·6 PILOT VALVE FREQUENCY RESPONSE FOR DIFFERENT LOAD CONDITIONS

Fig 5·7

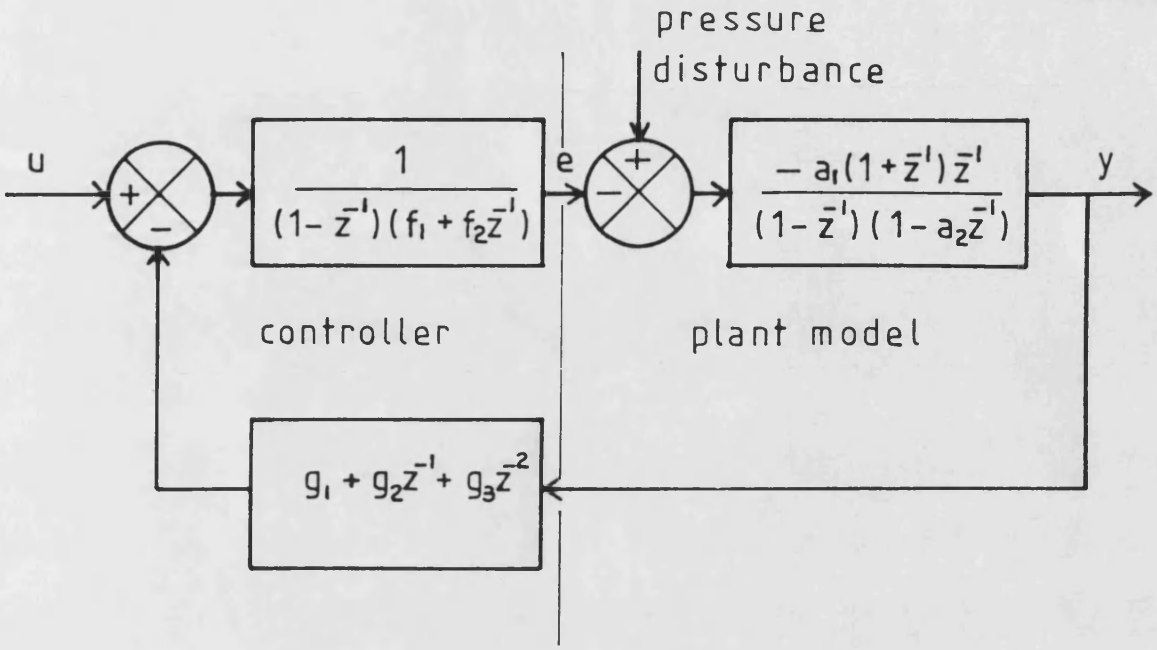

5·7 VALVE CLOSED LOOP BLOCK DIAGRAM

Fig 5·8

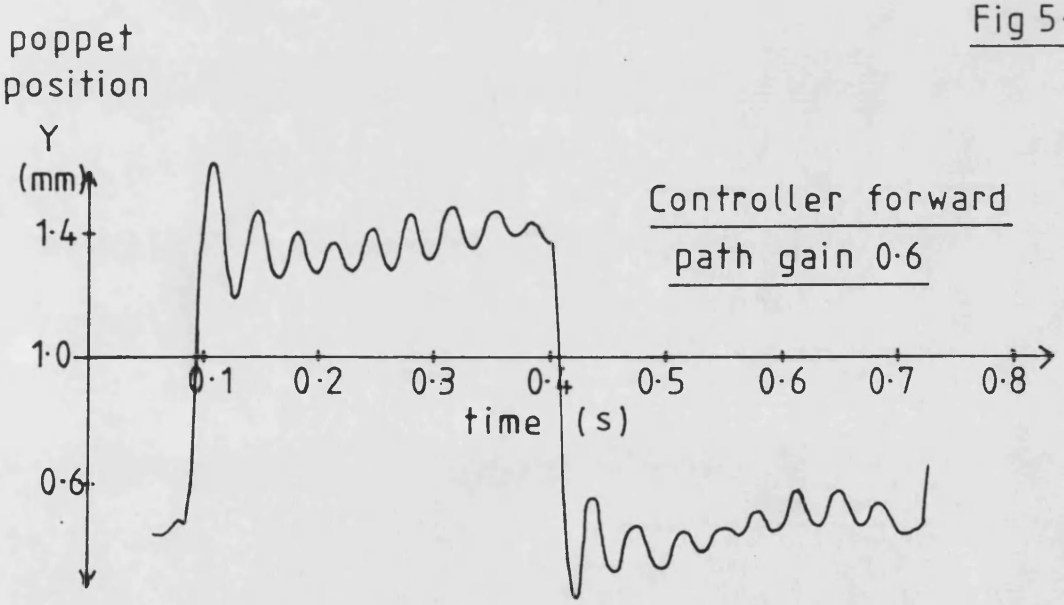

5·8 OVERALL VALVE UNCOMPENSATED STEP RESPONSE

Fig 5·9

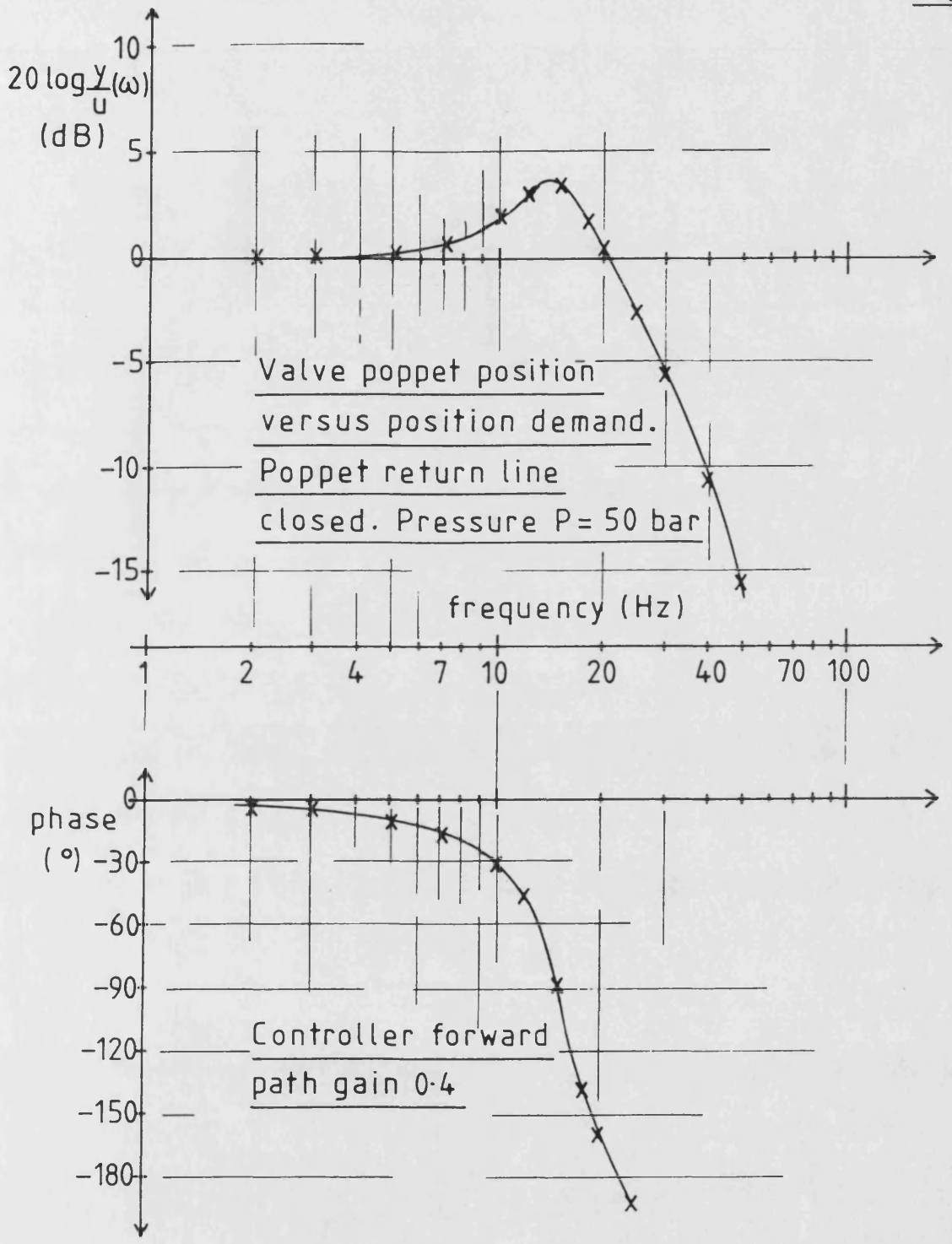

5·9 OVERALL VALVE UNCOMPENSATED CLOSED LOOP FREQUENCY RESPONSE

Fig 5·10

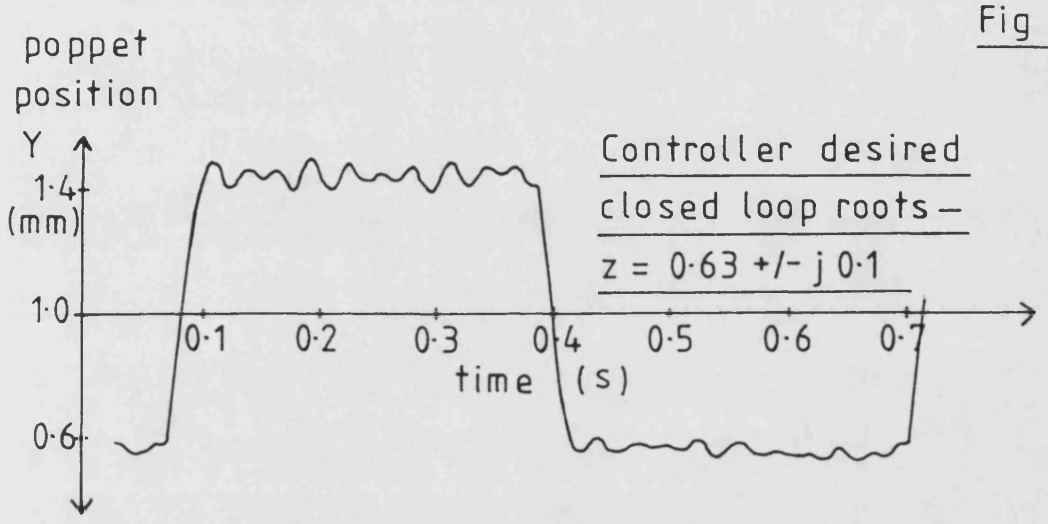

5·10 OVERALL VALVE COMPENSATED STEP RESPONSE

Fig 5·11

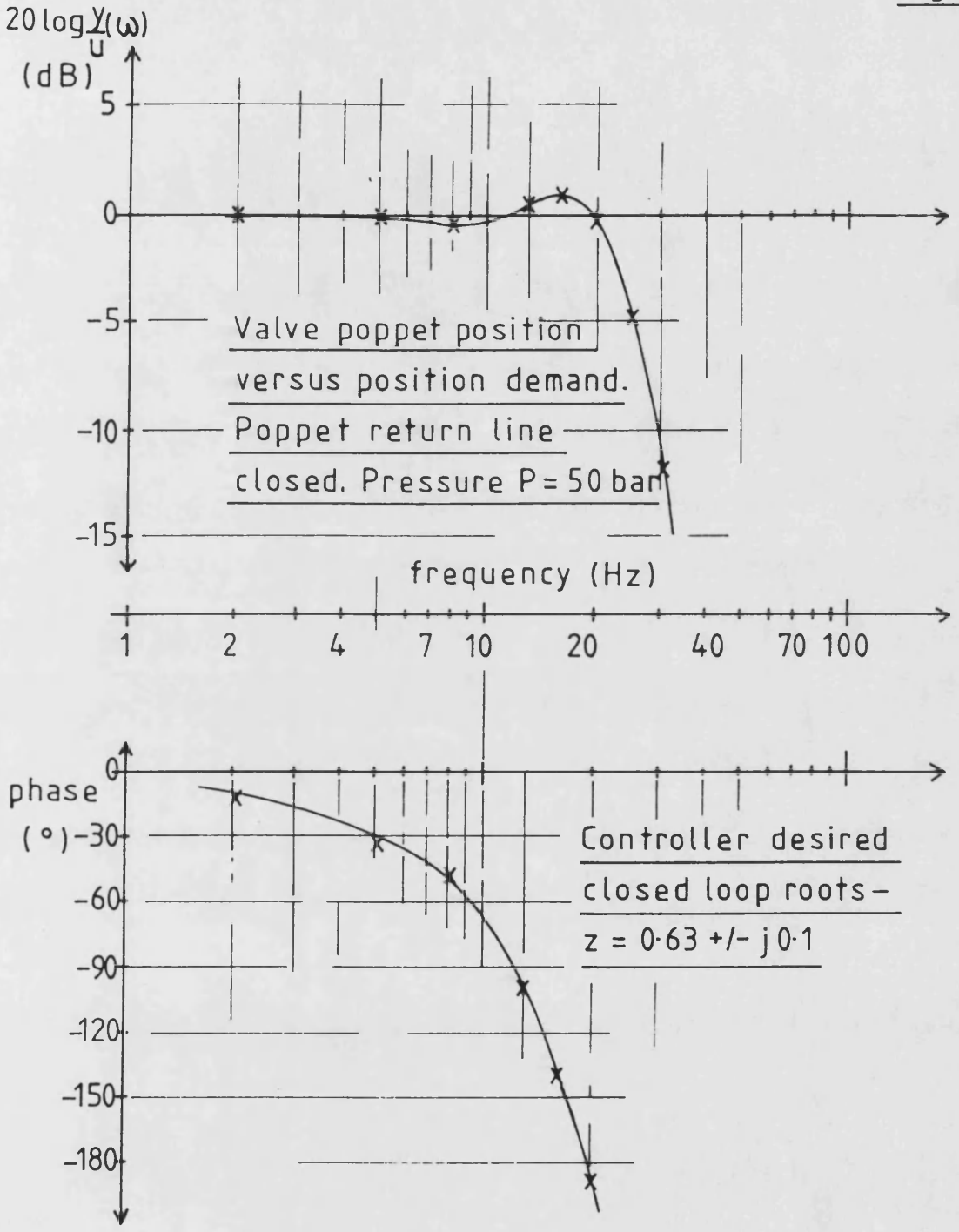

5·11 OVERALL VALVE COMPENSATED CLOSED LOOP FREQUENCY RESPONSE

Fig 5·12

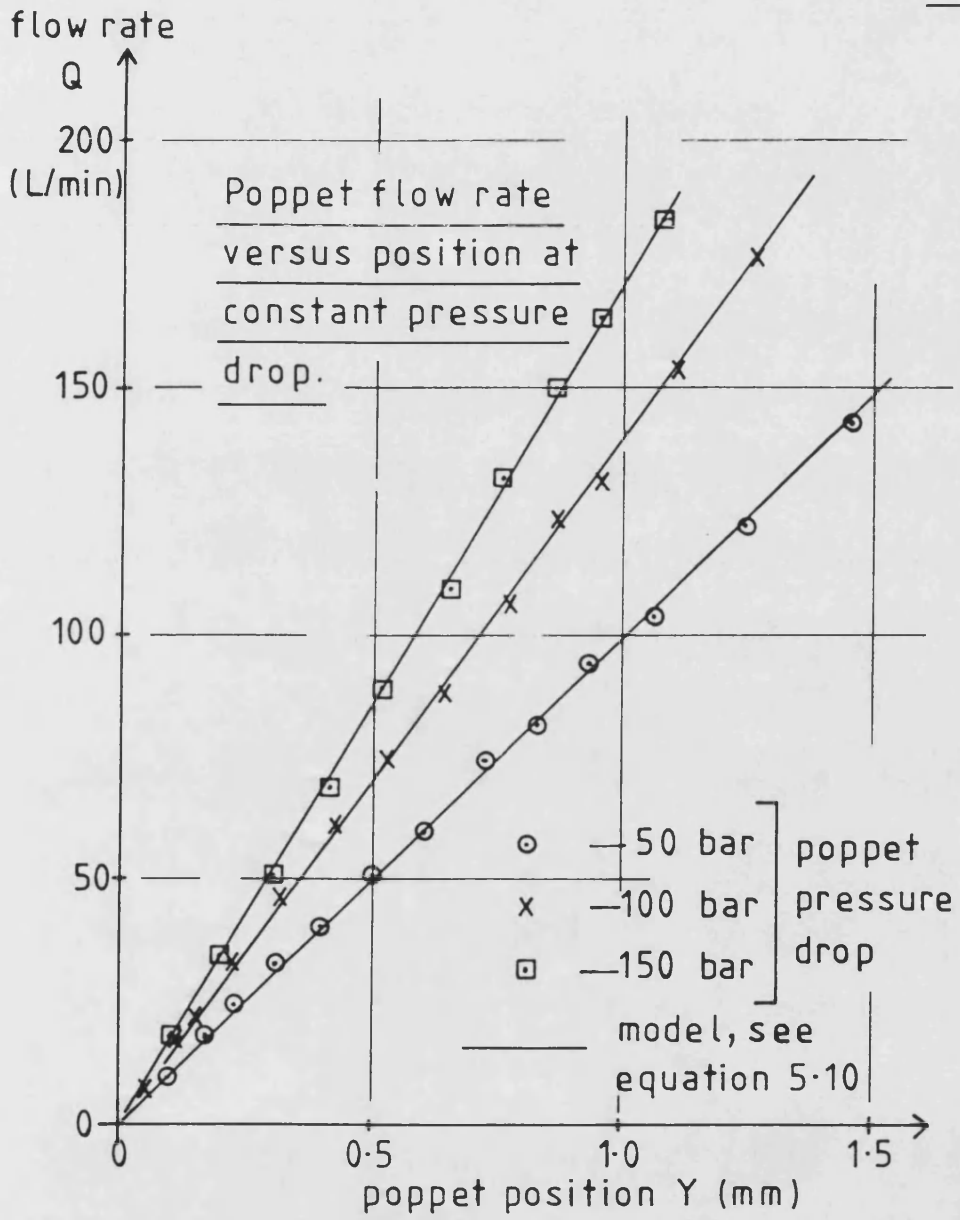

5·12 POPPET FLOW CHARACTERISTICS

Fig 5·13

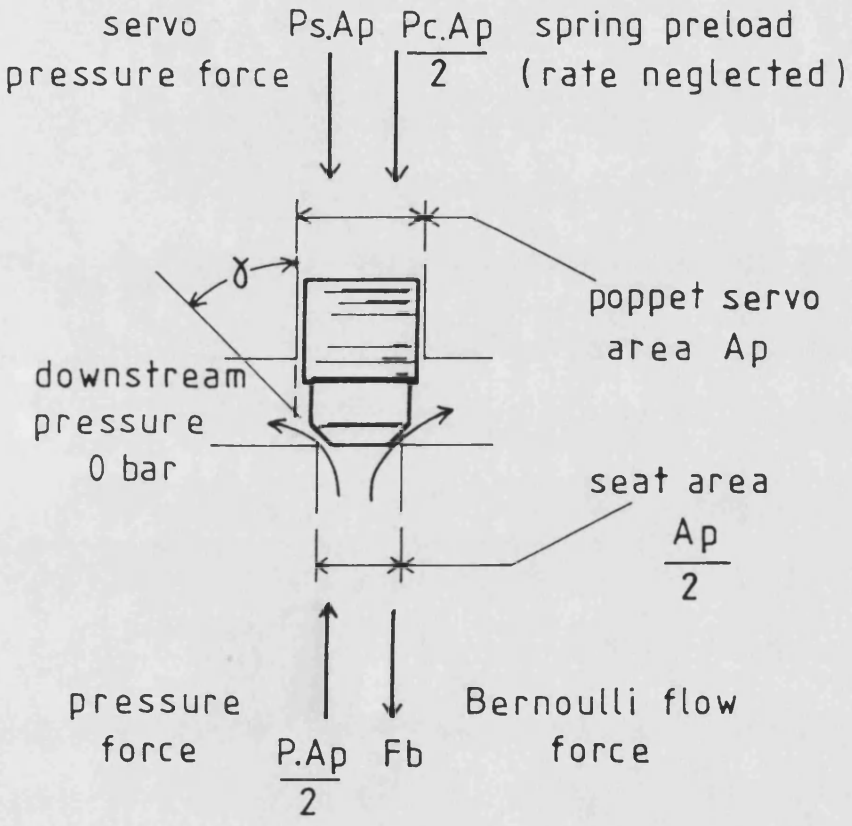

5·13 POPPET FREE BODY DIAGRAM

Fig 5·14

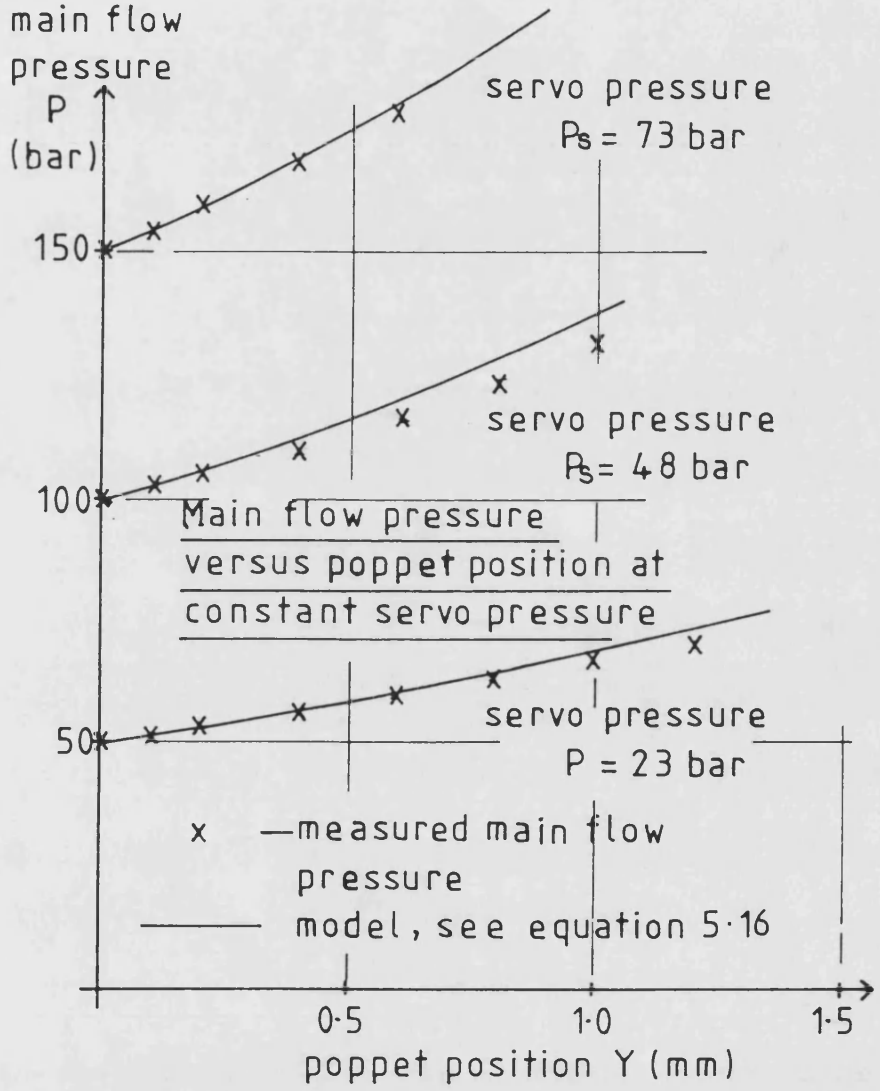

5·14 POPPET FORCE CHARACTERISTICS

Fig 5·15

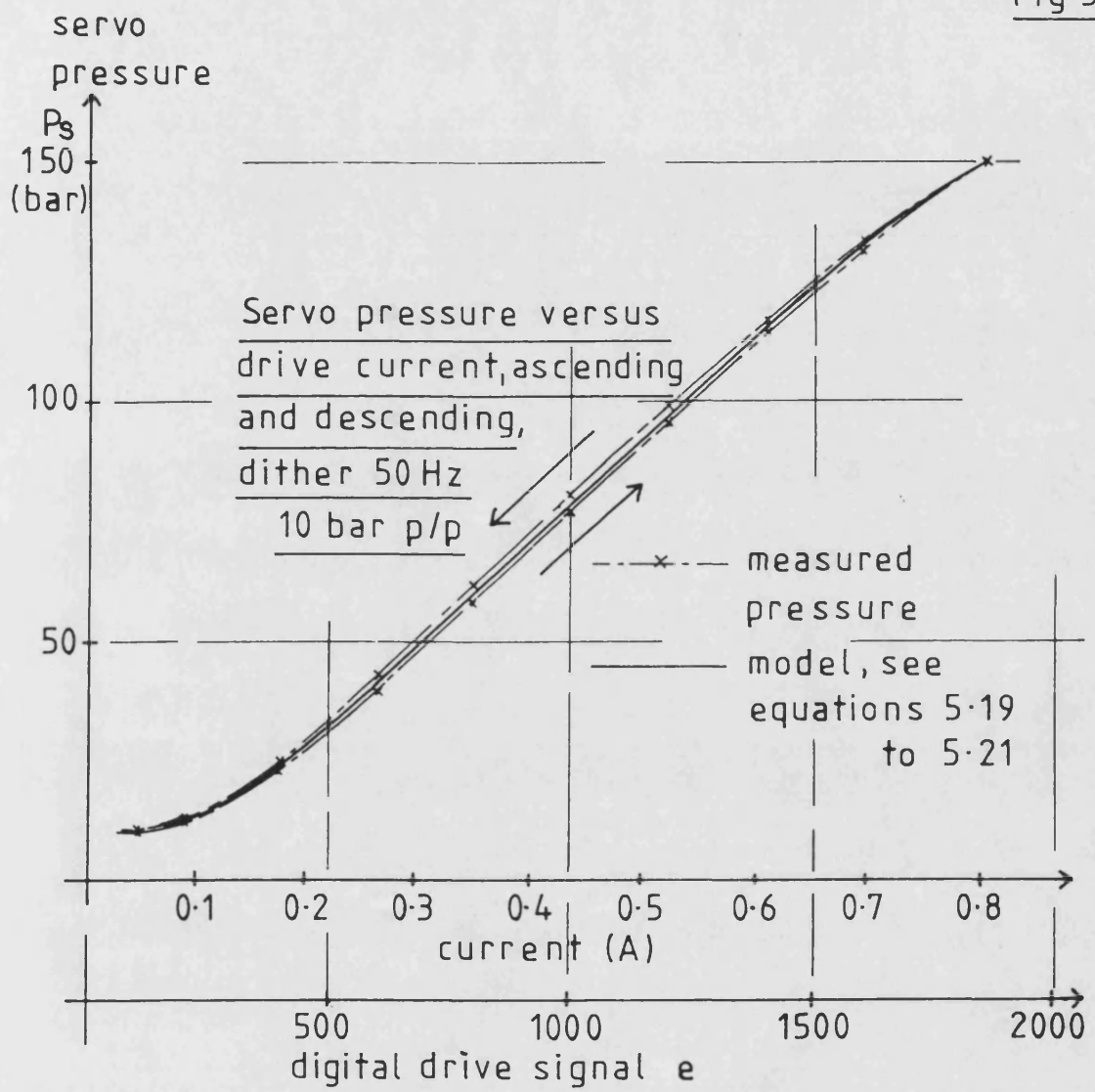

5·15 PILOT VALVE CHARACTERISTIC

Fig 5·16

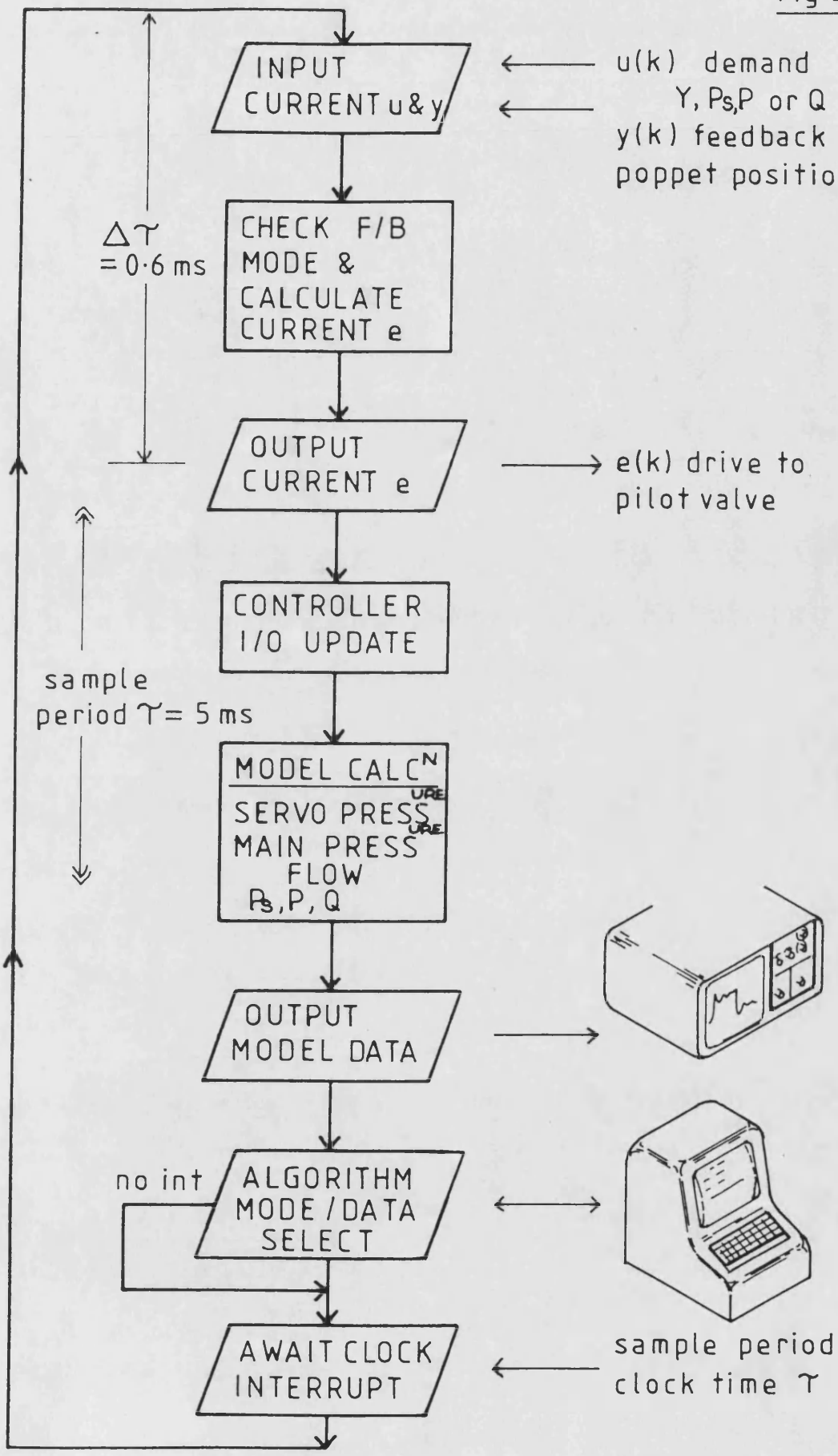

5·16 VALVE CONTROLLER FLOW CHART

Fig 5·17

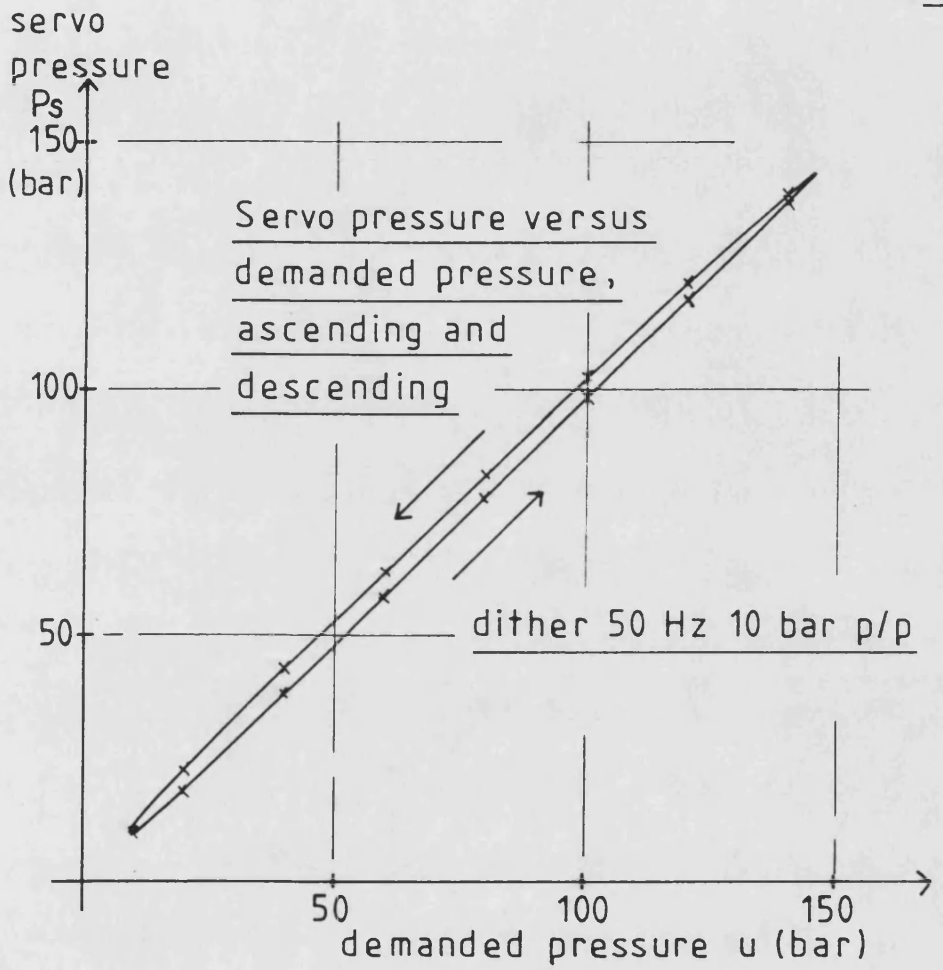

5·17 SERVO PRESSURE CONTROL MODE

Fig 5·18

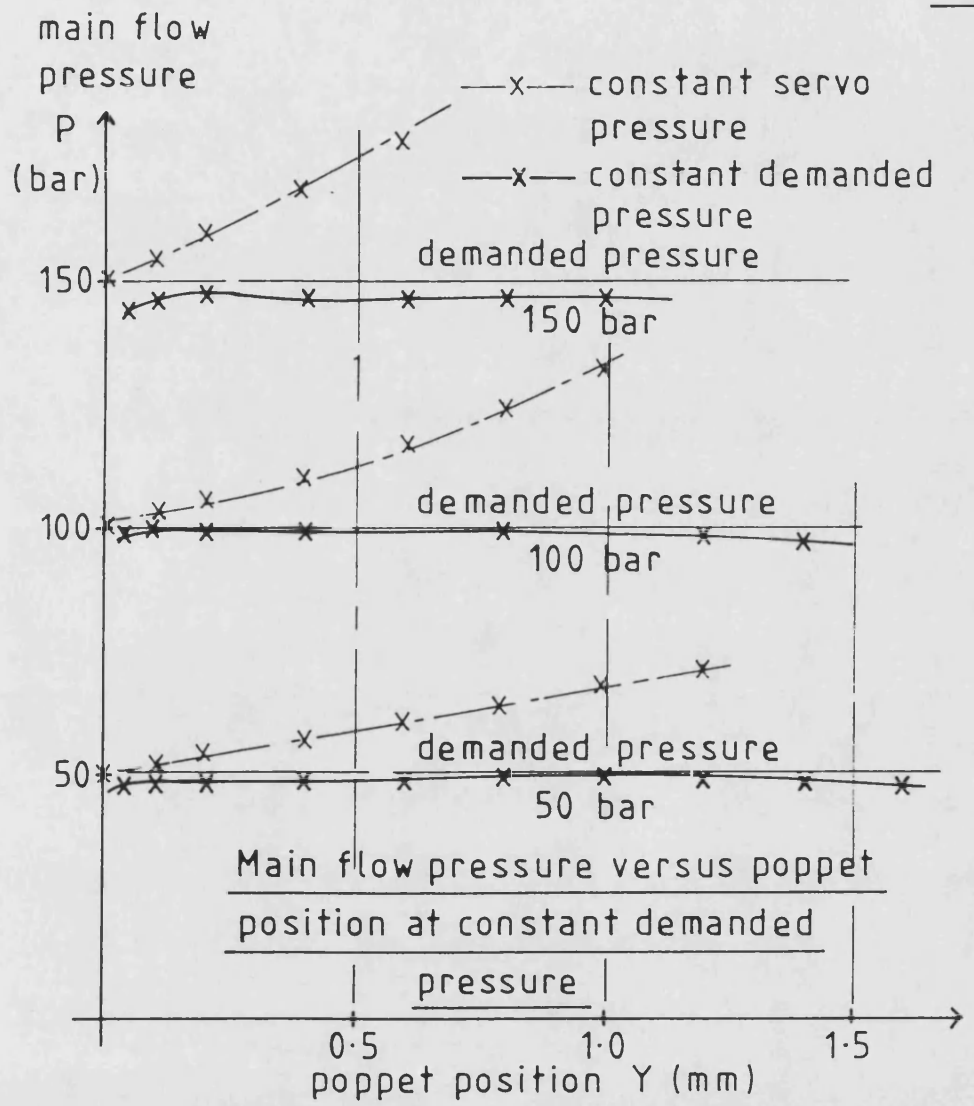

5·18 MAIN PRESSURE CONTROL MODE

Fig 5·19

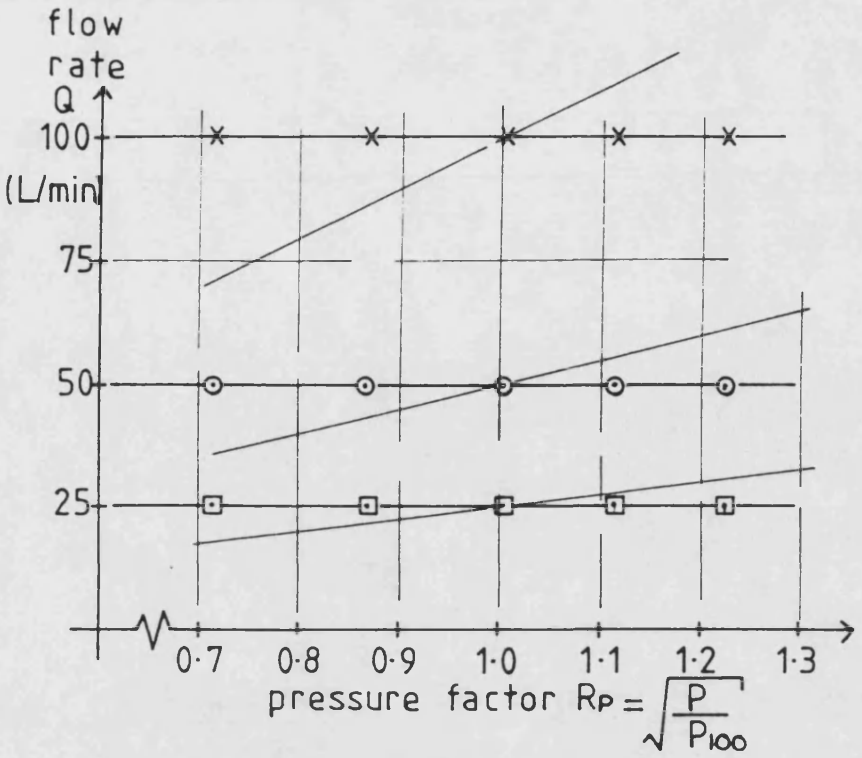

(a) FLOW RATE VERSUS PRESSURE

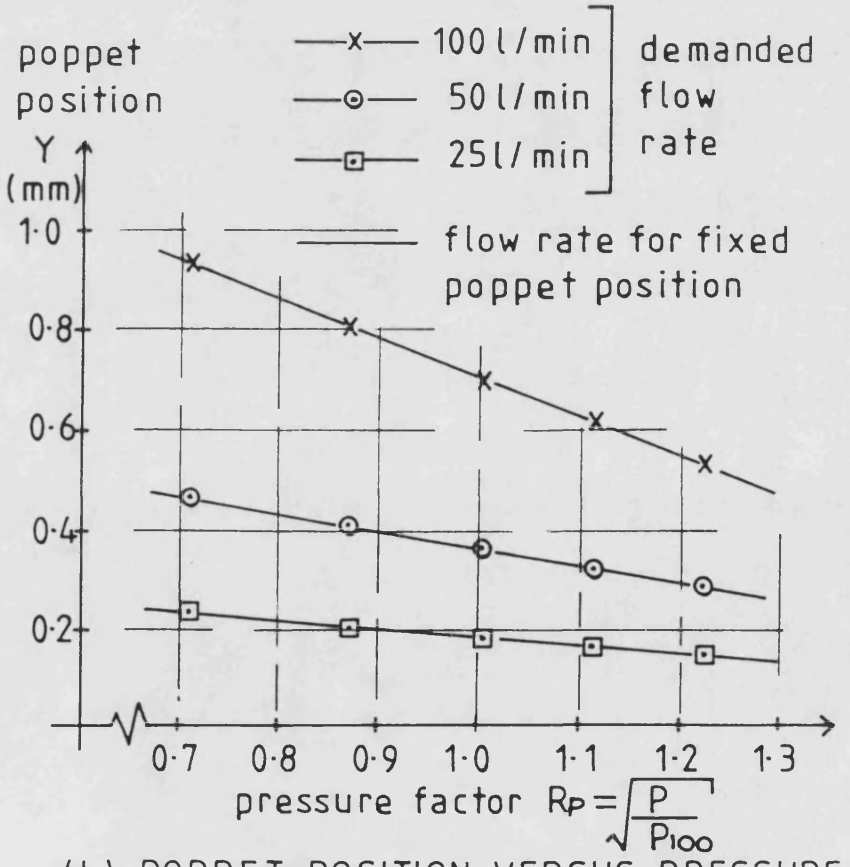

(b) POPPET POSITION VERSUS PRESSURE

5·19 FLOW CONTROL MODE

Fig 5·20

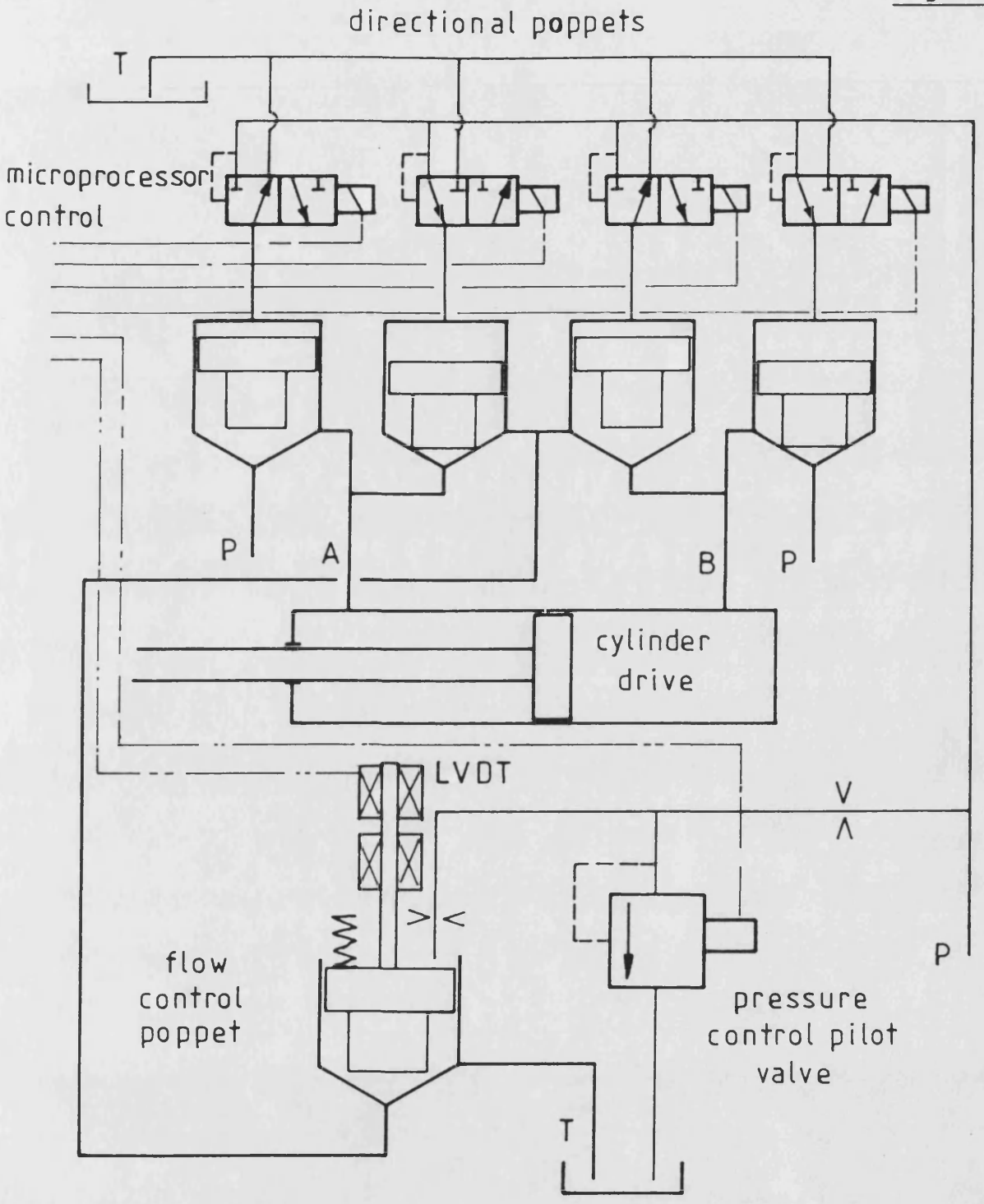

5·20 FOUR PORT FLOW CONTROL POPPET VALVE

Fig 5-21

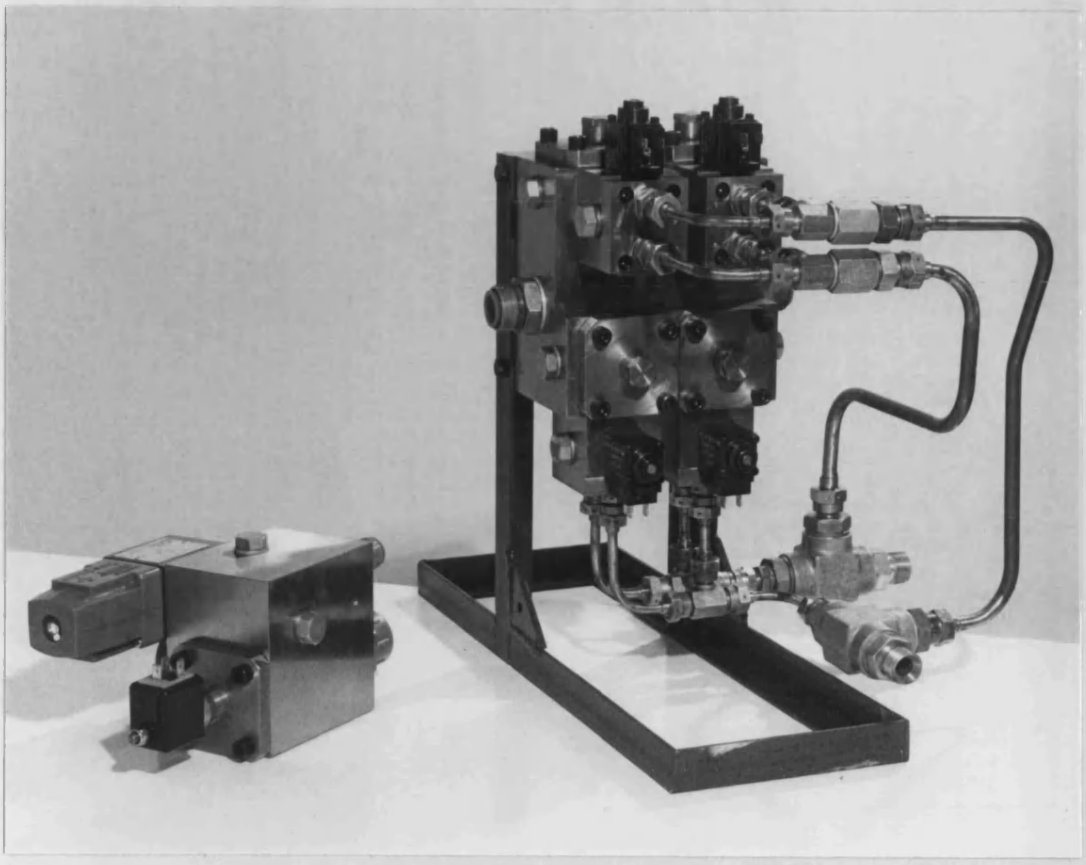

5·21 TWO PORT AND FOUR PORT POPPET VALVE HARDWARE

Fig 5·22

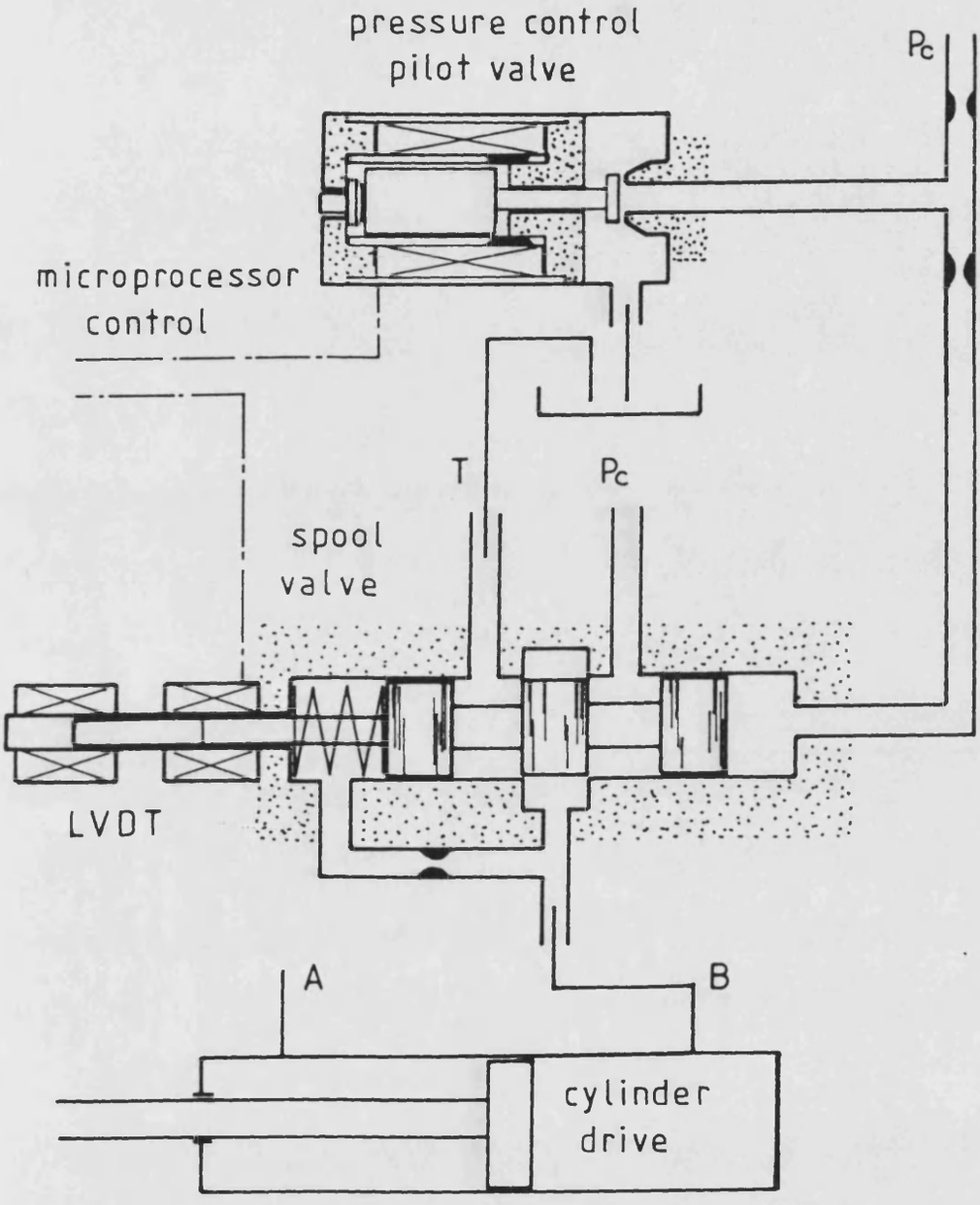

5·22 THREE PORT FLOW CONTROL SPOOL VALVE

6. DIGITAL VALVE INTERFACE

6.1 Introduction

601 The so called 'digital' valve techniques were discussed in section 2.8, and it was observed that significant hardware simplification, as well as potential improvement in the ease of interfacing to microcomputer systems, could be obtained using pulse width modulation (PWM) drive signals. In this chapter the new microprocessor controlled valve concept is extended to include a PWM driven pilot stage, providing the same function as before but at reduced cost. The proportional pilot valve used in Chapter 5 is replaced by a simple three way on/off ball valve element, which connects the back face of the poppet via a damping restrictor to either high or low pressure. The research presented is devoted to the design and investigation of the new pilot valve, and its application to the overall flow control valve.

602 In section 6.2 the new pilot stage hardware is introduced and the details of its design discussed. The test rig layout is also presented. The need for a high PWM switching frequency demands the use of an overdriving amplifier. In section 6.3 such an amplifier is presented, and the advantages of overdriving are demonstrated. A low power consumption version of the amplifier is also presented. The use of a programmable timer to create the PWM signal is explained in section 6.4, and it is shown that proportional pressure control can be obtained by applying PWM to the on/off pilot valve. In section 6.5 the dynamics of the pilot valve are considered and its effect on the overall flow control valve open loop performance investigated. The Pole Placement controller design method is used to derive an integral action controller which is shown to work successfully in practice. Finally in section 6.6, areas where further investigation is required are identified.

6.2 Valve Hardware Design and Test Rig Layout

603 A schematic of the modified flow control valve is shown in Fig 6.1, only the first stage pilot valve has been altered (compare fig 5.1). Instead of the proportional pressure control valve, a three port on/off solenoid valve is used, connecting the back face of the main stage poppet either to the constant supply pressure P_c, or tank via a demodulating restrictor. As described in section 2.8, the ball valve must be opened and closed at a very high frequency so that sufficient demodulation can

occur without using an excessively small and dynamically sluggish restrictor. The pressure downstream of the restrictor acting on the back face of the poppet, then takes up a mean value proportional to the Signal Modulation Ratio (SMR), with only small amounts of pressure fluctuation. Thus the on/off pilot valve provides the same function as the proportional pilot valve, except that now the servo pressure is proportional to the SMR rather than an analogue voltage. The function of the microprocessor is unchanged, being used in the same way as in Chapter 5 to implement the control law, and calculate the valve model.

604 The design of the alternative pilot valve is shown in the engineering drawing of Fig 6.2, the scale is twice full size. A parts list referring to the principal components is shown in Fig 6.3, the part numbers corresponding to those in Fig 6.2. In the following text the part numbers are referred to in brackets thus '( )'. All of the components are mounted inside or on the the pilot valve block (1), which itself is designed for mounting on the main valve block (2), to mate up with the same port arrangement as was previously provided for the proportional pilot valve.

605 Mounted inside the pilot valve block is the three port ball valve assembly. The ball switching time is minimised by using small valve seating elements and restricting the switching travel to the absolute minimum. The ball (4), is a 1.587 mm (1/16 in) diameter ball bearing, switched between two identical seats (6) of diameter 1.32 mm. The ball travel is restricted by the seat spacer (5), which limits the total ball travel from seat to seat to about 0.3 mm. One seat is connected to a constant high pressure supply, and the other to tank. The third port, providing the servo line to the main stage poppet, is connected to either seat by slots cut in the seat spacer (5). The ball valve allows a maximum flow of about 3 L/min at 150 bar pressure drop. If the valve is not activated then the high pressure naturally causes the ball to close off the low pressure seat, thereby connecting high pressure to the poppet back face and ensuring that the poppet is closed during an electrical failure.

606 Activation of the ball to close off the high pressure seat, thereby connecting the servo line to tank, is provided by an on/off solenoid (8), which transmits the electromagnetic unseating force along a push pin (7), to the ball. The push pin is made from precipitation hardened Beryllium Copper, thus cutting down magnetic flux leakage from the solenoid and providing a hard wearing tip where impact with the ball occurs. Ideally the electromechanical conversion device should have fast

dynamics for quick switching. However whilst a solenoid device may not be the best suited for this purpose, a solenoid has been used here because of its low cost, robustness, and simplicity in construction. The force generated from an on/off solenoid changes approximately in an inverse square fashion with the armature air gap. Thus to minimise the solenoid size and give maximum force, the push pin length was machined to give an activated minimum air gap of less than 0.3 mm. The solenoid was nominally rated at 12 V and 2.4 A for continuous operation [71], but greater switching speed was obtained using an overdriving amplifier with a 50 V supply.

607 The test rig layout is basically the same as discussed in section 5.2, and is shown in Fig 6.4. Apart from the pilot valve itself, the only additional requirements were, the overdriving amplifier and power supply and the use of the Darkstar's timer chip to generate the PWM drive signal.

6.3 Pilot Valve Switching Characteristics

608 In order for there to be some proportionality between the SMR and the demodulated servo pressure, the time spent in the ball switching transient compared to that at rest on one or the other valve seat must be small. The duration of the switching transient, is influenced by both electrical and mechanical factors which will now be discussed. The test results which follow were obtained with the main stage poppet fully closed at all times, thus removing the possibility of interaction with the pilot valve.

609 The build up of electromagnetic force on the armature after the solenoid has been activated, depends on the build up of current in the solenoid. Initially a constant voltage supply set at 12 V was used and the build up of current in the solenoid after switching observed. The results of these tests are shown in Fig 6.5, the voltage switching step being shown in Fig 6.5(a). Fig 6.5(b) and (c), compare the results of two different minimum air gaps with and without the hydraulic pressure supply switched on. With the supply off, the ball remains on the high pressure seat even when the solenoid is not activated, thus though the solenoid may be switched, no ball or push rod movement occurs (see Fig 6.2). When the supply pressure is applied then power is available for the return stroke, and the valve is moved back and forth.

610 In the 0.2 mm minimum air gap case of Fig 6.5(b), a very high maximum force of over 70 N is generated, this can be seen from the force versus air gap characteristic of Fig 6.6. With no pressure applied, Fig 6.5(b) shows that the current rises exponentially because of the inductive effect of the solenoid, the curve having a time constant of about 5 ms. Carrying out the same test with the valve moving, a blip in the current characteristic is observed, and is a result of the back EMF generated when the moving parts of the solenoid travel through lines of magnetic flux. The sharp discontinuity in response is the point at which the ball comes to rest on the valve seat, and switching is complete. In this case it is seen that the ball switching transient takes 11 ms to close off the supply, and about the same period to close off the return line after deactivation of the solenoid.

611 A repeat of this test for an air gap of 0.6 mm in Fig 6.5(c) shows the effect of having less force available to activate the solenoid. Fig 6.6 shows that with this air gap the maximum force is reduced to about 50 N. When the supply pressure is applied, the blip in the current rise characteristic indicates a switching time of 23 ms after activation. However the return stroke only takes 6.5 ms due to the more rapid decay of the electromagnetic force for larger air gaps.

612 The required switching transient period depends on the PWM frequency used, which in turn is a function of the overall valve desired bandwidth and the amount of demodulation of the PWM signal that is required. For example, a larger demodulation restrictor diameter improves the valve bandwidth, but also demands a higher PWM frequency if the demodulated pressure fluctuation is to be kept at the same level. In practice, PWM frequencies about ten times the desired valve closed loop bandwidth were found to be necessary, thus for example, a 20 Hz valve bandwidth requires a PWM frequency as high as 200 Hz. None of the tests shown in Fig 6.5 are capable of switching anywhere near this fast and alternative solenoid drive methods must be sought.

613 There are three things which can be done to improve the switching speed: firstly, the air gap can be kept small so that large accelerating forces are generated in the armature; secondly, an overdriving amplifier can be used to give a good current response; and thirdly, the solenoid can be constructed so that the eddy current generation during transients is reduced. The last point is important as the generation of eddy currents represents a loss of power, and dynamically a lag in the

build up of the force producing magnetic field. In the research presented here the first two of these options have been pursued, the third option being more difficult to implement as it requires redesign and development of the solenoid components.

614 The overdriving amplifier used to activate the solenoid, was a current feedback device employing a power FET to amplify the PWM drive signal. A circuit diagram of the amplifier is shown in Fig 6.7. The input is a unipolar PWM signal of 15 V amplitude generated by the microprocessor timer chip, which is then passed through an absolute rectifier circuit. An 11 V Zener diode limits the output from this stage to just over 10 V. The PWM signal then passes through an adjustable gain amplifier where the 10 V signal can be modified prior to input to the current feedback circuit. A gain of about 0.2 was used limiting the demanded current to 2.1 A. The current feedback circuit uses feedback from a 1 Ω current sensing resistor placed in series with the solenoid coil. The error between the demand and feedback signals is used by the 741 operational amplifier to generate the gate signal of the power FET, the correct solenoid current being maintained by resistive dissipation in the FET. The high current circuit around the solenoid is supplied from a 50 V power source for overdriving purposes.

615 To activate the valve the current circuit is switched to 2.1 A demand, and the FET opens up allowing nearly 50 V to be applied across the solenoid. This is shown in Fig 6.8(b). The full over voltage is applied until the current has built up to its rated value. Then the current feedback loop increases the FET voltage drop, and as shown in Fig 6.8(b), the 2.1 A current is maintained with a constant 11 V voltage drop across the solenoid. Comparison of Fig 6.8(c) with 6.5 shows that the current builds up far more rapidly using the overdriving amplifier. The slight kink in the voltage characteristic as it drops from 50 V to 11 V is caused by the push rod moving and corresponds to a 2 ms switching time, which is a dramatic improvement compared to the results shown in Fig 6.5.

616 When the solenoid is deactivated, the inductance of the coil causes a high reverse voltage to occur. The FET is protected from this voltage by a 70 V Zener diode connected to the FET gate which limits the overvoltage by turning back on the FET when 70 V is reached. The value of diode chosen is seen in Fig 6.8(c) to give a current decay time similar to the rise time.

617 Whilst the amplifier design used during the research was functionally adequate, its internal power dissipation was high. With the valve on continuously, the total power absorbed was about 115 W, only 22 W of which occurred in the solenoid. This is because the solenoid current was maintained by having a high voltage drop across the FET, thus dissipating large amounts of electrical power. The use of PWM signals gives the opportunity for power saving in the amplifier which greatly reduces the current requirement of the power supply. An alternative circuit still under development is shown schematically in Fig 6.9 [72]. In this arrangement two FET's are used, one connecting the solenoid to high voltage (FET1), and the other to earth (FET2). Both of the FET's are operated either fully on or off thereby dissipating very little power.

618 To activate the solenoid a positive signal is applied at the amplifier input and both FET's are turned on. The solenoid is subject to a high supply voltage, and the current builds up until the current sensing resistor voltage exceeds the reference level input to the comparator. Switching of the comparator then turns off FET1 via an optoisolator thereby turning off the power supply. The current then decays slowly through diode D2. When the current falls below a preset tolerance band, the comparator turns FET1 on again. The current is thus maintained at the correct level by a chopping action due to the switching of FET1.

619 When the input signal goes low, demanding the solenoid be turned off, FET2 is switched off and the comparator input is set high, switching off FET1 also. The voltage at point A falls via Diode D2 to earth, and the voltage at point B rises, reaching just over 50V before discharging rapidly via diode D1 to the discharge capacitor. The electrical energy stored in the coil is thus returned to the supply rather than dissipated. In this valve drive design, the largest source of power dissipation both during on time and switching transients, is the unavoidable power loss in the valve coil itself. The total power loss is less than one third of that in the previous amplifier design.

6.4 Pulse Width Modulated Pressure Control

620 The PWM drive signal was generated using a S6840 programmable timer chip interfaced to the Darkstar microcomputer. This timer has three 16-bit binary counters which can be controlled in various ways by writing data to the

corresponding counter control register [73]. PWM signals of variable frequency and SMR were obtained using two counters as shown in Fig 6.10. The basic PWM frequency is obtained by setting up the control register of timer 2 for continuous operation, and then writing the correct number of clock pulses P, to the counter. The counter then outputs a square wave, P pulses high, and then P pulses low. Timer 1 is set up in the 'single shot' mode, ie stay high for a programmed number of pulses H, then go low indefinitely until a reset pulse is received, and then repeat the process. The negative going edge of timer 2 output is used as the reset for timer 1, thus every PWM period the output of timer 1 goes high for H out of 2P clock periods. The SMR of this PWM signal can be changed simply by writing a new value of H to the counter of timer 1. The sixteen bit counter registers give very good resolution, for example, at a PWM frequency of 150 Hz, the SMR can be set within +/- 0.01 % of the desired value.

621 Considering the valve switching results of the previous section, the choice of PWM frequency is a compromise between obtaining a good valve bandwidth at high PWM frequencies, or reducing the nonlinear effect of the switching transient by operating at a lower frequency. For example, in Fig 6.8(d), neither the pressure rise nor fall are complete until about 6 ms after the demand signal has switched, thus if the time to reach full value is used as a constraint, a maximum PWM frequency of 83 Hz is obtained. At 20 Hz, more time is allowed with the valve at rest (see Fig 6.8). However using a 0.32 mm diameter demodulation restrictor, it can be seen in Fig 6.8(e) that insufficient demodulation occurs, and a higher frequency is required. The maximum possible PWM frequency is obtained by having a minimal rest period, and since in Fig 6.8 the switching time is about 2 ms, a maximum frequency of 250 Hz can be obtained. However, as soon as the SMR is changed from 0.5, then an impossible switching period of less than 2 ms is demanded. Thus increasing the frequency too high reduces the range of SMR which can be used. After initial experimentation a frequency of 150 Hz was chosen and this was found to give a range of SMR from 0.3 to 0.75. The nonlinear effect of the switching transient was tolerated in the design.

622 Pressure traces both upstream and downstream of the demodulating restrictor for different SMR values are shown in Fig 6.11. At a ratio of 0.3 the valve is activated for only 2 ms and in this period the ball only just closes off the high pressure seat in time before the solenoid is deactivated and the solenoid is opened up

again. Thus even before passing through the demodulation restrictor the pressure only falls to about 110 bar before increasing back to 150 bar. At an SMR of 0.4 the pressure falls to about 30 bar before rising again to 150 bar, and at an SMR of 0.5 it reaches neither extreme. Thus it is seen that the pressure is partly demodulated even before passing through the demodulation restrictor.

623 As the SMR is increased beyond 0.5 the same effect is seen to occur at the low pressure end of the range, for example at an SMR of 0.75, the pressure does not have time to reach more than a fraction of its full value before the valve switches and it returns back to zero. Beyond an SMR of 0.75 the valve failed to switch at all.

624 When the poppet is held closed, the effect of the demodulating restrictor on the ball valve pressure output depends on the size of restrictor used, and the stiffness of the trapped volume of oil between the restrictor and the back face of the poppet. Increasing the volume would reduce the stiffness and slow down the pressure rise time, thus allowing the use of a larger restrictor diameter whilst maintaining the same degree of pressure demodulation. For the valve under investigation a restrictor size of 0.32 mm diameter was chosen by trial and error to obtain a compromise between the valve dynamic response, and the amount of demodulation obtained.

625 The effect of the choice of restrictor on the valve dynamic performance is discussed in the next section, and here, in Fig 6.12, the demodulated pressure signals are displayed. The mean level of pressure is seen to be dependent on the SMR, giving a degree of proportionality. However even with a 0.32 mm diameter restrictor, peak to peak pressure fluctuations as high as 20 bar occur in the worst case. The use of a still smaller restrictor would increase the contamination sensitivity of the valve and reduce the dynamic performance. When the valve is operated normally with the poppet off its seat, these pressure fluctuations are reduced due to interaction with the poppet. The poppet is made to dither about a mean position. To some extent this effect is desirable, as a small amount of dither helps to remove hysteresis problems.

626 The mean value of pressure is plotted against the SMR in Fig 6.13, and it can be seen that the characteristic does show reasonable proportionality within the SMR

range 0.3 to 0.75. The restrictions on the SMR limit the available mean servo pressure from between 20 and 145 bar. The low pressure end of the range is higher than would be desired, as this corresponds to a poppet main flow pressure of around 40 bar minimum. To increase the lower end of the pressure range, a higher SMR is required which can only be achieved by using a faster switching device or reducing the PWM frequency.

627 The characteristic shown in Fig 6.13 can be modelled in the same way as the proportional pressure control valve was in section 5.5, the rest of the flow control valve models remaining unchanged. The microprocessor would be employed in the same way as in Chapter 5 to calculate the internal pressures and flow through the poppet valve, any one of these signals being used as feedback. More significant is the effect of PWM dynamically on the overall closed loop response, and this is discussed in the following section.

6.5 Closed Loop Control

628 In order to derive a closed loop Pole Placement controller for the PWM operated valve, a knowledge of the overall valve transfer function is required. Previously a second order model was used, but now with the new pilot stage the choice of model must be reconsidered. An appreciation of the pilot valve dynamics can be obtained by noting the pressure traces in Fig 6.12 where the change in pressure appears to be exponential in form, the rise in pressure aiming at 150 bar and the fall at 0 bar. It is seen that the rate of rise and fall depends on the mean pressure. At an SMR of 0.5 the rise and fall rates are about the same, however at higher mean pressure levels the rise in pressure is at a reduced rate and the fall at an increased rate, and vice versa for a low mean pressure level. This effect also influences the amplitude of pressure fluctuation, the worst amplitude occurring at an SMR of about 0.5.

629 The shape of the pressure traces can be explained by considering the flow through the demodulating restrictor into the chamber behind the poppet, volume V_d, (see fig 6.1). Assuming no poppet movement and taking small perturbations, the restrictor flow equation is :

$$q_d = C_d (p_s - p_d) = \frac{V_d}{\beta} s p_d \qquad (6.1)$$

Where the flow gain: $C_d = \frac{\partial Q_d}{\partial P_s}$

is assumed constant for small changes about a mean operating pressure.

Now since from the orifice equation, for $P_s > P_d$:

$$Q_d = C_q A_d \sqrt{\frac{2(P_s - P_d)}{\rho}}$$

then the flow gain:

$$C_d = \frac{C_q A_d}{\sqrt{2\rho(P_s - P_d)}} \tag{6.2}$$

In a PWM system the effective value of C_d is easier to calculate than for a conventional proportional system. For a proportional system, small perturbations demand that the restrictor pressure drop $P_s - P_d$, tend to zero, and this gives an infinite flow gain. In a PWM system there is always an appreciable pressure drop first one way and then the other, and a mean value of flow gain can be calculated. Rearranging equation 6.1 gives the pilot valve transfer function:

$$\frac{P_d}{P_s}(s) = \frac{1}{1 + \frac{V_d}{\beta C_d} s} \tag{6.3}$$

The time constant:

$$T = \frac{V_d}{\beta C_d} \tag{6.4}$$

is thus dependent on the trapped oil volume, the oil compressibility and the restrictor size.

630 Equation 6.3 shows that demodulation occurs because of the natural attenuation of the oil compressibility lag. The equation also governs how fast a step change in the mean pressure can occur, and hence the valve bandwidth. If for example the mean pressure is to be increased, then even leaving the valve fully

deactivated, ie SMR = 0, the pressure rise would be no quicker than that governed by equation 6.3. The frequency response plot shown in Fig 6.14, indicates a first order transfer function, as expected. The test was carried out changing the SMR sinusoidally about a mean value of 0.5. A first order model fit to the plot gives a -3 dB bandwidth of 15 Hz, which is one tenth of the PWM frequency.

631 A first order model for the pilot valve, combined with the integral action of the poppet, leads to a second order transfer function of the form:

$$\frac{y}{e}(s) = \frac{K}{s(1+Ts)} \tag{6.5}$$

In this equation, y represents the digitised value of the poppet position measurement, and e the digitised value of the drive signal. This is the same nomenclature as used in the discrete block diagram representation described in section 3.4. The overall open loop frequency response plot of the valve is shown in Fig 6.15, and is seen to be very similar to that obtained using the proportional pilot valve shown in Fig 5.5. A similar nonlinear depression also occurs around the break point frequency (see section 5.3). This effect is neglected in the controller design, and the linear model of equation 6.5 is fitted to the frequency plot.

632 Great care must be taken when fitting the model to ensure that the correct gain is used in the s to z transformation. For controller design, the discrete model must be a transfer function with digital input/output signals as seen by the microprocessor. However the frequency plot was obtained using analogue signals at the microprocessor interface, and unlike previous occasions, the input and output gains for the converting devices were not the same. The arrangement used during the frequency test is shown in block diagram form in Fig 6.16. The digital input signals u and y seen by the microprocessor are the same as before, ie the digital value being obtained by multiplying the voltage by 200. For example, the feedback signal:

$$y = 200V_y \tag{6.6}$$

633 The poppet LVDT amplifier had a 0 to 10 V output range, giving a maximum value of y of 2000, thus the maximum error signal, assuming a unity forward path gain, was also 2000. Thus the SMR was chosen to be generated by dividing the

current e value by 2000, ie:

$$SMR = \frac{e}{2000} \tag{6.7}$$

The drive signal is no longer output via a D/A, but the SMR value is written to the timer chip, which is updated every sample period, (ie every 5 ms). However, the frequency plot of Fig 6.15, was obtained by measuring the analogue voltages V_y and V_e, where:

$$V_e = 10SMR \tag{6.8}$$

The relationship between y and e as seen by the microprocessor can be found from equations 6.6 to 6.8:

$$\frac{y}{e} = \frac{V_y}{V_e} \tag{6.9}$$

Thus with the control system arrangement as shown in Fig 6.16, the measured frequency response plot of Fig 6.15 is as seen at the microprocessor interface, (ie, using the y and e signals). Fig 6.15 was thus used directly in the controller design with no gain adjustment.

634 The model of equation 6.5 was fitted to the frequency plot using a lag time constant of 9.4 ms, and for the discrete model a sample period of 5 ms gives the Pole/Zero Mapping discrete transfer function:

$$\frac{y}{e}(z) = \frac{0.15(1+z^{-1})z^{-1}}{(1-z^{-1})(1-0.587z^{-1})} \tag{6.10}$$

635 If the loop is closed using this transfer function, with a unity feedback controller implemented, the theoretical characteristic equation roots are: z = 0.72 +/- j0.4. Plotting these roots on the root locus diagram of Fig 4.1, yields a natural frequency of 18 Hz, and damping ratio 0.3. This corresponds well with the measured uncompensated closed loop step response shown in Fig 6.17(a). Superimposed on the natural oscillations due to the root positions, is the much higher 150 Hz PWM frequency. The flow pulsations on the back face of the poppet are seen to cause the poppet to dither with a peak to peak amplitude of about 0.1

mm.

635 The 5 ms sample period used in the controller corresponds to an aliasing frequency of 100 Hz. Thus the prominent 150 Hz PWM frequency was reflected into the lower frequency range. This problem was resolved by using a two pole antialiasing filter which was available on the Darkstar. The filter was set up to have a natural frequency of 75 Hz and damping ratio 0.7, giving a flat frequency characteristic having a -3 dB bandwidth of 87 Hz. This attenuated the 150 Hz signal by 12 dB. If an antialiasing filter bandwidth significantly less than this had been used, then it would have been necessary to include the filter dynamics in the valve model.

636 A good closed loop controller design was obtained using integral action control in the same manner as described in section 5.4, with desired closed loop root positions chosen at z = 0.7 +/- j 0.0. The measured closed loop step response with this controller implemented is shown in Fig 6.17(b), and it is seen that integral action control has been achieved whilst removing the undesirable oscillations. The closed loop frequency response plots for both the compensated and uncompensated control loops are shown in Fig 6.18. It can be seen that the compensating controller removes the resonant peak, but this is achieved whilst reducing the overall -3 dB bandwidth to 15 Hz.

6.6 Conclusions and Recommendations

637 The preceding sections have shown that using a simple three port ball valve driven by an on/off solenoid, proportional pressure control can be achieved. Compared with the more conventional proportional pilot valve used in the valve of Chapter 5, the on/off valve is simpler in construction, and hence can be produced at reduced cost. The on/off action also helps to reduce the effects of contamination and eliminates hysteresis errors. However, other errors are introduced, for example, the consistency of the pressure versus SMR characteristic (see Fig 8.13) depends on the supply pressure being constant, and on the amount of long-term variation of the switching characteristics as the valve wears. These potential problems must be the subject of further investigation.

638 Dynamically, the pilot valve performance is dependent on the PWM frequency,

and for the valve in question a 150 Hz PWM frequency gave a bandwidth of about 15 Hz. Further improvements in bandwidth would require an increase in the size of demodulating restrictor, and a corresponding increase in the PWM frequency to reduce the fluctuation of the main flow poppet. The ball valve assembly and solenoid used in the pilot valve were chosen because of their availability, reducing the amount of in house manufacturing required. The complete pilot valve was larger than necessary to provide the required flows. A smaller valve arrangement would have allowed faster switching times and a consequent increase in performance.

639 Further switching speed improvements can be made by using larger overdriving voltages in the amplifier, and also allowing initial overdriving of current to accelerate the armature. This must be accompanied by modifications to the solenoid construction so that eddy current losses during switching transients are minimised, thus ensuring a rapid build up of flux and hence of the electromagnetic forces. Even greater improvements in switching speed may be obtained by considering alternative electromagnetic conversion devices, for example, torque motor or force motor constructions.

640 A significant problem limiting the application of PWM in valve design is that of noise, and the related problem of wear. This is especially a problem when positive seating elements are used as in this study. The noise was caused principally by the high frequency impacts of the ball on the valve seat. Generally this can be minimised by shaping the current pulse generated by the amplifier so that the large activating force is reduced just prior to reaching the valve seat. Noise would also be reduced by the use of smaller, faster acting devices.

641 In the test valve, wear and brinelling was seen to occur on both of the valve seats, and the push pin. After about 2 million cycles the combined effect of wear in all of the components had caused a 0.25 mm reduction in the air gap (see Fig 6.2). After this initial settling period, very little further wear was observed. The final state of the valve seats and push pin after completion of the tests can be seen in Fig 6.19.

Fig 6·1

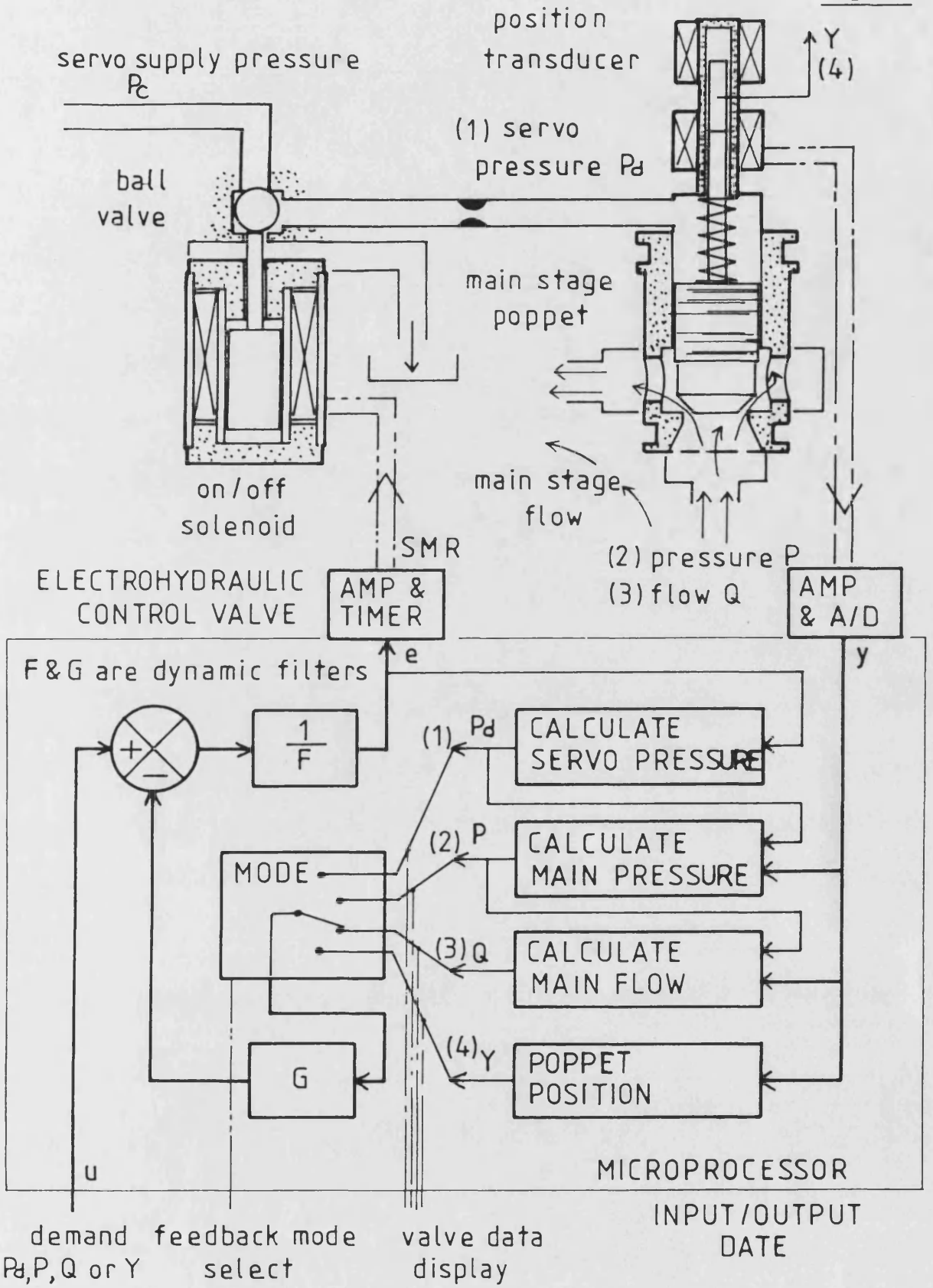

6·1 PWM DRIVEN FLOW CONTROL VALVE

Fig 6·2

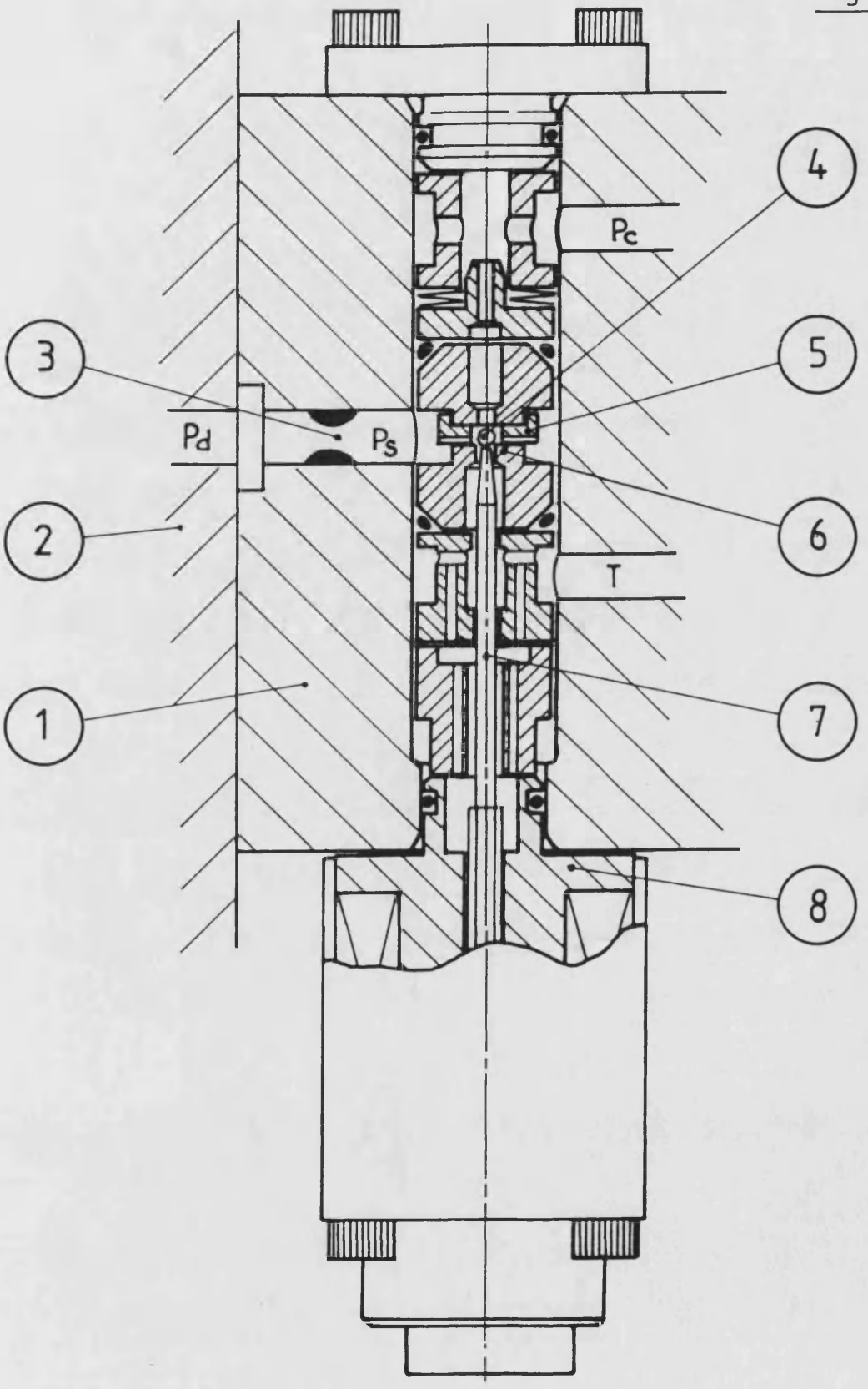

6·2 DIGITAL PILOT VALVE ASSEMBLY

DRAWING ~ SCALE 2:1

Fig 6·3

PART N°	NAME	COMMENTS
1	PILOT VALVE BLOCK	
2	MAIN VALVE BLOCK	
3	DEMODULATING RESTRICTOR	diameter 0·32 mm
4	BALL	diameter 1·587 mm (1/16 in)
5	SEAT SPACER	ball travel 0·3 mm nom
6	VALVE SEAT	diameter 1·32 mm
7	PUSH PIN	
8	ON/OFF SOLENOID	ref [71] 12 V dc 2·4A max

6·3 PARTS LIST FOR FIG 6·2

Fig 6·4

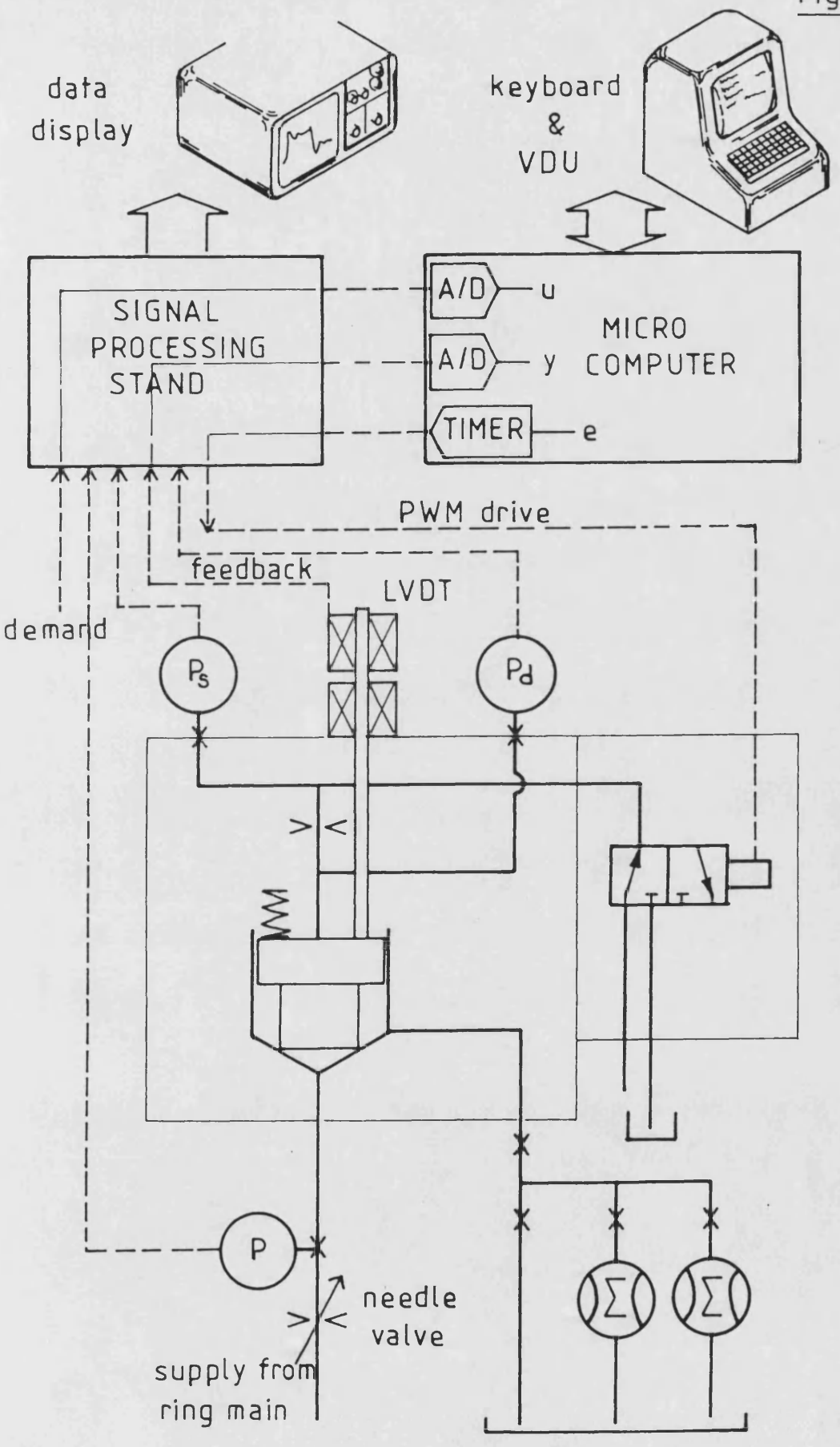

6·4 TEST RIG LAYOUT

Fig 6·5

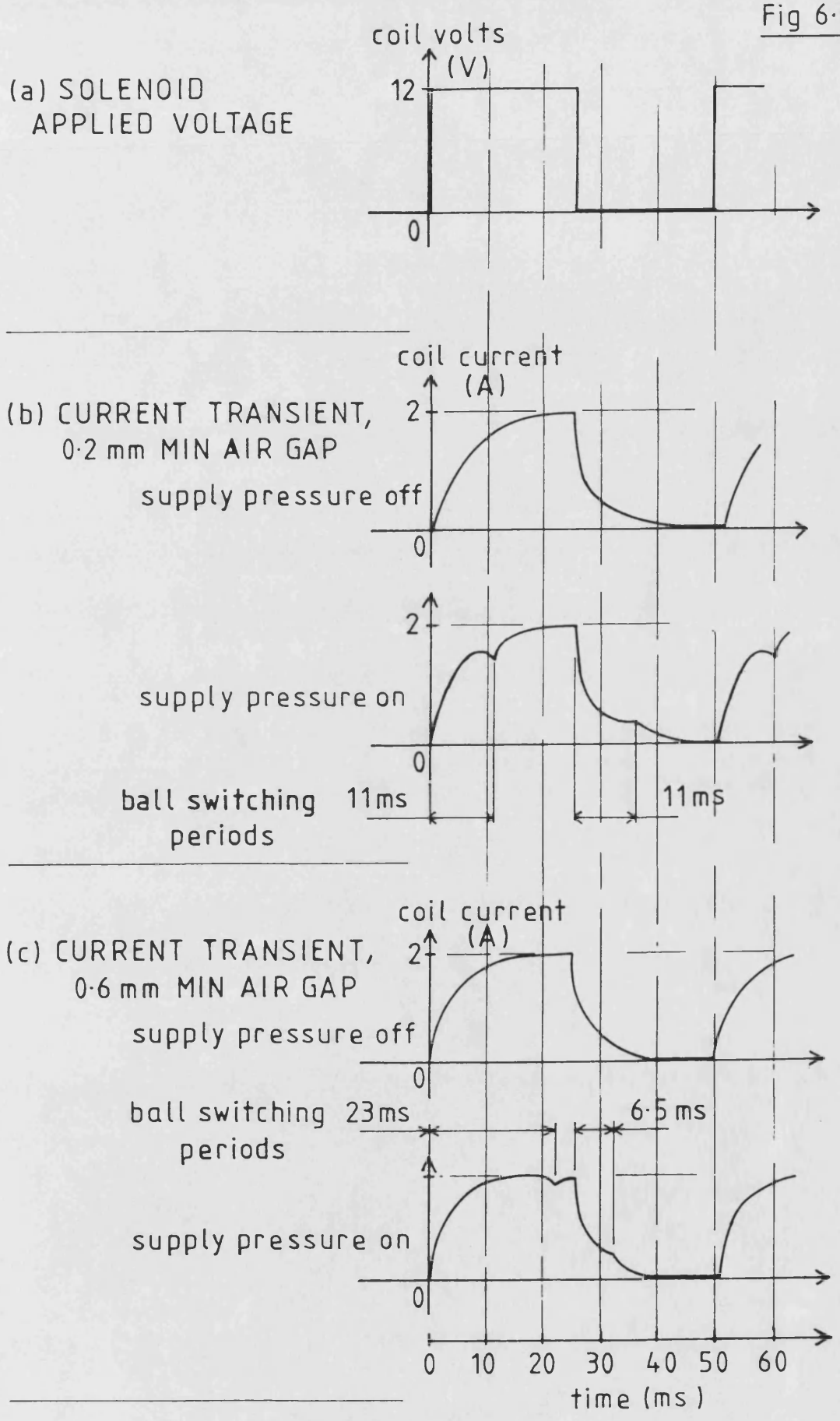

6·5 SOLENOID 12V SWITCHING TRANSIENTS

Fig 6·6

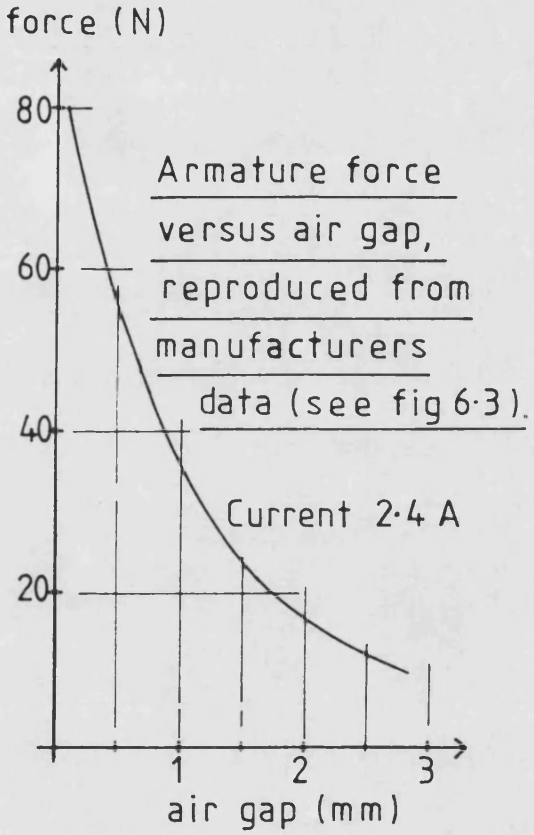

6·6 SOLENOID FORCE CHARACTERISTIC

Fig 6·7

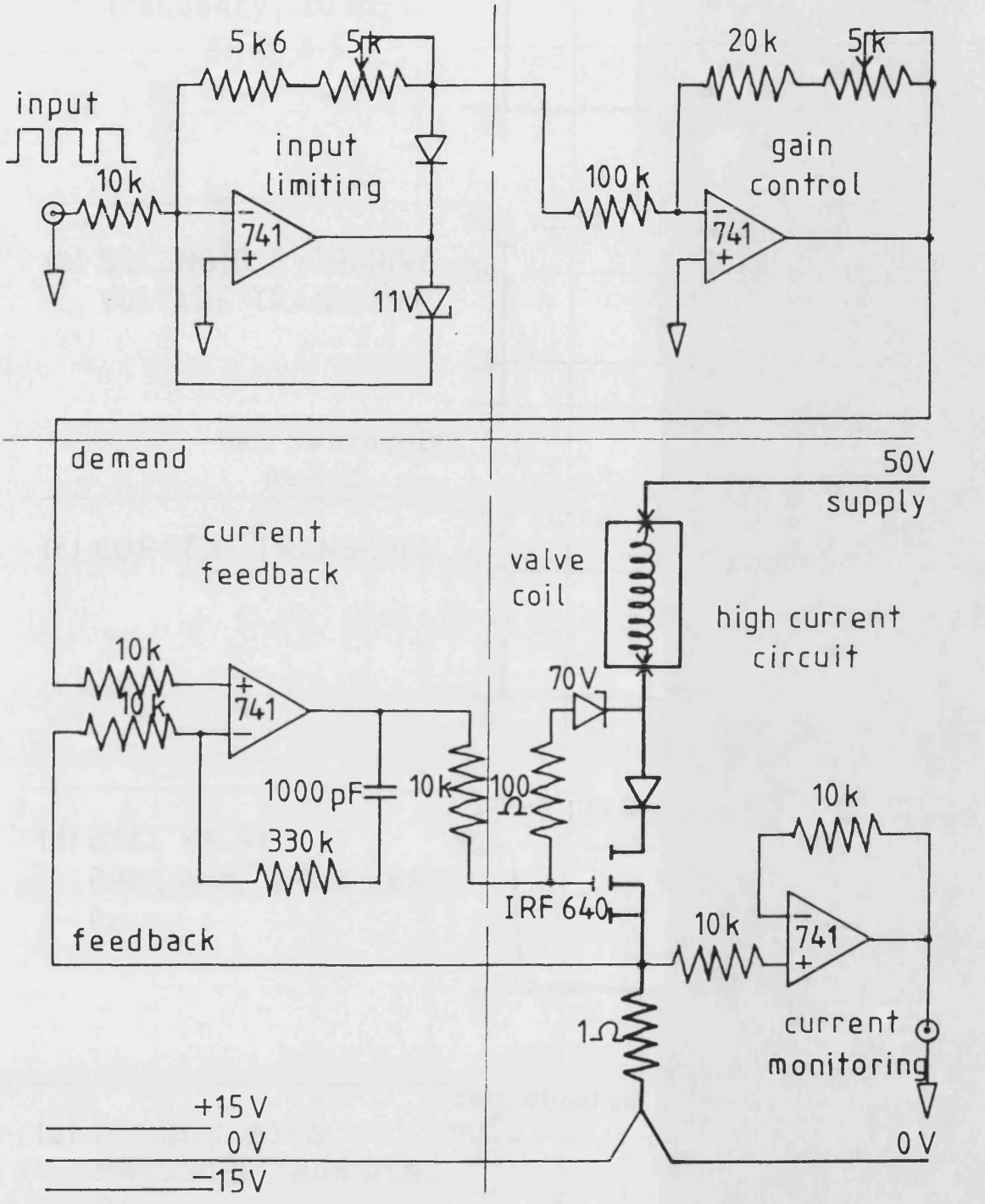

6·7 PWM VALVE DRIVE CIRCUIT DIAGRAM

Fig 6·8

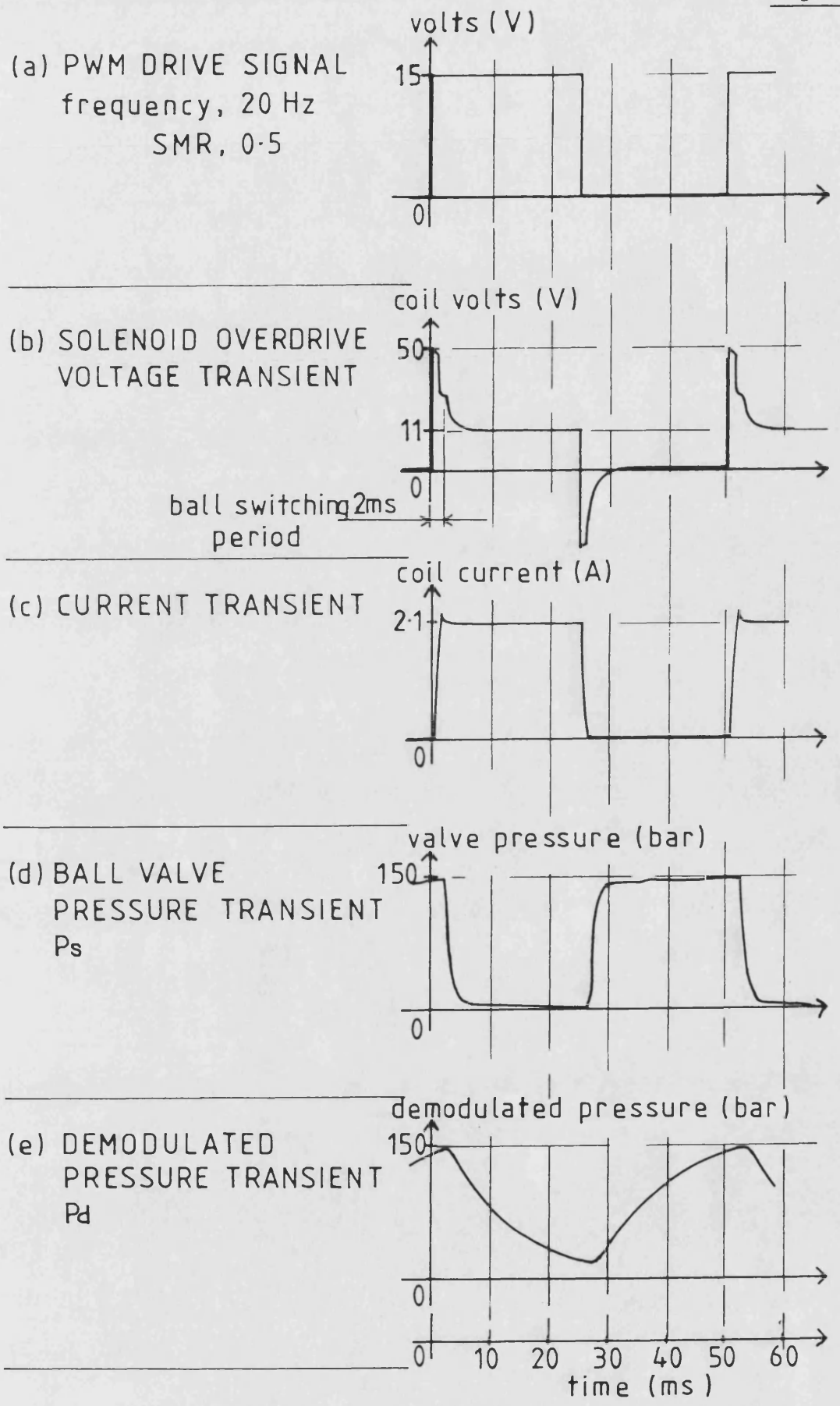

6·8 OVERDRIVE SWITCHING TRANSIENTS

Fig 6·9

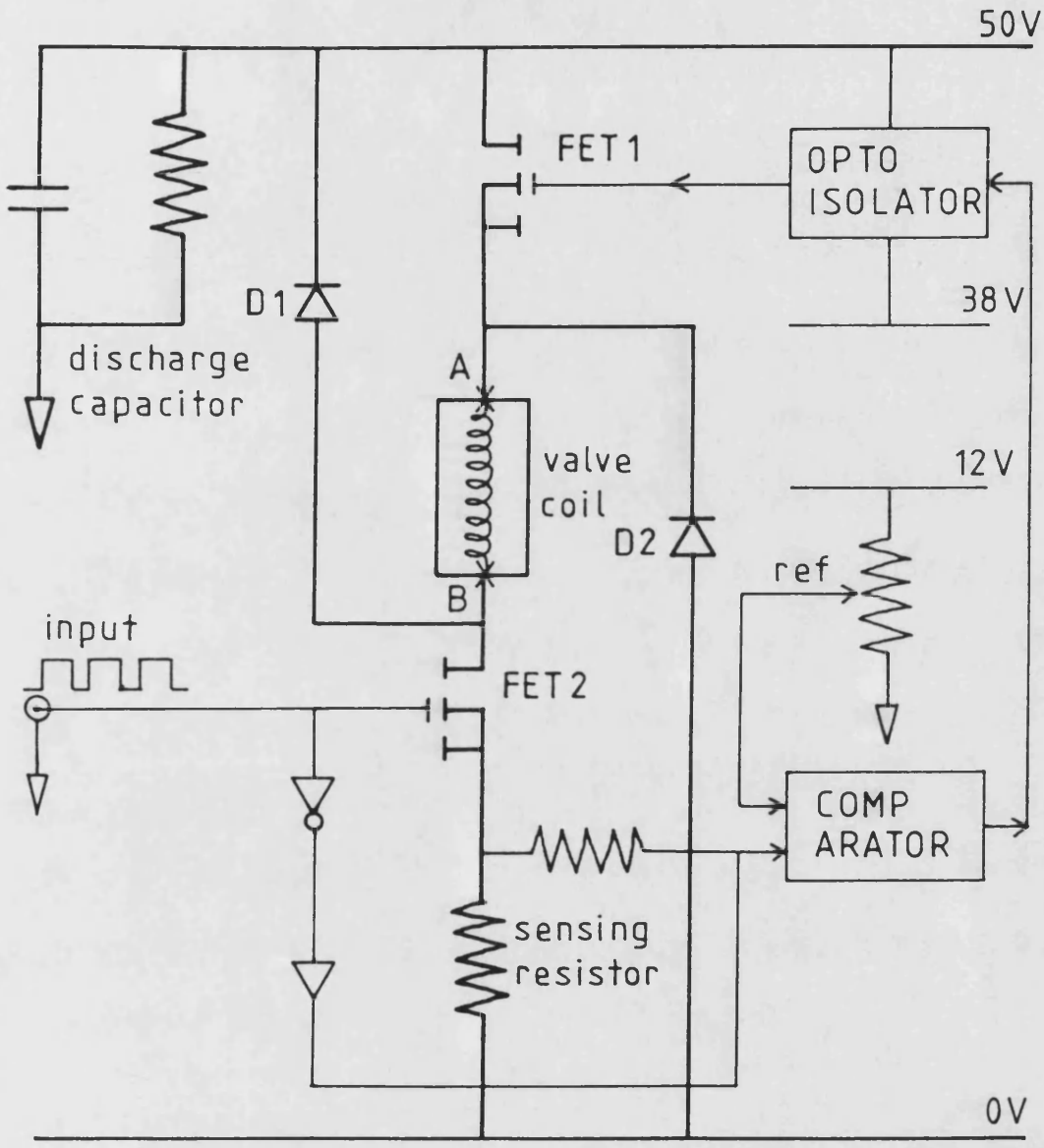

6·9 LOW POWER PWM VALVE DRIVE CIRCUIT DIAGRAM

Fig 6·10

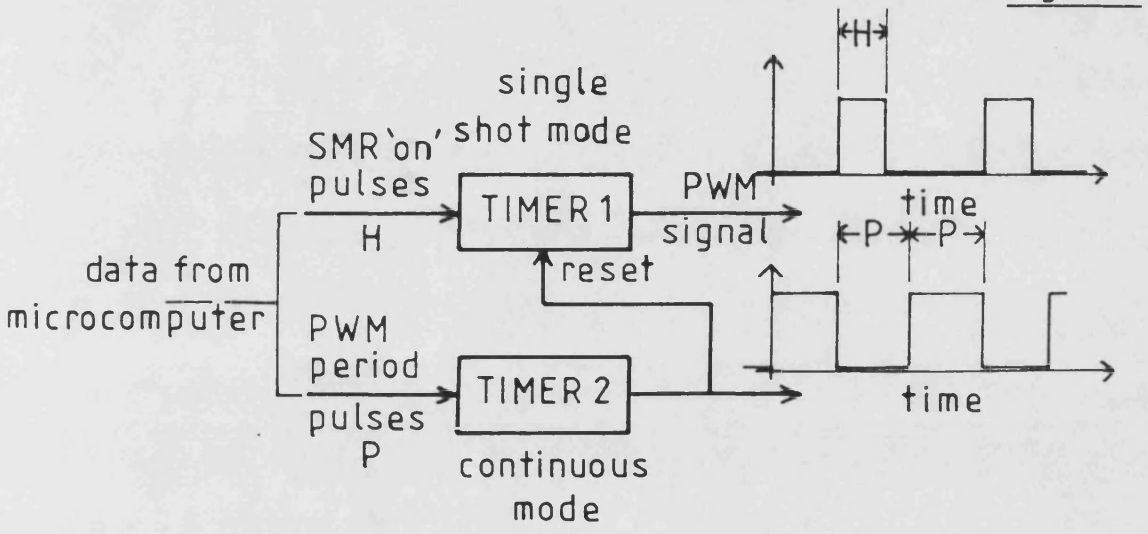

6·10 S6840 TIMER SET UP FOR PWM

Fig 6·11

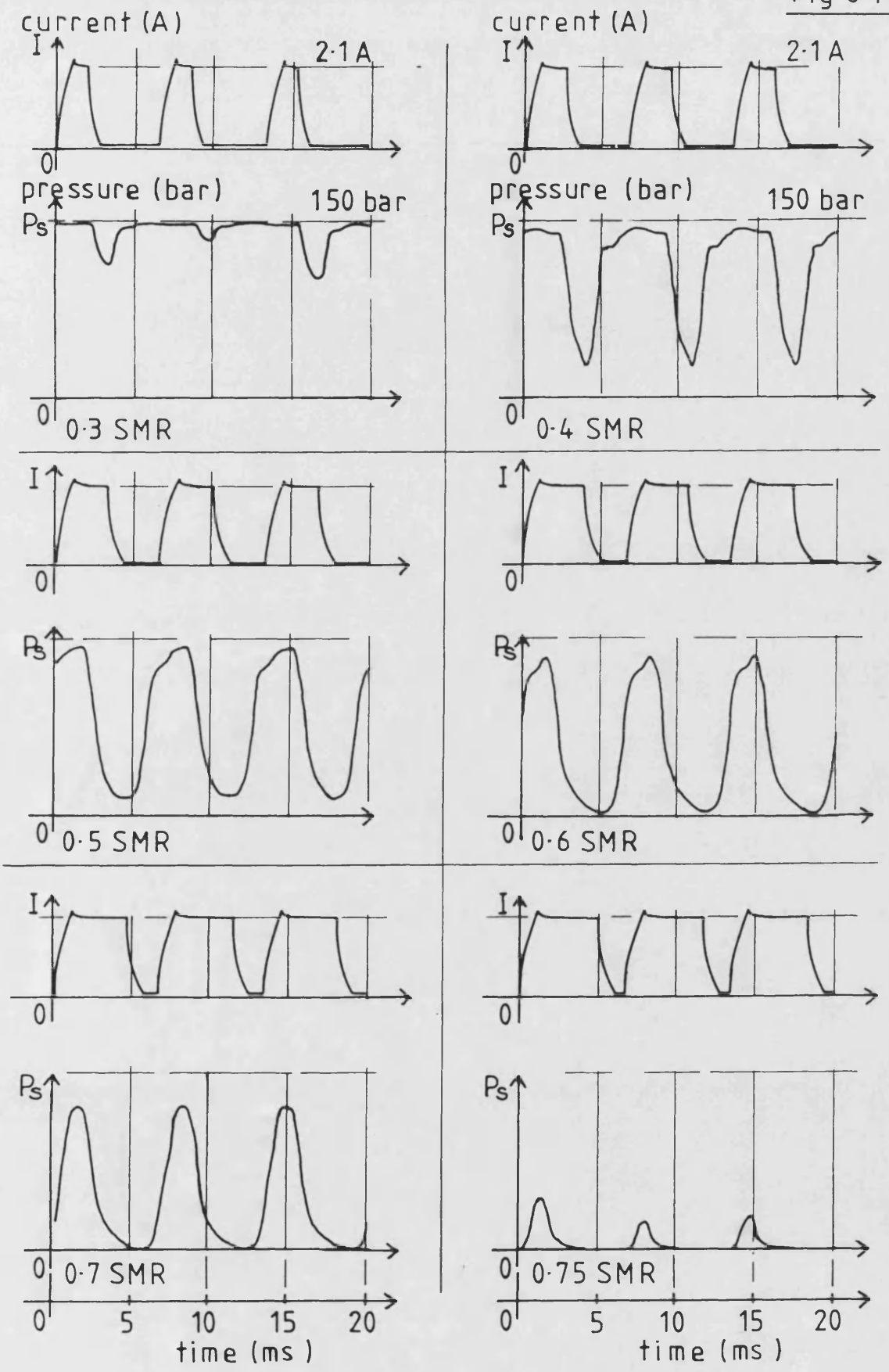

6·11 BALL VALVE PWM CURRENT AND PRESSURE WAVEFORMS

Fig 6·12

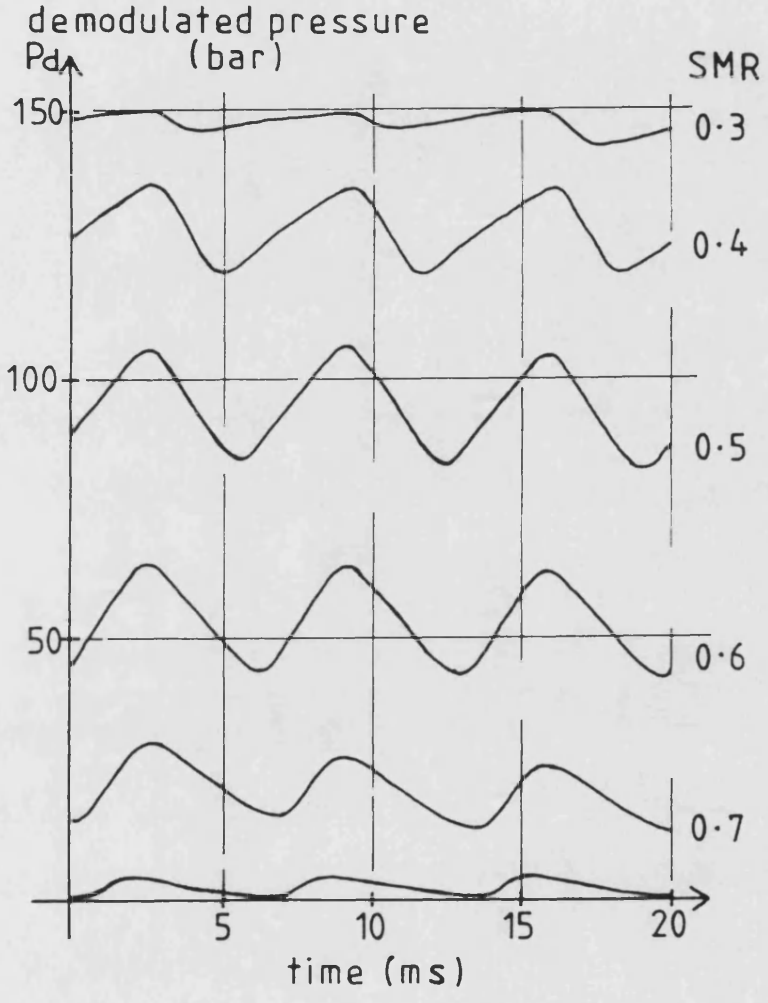

6·12 DEMODULATED PWM PRESSURE WAVEFORMS

Fig 6·13

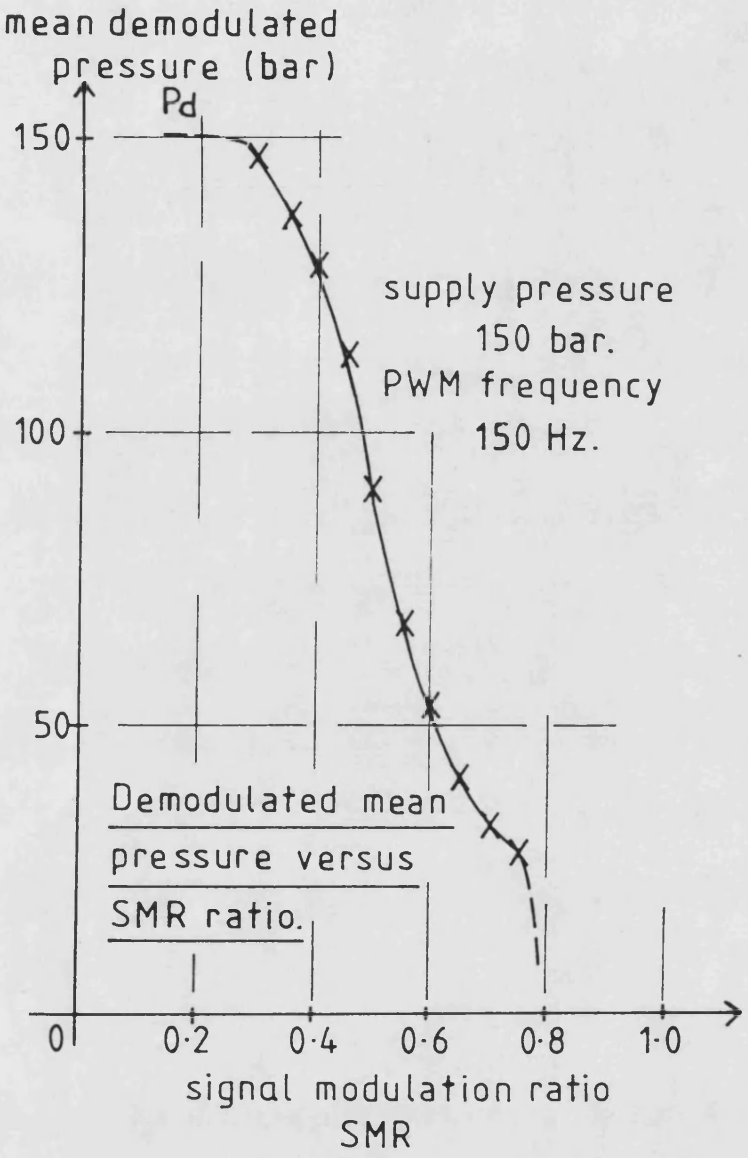

6·13 PWM PILOT VALVE CHARACTERISTIC

Fig 6·14

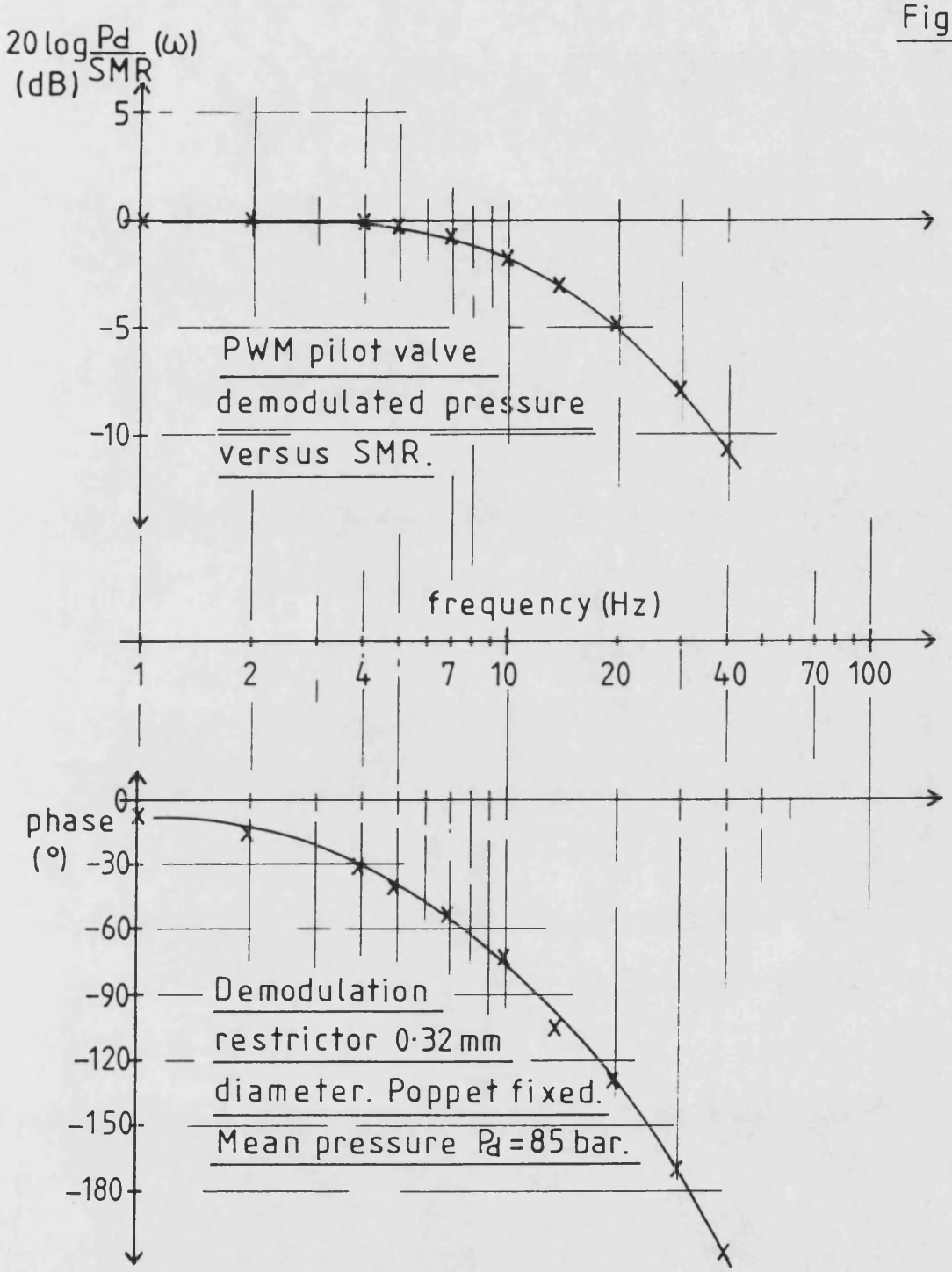

6·14 PWM PILOT VALVE FREQUENCY RESPONSE

Fig 6·15

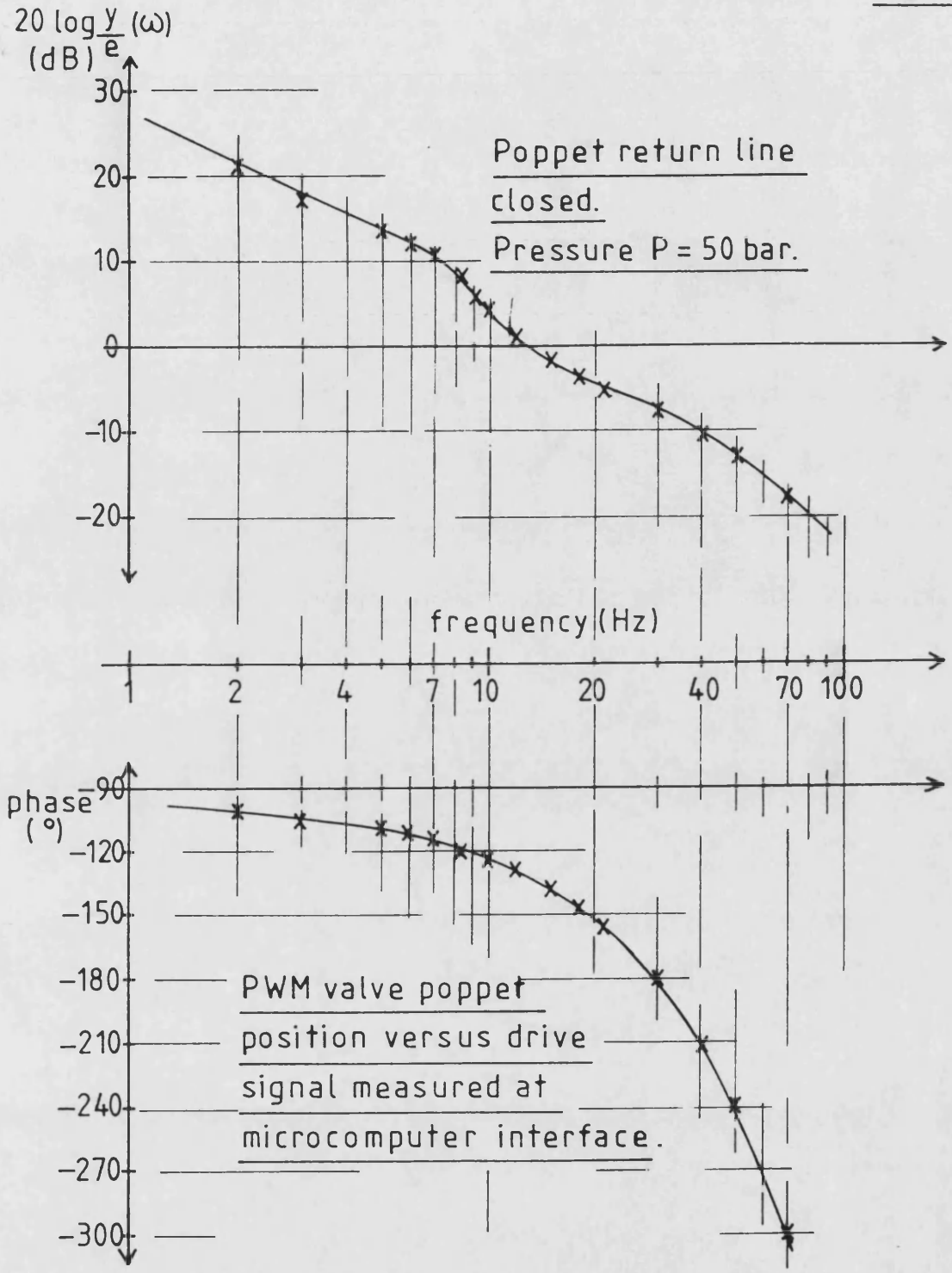

6·15 OVERALL PWM VALVE OPEN LOOP FREQUENCY RESPONSE

Fig 6·16

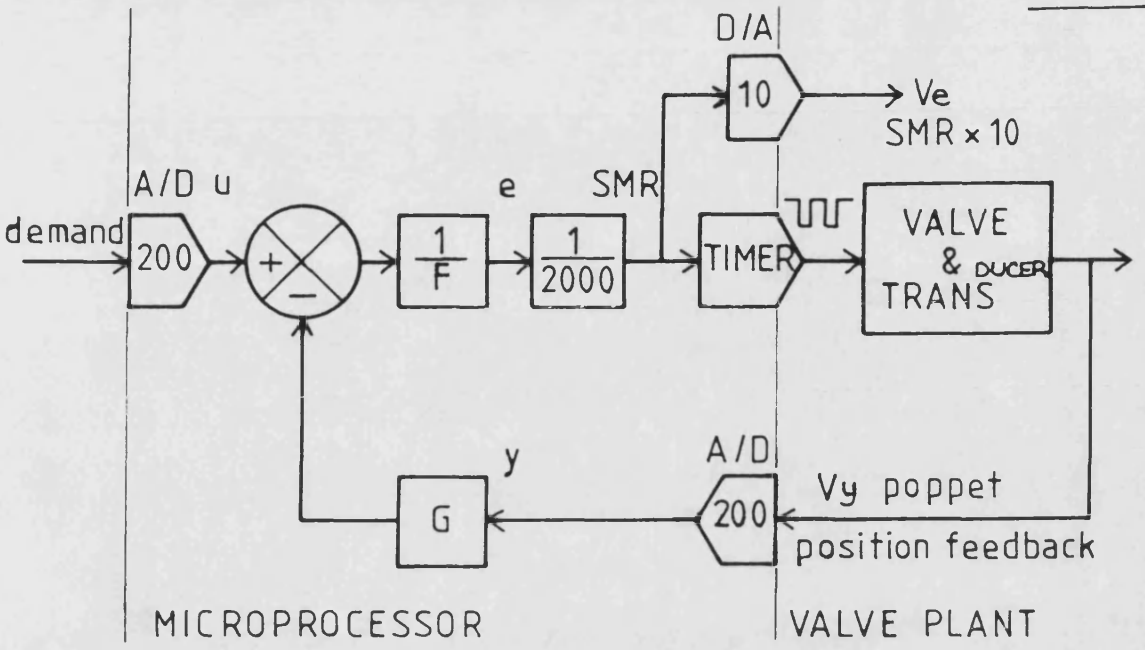

6·16 PWM VALVE CLOSED LOOP BLOCK DIAGRAM

Fig 6·17

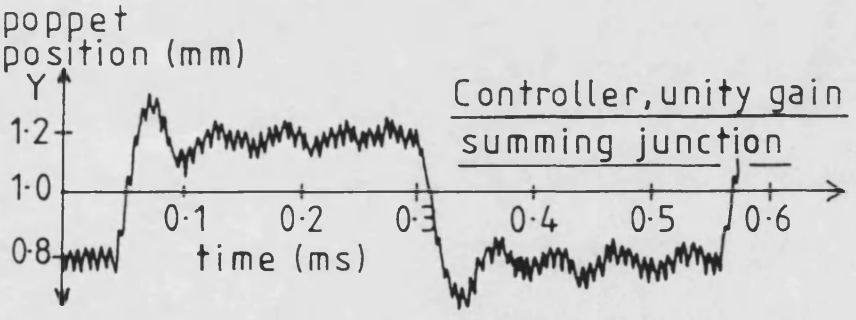

(a) UNCOMPENSATED STEP RESPONSE

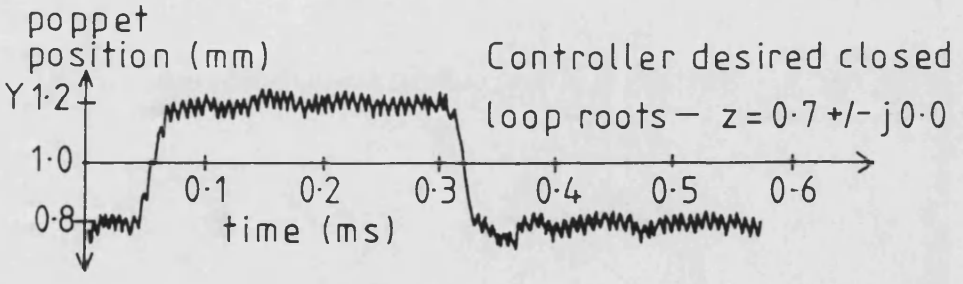

(b) COMPENSATED STEP RESPONSE

6·17 OVERALL PWM VALVE STEP RESPONSES

Fig 6·18

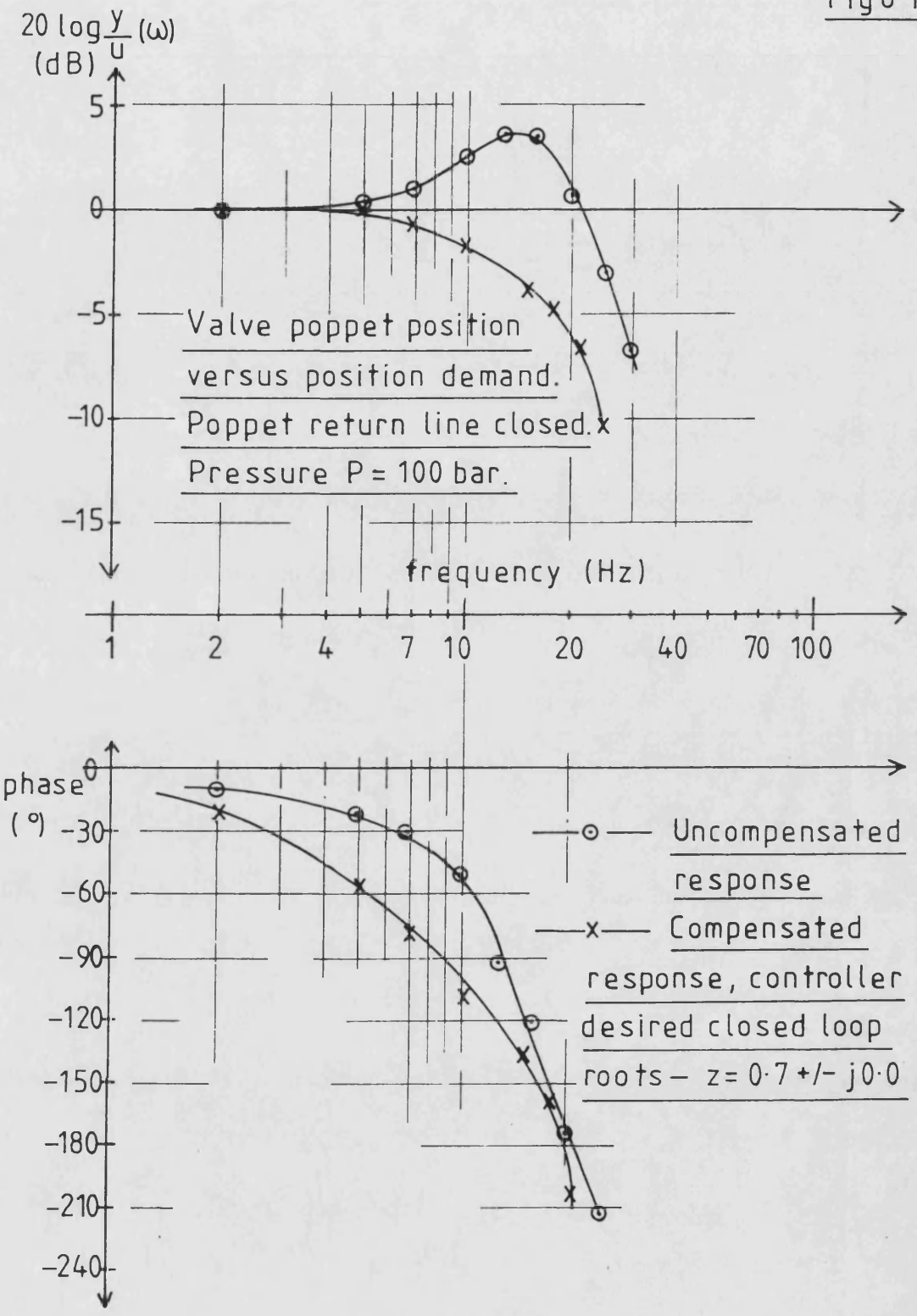

6·18 OVERALL PWM VALVE CLOSED LOOP FREQUENCY RESPONSES

Fig 6·19

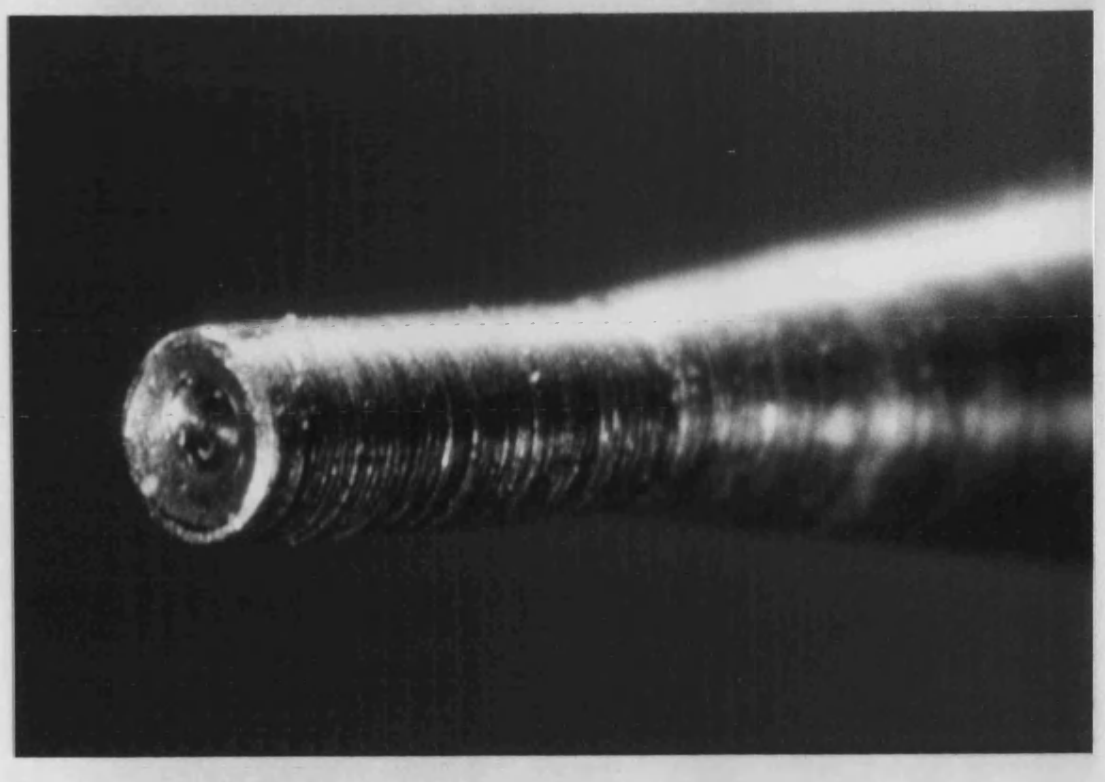

(a) CONCAVED END OF PUSH ROD

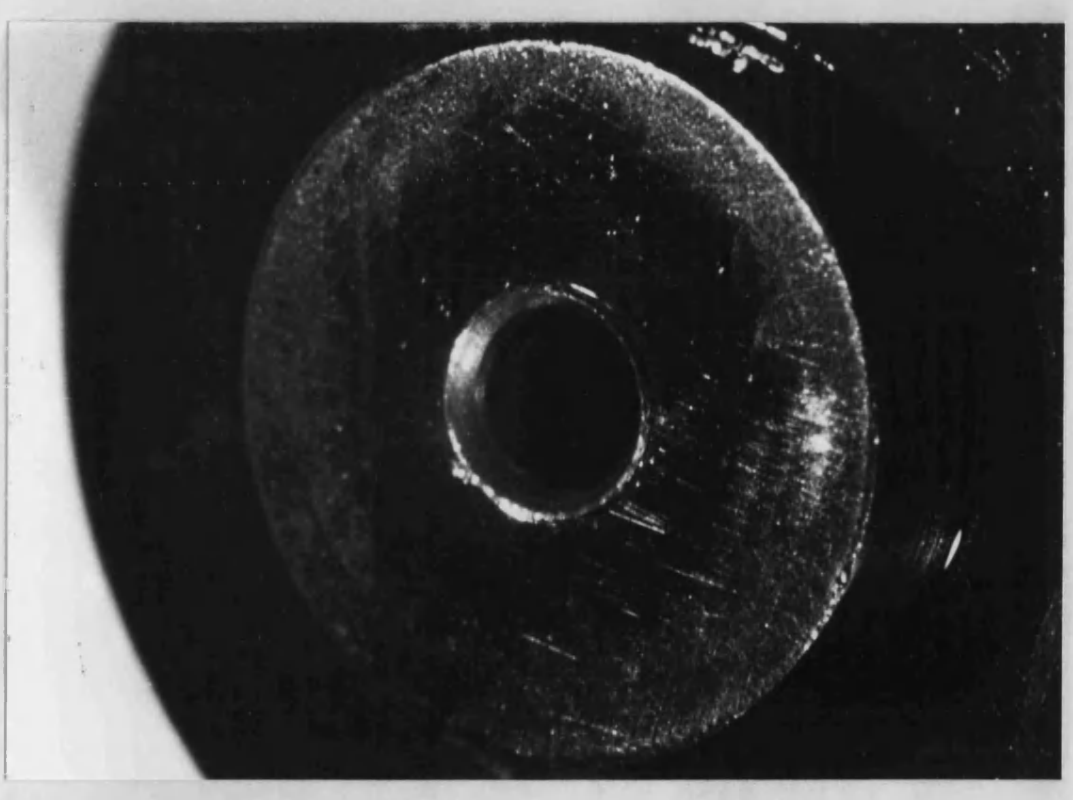

(b) DEFORMED VALVE SEAT

6·19 BALL VALVE SEAT AND PIN WEAR

7. ELECTROHYDRAULIC SERVOSYSTEM CONTROL

7.1 Introduction

701 An introductory discussion concerning electrohydraulic servosystems was presented in section 1.2, and closed loop microprocessor control was suggested as an alternative technique for improving the performance and flexibility of these devices. More specifically, it was claimed that in servosystems with naturally oscilliatory dynamic characteristics where derivative feedback is necessary, the microprocessor can be used to generate the appropriate feedback signal internally without any need for expensive feedback transducers. The methods used in achieving this end, based on classical control techniques and the Pole Placement method, were discussed in Chapters 3 and 4.

702 In the following chapters the feasibility of digital closed loop control techniques are demonstrated by application to an electrohydraulic cylinder drive, used to position a large load inertia. As is often the case with such systems highly oscillatory dynamics are exhibited, requiring the use of compensation in the closed loop controller to achieve a good dynamic response. The servosystem test rig layout is presented in section 7.2, and a number of deliberately introduced nonlinear characteristics which commonly occur in electrohydraulic systems are described. These have been included to test the robustness of the linear Pole Placement controller design method, and to show how these effects can be eliminated using nonlinear controller designs.

703 The servosystem dynamic equations are investigated in section 7.3, and the effects of the nonlinearities considered. This leads to an approximate linear model representation of the plant for use in controller design. The use of the Pole Placement method in designing a linear controller is discussed in section 7.4, and its application to the servosystem demonstrated both from step and frequency response plots, and by use of the root locus diagram. In section 7.5 the undesirable effects of nonlinearities inherent in the cylinder drive are presented, and the so called 'inverse filter' introduced, which improves both the steady state and dynamic closed loop performance. The disturbing effects of external time variable nonlinearities, such as change in the load inertia are investigated in section 7.6, and a linear controller is shown to be inadequate in these situations. External load disturbances which act on

the plant are shown in section 7.7 to be eliminated by integral action control, and the integral action Pole Placement method is used to design a controller for this purpose. The overall closed loop frequency responses before and after the use of compensation are compared in section 7.8, demonstrating clearly the advantages of the closed loop microprocessor controller.

7.2 Electrohydraulic Position Control System Test Rig

704 The accurate rectilinear positioning of a large inertia load over a wide range of stroke is a common requirement which can be met either by hydraulic or electrical actuation. However in the past the electrohydraulic solution has not always been favoured, and this in part is due to the troublesome dynamics associated with such systems. The low frequency underdamped oscillations which sometimes occur, arise from the interaction of the high inertia load with the compressibility of the oil in the cylinder [59]. If the natural frequency of oscillation is in the lower frequency range, then the forward path gain of the uncompensated closed loop system must be kept low to prevent excessive closed loop oscillation. Consequently the resulting bandwidth may then be inadequate and an alternative way of damping down the oscillations must be sought.

705 There are a number of mechanical solutions to the problem, all of them depending on dissipative effects to increase the damping and reduce oscillations [74]. However these methods often achieve the desired result by compromising the closed loop steady state accuracy and stiffness. Alternatively, compensating methods using velocity and acceleration feedback to an analogue controller work successfully [14], but require the use of extra transducers to provide the feedback signals. The generation of derivative feedback signals using electrical networks are prone to excessive amplification of high frequency noise, and for this reason their practical use is often restricted to the first derivative of the signal only. The most recent and most attractive solution is to use a closed loop microprocessor controller. In addition to eliminating the need for extra transducers by generating feedback signals internally, the microprocessor also introduces a great degree of flexibility and ease of implementing complex nonlinear controllers.

706 A test rig was developed where the electrohydraulic servosystem exhibited undesirable dynamics typical of those just described. The schematic in Fig 7.1

shows the basic components and the digital controller arrangement. The electrohydraulic servosystem consisted of a large inertia load of low damping driven by a servovalve controlled cylinder drive. During operation, the valve drive signal e, is supplied from the microprocessor controller, and is generated by comparing an external input demand signal u, with the feedback signal y, this being derived from measurement of the load position. The requirement was to position the inertia load with good steady state accuracy and dynamic performance, and this was achieved using the Pole Placement method developed in Chapter 4 to obtain the F and G filter coefficients. The same nomenclature is used as defined in section 3.4.

707 A more detailed drawing showing the test rig layout is shown in Fig 7.2, and details of the various components used in the rig are recorded in Fig 7.3. The cylinder was of single ended construction, a choice often made in practice because of the more compact design. However a directional nonlinearity is introduced as a result (see Appendix 1). The ratio of piston side area to annulus side area was 1.47, and this resulted in the cylinder extend stroke being about 1.2 times faster than the retract stroke for the same valve opening. The cylinder rod moved a total load inertia of 890 kg, which was rigidly located on a free running rail mounted trolley. The load position was indicated using a wire wound potentiometer, and the 61 cm cylinder stroke utilised about 95 % of the -10 to +10 V range of the 12 bit A/D. The resulting measurement accuracy being about 0.1 mm. The majority of the dynamic response tests were carried out about $Y = 0$, ie the mid stroke position of the cylinder.

708 In addition to inherent servosystem nonlinearities, some time variable external nonlinearities were included in the test rig, and these are shown in Fig 7.2. A proportional electrohydraulic pressure relief valve was used to control the system supply pressure continuously within the range 60 to 150 bar, and this had the effect of changing the valve flow gain, and hence the forward path gain of the closed loop system. The test rig load inertia was not changed during the course of the tests, but the effect of this was simulated by adding 2 litres of oil capacity on each of the lines between the valve and cylinder. Switching in these dead volumes resulted in bringing the open loop damped natural frequency down from 13 Hz to about 7 Hz, this corresponding to a load inertia increase of between 3 and 4 times.

709 All of the control system signals and other measurement signals were processed

and monitored from a central signal processing stand. The stand housed a signal generator from which the demand signals were derived, a digital oscilloscope and plotter for data observation and recording, and a frequency response analyser. A photograph showing the complete test rig is shown in Fig 7.4.

710 The servovalve dynamic characteristics as stated by the manufacturers were well in excess of the overall servosystem closed loop dynamics, thus the valve dynamics were not included in the plant model. However, the valve chosen for the test rig did have significant dead band and a dual gain characteristic, the details of which can be seen in Fig 7.3. These exaggerated nonlinearities were included to show how the microprocessor controller could be programmed to modify their effects on the system. The practical implications of these characteristics can be seen in Fig 7.5 from the measured cylinder velocity versus valve drive characteristic. Considering the retract stroke, ie positive cylinder displacement, 100 % current ie 8 mA, corresponds to a velocity of 28 cm/s. Between this point and the 0 % current point the characteristic is seen to follow one of three approximately constant gains depending on the current. From 0 to 2.5 % current, the flow gain is very low and assumed zero, from this point to the 25 % current point a constant but low flow gain can be observed, and for currents higher than this the gain is at a higher constant level. When the current polarity is reversed, Fig 7.5 shows a similar characteristic for cylinder extend velocities, due to the symmetrical valve characteristic. However this symmetry is upset by the differential cylinder areas, generating extend velocities faster than the retract velocities by a factor of about 1.2 for the same spool opening.

7.3 Servosystem Modelling

711 The Pole Placement controller design technique derives its simplicity from the assumed linearity of the electrohydraulic system being controlled. However in practice electrohydraulic systems are far from linear, thus the objective of this part of the research was to see if an adequate linear model suitable for controller design could be derived, in spite of nonlinear effects.

712 A typical step response of the closed loop test rig servosystem is shown in Fig 7.6(a), using an analogue summing junction controller to close the loop. The 1 cm step change in load position corresponds to a 3 mA peak valve drive current, thus

from Fig 7.5 it can be seen that the valve is acting in the high flow gain region for a significant part of the time. This has the effect of giving a very rapid initial rise time. The 0.5 cm step response in Fig 7.6(b) is within the low gain region of the valve and results in a slower initial rise time, and consequently the oscillations are less pronounced. The frequency of the oscillations are at about 13 Hz, but this value changes depending on the the operating point of the plant.

713 A linear representation of the servosystem can be obtained from a small perturbation analysis as carried out in Appendix 1. Taking into account the effects of oil compressibility, the simplest representation of the system is given in equation A1.10:

$$\frac{y}{e}(s) = \frac{K\omega_n^2}{s(s^2+2\zeta\omega_n s+\omega_n^2)} \qquad (7.1)$$

The equation is obtained neglecting the servovalve dynamics and assuming the cylinder piston is so positioned that the compressibility lag time constant is the same in the oil volumes on each side of the actuator. At other positions a fourth order equation results, however this is not a dominant effect, and generally the servosystem can be adequately modelled by equation 7.1. Derivation of the uncompensated closed loop transfer function from equation 7.1, yields a first order lag term and an oscillatory second order term, which describes well the shape of the step responses seen in Fig 7.6.

714 From equation A1.14 of Appendix 1, the damping ratio in equation 7.1 is seen to change depending on the natural damping of the load C, and the valve flow/pressure gain C_p. Since in the test rig an overlapped valve is used C_p is very small about the null point, thus the valve provides very little damping. The natural frequency in equation 7.1 changes as the piston moves. Equation A1.13 of Appendix 1 indicates that the lowest frequency is obtained when the piston is near the middle of its stroke, increasing as the piston moves towards either end of the cylinder. The effect of this nonlinearity on the closed loop system was observed by measuring the closed loop damped natural frequency at different piston positions, and the results shown in Fig 7.7 can be seen to agree with the theory. The frequencies were measured as mean values from the system step responses similar to that shown in Fig 7.6, and it can be seen that the extend stroke frequency is higher than the retract stroke frequency. This is a result of the unequal piston

areas which cause a change in forward path gain when the direction of motion is reversed.

715 In Appendix A1.4 it is shown that the extend stroke gain exceeds the retract stroke gain by the ratio:

$$R_G = \sqrt{\frac{A_p}{A_a}} \tag{7.2}$$

Using the data of Fig 7.3 this comes out to be: $R_G = 1.21$. This is verified by the result shown in Fig 7.5. The effect of this gain change during closed loop control can be seen in Fig 7.6, where larger oscillations are seen to occur on the extend stroke of the cylinder.

716 The validity of the small perturbation model equation 7.1, is also verified by the measured open loop frequency plot shown in Fig 7.8, which was derived using an analogue summing junction controller. At low frequencies the plot descends at -20 dB/decade, corresponding to an inherent integral action. At higher frequencies the second order oscillatory term causes a resonant peak at about 13 Hz. A good s plane model fit of equation 7.1 to the frequency response data is seen in Fig 7.8 to be obtained by putting:

$K = 4.45$ /s $\quad \zeta = 0.1 \quad \omega_n = 13$Hz

Whilst this model based on the frequency response test provides some useful information about the plant, it lacks vital information about the nonlinearities which occur. Different frequency response results were obtained simply by changing the amplitude of the sinusoidal signal, or moving the position of the load about which the sinusoidal motion occurred. Dramatic changes in the plant dynamics also occured when the dead volumes were switched in, (simulating an increase in load inertia). The effect on the step response can be seen in Fig 7.9, where compared to Fig 7.6, the frequency of oscillation is seen to be reduced. Thus it is seen that in controller design the fixed coefficient linear model must be used with caution. The practical problems associated with the design of a linear Pole Placement controller are discussed in the following section.

7.4 Digital Closed Loop Servosystem Control

717 The plant modelling and Pole Placement controller design technique for the plant transfer function of equation 7.1, was discussed in Chapters 3 and 4 to illustrate the proposed general methods and the effects of sampling. Details of the theory behind the practical application of these methods, described in this section, can be obtained by reference to these chapters. Prior to calculation of the F and G coefficients it was necessary to select a sample period and discrete model of the plant. The method of selection of both of these was discussed generally in sections 3.8 and 3.6 respectively. In the case of the servosystem test rig, the sample period was selected on the basis of the 13 Hz natural frequency which must be controlled. Using the guide lines of section 3.8, sampling at five times this frequency corresponds to a sample period of 15 ms, and this value was used throughout the servosystem test program. The corresponding aliasing frequency is about 33 Hz, and since the plant dynamics shown in Fig 7.8 are well attenuated at this frequency, no antialiasing filters were used.

718 The introduction of a Sample and Hold circuit into the plant when converting from an analogue to a digital control system, alters the dynamics of the plant dependent on the sample period used. The consequencies of the chosen 15 ms sample period can be seen from the measured step response plots shown in Fig 7.10. In Fig 7.10(a) an analogue summing junction controller was used, and this is compared with the digital system step response in Fig 7.10(b). In the second case, the amplitude of the oscillations has been reduced, which from the simulation work of section 3.7 is to be expected. The effect of slow sampling was not detrimental to the closed loop performance of the system, but it was essential that it be taken into account in the controller design method, thus demanding the use of discrete plant modelling.

719 The discrete model used in the controller design is based on the Pole/Zero Mapping method (see Appendix 2). The application of the method to equation 7.1 was discussed in sections 3.6 and 3.7, and from equation 3.14 the resulting discrete model is:

$$\frac{y}{e}(z) = \frac{a_1(1+z^{-1})^2 z^{-1}}{(1-z^{-1})(1-a_2 z^{-1}-a_3 z^{-2})} \qquad (7.3)$$

This transfer function has the advantage over those derived by other s to z methods of having a small number of coefficients, and fixed zeros. This helps to simplify the controller design process. The coefficient values of paragraph 716 yields the 'a' coefficients of equation 7.3 to be:

$a_1 = 0.0204 \quad a_2 = 0.633 \quad a_3 = -0.799$

The frequency response using these coefficients is shown by the dashed lines in Fig 7.8, indicating a good comparison with the measured frequency response, and a characteristic reduction of the higher frequency amplitude ratios.

720 The F and G controller transfer functions, based on equation 7.3 as the plant model and assuming a third order desired model, are of second order, yielding a total of six coefficients. Here results are shown where the controller design equations have been solved for a particular demanded performance. The behaviour of the calculated controller in handling the various servosystem nonlinearities is discussed.

721 When a linear control law is applied to a highly nonlinear plant such as the servosystem, the effects of the nonlinearities on the closed loop response are unknown. Calculation of an unsatisfactory control law can occur for a number of reasons, for example, it could be a result of neglecting significant higher order dynamics at the modelling stage, or of bad fitting of the model due to nonlinear distortions of the measured frequency plot. During the course of the research, the biggest single source of error was found to occur as a result of small test signals, used to obtain the frequency response, being used to design controllers for relatively large step changes in demand. It is all very well having elaborate techniques for fitting models to experimental data, but if the raw data is unrepresentative to begin with, then it is all to no avail. Small sinusoidal input signals normally used in frequency response tests, only move the servovalve spool slightly about the null point, and here the characteristics are often quite different from those at larger openings. This was especially the case for the servosystem since the frequency response test never entered into the high gain region of the valve. High amplitude sinusoidal signals could not be used during frequency testing, especially at frequencies near resonance, as this caused undesirable excitation of the system.

722 The frequency response plot obtained in Fig 7.8 using small signals, ie in the low gain region of the valve, caused an underestimation of the mean forward path gain which occured with larger operating signals. Consequently at the controller design stage the calculated controller coefficients gave an overestimated controller forward path gain and instability resulted. Thus the 'a' coefficients in paragraph 719, derived from the frequency response test in Fig 7.8, do not give a suitable plant model. Having a knowledge of the reasons for the instability, enables intelligent guesses to be made as to what the 'a' coefficient values should be to give good control results, however generally such a trial and error approach, though it can be successful, is not acceptable or reliable.

723 A technique for obtaining a more representative plant model using the normal operating signals of the control system is the Recursive Least Squares (RLS) identification method presented in the next chapter. RLS identification has a number of other advantages, besides giving a good model, which also will be discussed. Here, the result of RLS identification of the servosystem is presented, and its successful use in controller design demonstrated. RLS identification of the servosystem using a 1 cm square wave demand signal, and a 100 bar supply pressure, gave the 'a' coefficient values:

$a_1 = 0.0263 \quad a_2 = 0.792 \quad a_3 = -0.566$

The frequency response of equation 7.3 using these coefficients is shown by the heavily marked lines in Fig 7.8, and it can be seen that the RLS model gives a large increase in forward path gain as expected, and also reduces the damped natural frequency. In fact the RLS model bears little resemblance to the original frequency plot. These differences demonstrate the caution which must be exercised in the interpretation of small signal frequency response test results.

724 The modified 'a' coefficients were used to design a controller for the servosystem which was tried out at the RLS test condition, ie using a 1 cm square wave demand signal. A good indication of where to select the desired root positions was given by calculating the uncompensated closed loop positions. Calculation yields roots at, $z = 0.854$, and $z = 0.456 +/- j0.652$. By plotting these root positions on the root locus diagram of Fig 4.1 and moving the roots similarly to that shown in Fig 4.2, the desired performance was reached. The final choice of root positions

was decided upon by observation of the closed loop step response, and were chosen to be at $z = 0.7$, and $z = 0.3 +/- j0.2$. The controller 'f' and 'g' coefficients corresponding to these root positions are:

$f_1 = 0.662 \quad f_2 = 0.330 \quad f_3 = 0.081$

$g_1 = -0.179 \quad g_2 = -0.564 \quad g_3 = 1.743$

The effect of the controller can be seen in Fig 7.11(b) , the step response is much improved compared with the uncompensated step response shown in Fig 7.11(a).

725 The action of the controller can be best umderstood from the root locus diagram. Fig 7.12 shows the general shape of the root locus for increasing forward path gain, both before and after compensation. In the uncompensated case the closed loop system is of third order having the same pole and zero positions as equation 7.3. Thus the root locus diagram shown in Fig 7.12(a), has three poles and three zeros one of which is imaginary. The two complex roots of the closed loop characteristic equation are very close to the umit circle, indicative of highly oscillatory behaviour, and it is seen that further increase in the forward path gain causes the onset of instability. The two zeros at $z = -1$, are forced by the Pole/Zero Mapping approximation, but this only effects the loci at very high impractical gain values, and has a marginal effect on the plot inside the unit circle. The same applies to the compensated root locus shown in Fig 7.12(b), but here the locus inside the unit circle has been deliberately altered by the controller to improve the dynamic performance. The use of a second order controller with a third order plant increases the order of the closed loop system to five, but since the desired characteristic equation is only third order, two of the roots are thus forced to the origin of the root locus diagram. The important point about Fig 7.12(b), is that the loci of the complex pair of roots has been made to move in the opposite direction, and to pass through well damped regions of the root locus diagram.

726 A more detailed locus of the compensated case is shown in Fig 7.13, and the effects of changing the forward path gain can be clearly seen. As soon as the forward path gain is changed from the controller design point, the two zero roots move and the fourth and fifth order coefficients of the characteristic equation are no longer zero, however these roots are very fast and have very little effect. More

significant is what happens to the complex pair of roots. It is seen that there is some room for changes in gain before these roots are moved into dangerous positions, thus the Pole Placement method has generated a robust fixed coefficient controller. In the following sections, the effects of system nonlinearities using this fixed coefficient controller are investigated.

7.5 Plant Inherent Nonlinearities - Inverse Filter Design

727 In sections 7.2 and 7.3 some of the nonlinear mechanisms in the servosystem and their effect on the system response was discussed. Two categories of nonlinearity can be established: first, the inherent nonlinearities occurring within the cylinder drive, which can be quantified in terms of the valve drive and feedback signals; and secondly, external nonlinearities, which are time variable and change independently of the control signals. In this section the method of handling the former category of nonlinearities is considered.

728 The fixed coefficient controller of paragraph 724 was designed for a specific set of servo system operating conditions. The supply pressure was held at 100 bar and a 1 cm step demand signal was used. Even when operating the controller under these conditions some undesirable effects can be observed from the step response trace Fig 7.11. The extend stroke rise time is greater than that of the retract stroke, and is a consequence of the directional gain nonlinearity discussed in section 7.3. Also the large valve overlap creates a null deadband and as a result a considerable load position steady state error occurs, giving errors of up to +/- 1 mm. The dual gain characteristic of the valve is noticed when different step sizes are demanded. In Fig 7.14, the 1 cm design step size is changed to 0.5 cm and 2 cm. In the 0.5 cm case the valve operates completely in the low gain region and the step response is sluggish. Conversely the 2 cm response is predominantly in the high gain region of the valve and undesirable overshoot results.

729 With the exception of the nonlinear change of the natural frequency with movement of the cylinder piston, all of the inherent nonlinearities mentioned in section 7.3 are related to the valve drive signal e, and are a consequence of the characteristic shown in Fig 7.5. The characteristic effectively shows how the forward path gain changes with valve spool position, and this can be corrected by programming a so called 'inverse filter' to linearise the characteristic.

730 The inverse filter was designed so that the forward path gain, ie the change of load velocity for a change in drive signal, was constant over all the range of valve drive signals. The linearised forward path gain was chosen to be the same as that for the lower of the valve gain characteristics when the cylinder is extending the load, this is shown in Fig 7.15(a). The actual valve characteristic is shown in Fig 7.15(b), and using these first two figures the inverse characteristic can be derived, and is shown in Fig 7.15(c). The conventional drive signal e, derived from the controller, is passed into the inverse filter, and e_o, the error signal after modification by the inverse filter, is output to the plant. The final figure 7.15(d), shows how the inverse filter is implemented.

731 Fig 7.15 deals with the directional gain and dual gain nonlinearities, but does not include the null point eliminator, this is shown in Fig 7.16. Effectively the valve is never allowed to come to rest in the null region, ie within +/- 2.5 % current. When the drive signal is decreasing from a positive value and the start of the overlap region begins, the drive signal jumps through to a negative value just outside of the overlap region, the drive signal then tries to move from here into the overlap region and another jump occurs back outside of the positive overlap region. Thus the valve spool never comes to rest, but in the steady state dithers about the valve null point. A typical control signal is shown iin Fig 7.17.

732 The overall effect of the full inverse filter cam be seen from the step response plot Fig 7.18, the steady state error is much reduced, and the directional nonlinearity eliminated. A similar step response was maintained irrespective of the amplitude of the control signal.

733 The method of implementing the full inverse fillter is shown in Fig 7.19. In step 1, if the cylinder is retracting, ie a positive drive signal, then e is multiplyed by the gain R_G. Then in step 2, a test is made to see if the signal is in the high gain region, and if it is, e is reduced to correspond effectively tto the low gain level. In step 3 the null zone eliminator is applied, and in the final step the saturation limits are tested and corrected if necessary. All of these ssteps took less than 0.5 ms to implement, which is a very small part of the overalll 15 ms sample period.

734 The change in damped natural frequency with load position, shown in Fig 7.7, could be expressed in terms of the load position and used to modify the control

action, however this was not found to be necessary, the fixed coefficient controller giving a good response over all the range of load position. In the following chapters, the test results presented for the most part include only stages 1 and 4 of the inverse filter (see Fig 7.19), ie the directional gain adjustment and the saturation limits, the dual gain characteristic being left out so that its effect on the control algorithms can be tested.The inclusion of the other parts of the filter will be indicated where applicable.

7.6 Plant Time Variable Nonlinearities

735 Two time variable nonlinearities were deliberately introduced into the servosystem, the changing supply pressure and the extra dead volume (designed to simulate an increase in load inertia). The latter is considered first.

736 The effect of introducing the dead volume on the uncompensated control system was shown in Fig 7.9, and compared with the no extra dead volume case (see Fig 7.10(a)), the damped natural frequency is reduced from about 13 Hz to 7 Hz. When the fixed controller design of paragraph 724 was implemented, and the dead volumes switched in, the step response changed as shown in Fig 7.20. The controller is no longer matched to the plant conditions, and excessive oscillations are seen to occur. The correct controller design can only be calculated and implemented from a knowledge of the new plant conditions.

737 The effect of the dead volume on the closed loop controller can also be seen from the root locus diagram of Fig 7.21. The plot was derived using the fixed controller coefficients of paragraph 724, and newly identified 'a' coefficients for the plant model. The poles of this model are those shown in the right hand part of the root locus plane, and compared to the plot with no dead volume present in Fig 7.13, it is seen that the model poles have been moved to the right, corresponding to a reduced natural frequency (see Fig 4.1). In Fig 7.21 it is also seen that the closed loop characteristic equation roots have moved to undesirable positions, the complex pair moving away from the originally specified locations at $z = 0.3 +/- j0.2$, to new positions at $z = 0.68 +/- j\,0.43$, corresponding to a low damping ratio of about 0.35. Also it is seen that the two roots ideally chosen to be at the origin have moved to new positions at $z = -0.22 +/- j\,0.23$.

738 Variations in the supply or load pressure applied to the servovalve, alters the pressure drop across the valve flow orifices and effectively changes the forward path gain of the control loop, the gain changing according to the square root of pressure drop across the valve. As the load is moved back and forth the cylinder pressures are changing all of the time, however the pressure drop across the valve is kept high compared with that across the load and this nonlinear effect is thus small, posing no real problem in the closed loop performance. However if large changes in supply pressure occur the step response is detrimentally affected.

739 The electrohydraulic pressure control valve was used to change the supply pressure within the range 60 to 150 bar. The fixed controller design was for a supply pressure of 100 bar, and Fig 7.22 shows that reducing the pressure to 60 bar gives a sluggish response, whilst increasing it to 150 bar gives excessive overshoot. The root locus diagram for the 150 bar case is shown in Fig 7.23, and is seen to have a shape very similar to that of the 100 bar case in Fig 7.13. This is to be expected as changing the supply pressure corresponds simply to a change in forward path gain of the plant. The real roots that were at $z = 0.7$ and $z = 0$, have moved up the breakout branches to new positions at $z = 0.69 +/- j0.3$. The other zero root has moved to $z = -0.27$, and the complex pair that should be at $z = 0.3 +/- j0.2$, have moved to $z = 0.04 +/- j0.57$. It is this pair of roots which are responsible for the high frequency oscillation of the step response shown in Fig 7.22.

740 In spite of the fixed coefficient controller being robust, it is seen that in situations where large plant parameter changes occur the controller gives an inadequate response. However the flexibility of the microprocessor makes it easy to make variable coefficient controllers which are able to cope. A method of implementing time variable controllers will be discussed in the following chapters.

7.7 Integral Action Control

741 In Appendix A1.1, the influence of external forces on the load position is derived using small perturbation analysis, and in section A1.3 it is shows that in order to supply the pressure required to sustain a force in equilibrium, the spool valve must be cracked open. The amount of opening, corresponds to the steady state error and depends on the valve flow gains C_x , and C_{ip} , which are determined by the spool characteristics and the prevailing operating conditions.

742 Integral action control removes steady state errors by including integral action in the forward path of the controller. The required valve drive offset necessary to sustain the load can then be maintained with zero steady state error between the demand and feedback signals. The method of calculating an integral action controller was discussed in section 4.6. The equations are solved in the same way as for a non integral action controller, but a $(1-z^{-1})$ factor is required in the forward path controller polynomial. The order of the controller goes up to three in accordance with equation 4.18, and since the closed loop performance is still specified as third order, three of the characteristic equation roots are set to $z = 0$.

743 In theory the same desired root positions should be demanded as before, ie at $z = 0.7$, and $z = 0.3 +/- j0.2$. However the resulting controller lacked robustness, since for relatively small increases in supply pressure from the design value, intersample rippling occurred (see paragraph 415). This phenomena is a result of choosing root positions too close to the negative real half of the unit circle [65]. The undesirable sensitivity of the controller was reduced by choosing new root positions at $z = 0.5$, and $z = 0.8 +/- j 0.2$. The corresponding step response is shown in Fig 7.24. The integral action of the controller was demonstrated by switching an offset in the valve driver to simulate an external load. For a step change in offset, Fig 7.25 shows for the normal controller a corresponding position error, but for the integral action controller a small transient occurs and then the position accuracy is restored.

744 The integral action controller increases the order of the controller by one, thus the overall system is now sixth order and a completely different root locus plot can be expected. Using the controller design of the previous paragraph, and the model 'a' coefficients from which the controller was designed, the corresponding root locus plot is shown in Fig 7.26. It is seen that integral action causes two poles to be placed at $z = 1$, one corresponding to the plant and one to the controller F polynomial. This root locus plot is seen to be relatively insensitive to changes in forward path gain. In particular the real root at $z = 0.5$ is seen to move to the right when the forward path gain is increased, corresponding to a more sluggish rather than a faster system. This apparent low sensitivity to gain changes was verified in practice as it was found that the shape of the step response was similar for supply pressures anywhere within the 60 to 150 bar range (see Fig 7.27), thus from this point of view also integral action gives a better result.

7.8 Closed Loop Frequency Response

745 The use of the inverse filter developed in section 7.5 makes the closed loop response less sensitive to changes in signal amplitude, the step response at small amplitudes being similar to that at large amplitudes. This means that the small signal frequency response is made to be more representative of the system generally, and thus it is valuable to see what effect the Pole Placement controller design has had on the overall closed loop small signal frequency response. In Fig 7.28 the measured uncompensated closed loop frequency response shows a very poor bandwidth of around 0.8 Hz. Even with this very low lag time constant, the resonant peak at 13 Hz reaches an amplitude ratio of -7 dB.

746 Even the best step response traces presented in this chapter show some oscillation in spite of over damped root positions being chosen. This is the result of unmodelled nonlinear effects such as backlash which have been observed to occur in the system. The presence of some remaining high frequency oscillation is also indicated by the compensated closed loop frequency plot in Fig 7.29, this peak also occurring at -7 dB. However the Pole Placement controller has allowed an improvement in -3 dB bandwidth from 0.8 Hz to 6.5 Hz.

7.9 General Discussion

747 The various methods of controlling the dynamics of long stroke high inertia servosystems was discussed in section 7.2, and the microprocessor solution demonstrated in this chapter compares favourably with analogue controller solutions, even if only a simple fixed coefficient controller is implemented. Whereas the analogue solution requires the use of expensive derivative feedback transducers, the digital solution could be implemented using an inexpensive single chip microprocessor system. However the greatest advantage over analogue systems is obtained from the flexibility and ease with which complex nonlinear controllers can be implemented.

748 In the servosystem test rig a sample period of 15 ms was chosen, and only about 1 ms of this time was used to implement the linear control law. The remaining 14 ms is the so called 'auxiliary processing time', (see section 3.4). A small fraction of this time was used to implement the inverse filter described in

section 7.5, which improved the linearity and steady state accuracy of the closed loop system. Such a filter could also be used to create any other nonlinear effect which may be desired.

749 The external time variable nonlinearities discussed in section 7.6 cause considerable upset when a fixed coefficient controller is used, and no solution to this problem was presented. In an analogue system the problem would be overcome by designing a compromise controller, where in order to maintain the stability margins in the worst nonlinear condition, a less than acceptable response would be tolerated elsewhere. Using a microprocessor controlled system it is possible to modify the controller so that the best control law is implemented at any given operating point of the servosystem, giving a good response at all times.

750 In consideration of the time variable nonlinearities, two problems arise: first, how does the microprocessor know that the nonlinearity has occurred; and secondly, even if the nonlinear change is known, what adjustment to the control law should be made? The obvious solution to this problem is to use Gain Scheduling. For example, if there are significant changes in the servosystem supply pressure as the system is running, then a transducer would be used to measure the pressure at any instant and the signal input to the microprocessor. Prior to operation of the closed loop system a discrete model of the electrohydraulic plant for a number of different pressure levels would be obtained, and the appropriate control action calculated using the Pole Placement technique. During operation, the supply pressure would be measured and the nearest corresponding controller design implemented from memory.

751 Whilst Gain Scheduling is simple to implement and uses very little auxiliary processing time, it has the drawback of requiring extra transducers, and the derivation of the plant model for each point of the schedule can be a very time consuming task. This is especially the case if a number of nonlinear changes are occurring simultaneously. The plant models can be generated either by simulation, which requires a detailed knowledge of the plant, or more usually by carrying out response tests. However, besides being time consuming the use of unrepresentatively small amplitude signals in such tests do not always give the correct results.

752 Ideally a method of identification is required which in a short time can derive directly the 'a' coefficients of the plant model, thereby eliminating both the model fitting stage and the s to z conversion stage. Such a technique is the Recursive Least Squares (RLS) identification method, which can be implemented either on or off-line to obtain the 'a' coefficients directly from the normal operating control signals. Employed off-line the technique can be used to very quickly calculate a plant model from which a control law can be calculated and a gain schedule established, all of this being implemented automatically with no quantitative information about the plant being required from the designer.

753 The most attractive use of the RLS identification method is on-line, where the RLS algorithm is implemented recursively using the auxiliary processing time. Ultimately the identification algorithm updates the 'a' coefficient estimates every sample period, from which the control law can also be recalculated every sample period, and the latest controller coefficients implemented. When a parameter change occurs in the plant, this is observed by the identification algorithm and there is a corresponding change in the 'a' coefficient estimates. The controller is then adjusted so that the demanded dynamic response is always maintained. This technique is known as Self Tuning Control (STC), and is one of a number of adaptive control methods. STC has the advantage of requiring no additional transducers to correct for the nonlinearities, and requiring no previous knowledge of the plant to be controlled. The theory and development of both RLS identification and STC adaptive control algorithms for the electrohydraulic servosystem test rig is the subject of the following chapters.

Fig 7·1

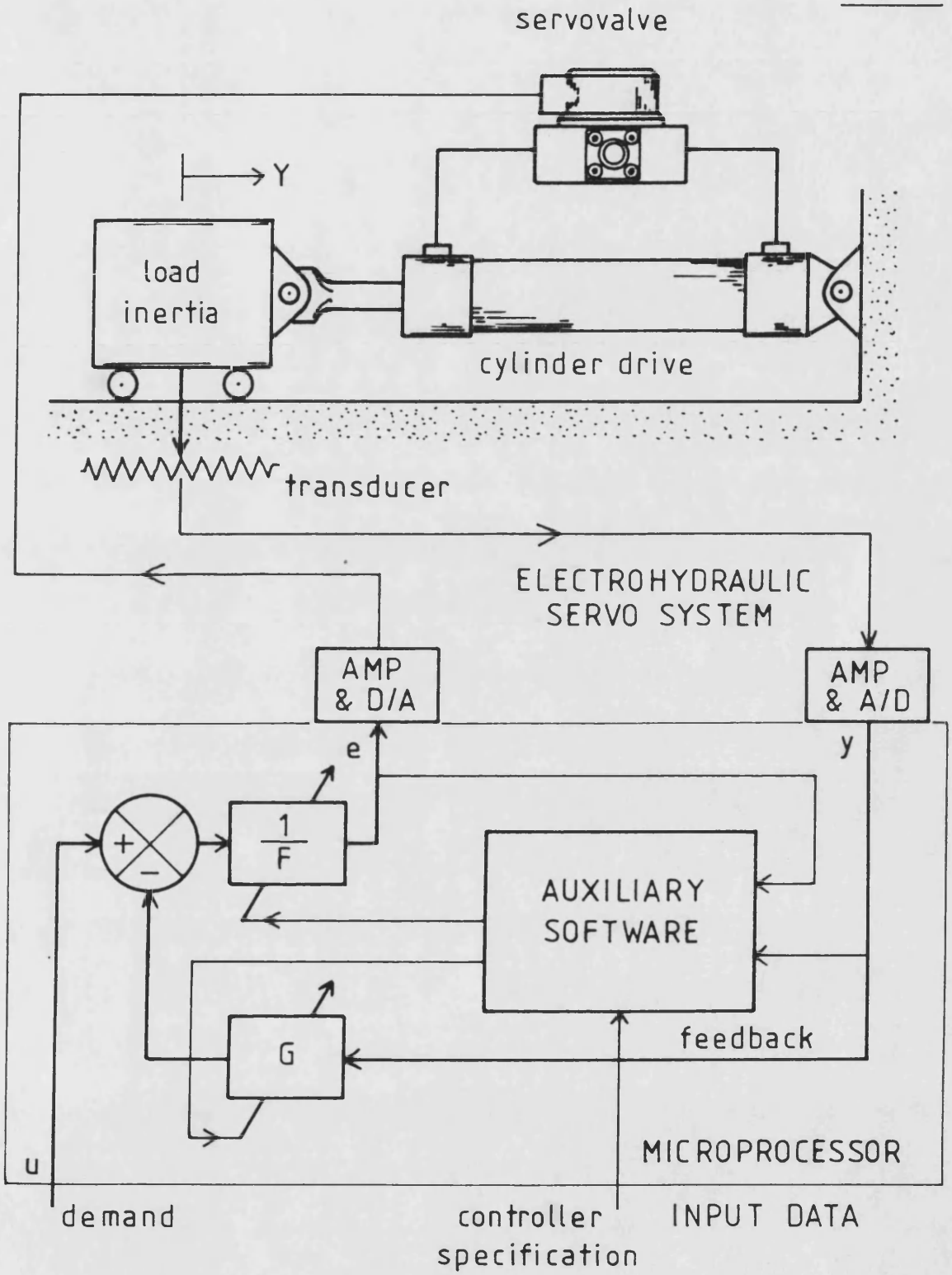

7·1 ELECTROHYDRAULIC SERVOSYSTEM SCHEMATIC

Fig 7·2

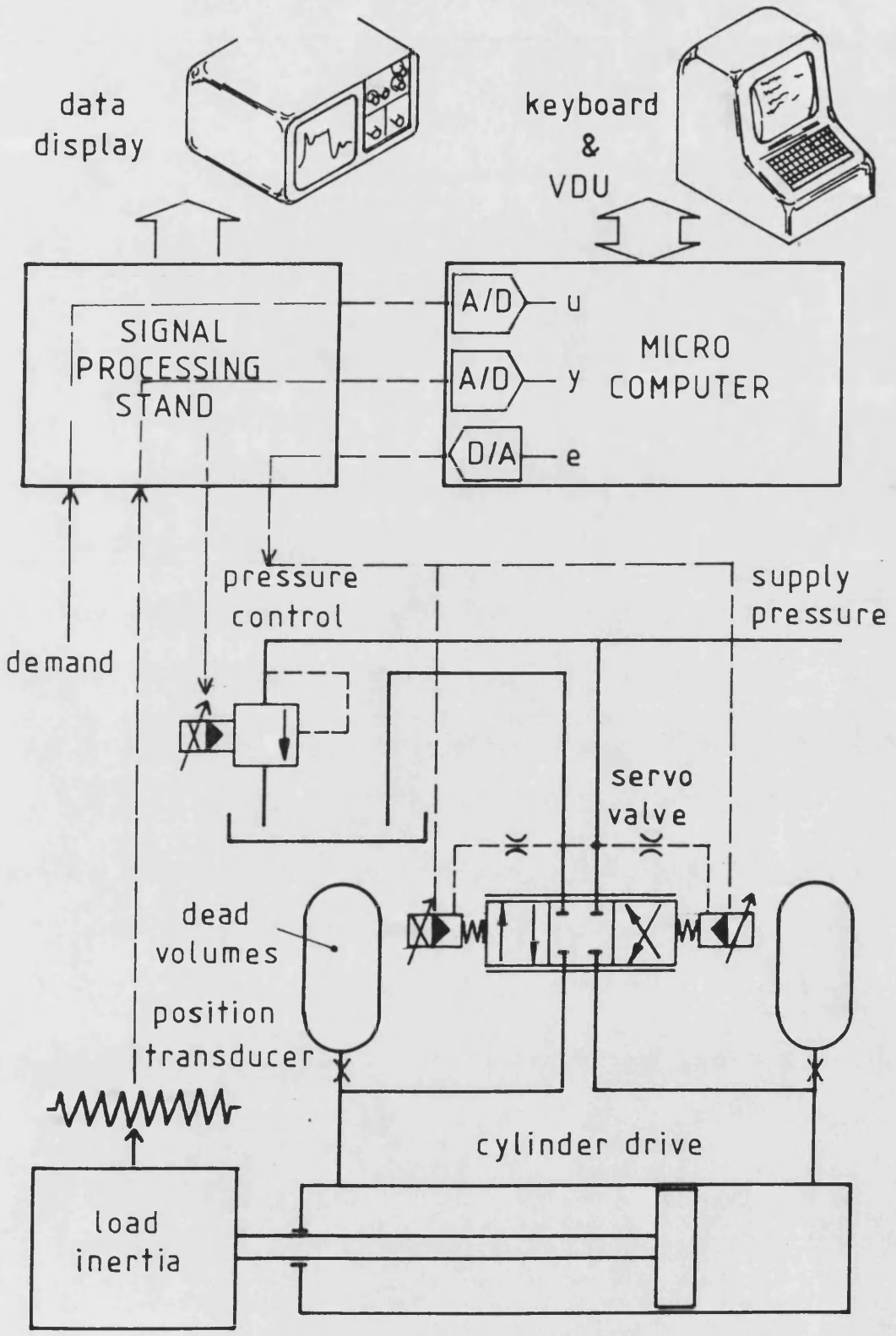

7·2 TEST RIG LAYOUT

Fig 7·3

SERVOVALVE: Moog series 76

−3dB bandwidth greater than 50 Hz
deadband +/- 2·5 % spool travel
flow gain at 70 bar:
1·26 L/min/mA for spool travel < 25 %
5·4 L/min/mA for spool travel > 25 %

CYLINDER DRIVE:

stroke: 610 mm, Y = 0 at mid position
areas: piston 2025 mm^2, annulus 1380 mm^2
additional dead volume 2 L on each side

LOAD SYSTEM:
damping: very low
mass: 890 kg

SUPPLY PRESSURE CONTROL:
continuously variable from 60 to 150 bar

7·3 TEST RIG DATA

Fig 7·4

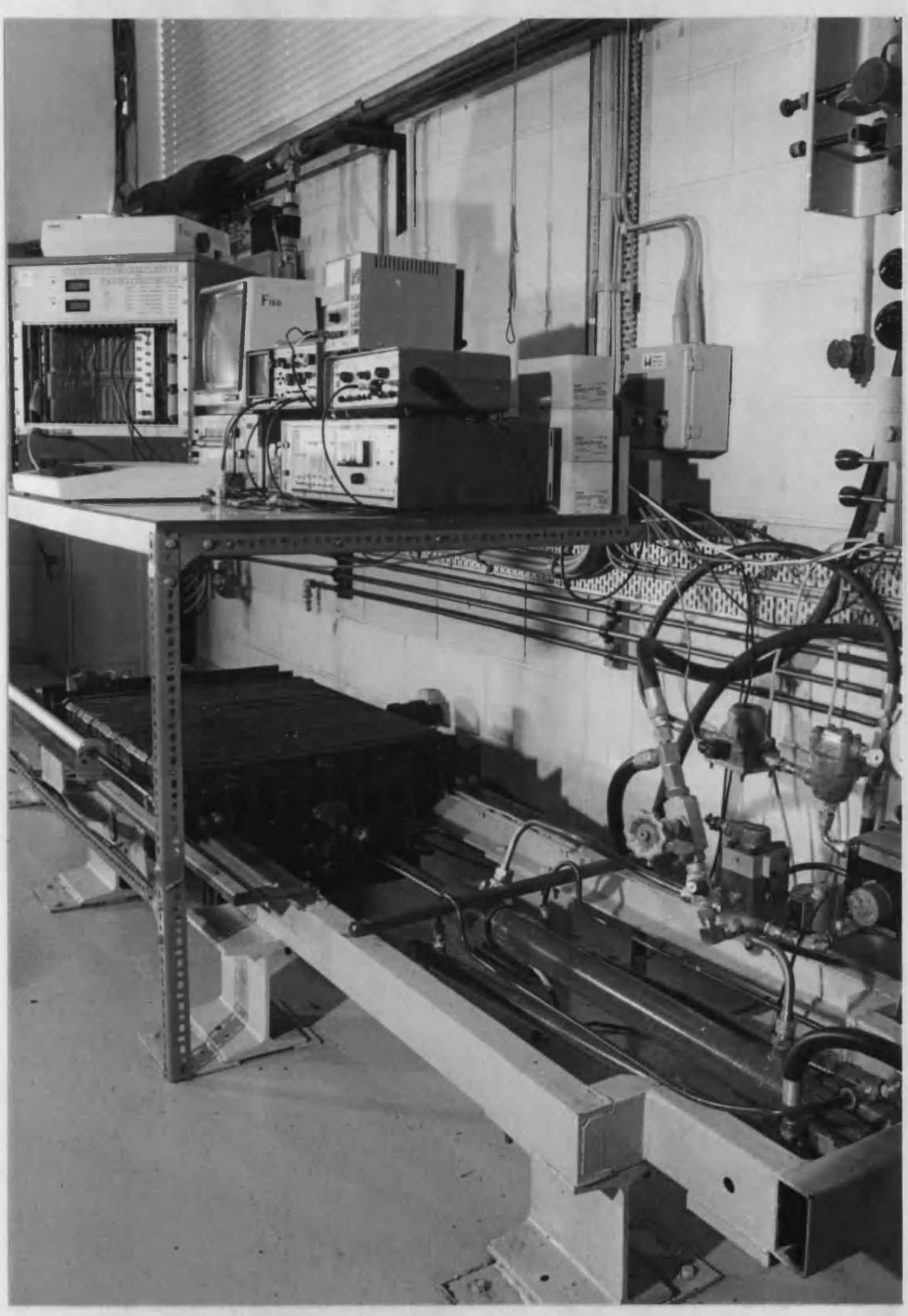

7·4 ELECTROHYDRAULIC SERVOSYSTEM TEST RIG

Fig 7·5

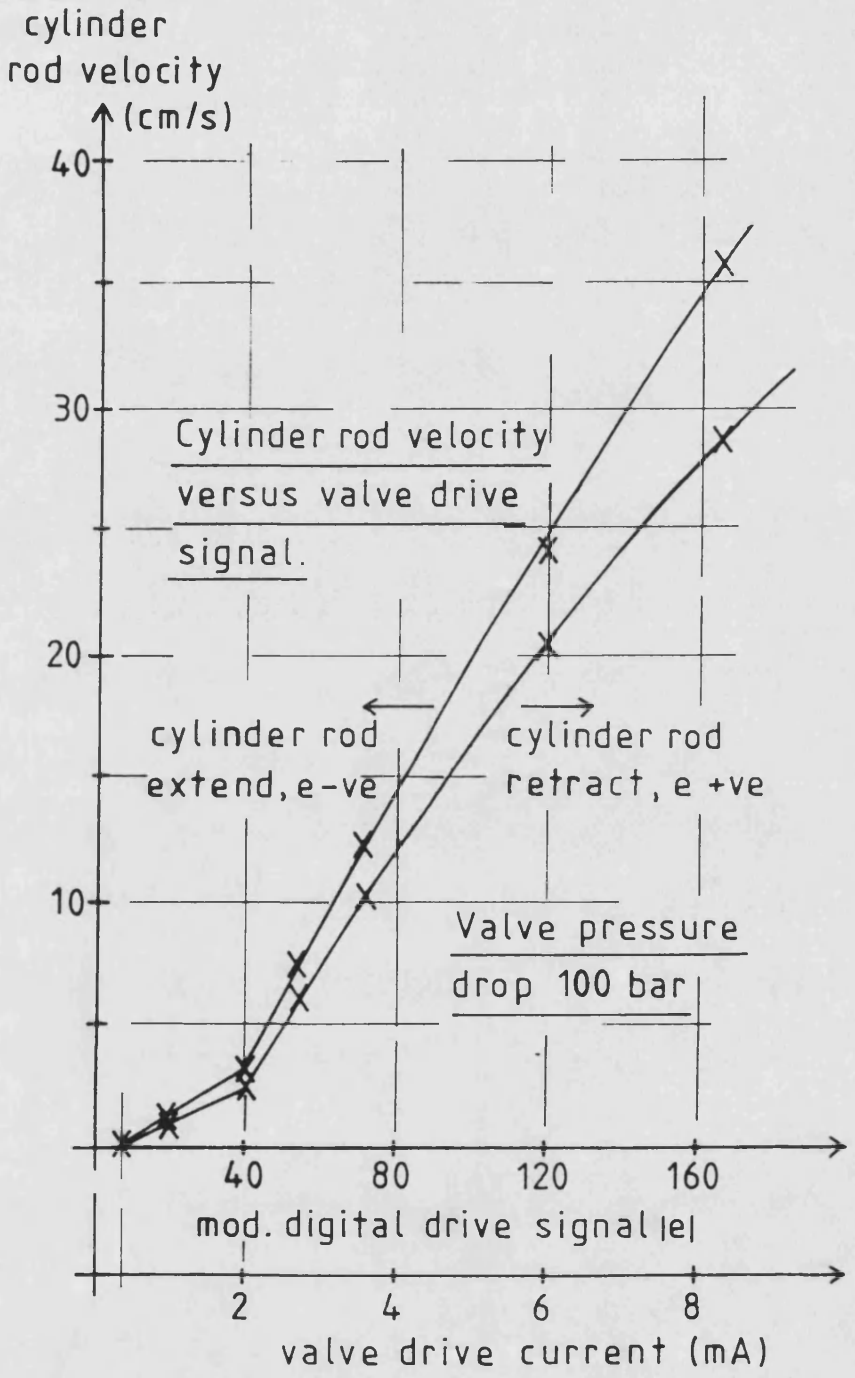

7·5 CYLINDER/VALVE FLOW GAIN SHOWING DUAL GAIN CHARACTERISTIC

Fig 7·6

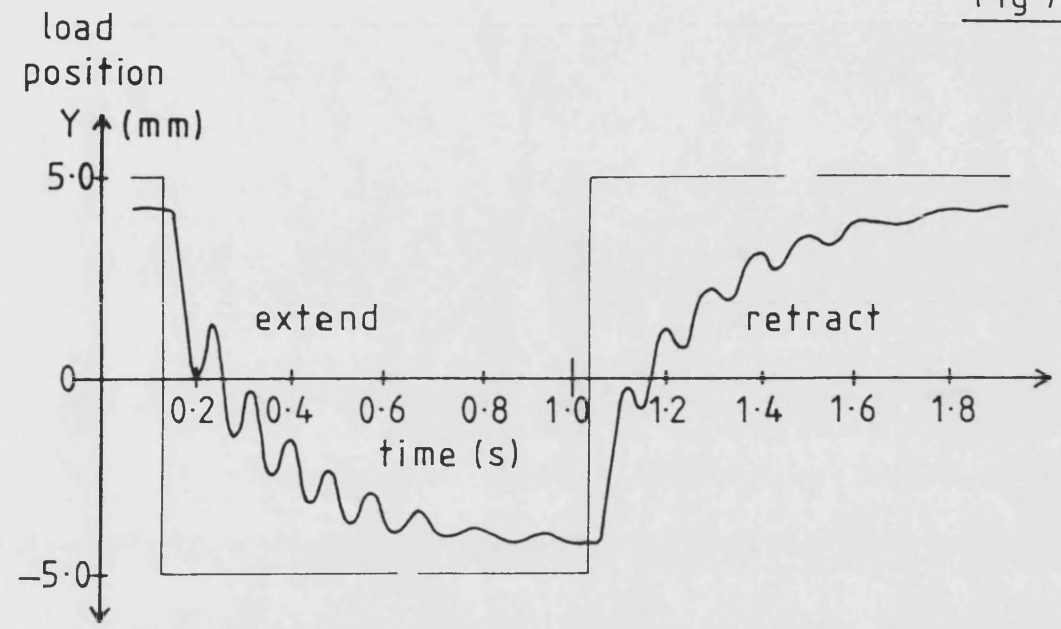

(a) 10 mm STEP RESPONSE

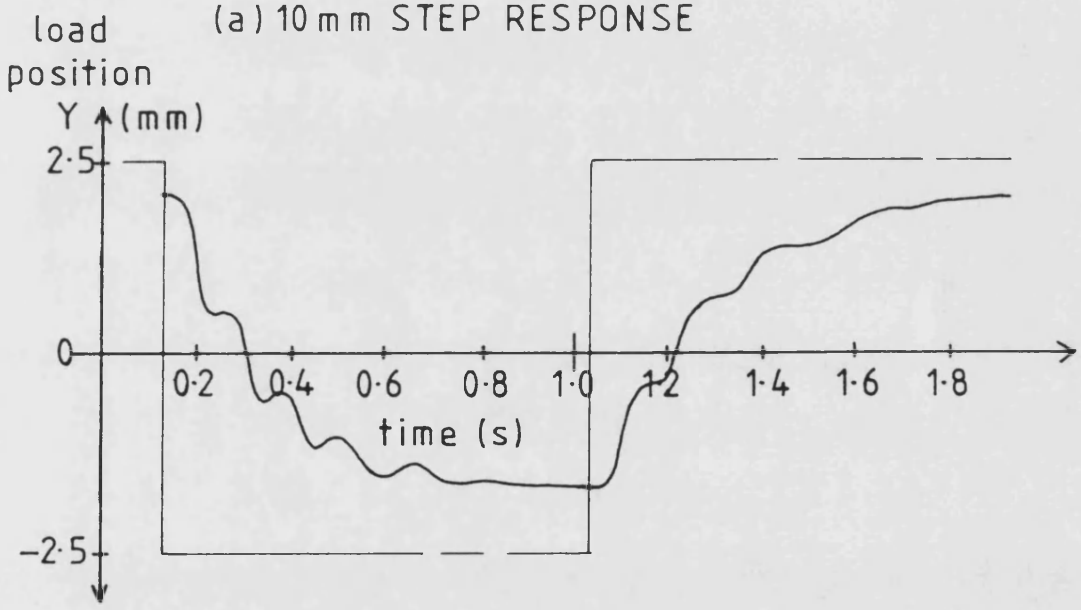

(b) 5 mm STEP RESPONSE

7·6 UNCOMPENSATED STEP RESPONSE ~ ANALOGUE CONTROLLER

Fig 7·7

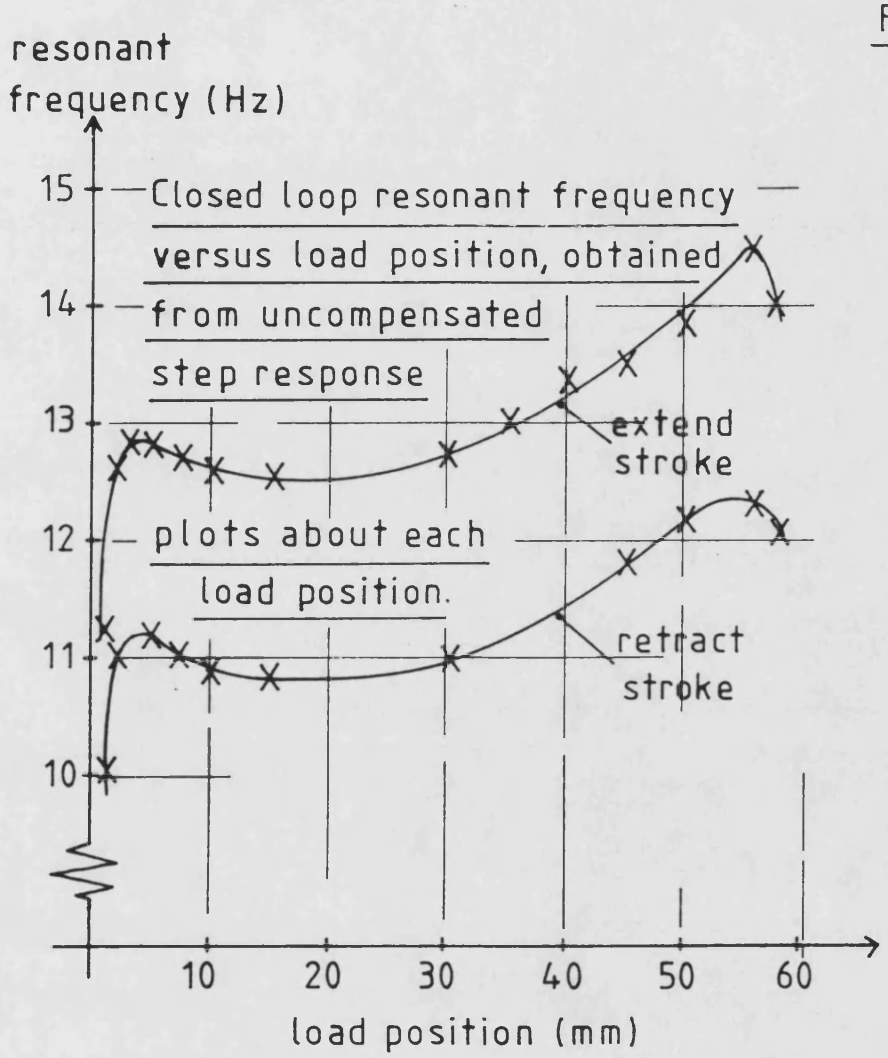

7·7 CHANGE OF RESONANT FREQUENCY WITH LOAD POSITION

Fig 7·8

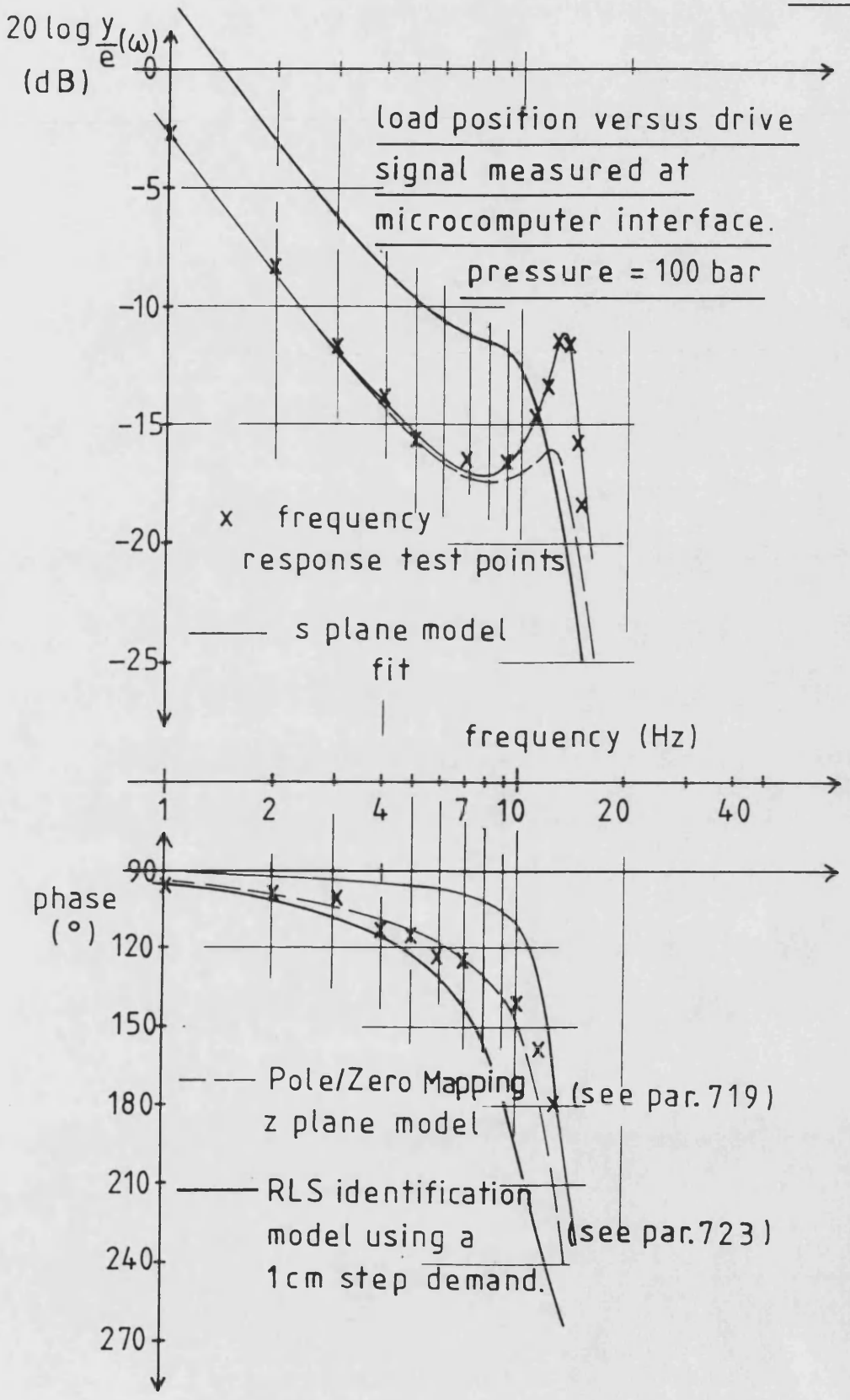

7·8 OPEN LOOP FREQUENCY RESPONSE

Fig 7·9

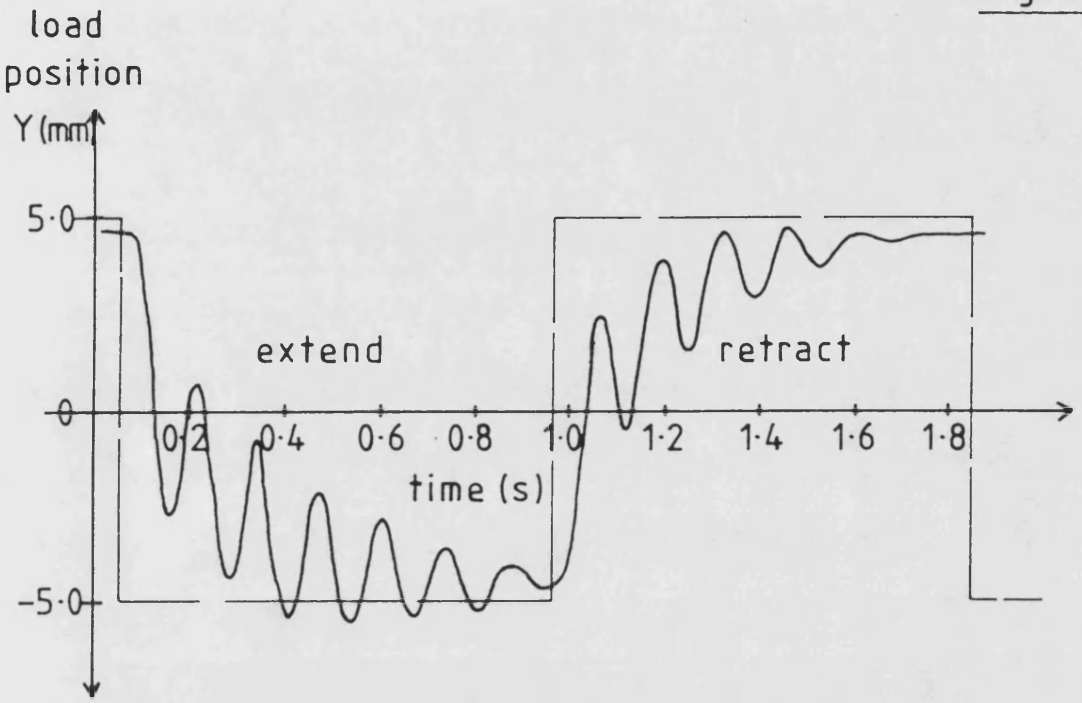

7·9 UNCOMPENSATED STEP RESPONSE ~ DEAD VOLUME ADDED

Fig 7·10

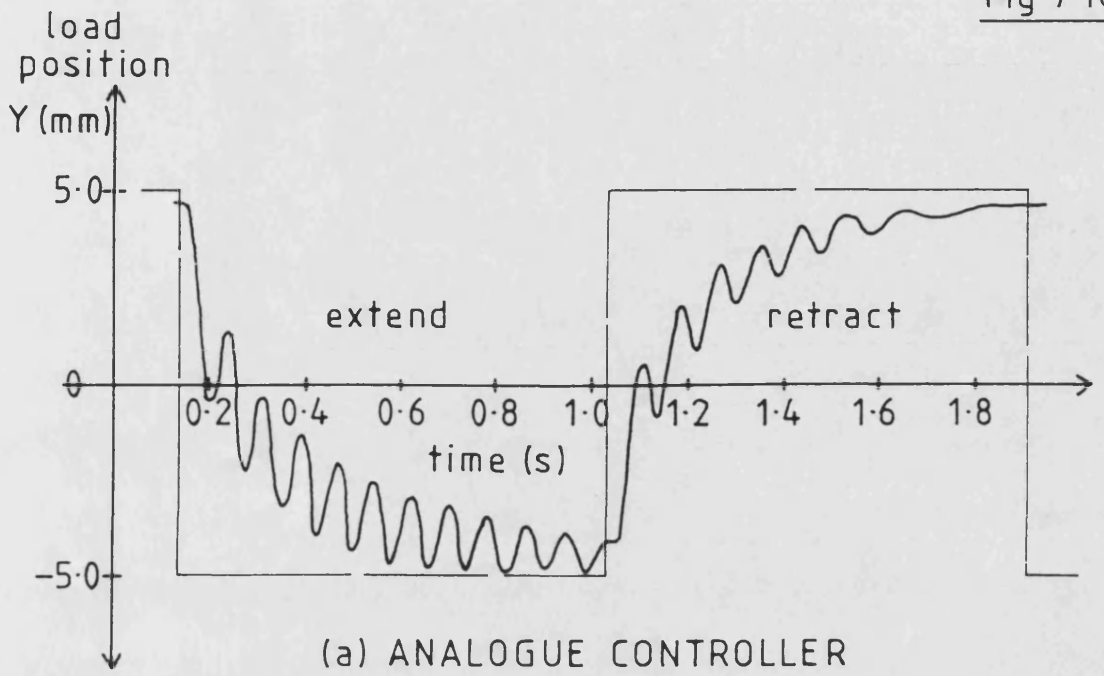

(a) ANALOGUE CONTROLLER

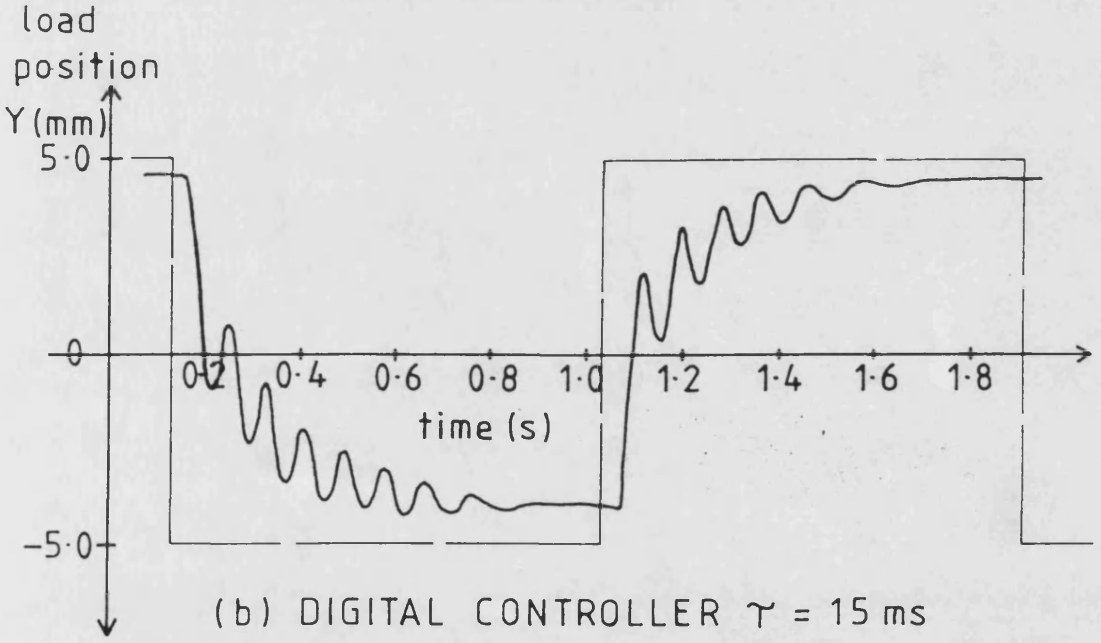

(b) DIGITAL CONTROLLER τ = 15 ms

7·10 UNCOMPENSATED STEP RESPONSE ~ EFFECT OF SAMPLING

Fig 7·11

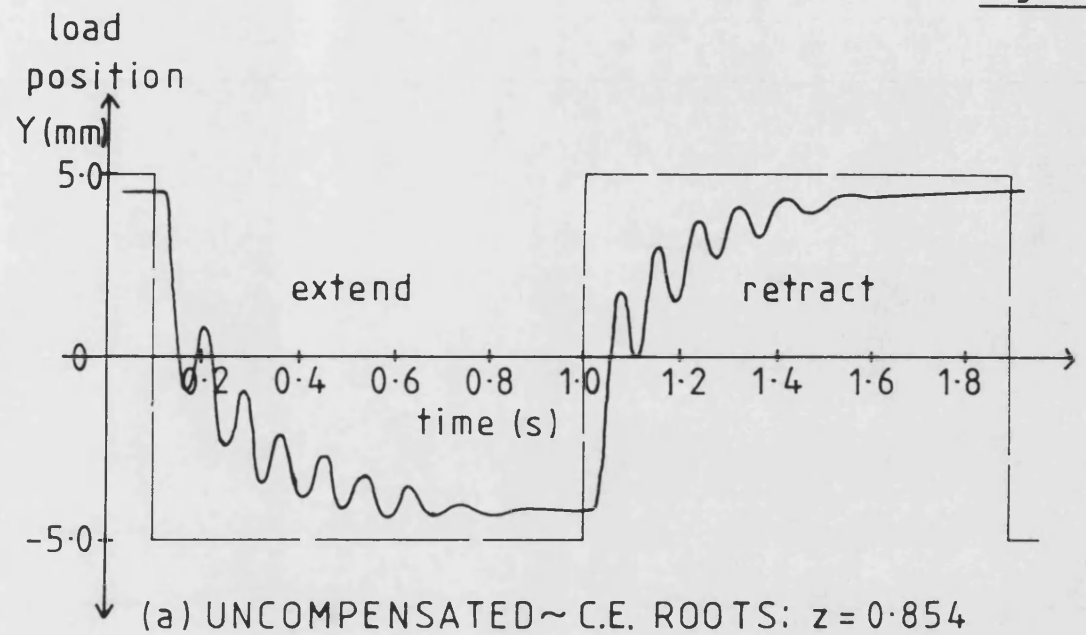

(a) UNCOMPENSATED ~ C.E. ROOTS: z = 0·854
z = 0·456 +/- j0·652

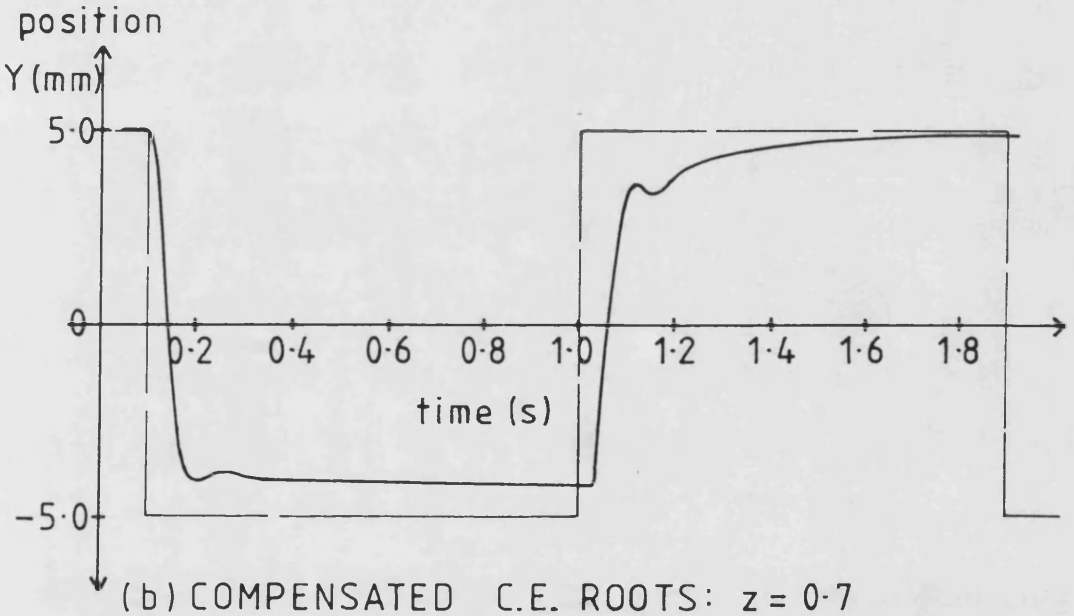

(b) COMPENSATED C.E. ROOTS: z = 0·7
z = 0·3 +/- j0·2

7·11 STEP RESPONSE BEFORE AND AFTER COMPENSATION

Fig 7·12

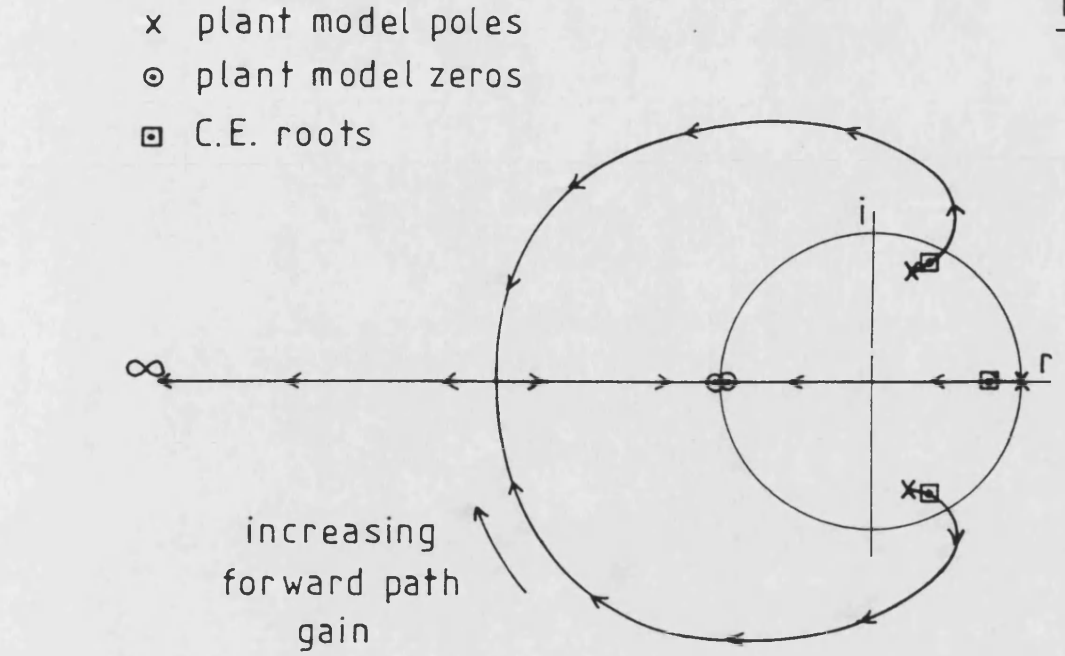

(a) UNCOMPENSATED ~ C.E. ROOTS: z = 0·854
z = 0·456 +/- j 0·652

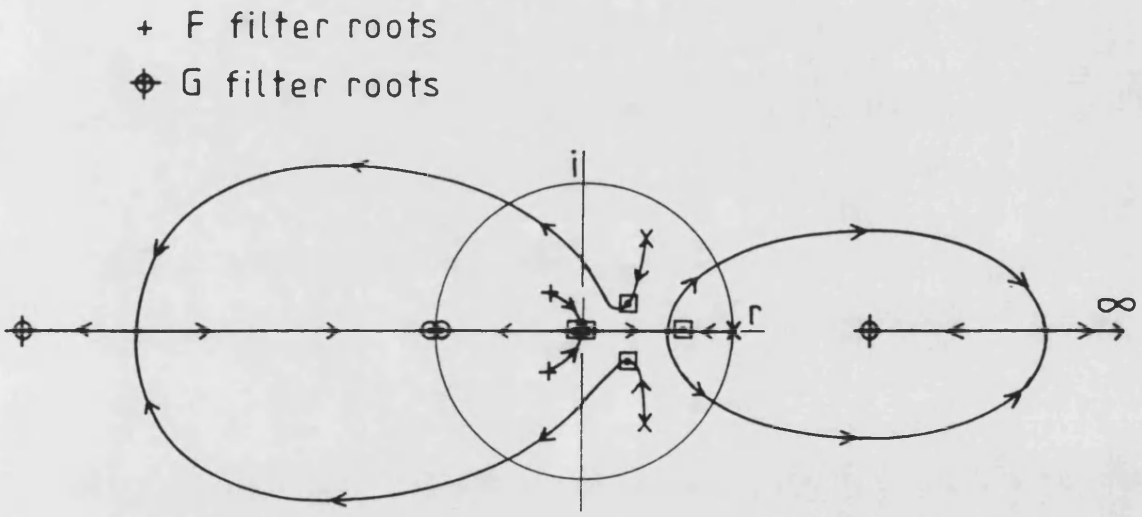

(b) COMPENSATED ~ C.E. ROOTS: z = 0·7
z = 0·3 +/- j 0·2

7·12 ROOT LOCUS PLOTS BEFORE AND AFTER COMPENSATION

Fig 7·13

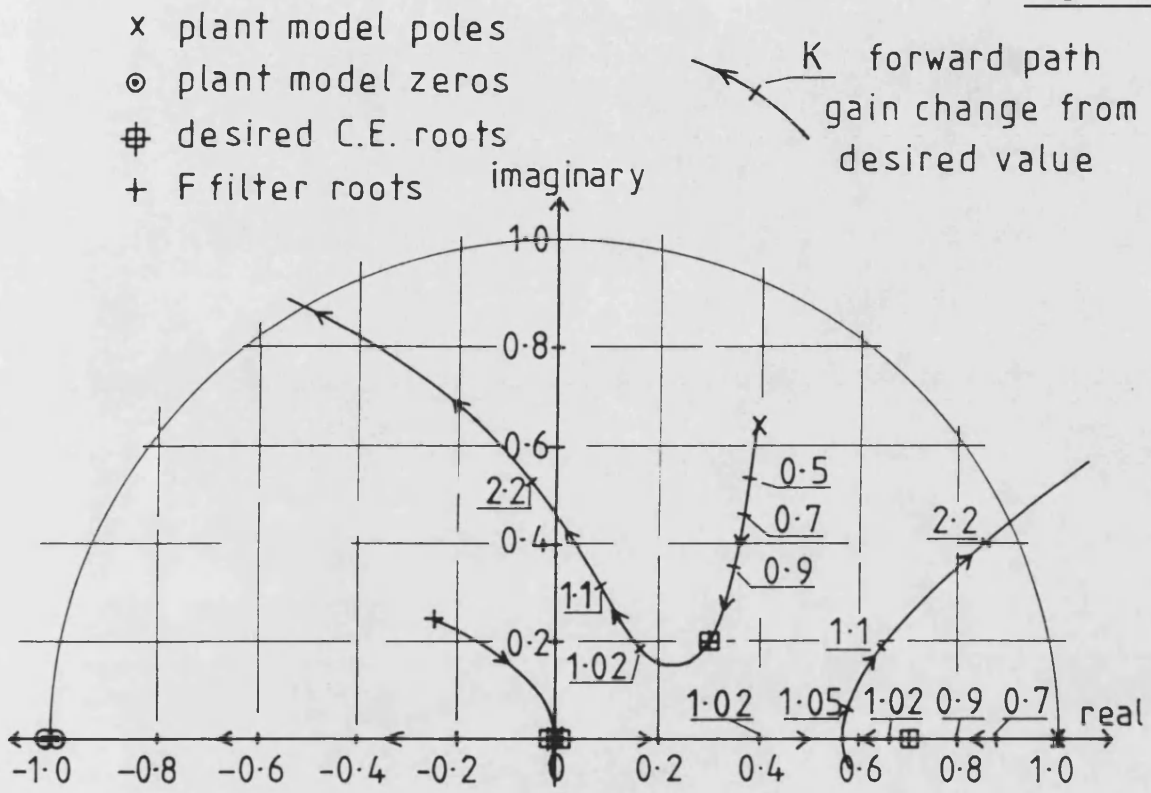

desired C.E. roots : $z = 0{\cdot}7$, $z = 0{\cdot}3 \pm j0{\cdot}2$

7·13 COMPENSATED ROOT LOCUS PLOT ~ PLANT AT DESIGN POINT

Fig 7·14

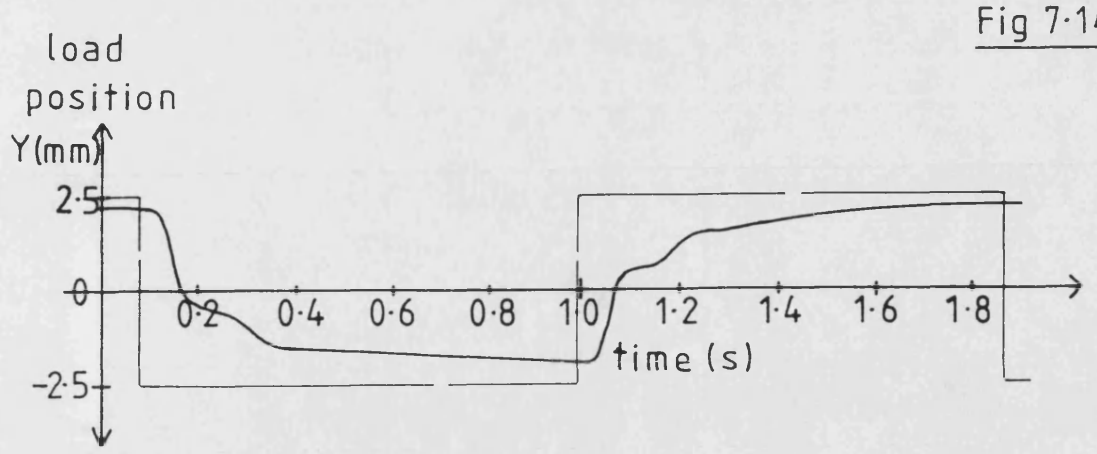

(a) 5mm STEP RESPONSE

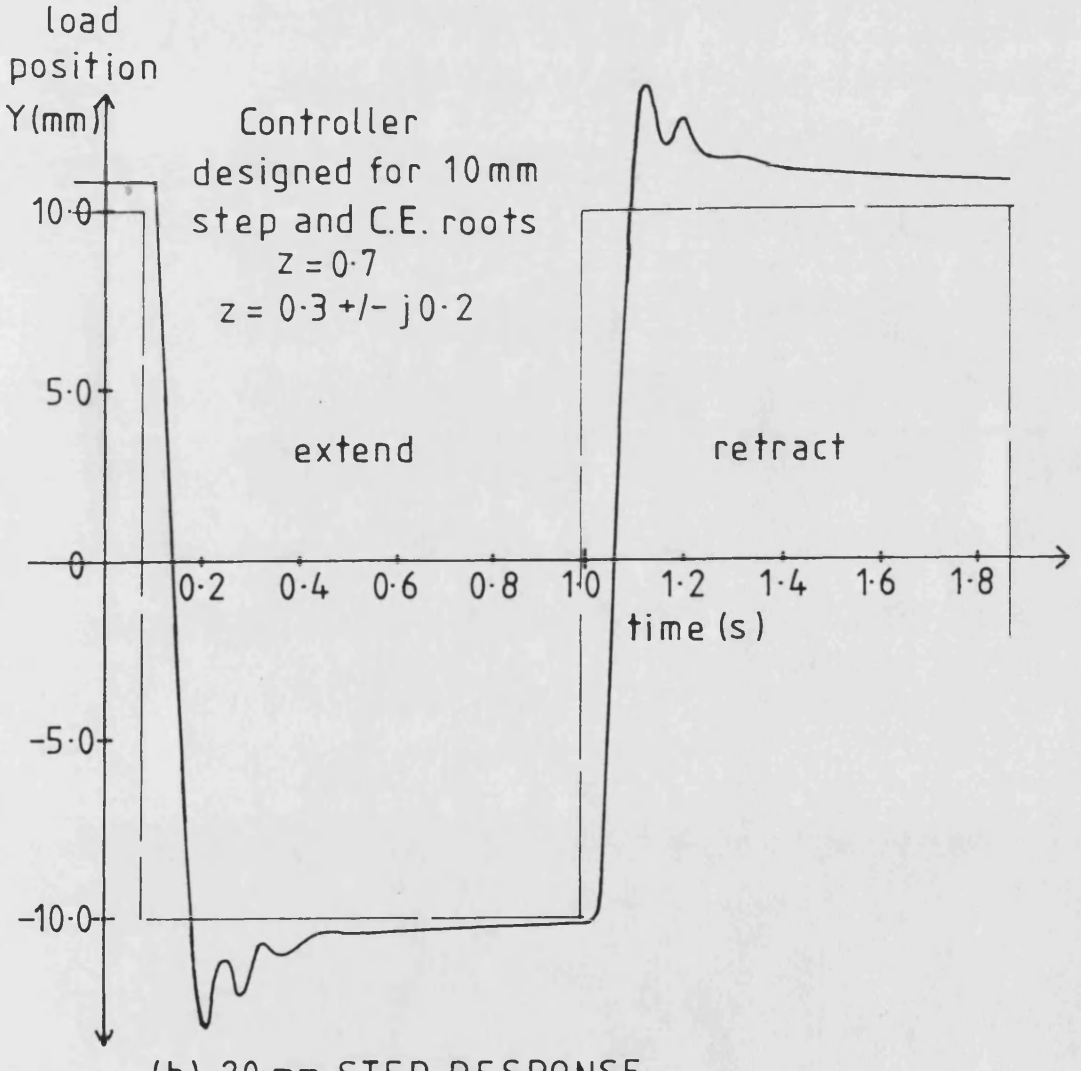

(b) 20 mm STEP RESPONSE

7·14 COMPENSATED STEP RESPONSE ~ EFFECT OF STEP AMPLITUDE

Fig 7·15

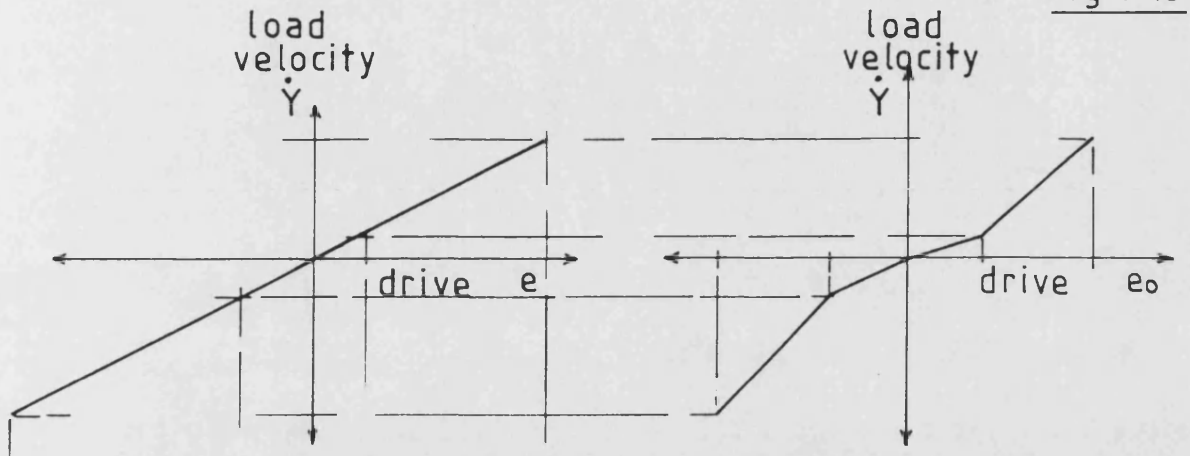

(a) DESIRED FORWARD PATH GAIN CHARACTERISTIC

(b) CYLINDER DRIVE CHARACTERISTIC (see Fig 7·5)

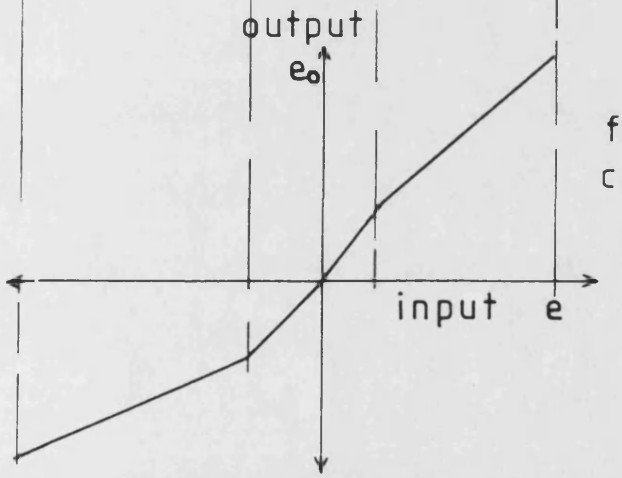

(c) INVERSE FILTER I/O CHARACTERISTIC

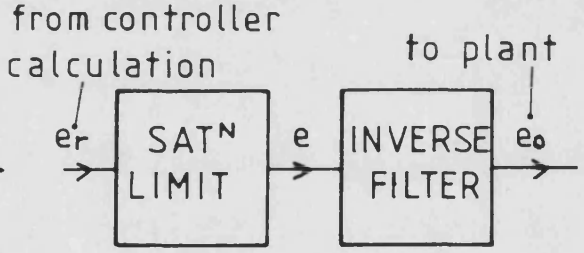

(d) INVERSE FILTER LOCATION

7·15 INVERSE FILTER DESIGN

Fig 7·16

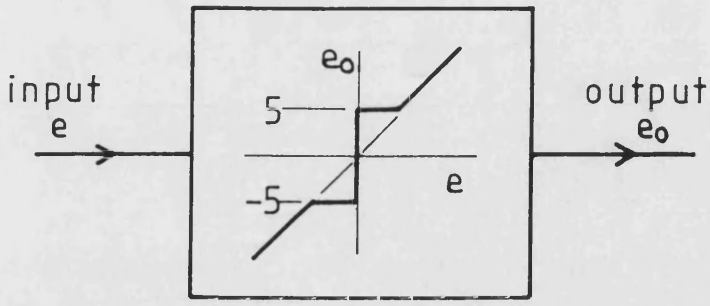

7·16 NULL POINT ELIMINATOR

Fig 7·17

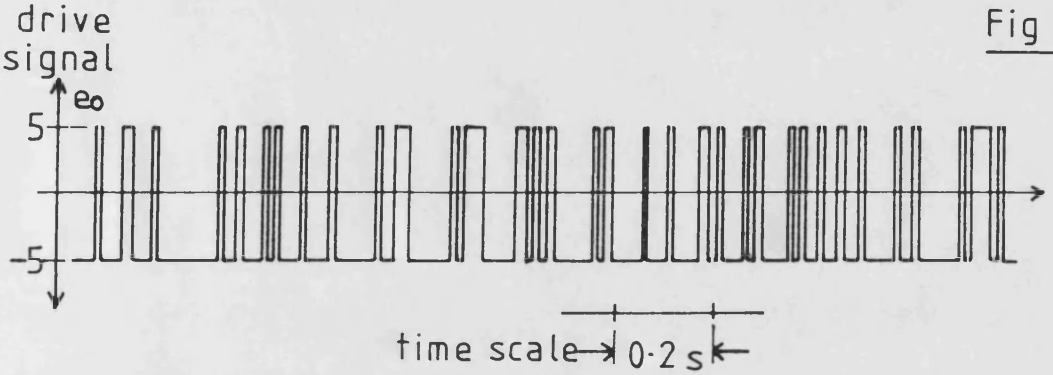

7·17 NULL POINT DITHER SIGNAL

Fig 7·18

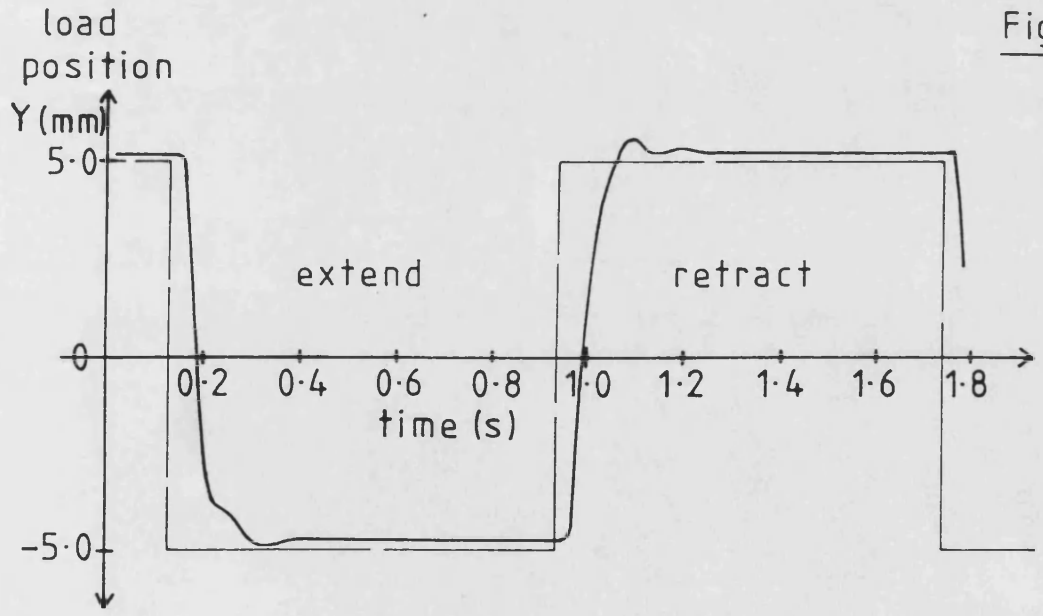

7·18 COMPENSATED STEP RESPONSE WITH INVERSE FILTER ADDED

Fig 7·19

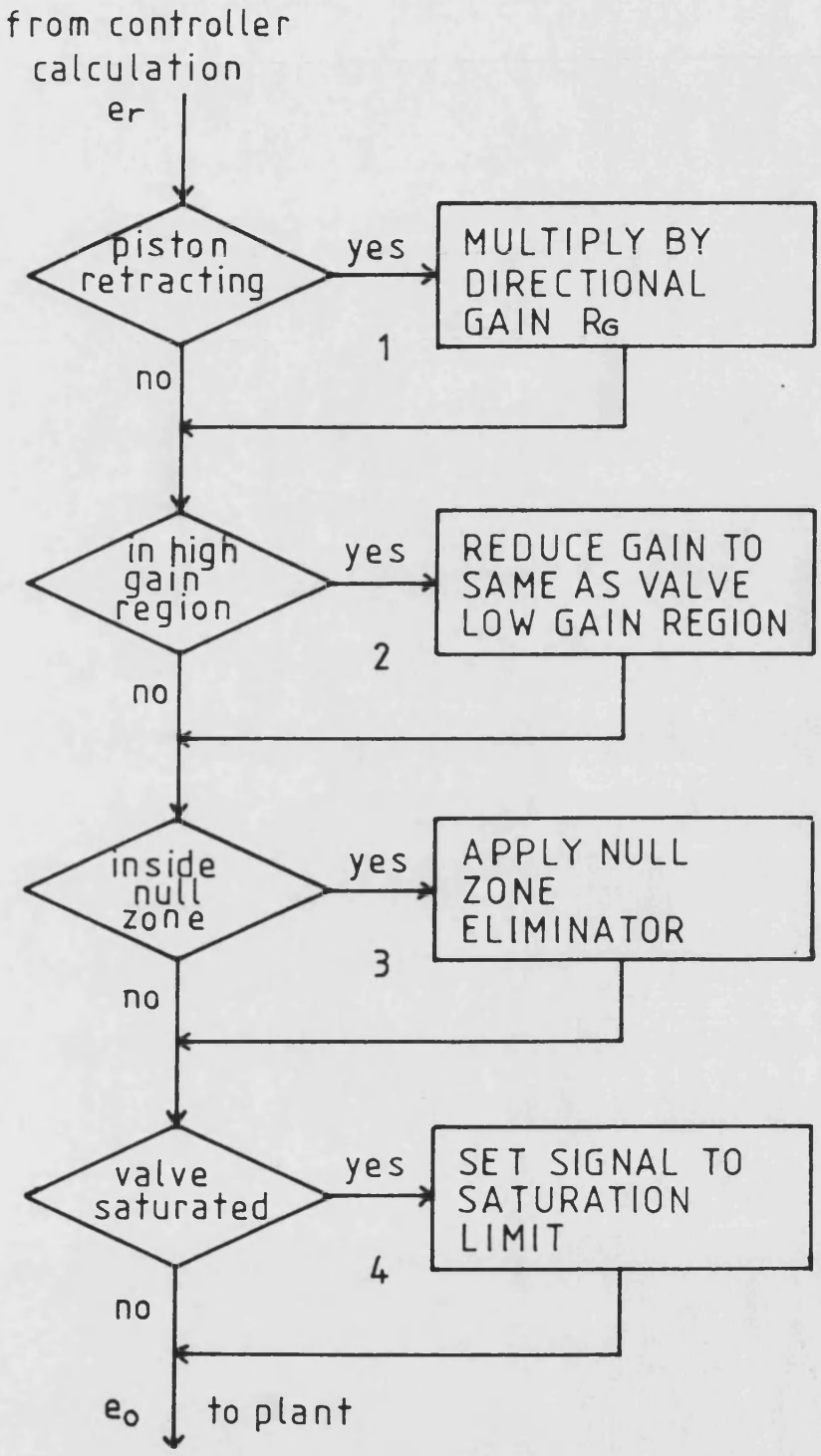

7·19 INVERSE FILTER FLOW CHART

Fig 7·20

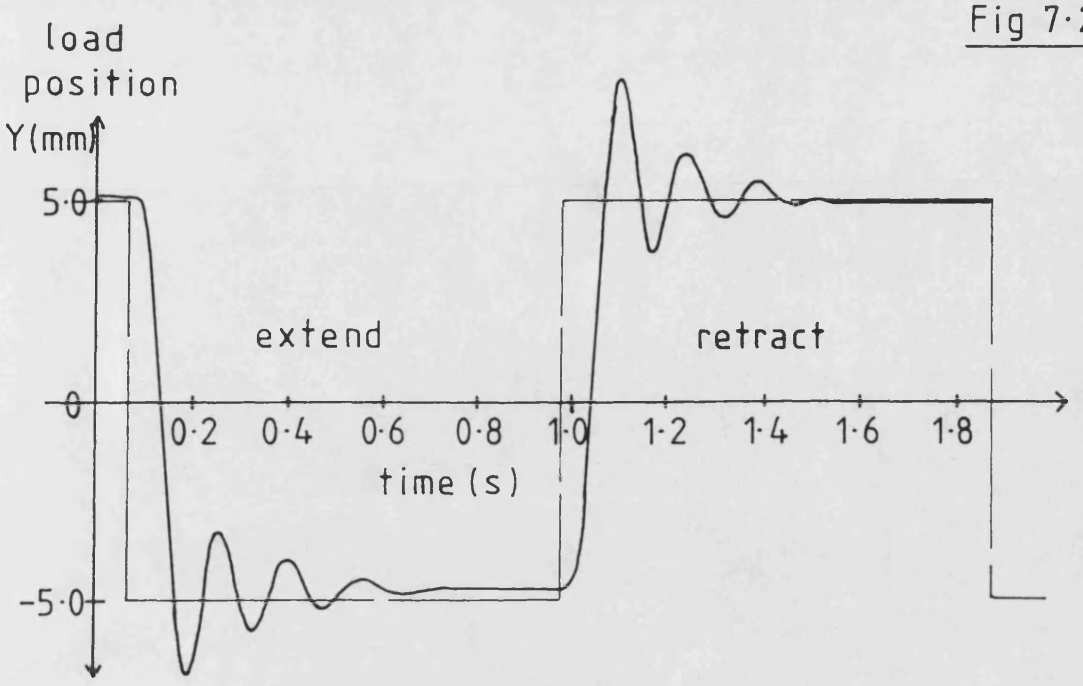

7·20 FIXED CONTROLLER STEP RESPONSE ~ DEAD VOLUME SWITCHED IN

Fig 7·21

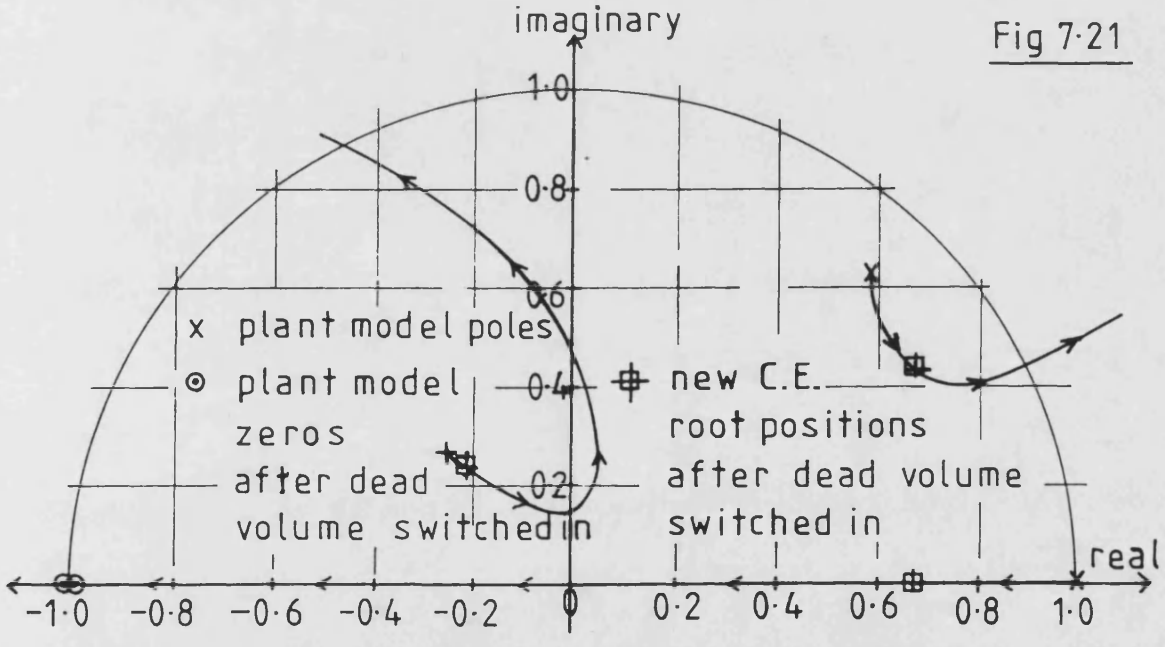

new C.E. roots: z = 0·68, z= 0·68 +/- j0·43

7·21 FIXED CONTROLLER ROOT LOCUS ~ DEAD VOLUME SWITCHED IN

Fig 7·22

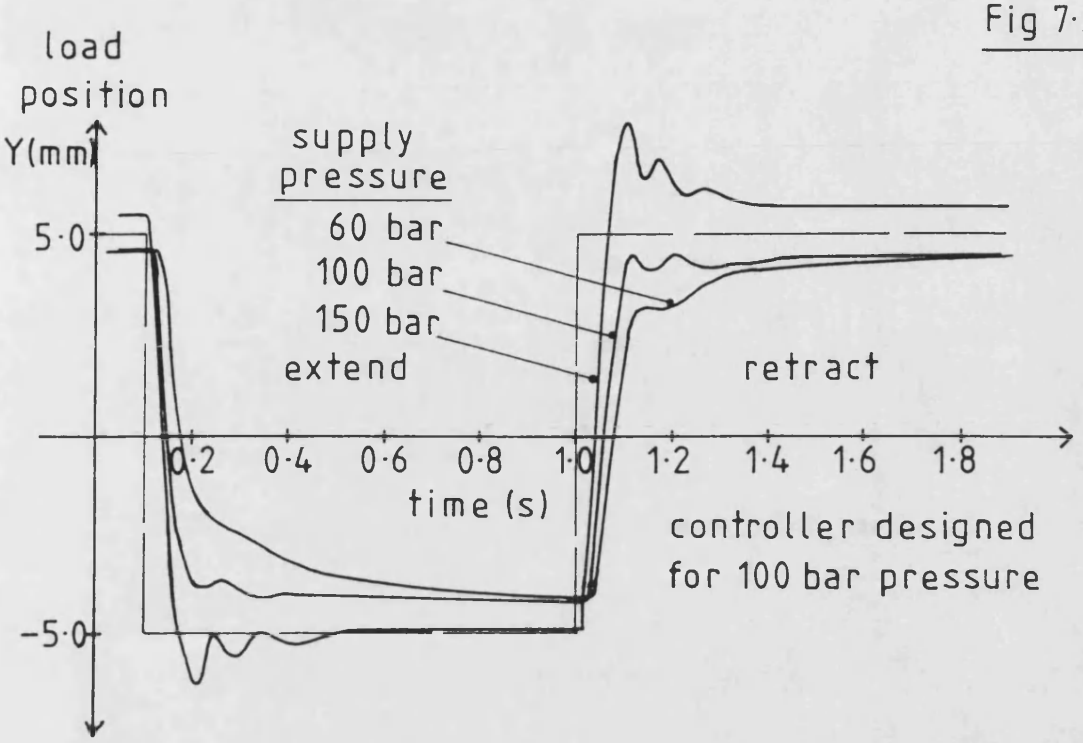

7·22 FIXED CONTROLLER STEP RESPONSE ~ SUPPLY PRESSURE CHANGES

Fig 7·23

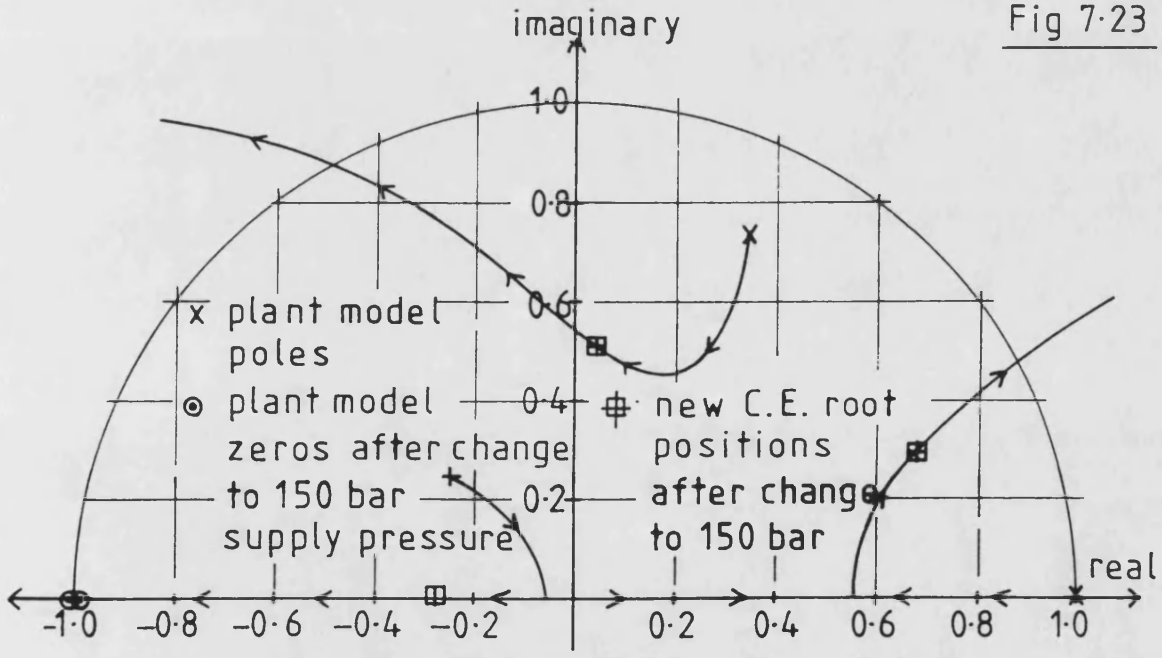

new C.E. roots: $z = -0{\cdot}27$, $z = 0{\cdot}69 \pm j0{\cdot}3$, $z = 0{\cdot}04 \pm j0{\cdot}57$

7·23 FIXED CONTROLLER ROOT LOCUS ~ 150 BAR SUPPLY PRESSURE

Fig 7·24

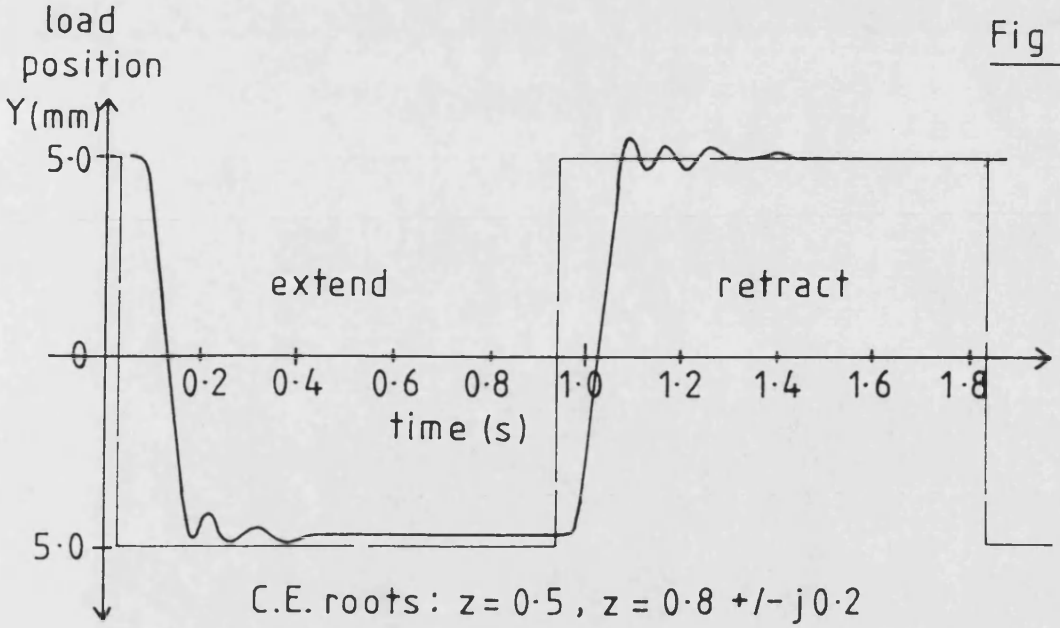

7·24 INTEGRAL ACTION CONTROLLER STEP RESPONSE

Fig 7·25

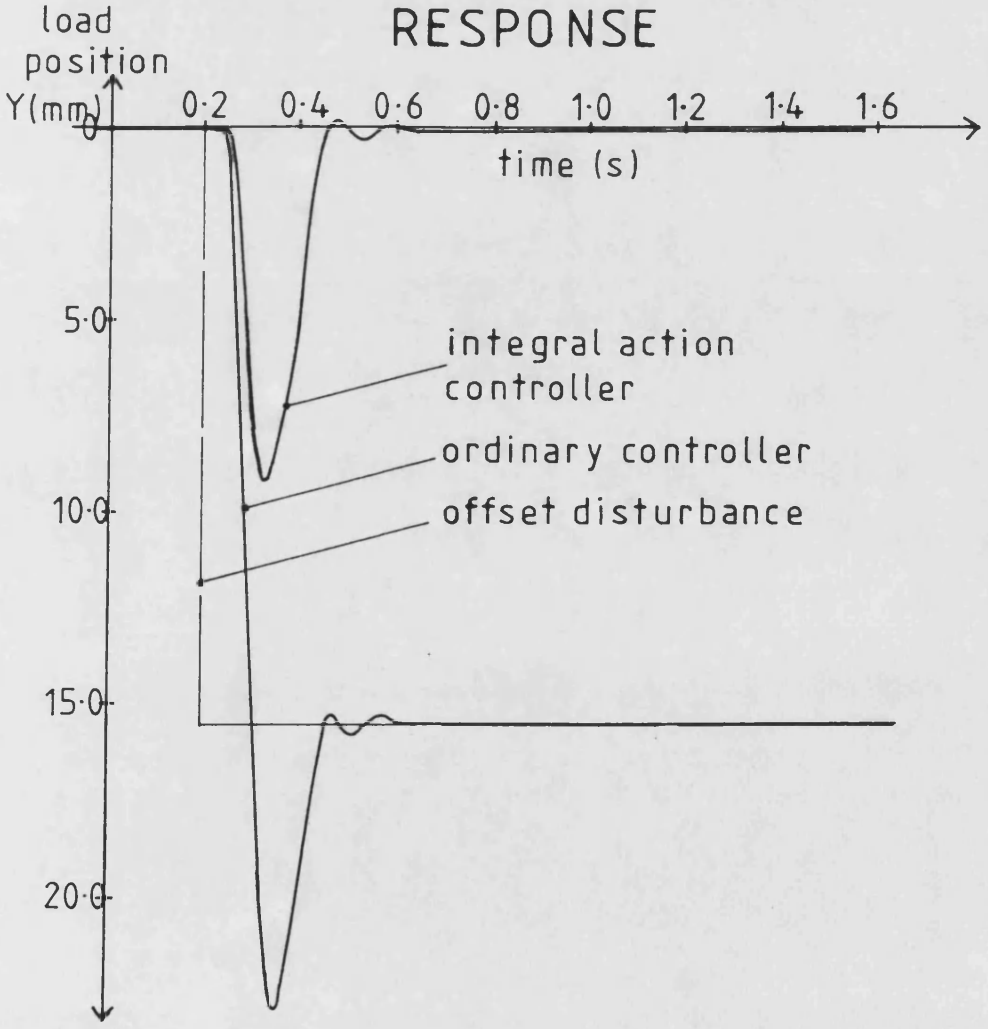

7·25 INTEGRAL ACTION CONTROL OF STEP DISTURBANCE

Fig 7·26

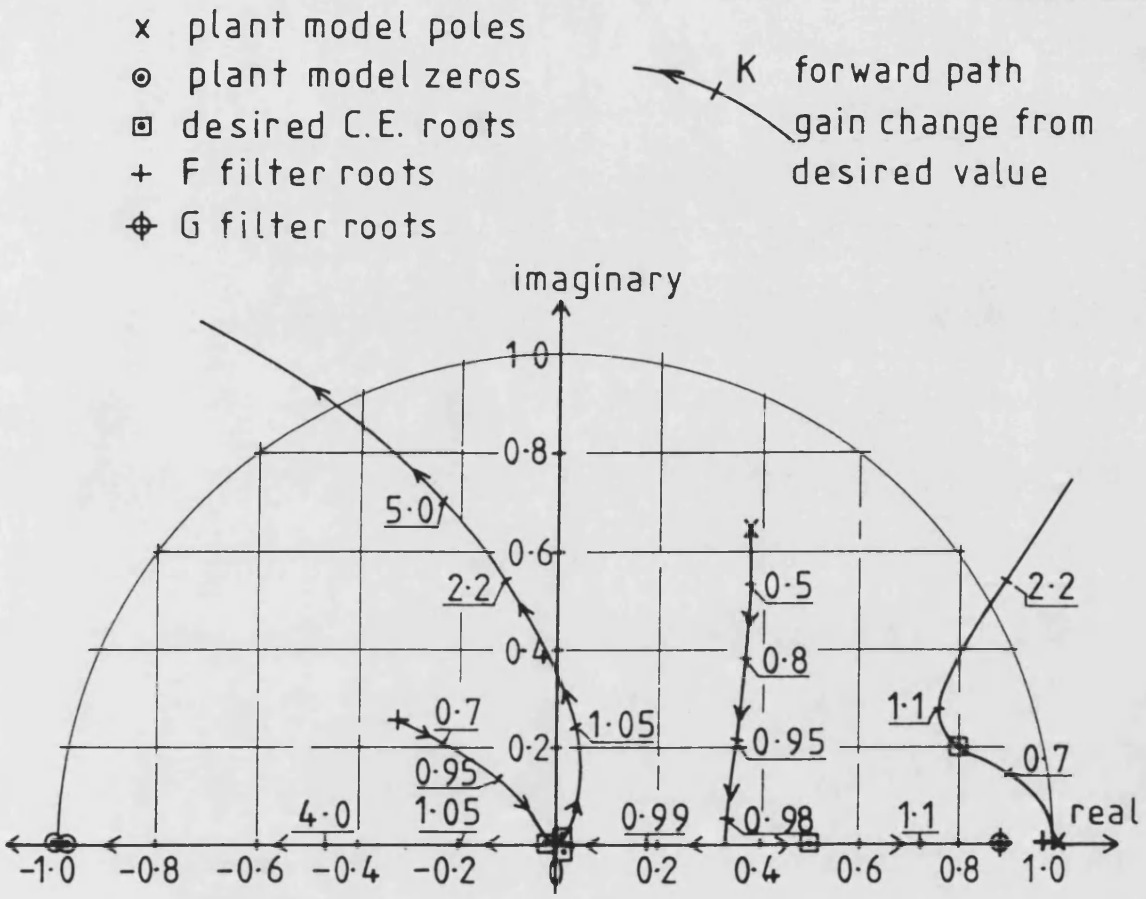

desired C.E. roots: $z = 0{\cdot}5, z = 0{\cdot}8 \pm j0{\cdot}2$

7·26 INTEGRAL ACTION CONTROL SYSTEM ROOT LOCUS

Fig 7·27

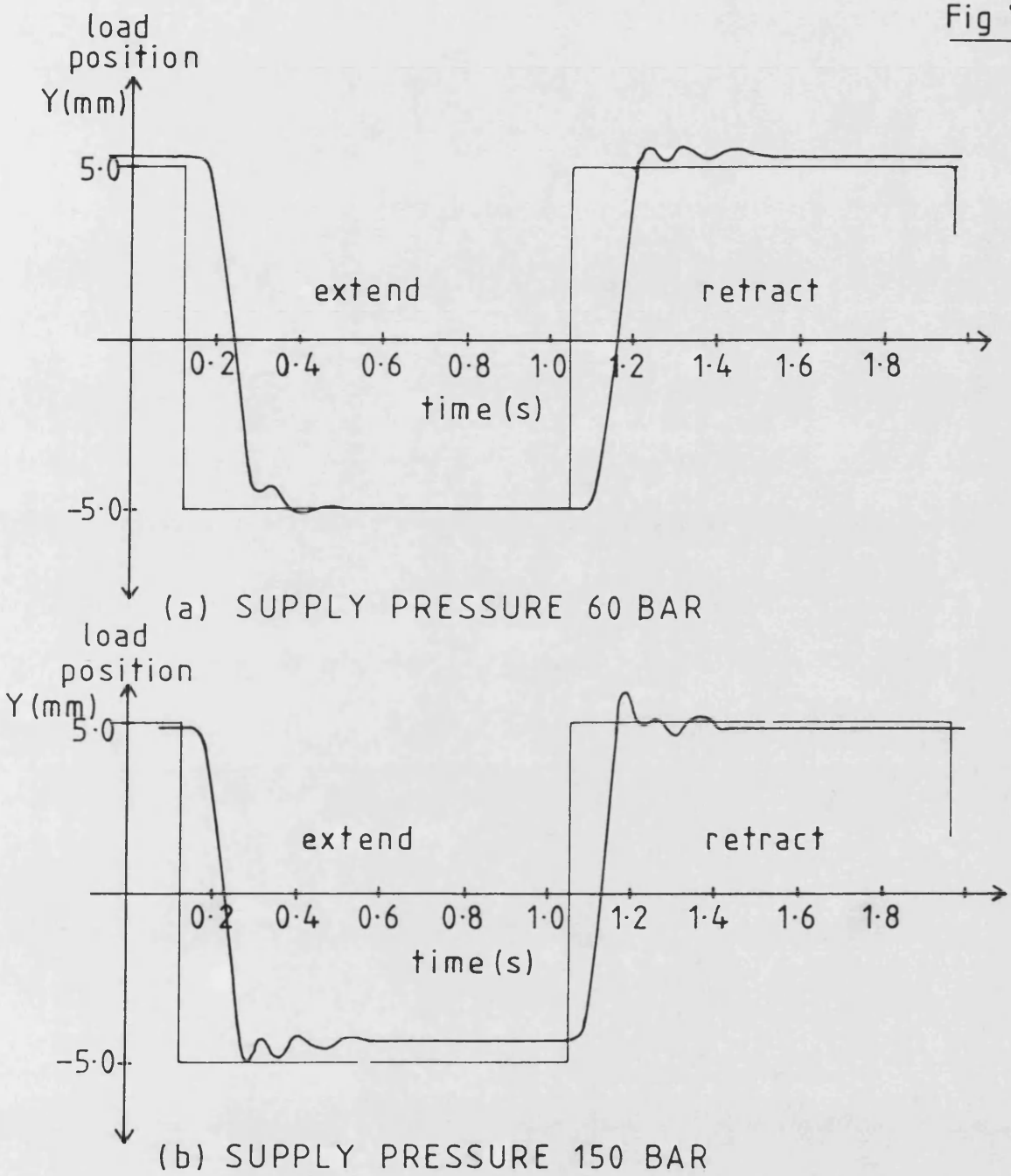

7·27 FIXED INTEGRAL CONTROLLER STEP RESPONSE ~ SUPPLY PRESSURE CHANGES

Fig 7·28

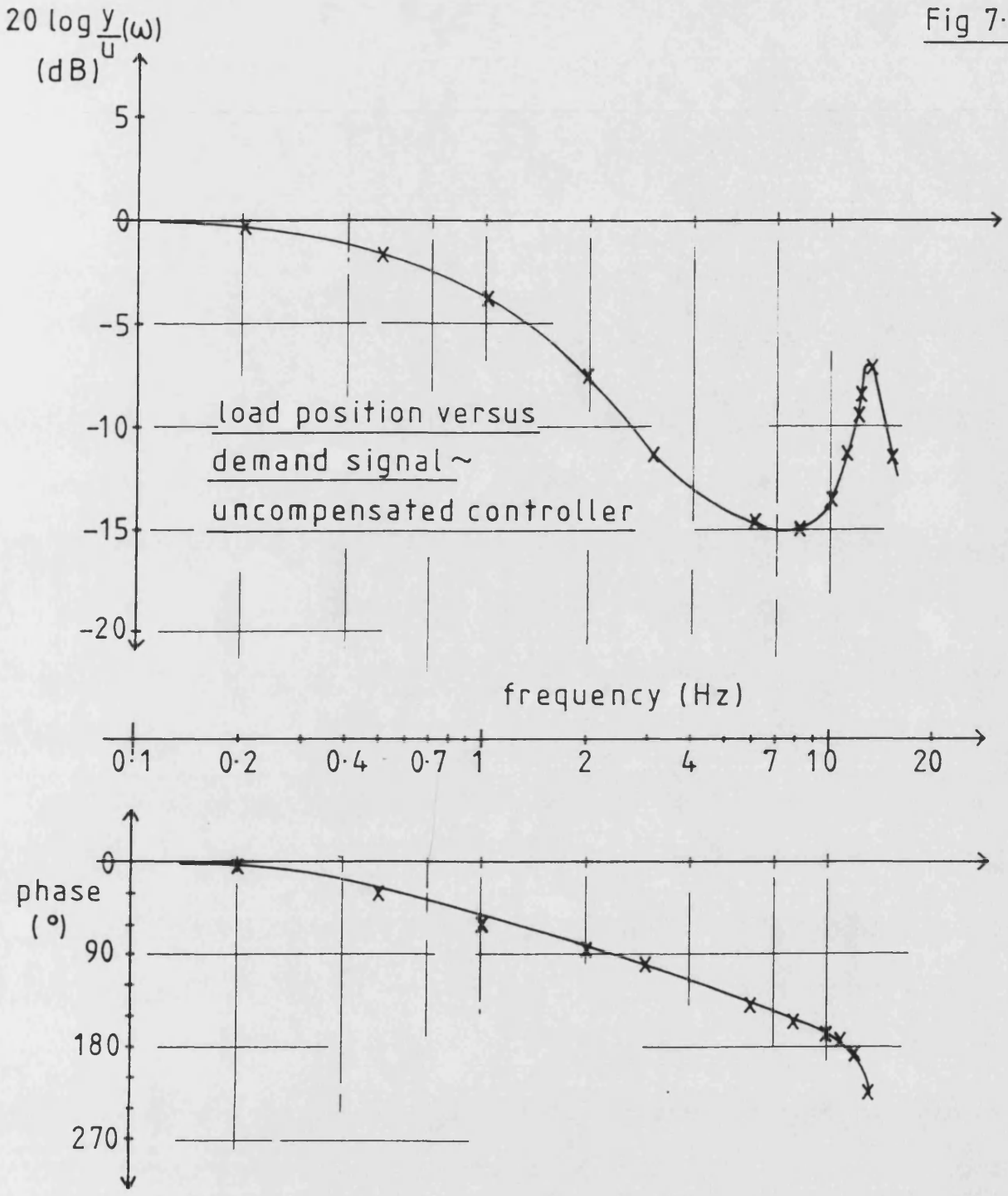

7·28 UNCOMPENSATED CLOSED LOOP FREQUENCY RESPONSE

Fig 7·29

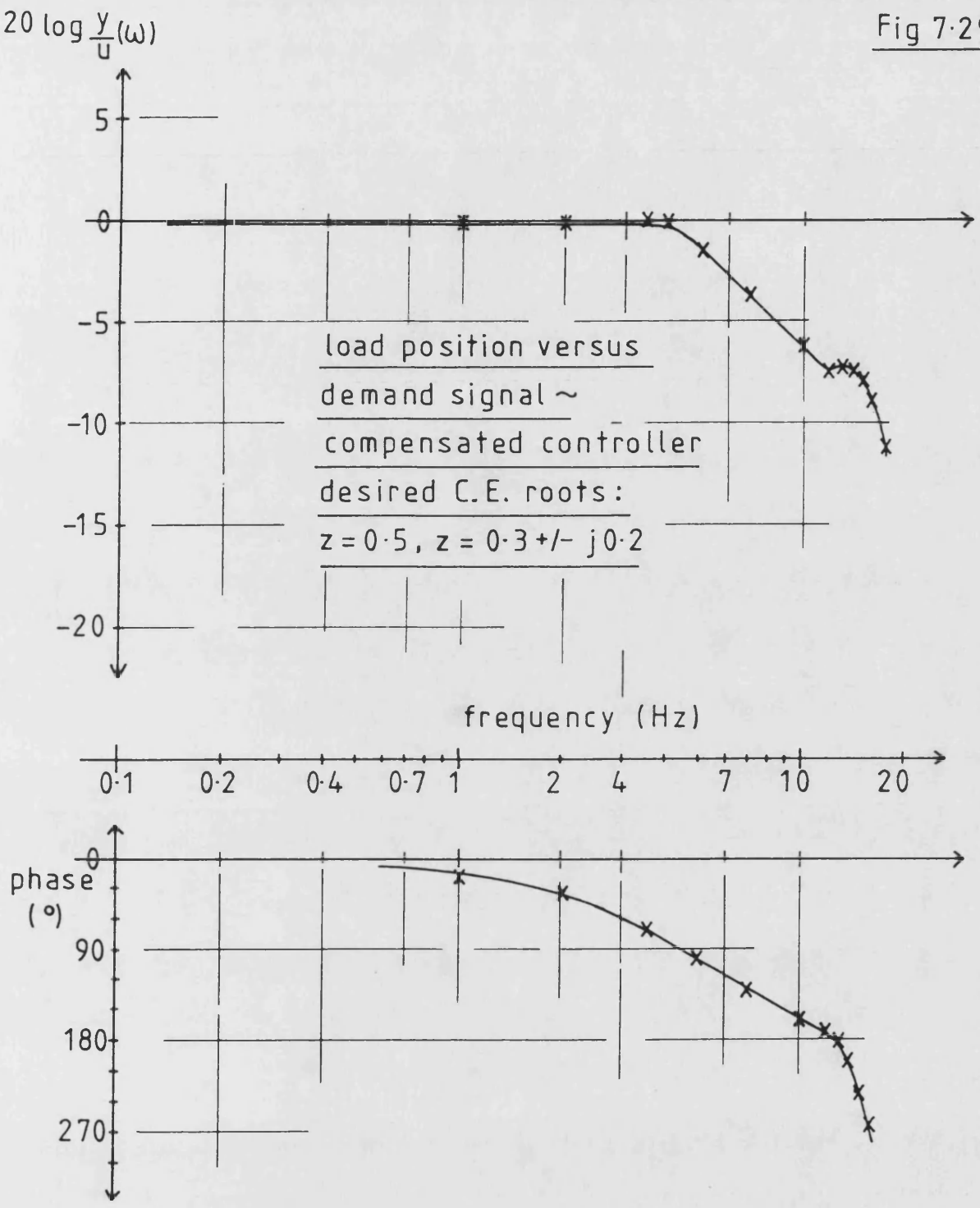

7·29 COMPENSATED CLOSED LOOP FREQUENCY RESPONSE

8. SERVOSYSTEM IDENTIFICATION

8.1 Introduction

801 The previous chapter showed that in of spite nonlinearities in the servosystem a good control system could be designed assuming a linear plant model. However difficulties arose in obtaining appropriate plant model coefficients from which to derive the controller. Frequency response tests were found to give inappropriate models and to be time consuming in implementation.

802 A solution to these problems is found in the rapidly expanding field of parameter identification. Discrete model parameter identification techniques provide an alternative to conventional methods which is relatively quick to implement, and requires no specialised test equipment other than the microprocessor. Additionally, since the 'a' coefficients are calculated as output, these values can be used directly in the Pole Placement algorithm. In this chapter a Recursive Least-Squares (RLS) discrete identification method is proposed, and is developed specifically to complement the servosystem controller design algorithm discussed in Chapter 4.

803 In section 8.2 the RLS method is compared with conventional response methods used in electrohydraulic servosystem identification. The equations of the RLS algorithm are presented in section 8.3, and the specific case of an identification algorithm for the servosystem test rig is discussed in section 8.4. The RLS algorithm is based on an approximate Pole/Zero Mapping model of the plant, and in section 8.5 test results are presented verifying the accuracy of the algorithm in application to the electrical simulation network (see section 3.5).

804 Practical application of the identification algorithm to the servosystem is described in sections 8.6 to 8.9. The effect of the servosystem inherent and time variable nonlinearities are shown in section 8.6, leading to a discussion of algorithm robustness in sections 8.7 and 8.8. Finally in section 8.9 the factors influencing the model parameter convergence speed are demonstrated.

8.2 Identification Methods

805 There are two approaches in the derivation of a plant model for controller synthesis: physical modelling, or black box modelling. In the former an attempt is made to derive a set of equations describing every aspect of the plant behaviour, and in the latter a simple mathematical equation is sought describing a relationship between the measured input and output signals of the plant, a process known as plant identification. The derivation of the equations of a physical model can be a complex and time consuming process, and even when the model is complete, its accuracy often cannot be guaranteed unless verified by testing against real plant behaviour. Physical modelling is most useful at the design stage, where due to the absence of any hardware, black box testing is not possible. At this stage the analysis of physical equations can help to shape the design. However at the controller synthesis stage where hardware is already existing, almost invariably the black box approach is used for fine tuning.

806 In the identification of electrohydraulic servosystems the conventional methods of black box testing have been by step and frequency response tests. In recent years the wider availability of microprocessor systems has allowed these methods to be augmented by various computational curve fitting techniques, from which the relevant discrete domain data can be derived [75,76]. However the basic problems remain: such tests are still time consuming, and they still require the use of specific and often unrepresentatively small input signals which can lead to spurious results. In addition specialised test equipment is required.

807 A more attractive alternative which has been proposed is identification by the use of pseudo random binary signals (PRBS). Here a pulse sequence simulating white noise is passed through the system, and by the correlation of the input and output signals the pulse response of the plant can be obtained [77]. Processing of the data beyond that point depends on the form of the model required. Typically the data is translated into the frequency domain from where the appropriate controller can be designed. PRBS black box modelling of electrohydraulic systems has been shown in specific cases to compare favourably with the more conventional methods [75,78]. However, many researchers having studied identification, stop short of actually synthesising a controller from the test data, thus the real test of the usefulness of the identified model has not been applied.

808 PRBS testing offers some potential for on-line identification as the pulse train can be superimposed on the normal operating signal. However to avoid distortion caused by the operating signal, PRBS must be applied at times when the plant is at rest. This method was proposed in the early days of adaptive control as a means of updating process plant controllers on-line to minimise set point errors [79,80]. In servosystem situations where the set point, ie demand signal, is moving about continually, on-line identification using PRBS is more difficult to implement. Also since the response times of electrohydraulic servosystems are considerably faster than process plants, the time spent processing the large PRBS data records may be too long to enable any useful update of the controller.

809 The advent of powerful computational devices has opened up the whole concept of black box identification, and in the past fifteen years a vast amount of literature describing new methods has been published, and numerous surveys have been carried out [81,82,83,84]. The increasing use of microprocessors for digital control has especially encouraged the development of discrete linear transfer function identification which can be used directly with digital control theory. The most widely discussed and tested method of parametric identification is the Least-Squares method. Here, the plant model to be identified is first chosen in general form, ie the number of model poles and zeros, the actual values of the roots are then found by least squares fitting of the model to the experimental data. The choice of plant model form is based on a knowledge of the behaviour of the plant. For example, for the servosystem, the obvious choice in the light of the results of Appendix 1 and Chapter 7 is to use the model:

$$\frac{y}{e}(z) = \frac{a_1(1+z^{-1})^2 z^{-1}}{(1-z^{-1})(1-a_2 z^{-1}-a_3 z^{-2})} \qquad (8.1)$$

The objective is to estimate the 'a' coefficients of the above model such that the model input/output relationship follows that of the plant irrespective of the input signal.

810 The Least-Squares method works by passing the same drive signal e, into both the plant and the model, which initially is based on guessed 'a' coefficient values. The plant output measurements are compared with the model output and the 'a' coefficient values are adjusted so that over a batch of plant input/output samples, the sum of the squares of the errors between the plant output and the model output

is minimised. This process is illustrated in Fig 8.1.

811 The Least-Squares identification technique has a number of advantages over the conventional black box testing methods: most importantly, the technique does not demand small unrepresentative servosystem drive signals, the 'a' coefficients being derived from the normal plant operating signals. If there are significant nonlinear effects taking place during operation, then the best linear model fit to the nonlinearly related sampled data points is sought. Thus nonlinearities are accounted for to some extent, and during the research it has been found that good controllers can be designed from linearised models derived in this way.

812 In the work presented in this thesis the Least-Squares method is used in recursive form, ie RLS identification. Here, exactly the same process as described above is carried out to obtain the 'a' coefficients, but each pair of sampled data points is dealt with within the sample period using the controller auxiliary processing time. The basic equations are also modified so as to enable exponential forgetting of old data, thus by using only recent data points to calculate the 'a' coefficients the algorithm responds to changes in plant parameters. In this form the identification algorithm can be used in conjunction with the the Pole Placement algorithm either for automatic controller design or more attractively for STC adaptive control.

8.3 Recursive Least-Squares (RLS) Identification

813 The equations for both the Least-Squares and RLS identification techniques are summarised in Appendix 5. More detailed derivation and discussion of the general equations can be found in abundance in the control and identification literature [58,85,86]. In this section the objective is to give an appreciation of the working of RLS used in servosystem identification. It is assumed that a plant model with three coefficients has been specified, (for example equation 8.1), which from equation A5.3 can be expressed recursively as:

$$\hat{y}(k) = a_1x_1+a_2x_2+a_3x_3$$

or in matrix form:

$$\hat{y}(k) = \underline{X}^T(k)\underline{A}(k) \tag{8.2}$$

Where $\hat{y}(k)$ is the next estimated plant output, in terms of the previous measured plant input/output data x_1, x_2, x_3. Every sample period the information vector $\underline{X}(k)$, and the parameter vector $\underline{A}(k)$, are updated, and the next estimate of the plant output calculated.

814 If a large batch of input/output samples e, and y, during a plant transient has been stored in memory, then equation A5.6 can be used to calculate the parameter vector $\underline{A}(k)$. The equation is restated here choosing unity forgetting factor, ie giving equal weights to all of the data points:

$$\underline{A}(k) = \frac{\sum_{i=1}^{i=k} \underline{X}(i)y(i)}{\sum_{i=1}^{i=k} \underline{X}(i)\underline{X}^T(i)} \tag{8.3}$$

The procedure for calculating a batch of samples from $i = 1$ to k, say N samples, is lengthy. For the i th pair of the N pairs of input/output samples, the procedure is: firstly, update the information vector $\underline{X}(k)$, ie using previous measured input/output data. Secondly, multiply this by the i th measured y value giving the i th numerator term of equation 8.3; and thirdly, add this to all of the previously calculated numerator terms. Next the i th denominator square matrix elements are calculated and likewise added to all of the previous terms. Calculation of the square matrix is made simpler due to its symmetry, thus the upper triangle only need be calculated. After repeating these calculations N times, the denominator matrix must be inverted to obtain $\underline{P}(k)$, known as the covariance matrix. Finally, multiplying by the numerator vector, the plant parameter vector $\underline{A}(k)$, can be calculated.

815 If it is assumed that the noise on the plant input/output measurements is white with variance σ^2, then the calculated 'a' coefficient estimates converge asymptotically to their correct values, ie are unbiased, and it can be shown that the covariance matrix of the estimation errors at the kth instant is:

$$\underline{C}(k) = \sigma^2\underline{P}(k) \tag{8.4}$$

ie, the accuracy of the estimates is seen to be dependent on the nature of the noise on the input/output signals [85]. Noise in this context refers to any departure of the real plant from linear behaviour, whether caused by genuine noise on the signal measurements, or by bad modelling of the plant. In practice, noise in the system is generally not white, and the presence of unmodelled dynamics and load disturbances creates some biasing of the estimates. If the biasing is severe then a model of the disturbances also must be included in the scheme [87].

816 Now from equation A5.8 it can be seen that $\underline{P}(k)$ gets smaller, corresponding to greater parameter accuracy (see equation 8.4), when large numbers of samples are processed. Generally, the larger the noise levels on the signals, the larger the batch of data points required to achieve the same accuracy. The effect of N on the coefficient estimates can be seen from equation A5.11 of Appendix 5, ie the recursive form of the 'a' coefficient update equation:

$$\underline{A}(k) = \underline{A}(k-1) - \underline{P}(k)\underline{X}(k)[\underline{X}^T(k)\underline{A}(k-1) - y(k)] \qquad (8.5)$$

It is seen that the adjustment to the 'a' coefficients as a result of the last set of processed data points, depends on the plant/model error shown inside the square brackets of equation 8.5 (see equation 8.2), and on $\underline{P}(k)\underline{X}(k)$, commonly known as the 'Kalman Gain'. At the start of a calculation $\underline{P}(k)$ is large and the 'a' coefficients are rapidly adjusted towards the correct values. After many sets of data points have been processed when $\underline{P}(k)$ becomes small, very little further adjustment is made to the parameter vector, and full convergence is reached.

817 Although converged 'a' coefficients are desirable, the small values in the $\underline{P}(k)$ matrix presents a problem in situations where the plant parameters change. If as is intended, equation 8.5 is to be able to adapt to plant parameter changes, then having small elements in the covariance matrix $\underline{P}(k)$, will not allow rapid convergence to the new parameter values. Thus a means of artificially increasing $\underline{P}(k)$ is required, and this is provided by the forgetting factor α. Appendix 5 shows that the covariance matrix can be updated recursively, eliminating the need for a tedious inversion. Also included in the $\underline{P}(k)$ update equation A5.10 is the forgetting factor as shown below:

$$\underline{P}(k) = \frac{\underline{P}(k-1)}{\alpha} - \frac{\underline{P}(k-1)\underline{X}(k)\underline{X}^T(k)\underline{P}(k-1)}{\alpha[\alpha+\underline{X}^T(k)\underline{P}(k-1)\underline{X}(k)]} \tag{8.6}$$

If $\alpha = 1$ then it is seen that $\underline{P}(k)$ continues to get smaller and smaller each sample period, but if it is set to less than 1, say 0.98, then each sample period the previous $\underline{P}(k)$ elements are divided by 0.98, ie increased by 2 %. Thus after a large number of samples , an equilibrium point is reached with the coefficients of the covariance matrix tending to positive nonzero values. The smaller α is made, the larger the equilibrium values of the $\underline{P}(k)$ matrix coefficients become, and the more rapidly can the 'a' coefficient values be changed to adapt to a new set of plant conditions. It can be shown that the speed of convergence to a change in plant parameters is exponential [88] and has a time constant of N_T sample periods,where:

$$N_I = \frac{1}{1-\alpha} \tag{8.7}$$

Thus for the servosystem test rig sample period of 15 ms, $\alpha = 0.98$ corresponds to convergence with a time constant of 0.75 s, and a forgetting factor $\alpha = 0.9$ gives a time constant of 0.15 s. If the forgetting factor is set too low then the large covariance matrix elements lead to increased estimation errors (see equation 8.4). In practice the choice of forgetting factor is a compromise between fast convergence, according to equation 8.7, and robust estimation according to equation 8.4. Typically, forgetting factors fall in the range 0.9 to 1 depending on the signal to noise ratio of the system and the modelling accuracy.

818 The use of a fixed forgetting factor less than unity unfortunately is not the complete answer, the situation when the closed loop system is at rest must be considered. When the system is at rest the information vector $\underline{X}(k)$, goes to zero, and equation 8.6 becomes:

$$\underline{P}(k) = \frac{\underline{P}(k-1)}{\alpha} \tag{8.8}$$

Thus the elements of $\underline{P}(k)$ increase exponentially. Several things could happen depending on how long the plant remains in this state of rest. Eventually a numerical overflow will occur, but if the RLS algorithm is being used for adaptive control, then generally the drift of the 'a' coefficient estimates will give an unstable closed loop system prior to this. The closed loop system will either persist in

dangerous high amplitude unstable oscillations, or the dynamic information obtained from the instability will cause the RLS identification algorithm to reconverge for a period. In this latter case a limit cycling type instability results.

819 This phenomena is caused by the lack of dynamic information in the plant signals, and is known as 'estimator wind up', a number of solutions have been proposed [89,90]. In the work presented in this thesis it was found adequate simply to set the forgetting factor to unity when the signal quality was poor. In this situation the current 'a' coefficient values are maintained, and since the plant is at rest the plant/model error is small and the drift in 'a' coefficient estimates slight, unless the plant is at rest for extremely long periods of time. The difficulty in this approach is knowing when is the right time to set the forgetting factor to unity or to switch it back to its normal operating value.

820 The best algorithm adaptation speed to plant parameter variations is obtained by having a continuously variable forgetting factor. In such a scheme, the forgetting factor is designed to go to a low value only when the plant model error is large, as is the case when the plant parameters suddenly change [90]. When the correct model coefficient values are once again reached, the plant/model error is again small and the forgetting factor is set to near unity thereby giving robust estimation.

8.4 Application to Third Order Servosystem Model

821 The on-line calculation of equations 8.5 and 8.6 to obtain the covariance matrix and parameter estimation vector is very demanding on processor time, and from this point of view it is important to choose a plant model with the minimum of 'a' coefficients. In section 3.6, it was pointed out that depending on the method of converting from the s plane to the z plane the three coefficients of the s plane model:

$$\frac{y}{e}(s) = \frac{K\omega_n^2}{s(s^2+2\zeta\omega_n s+\omega_n^2)} \tag{8.9}$$

could be converted to a z plane model having a varying number of coefficients in the numerator. For example, the use of either z transform tables or the bilinear transformation method leads to three numerator coefficients and three denominator

coefficients [55]. After comparison of the methods, the Pole/Zero Mapping method which has only one numerator coefficient was found to be most suitable. Conversion of equation 8.9 using this method gives the already stated equation 8.1.

822 The number of coefficients in equation 8.1 is also reduced by the use of an integral action model rather than a general third order model. In the latter case three rather than two denominator coefficients would be required. Since servosystem plants contain inherent integral action, the model of equation 8.1 can be used with no adverse effects. Equation 8.1 is reduced by multiplying both sides by the factor $(1-z^{-1})$ yielding:

$$\frac{y_d}{e}(z) = \frac{a_1(1+z^{-1})^2 z^{-1}}{1-a_2 z^{-1}-a_3 z^{-2}} \tag{8.10}$$

where:

$$y_d(k) = y(k)-y(k-1) \tag{8.11}$$

ie, the difference between the present and previous y values. Thus the model is implemented taking y_d rather than y as the plant output. Equation 8.10 can now be expressed in recursive form:

$$y_d(k) = a_1[e(k-1)+2e(k-2)+e(k-3)]+a_2 y_d(k-1)+a_3 y_d(k-2) \tag{8.12}$$

By comparison with equation 8.2, it can be seen that the elements of the parameter vector are a_1, a_2 and a_3, and the elements of the information vector are:

$$\begin{bmatrix} x_1 \\ x_2 \\ x_3 \end{bmatrix} = \begin{bmatrix} e(k-1)+2e(k-2)+e(k-3) \\ y_d(k-1) \\ y_d(k-2) \end{bmatrix} \tag{8.13}$$

The $\underline{P}(k)$ matrix update equation 8.6, looks to be lengthy in implementation, but since the matrix is symmetric then:

$$[\underline{P}(k-1)\underline{X}(k)]^T = \underline{X}^T(k-1)\underline{P}(k-1) \tag{8.14}$$

Thus this term need be calculated only once and can be used in three places in

equation 8.6.

823 The RLS algorithm is updated on-line every sample period, and thus forms part of the auxiliary processing time in the closed loop control algorithm. The structure of the RLS algorithm is shown in Fig 8.2. Every sample period the input signals are read and the next control signal is calculated and output, as shown in Fig 3.6. Then in the identification algorithm, the control and feedback signals are first tested to ensure there is sufficient dynamic information for convergence, and the forgetting factor is set appropriately. The difference between the present and previous plant output is then calculated, followed by the calculation of $\underline{P}(k-1)\underline{X}(k)$, from which the covariance matrix can be updated. Only six elements need be calculated since the matrix is symmetric. Calculation of the plant/model error $\hat{y}_d(k)-y_d(k)$, and the Kalman gain $\underline{P}(k)\underline{X}(k)$, then allows the update of the parameter vector $\underline{A}(k)$. Finally the information vector must be updated in preparation for the next sample period.

824 The whole identification process with three 'a' coefficients took 9 ms to implement on the Darkstar microcomputer using floating point arithmetic. If a general third order model rather than an integral action model had been used, the introduction of a fourth coefficient would have increased this time to 15 ms due to the large increase in the number of covariance matrix elements. Thus the need to use the absolute minimum number of 'a' coefficients is seen.

8.5 Identification of Electrical Simulation Network

825 In section 3.7 the dynamics of the approximate Pole/Zero Mapping model was compared with the exact discrete plant model, (derived from z transform tables). The electrical simulation network was set up to behave as the third order equation 8.9 with the parameters:

$K = 5.4\ /s \quad \zeta = 0.172 \quad \omega_n = 4.1\text{Hz}$

The effect of converting from the s to z plane for various sample periods was considered. Fig 3.9 showed that the approximate $z = -1$ zero positions of the Pole/Zero Mapping model caused excessive attenuation of the transfer function at frequencies approaching the aliasing frequency. For very slow sample frequencies

the effect was all the more marked.

826 Here the same comparison test is carried out, but the Pole/Zero Mapping transfer function frequency plots are obtained directly by RLS identification of the simulation network rather than by s to z transformation of the s plane model. Fig 8.3 shows the plant model frequency response before sampling, and the exact effect of sampling at different frequencies, (derived from the s plane model using the Hold Equivalence method). The corresponding frequency plots derived by RLS identification of the Pole/Zero mapping transfer function, equation 8.1, is shown in Fig 8.4, and it is seen that the resonant peak amplitudes agree well with those of Fig 8.3. It is only at frequencies higher than this, which are not prominent in the step response, that the erroneous effect of the model zeros is seen. The phase information is also seen to agree well with the exact model. The RLS identification was carried out at the sample periods shown, using a square wave demand signal and a closed loop summing junction controller.

827 Comparing Fig 8.4 with the s to z calculated model in Fig 3.9, it is seen that using RLS identification, the excessive attenuation at the resonant frequency has been corrected, the RLS identification algorithm thus giving a better result than s to z transformation in this case. The Pole/Zero Mapping method can thus be used with confidence for RLS identification. In situations where the modelling of the plant is not quite exact, ie as is the case for the Pole/Zero Mapping model, the identified parameter estimates are sensitive to the dynamic content of the servosystem input/output signals. Slightly different coefficient values will result depending on the the signals used. For the test results shown in Fig 8.3 and 8.4, the good result at the resonant frequency can be expected, since for the step response signal used, that frequency was dominant. In other situations the result may not have been so good. In a real servosystem there are always errors between the plant and model, and likewise a different RLS model will be identified depending on the signal content. The question which must be answered is whether these modelling errors are detrimental to the usefulness of the identified model in controller design.

8.6 Nonlinear Servosystem Identification

828 The application of the RLS identification method to the servosystem is discussed in the remaining sections of this chapter. The algorithm (shown Fig 8.2) was based

on the model equation 8.10, and equations 8.5 and 8.6 to obtain the model 'a' coefficients. The tests were carried out using a summing junction controller sampling at 15ms as shown in Fig 8.5. The position of the optionally implemented inverse filter should be noted. The signal e, was taken as the plant input, thus effectively including the inverse filter as part of the plant. The identification was thus of the linearised transfer function from e to y. The majority of the test results presented are with the inverse filter left out, and this mode of operation may be assumed unless otherwise stated. Almost all of the results were obtained using square wave demand signals which are both persistently exciting and sufficiently rich for good identification.

829 The nonlinearities of the servosystem had a significant effect on the identified plant model, and here each nonlinearity is considered in turn. The differential area piston used in the cylinder drive was shown in section 7.3 to have an effect on the forward path gain of the plant. It was found theoretically that the gain on the extend stroke compared to the retract stroke was increased by a factor:

$$R_G = \sqrt{\frac{A_p}{A_a}} \tag{8.15}$$

This was verified in practice as shown in Fig 7.5. The effect was evident from the identification algorithm by stepping the cylinder drive staircase fashion, first in one direction and then in the other direction. The cylinder drive was extended in 1 cm steps from the fully retracted position, and the estimated plant parameters were fully converged after about twenty steps. The frequency response of the resulting plant model transfer function is shown by the chain dotted lines of Fig 8.6, and shows a large resonant peak at 13 Hz as expected. The test was then repeated from the fully extended position, retracting the cylinder drive in 1 cm steps. The resulting model frequency response is shown by the dashed lines in Fig 8.6. As expected the retract stroke gain is less than that for the extend stroke. The gain change measured from Fig 8.6 is 1.15 compared to 1.21 measured from Fig 7.5.

830 It can also be noticed from Fig 8.6 that the amplitude of the resonant peak is considerably reduced on the retract stroke, corresponding to a higher damping ratio. This nonlinearity can be explained by considering two effects: firstly, there is more energy associated with the extend stroke to overcome Coulomb friction effects in the cylinder. Higher energy levels take longer to dissipate, leading to prolonged

oscillation. Secondly, the damping created by the servovalve is related to the direction of motion. This can be seen from equation A1.14 of Appendix 1, where it is shown that the damping ratio is proportional to the flow/pressure gain C_p, of the spool orifices. In equation A1.28 the ratio between extend and retract stroke gains is stated as being:

$$R_P = \frac{C_p^-}{C_p^+} = \sqrt{\frac{A_a}{A_p}} \tag{8.16}$$

In other words, the extend stroke damping ratio is less than the retract stroke damping ratio by a factor R_P, which from Fig 7.3 works out to be 0.83.

831 Although the identification algorithm is shown in Fig 8.6 to be sensitive to the directional nonlinearity, the significant time taken for convergence makes it of little value in controlling this effect in an STC adaptive controller. If a square wave demand is input, stepping backwards and forwards alternately, the identification model converges to a mean transfer function shown by the continuous line in Fig 8.6. The undesirable effect of the gain nonlinearity is best eliminated by the inclusion of the inverse filter. The use of the directional gain part of the filter only, was found to produce a similar identified plant model in the extend and retract strokes.

832 When the supply pressure is increased or decreased, the controller forward path gain needs to be decreased or increased respectively to maintain the same closed loop dynamic performance. The ability of an adaptive controller to perform this function depends on how well the change in gain is identified. Some test results using the RLS identification algorithm are shown in Fig 8.7 for supply pressures at 150, 100 and 60 bar. As expected increasing the supply pressure has increased the identified plant model gain. The differences in gain measured from the low frequency region of Fig 8.7 agree well with the theoretically calculated gains derived from the orifice equation. As in Fig 8.6 considerable changes in the resonant peak amplitude are seen, and again this could be due to the reduced energy levels at lower pressures which are quickly dissipated by Coulomb friction effects. There is also an increase in the valve flow/pressure gain C_p at lower pressures, which effectively increases the valve damping (see equation A1.14). The change in both gain and damping ratio can also be observed from the step response traces shown in Fig 8.8.

833 When the dead volume valves were opened, the compliance of the oil on both sides of the piston was increased, and the effect on the natural frequency was similar to that incurred by increasing the load inertia. The natural frequency was found to reduce from 13 Hz to 7 Hz, corresponding to increasing the load by between 3 and 4 times. This effect can be observed from the identified plant frequency response plots of Fig 8.9. The plots also show a small change in forward path gain which is unexplained by the theory of Appendix 1. The change in gain may have been caused by the valve dual gain characteristic, since the mean valve gain during a step response was found to be very sensitive to the nature of the response.

834 The constant amplitude 1.6 cm peak to peak square wave signal used in all of the identification test results so far presented, corresponds to an error signal in the range +/- 5 mA, which from Fig 7.5 is seen to reach into the high gain region of the valve flow characteristic. The influence of this nonlinearity was not noticed until the amplitude of the demand square wave was altered. A typical step response where the valve enters the high gain region is shown in Fig 8.10(a), and is characterised by a very rapid initial rise time and correspondingly high oscillations. At smaller amplitudes where the valve operates only in the low gain region, ie less than +/- 2 mA, the initial rise velocity following a step change in demand is less, this also causing a reduction in the severity of the oscillations. This reduced gain effect was made to occur over all of the amplitude range by the introduction of the inverse filter. A typical step response is shown in Fig 8.10(b). The corresponding identified model frequency response for the two signal amplitudes is shown in Fig 8.11, the dashed lines corresponding to a high step amplitude and the continuous lines to a small step amplitude. It is seen that in the small step case, the model produces the expected lower gain and resonant peak. A similar response could be made to occur for any signal amplitude by including the inverse filter.

835 In spite of its ability to adjust to signal amplitude dependent nonlinearities as shown in Fig 8.11, the identification algorithm was limited in its usefulness in this respect because of the slowness in adapting to these rapid and frequently occurring changes in the plant. Similarly to the directional nonlinearity, a better solution is to control the plant with the full inverse filter included, thus eliminating these nonlinear effects.

8.7 Servosystem Identification Robustness

836 In on-line RLS identification implementations, the accuracy with which the identified parameters are calculated in each sample period depends on the forgetting factor, the quality of the control signals and the model accuracy. However, in the great majority of applications the nature of the control signals is determined by the process in which the control system is being used, and the plant model is restricted to being a linear reduced order representation of the plant. Thus the only real control over the robustness of the identification algorithm is via the forgetting factor.

837 In each application the choice of forgetting factor required will depend on the the modelling errors present. For the electrical simulation network it was found that forgetting factors as low as 0.9 could be used whilst maintaining good coefficient estimates. The servosystem test rig on the other hand was found to require factors greater than 0.95 to produce satisfactory results. Fig 8.12 shows the change with time of the plant model 'a' coefficients for a 0.99 forgetting factor and with no change in the plant operating conditions. Some fluctuation in the parameter estimates is seen to occur synchronised to the step frequency, the biggest changes occurring immediately after the demand has been switched. The same test carried out with a 0.96 forgetting factor is shown in Fig 8.13 and considerable parameter fluctuation is seen to occur, again the biggest fluctuations synchronised with the step changes in demand.

838 In both Fig 8.12 and 8.13 the largest percentage fluctuation is exhibited by the numerator coefficient a_1. This sensitivity is due to the very small value of the numerator coefficient compared with the other two. In the Least-Squares equation A5.5, the objective is to determine the 'a' coefficients such that the plant/model error is minimised. All three coefficients contribute equally to the calculation, but since the numerator coefficient is small, the same magnitude of plant/model error can be tolerated whilst allowing greater percentage changes in its value than is the case with the other coefficients. This was found to be another good reason for using the Pole/Zero Mapping model. Here, the use of only one numerator coefficient and fixed zeros, was found to reduce the amount of coefficient fluctuation compared with identification using the Hold Equivalence model, where the roots were found to

drift, moving in and out of the unit circle.

839 The reduction of numerator coefficient fluctuation is important for adaptive controller schemes as it effects directly the forward path gain used in the controller, causing a lack of consistency in the step response. Apart from using larger forgetting factors coefficient fluctuation can be minimised by ensuring that the control system offsets are set up correctly. Offset introduced in the valve drive amplifier produces a steady state error in the control system. Thus while the plant is at rest with a nonzero drive signal applied, this same signal causes the integral action plant model to drift. The consequent plant/model error produces a corresponding drift in the 'a' coefficient values which can upset the identified model and hence the controller.

840 Even with careful tuning of the offset some inevitable drifting of 'a' coefficient estimates occurs when the system is at rest, the amount of drift depending on the choice of forgetting factor. This is shown in Fig 8.14 and 8.15 for forgetting factors of 0.996 and 0.98 respectively, where the square wave signal is suddenly switched off and held at zero. It is seen that in the former case the larger forgetting factor significantly reduces the speed of parameter drift. Notice in both cases that the numerator coefficient nose dives. In an adaptive scheme this would result in excessive controller forward path gains being implemented and the eventual instability of the control system.

8.8 Forgetting Factor Switching Strategy

841 The results of the last section show that some strategy is required to maintain the coefficient values during periods of poor signal quality. A number of schemes have been proposed [90,110] which change the forgetting factor in a continuously variable way dependent on the plant/model errors. These techniques have the advantage of giving good convergence speeds when adaptation is required, and holding the coefficient values steady when the signal quality is poor. However in the case of the servosystem test rig, a simpler more quickly implemented technique was used, whereby if the drive signal was slow moving and insufficient for identification then the forgetting factor was set to unity. In this condition none of the previous data used to identify the plant model is discounted, and thus the input of poor quality data, due to the plant being at rest, takes a long time to corrupt the

coefficient estimates.

842 The most difficult part of this technique was knowing exactly when to set the factor to unity and when to switch it to its original value. By experimentation it was found that a suitable switching strategy can be designed using two signals: the closed loop steady state error $(u-y)$, and the output difference signal y_d. If during operation the error signal is small, then either the servosystem is coming to rest exhibiting no further useful dynamic information, or an overshoot is about to occur. In the former case the forgetting factor should be set to unity, and in the latter it should be left at its original value. Hence the need for a second signal to establish whether the former or latter is occurring. If in addition to $(u-y)$ being small, the difference between the present and previous plant output signal values is also small, then a dynamically rich overshoot cannot be occurring. Thus if the test of both of these signals is positive then the dynamic content of the signals is poor and the forgetting factor should be set to unity.

843 The exact values of $(u-y)$ and y_d at which the forgetting factor should be switched was found by experimentation. If the limits were set too high, then useful dynamic information was wasted, and if set too low, parameter drifting occurred. Some results for the test rig are shown in Fig 8.16 where it is seen that after the most dynamically rich part of the step response the forgetting factor is set to unity, where it remains until the next step change in demand occurs. This strategy was found to give good results, allowing long periods of rest with no significant parameter drift. The developed switching strategy increases the robustness of the system for a wide variety of different signals, however in other applications more complex strategies may be required, or on the other hand, if the system is excited all of the time then no strategy may be needed.

844 All of the tests so far described have been based on the step response of the servosystem, which being dynamically rich is good for identification purposes. However some demand signals, though undergoing large changes, are insufficient for good identification. It is not easy to establish the presence of these signals so that identification can be stopped. For example Fig 8.17 shows the effect on the a_2 coefficient comparing identification of the plant at 150 bar and 60 bar supply pressure, the forgetting factor being set to 0.99. In the 150 bar case (Fig 8.17(a)), the signal is seen to be rich in dynamics giving good identification and small

coefficient fluctuation. At 60 bar however, the oscillations are less pronounced resulting in poor identification and greater coefficient fluctuation. In the 60 bar case it was found that the designed controller gave noticeably inconsistent step responses when implemented.

8.9 RLS Identification Parameter Convergence Speed

845 Having chosen a forgetting factor and devised a suitable switching strategy from the point of view of the robustness of the algorithm, it is useful to know how quickly the algorithm will adjust when a change in the plant parameters occur. For example Fig 8.18 shows how the plant model 'a' coefficients converge when the supply pressure changes from 60 bar to 150 bar, the forgetting factor being set to 0.996. As expected the most significant change is in the numerator coefficient, representing the forward path gain of the plant, and the convergence time is seen to be about 40 s, or after 10 demand square wave periods. In theory the convergence rate should be exponential according to equation 8.7:

$$\tau_C = \frac{\tau}{1-\alpha} \tag{8.17}$$

which for a sample period of 15 ms and a forgetting factor $\alpha = 0.996$ gives a convergence time constant of 3.75 s. However the convergence rate is also shown by Fig 8.18 to be a function of the dynamic content of the control signal, since the change in value of the coefficients is seen to be greatest immediately after a step change in demand has occurred. If a lower frequency square wave demand signal had been used, then the coefficients would have taken even longer to converge. The effect of changing the forgetting factor on the convergence speed is shown by comparing Fig 8.18 and 8.19. In the latter the forgetting factor was reduced to 0.98 and it is seen that the coefficients are converged after only about 10 s compared with 40 s in the previous case.

Fig 8·1

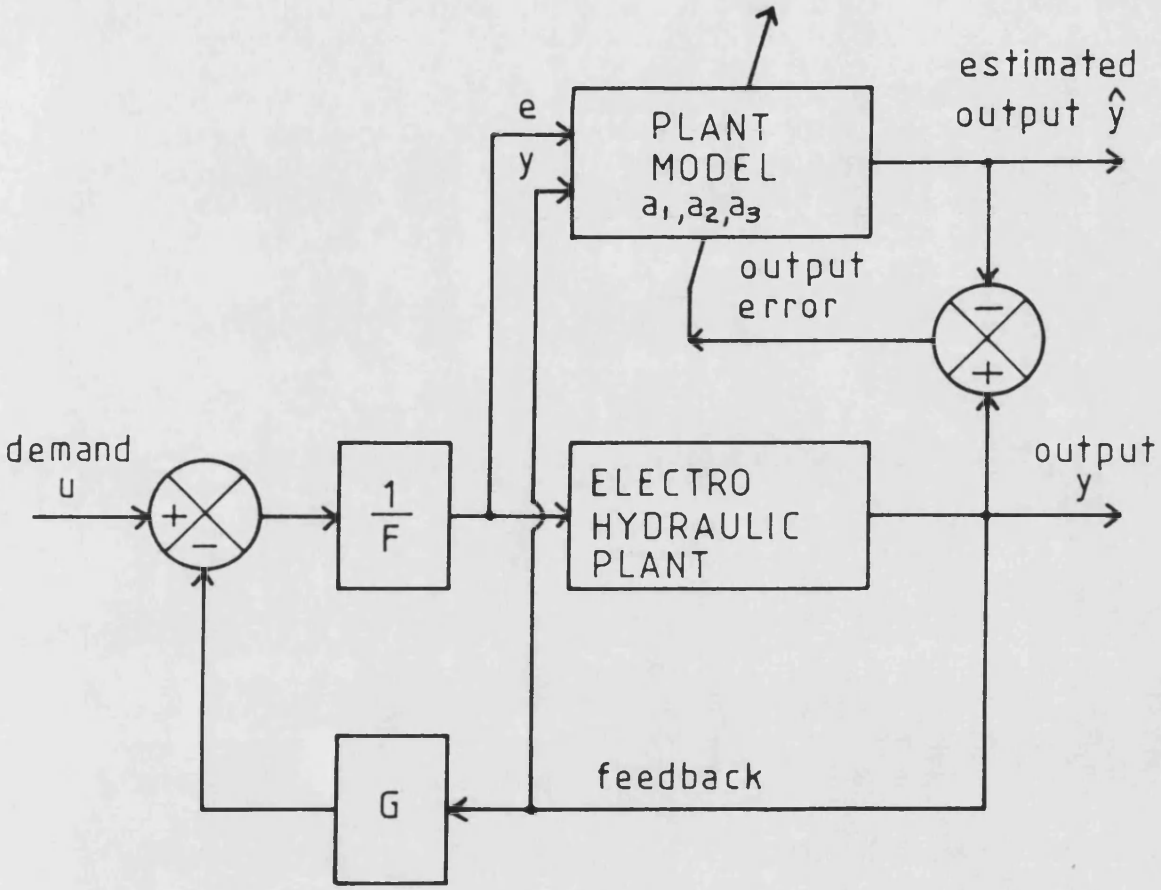

8·1 RECURSIVE LEAST-SQUARES IDENTIFICATION SCHEMATIC

Fig 8·2

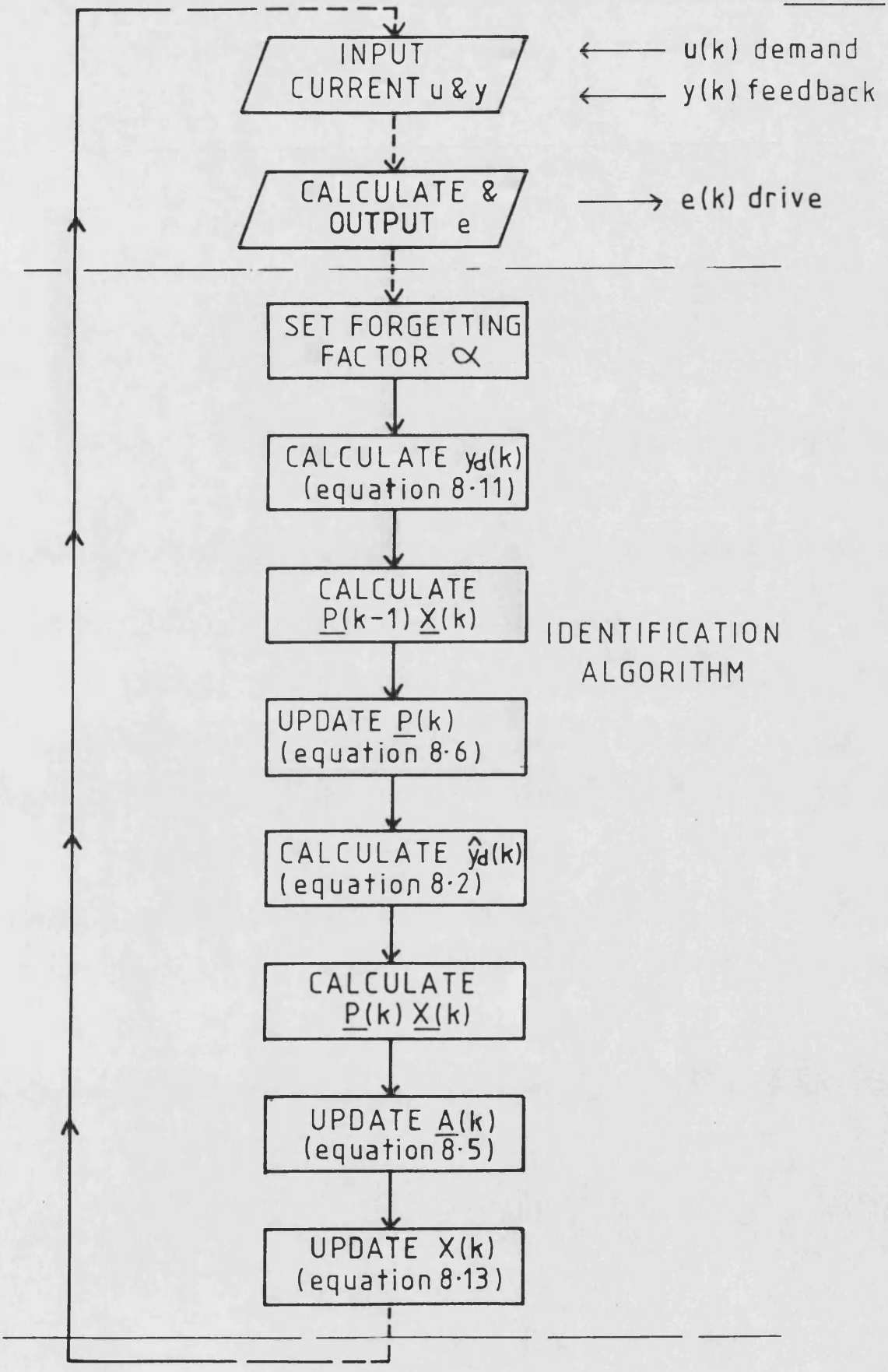

8·2 RLS IDENTIFICATION ALGORITHM FLOW CHART

Fig 8·3

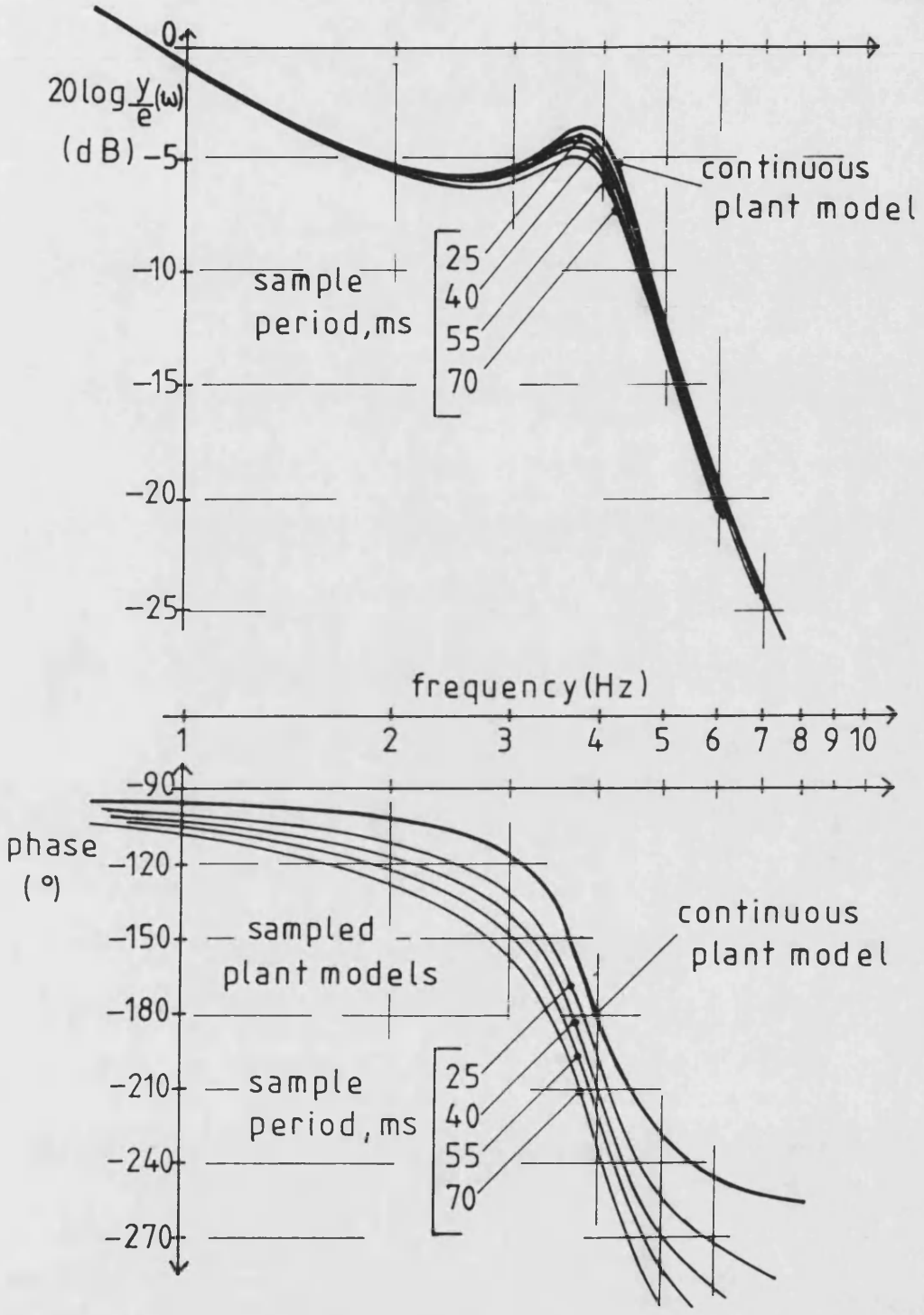

8·3 FREQUENCY RESPONSE OF SAMPLED PLANT ~ EFFECT OF SAMPLING

Fig 8·4

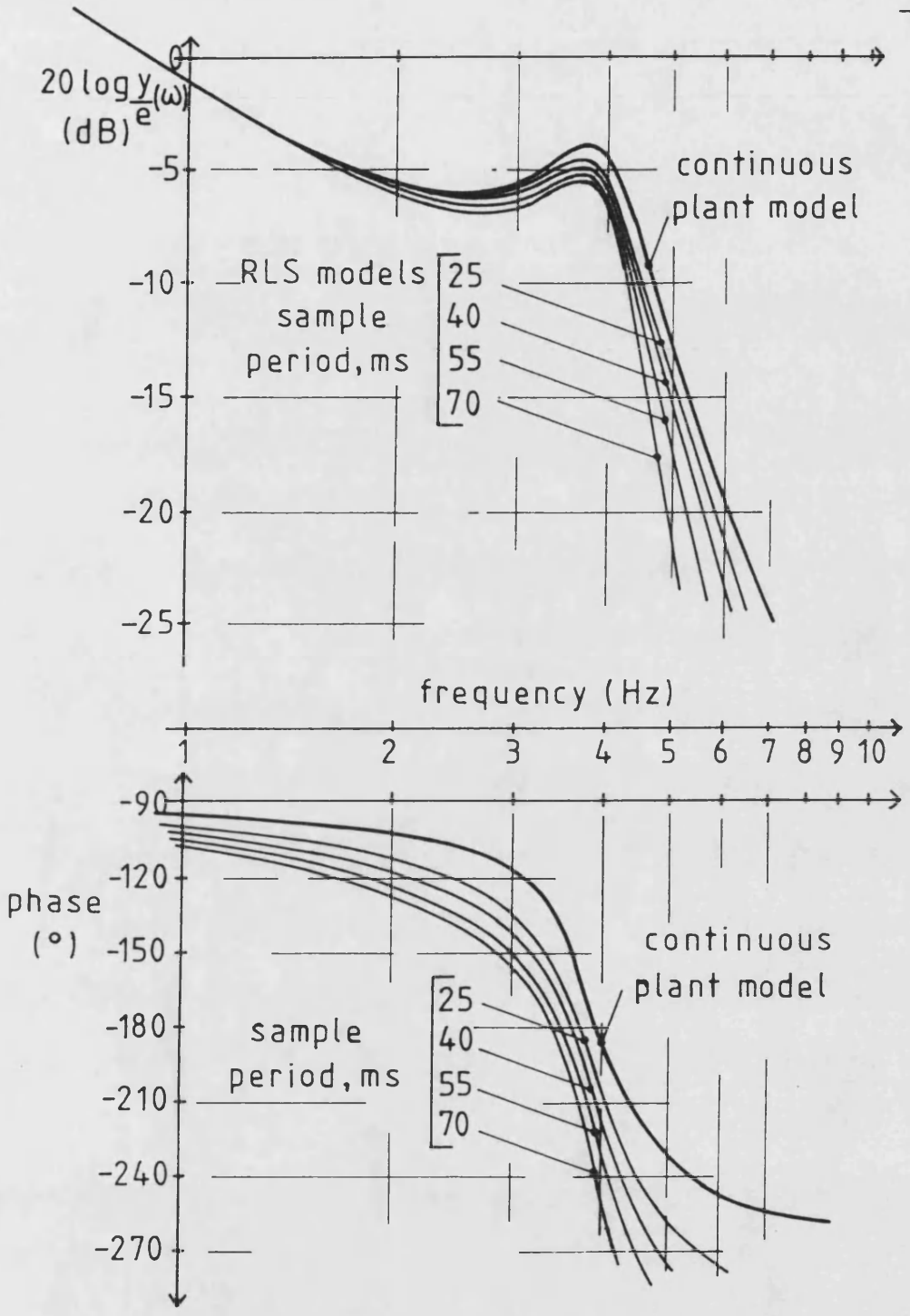

8·4 RLS IDENTIFICATION OF SAMPLED PLANT USING POLE/ZERO MAPPING

Fig 8·5

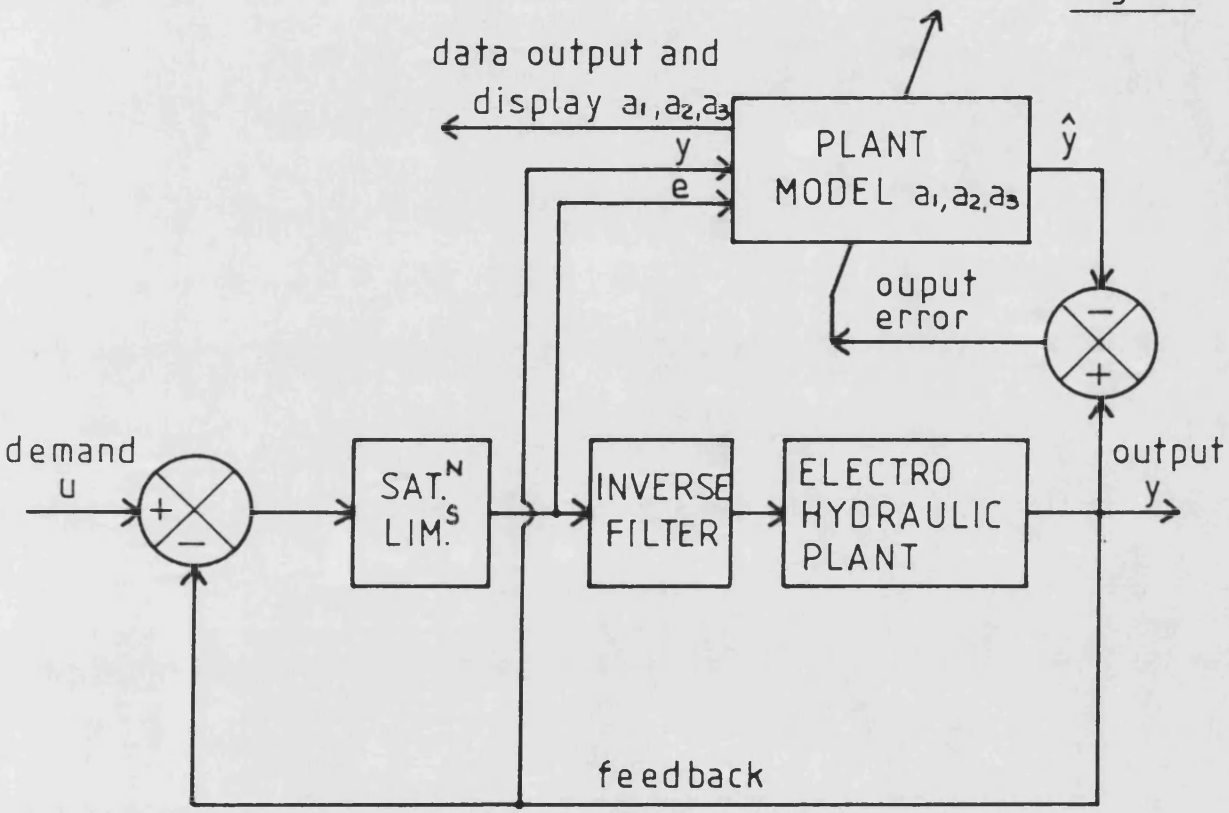

8·5 SERVOSYSTEM RLS IDENTIFICATION SCHEMATIC

Fig 8·6

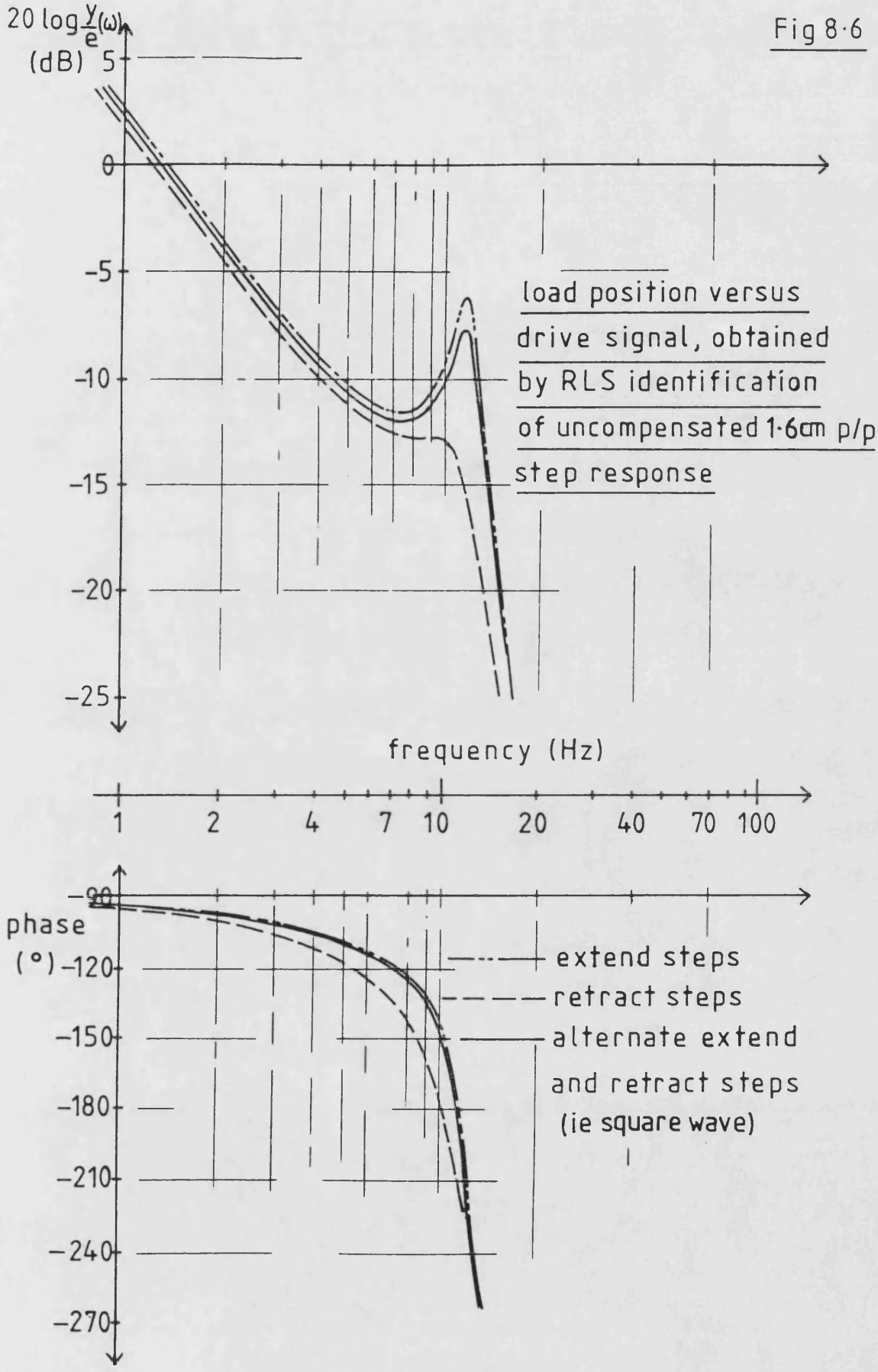

8·6 RLS IDENTIFICATION OF DIRECTIONAL NONLINEARITY

Fig 8·7

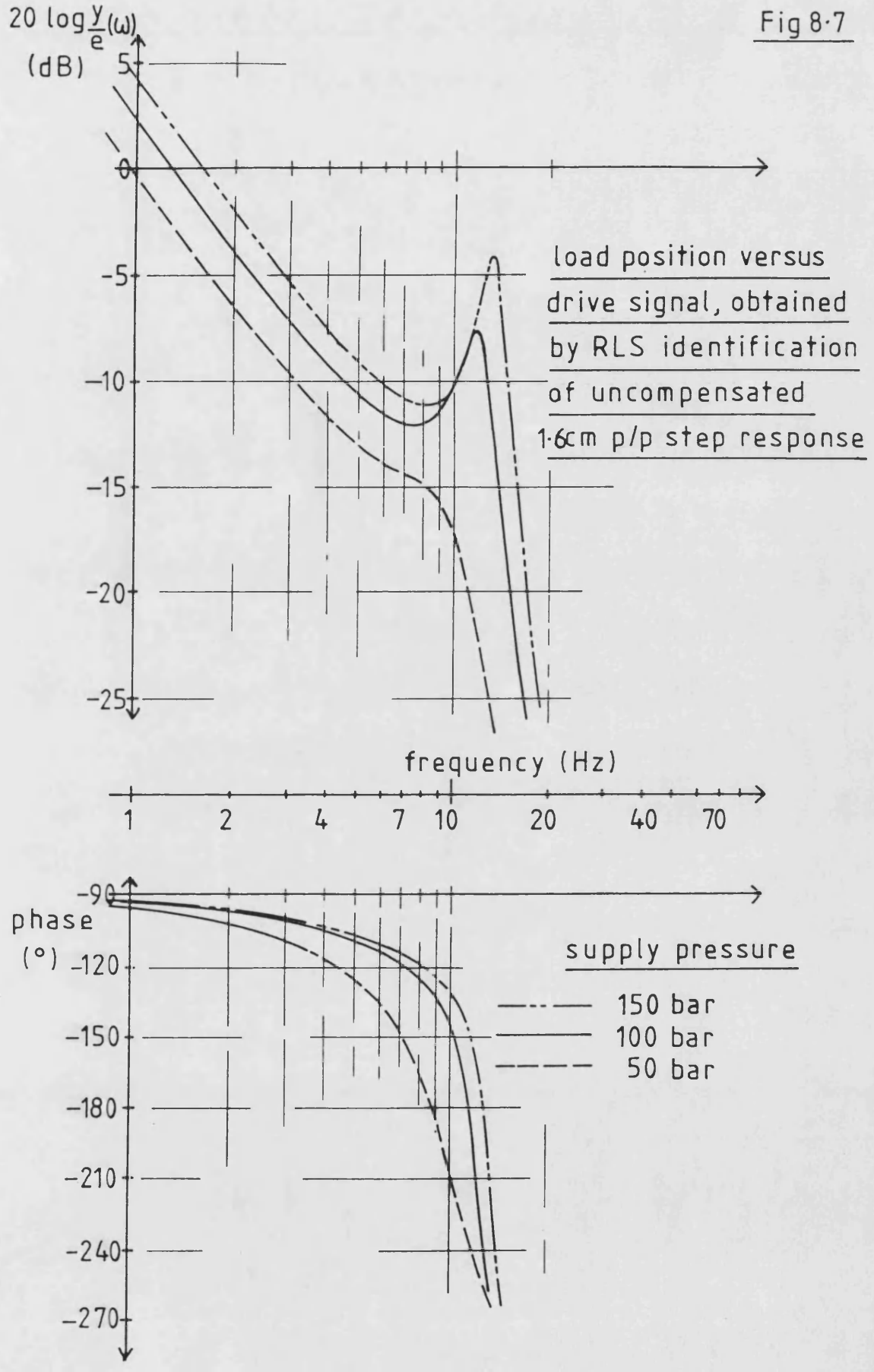

8·7 RLS IDENTIFICATION OF SUPPLY PRESSURE CHANGES

Fig 8·8

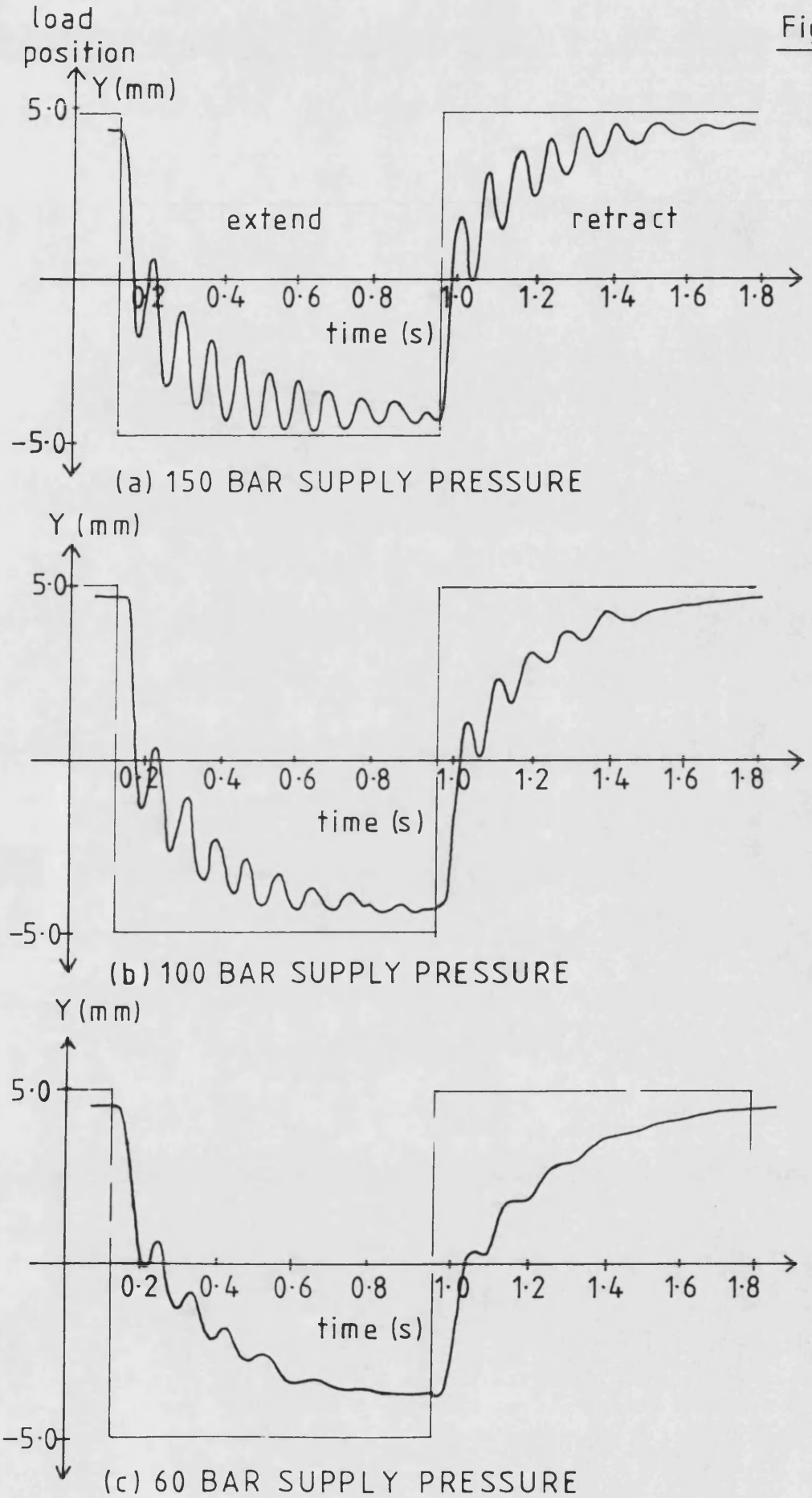

8·8 UNCOMPENSATED STEP RESPONSE ~SUPPLY PRESSURE CHANGES

Fig 8·9

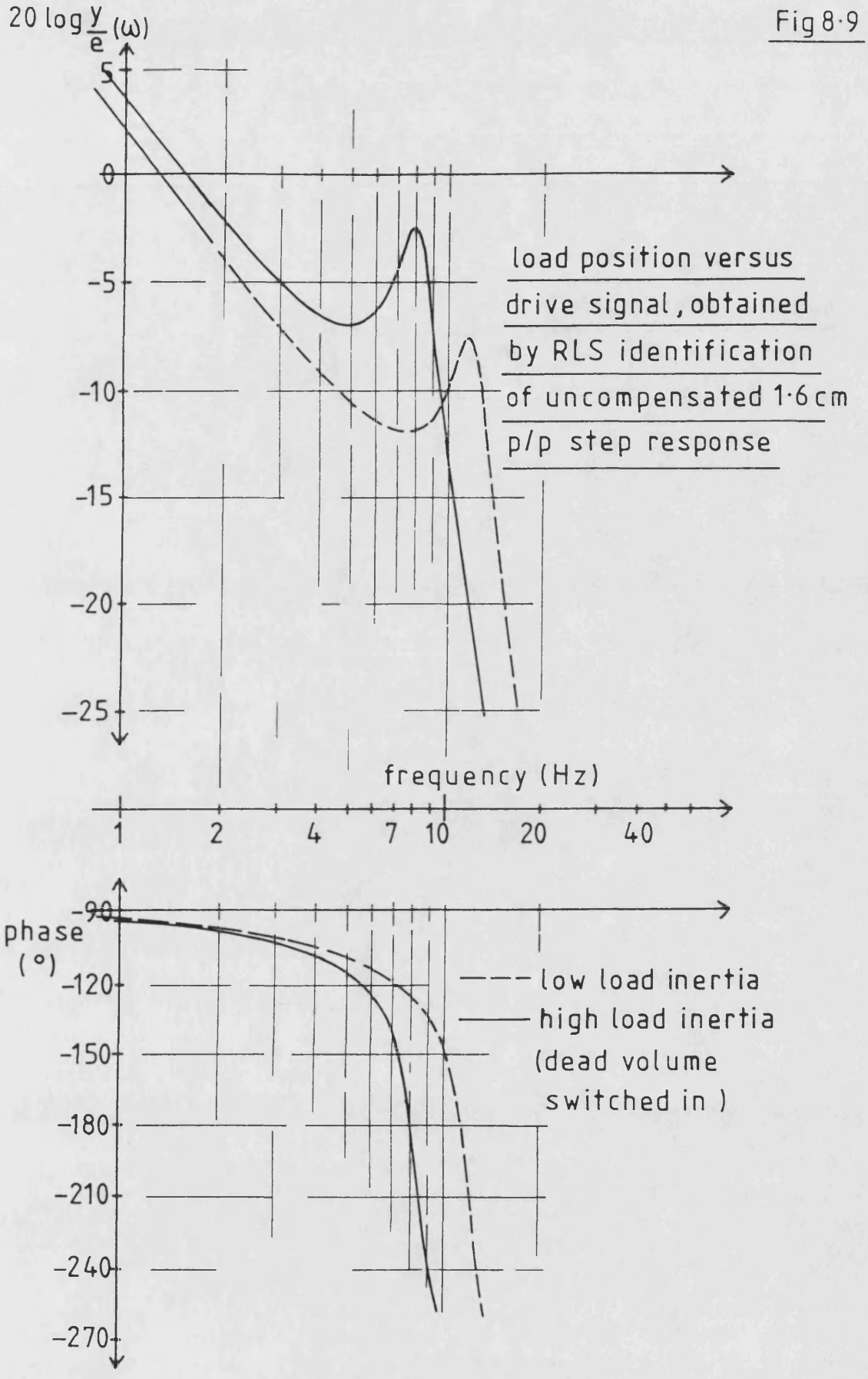

8·9 RLS IDENTIFICATION OF SIMULATED CHANGE IN LOAD INERTIA

Fig 8·10

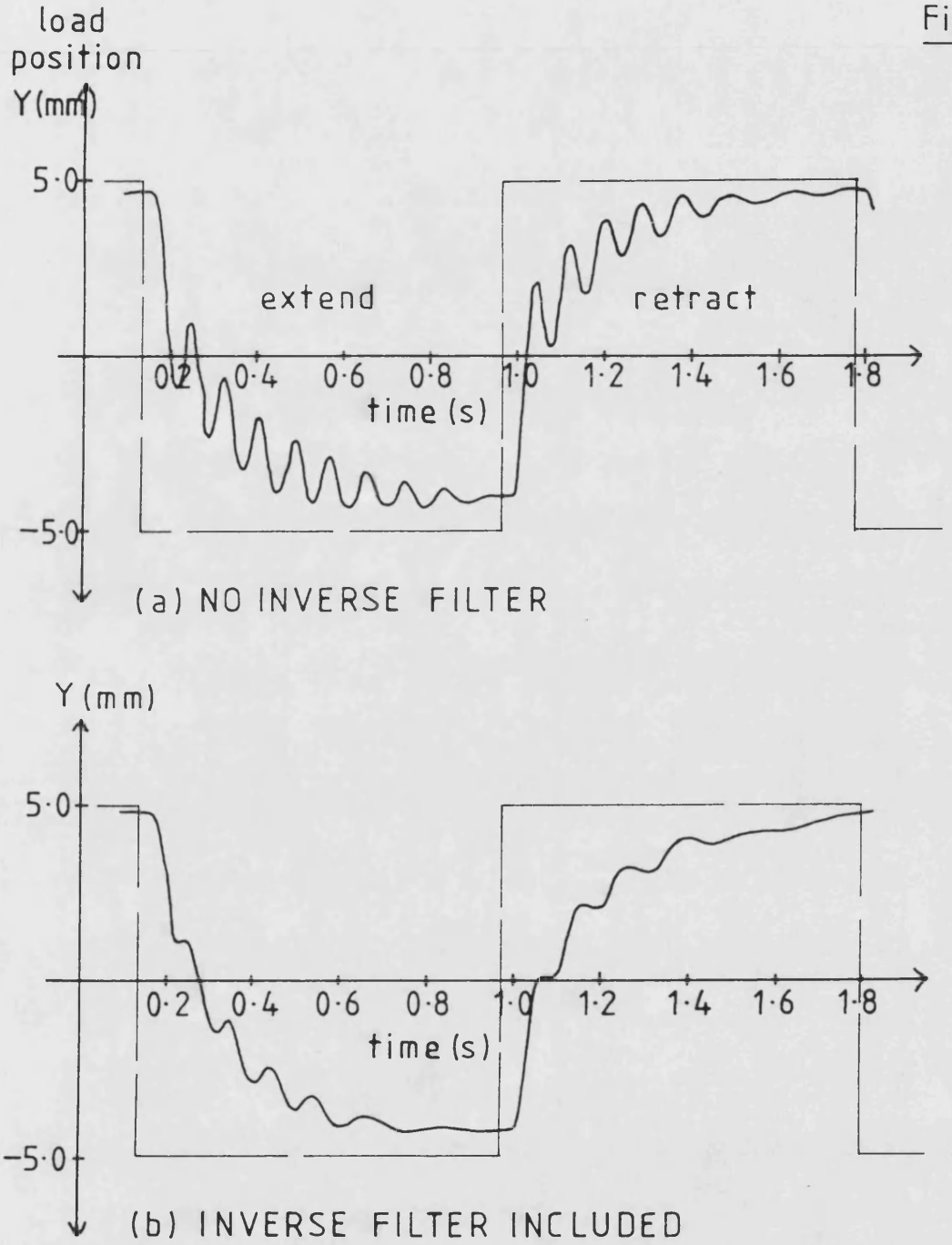

8·10 UNCOMPENSATED STEP RESPONSE ~ EFFECT OF INVERSE FILTER

Fig 8·11

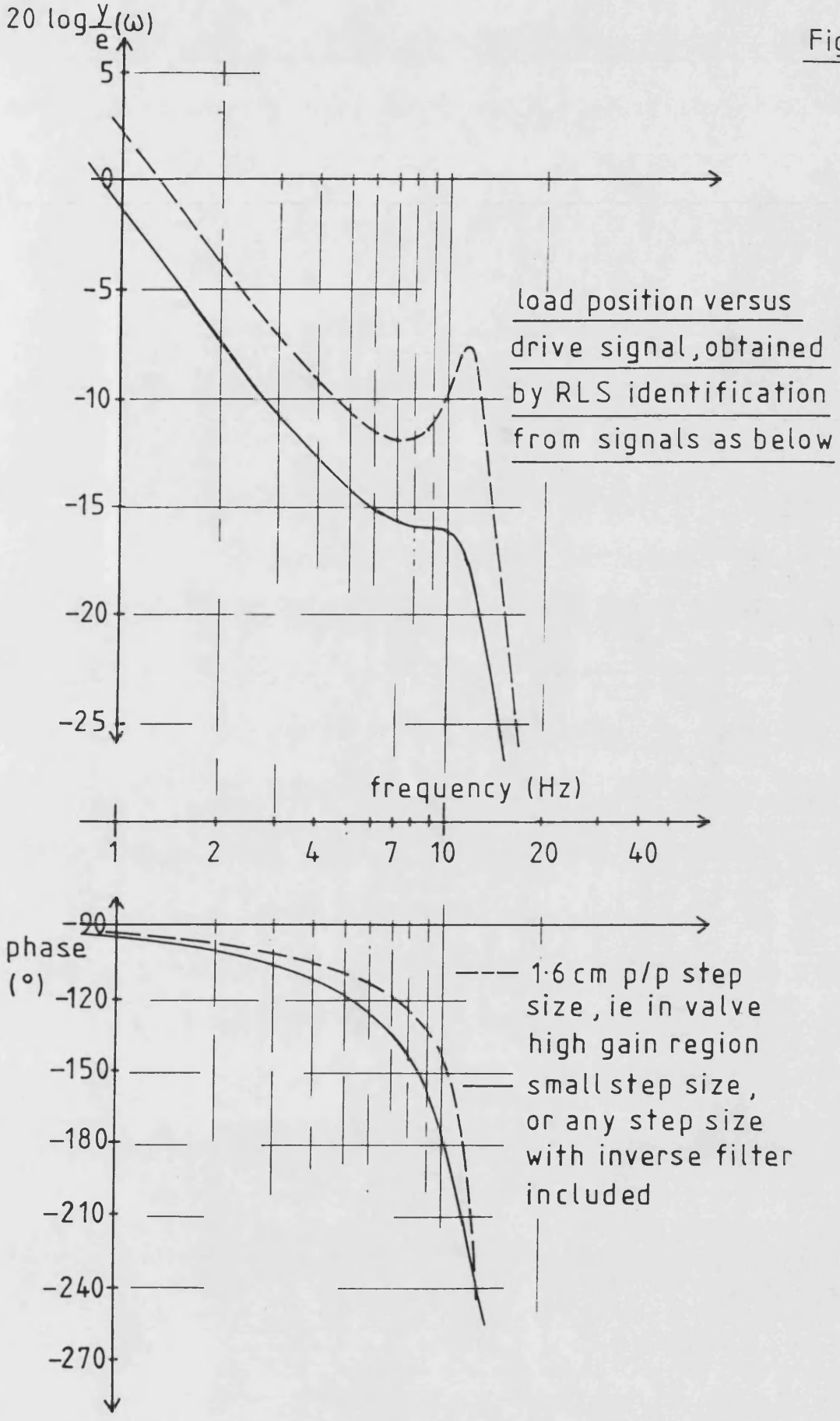

8·11 RLS IDENTIFICATION WITH AND WITHOUT INVERSE FILTER ADDED

Fig 8·12

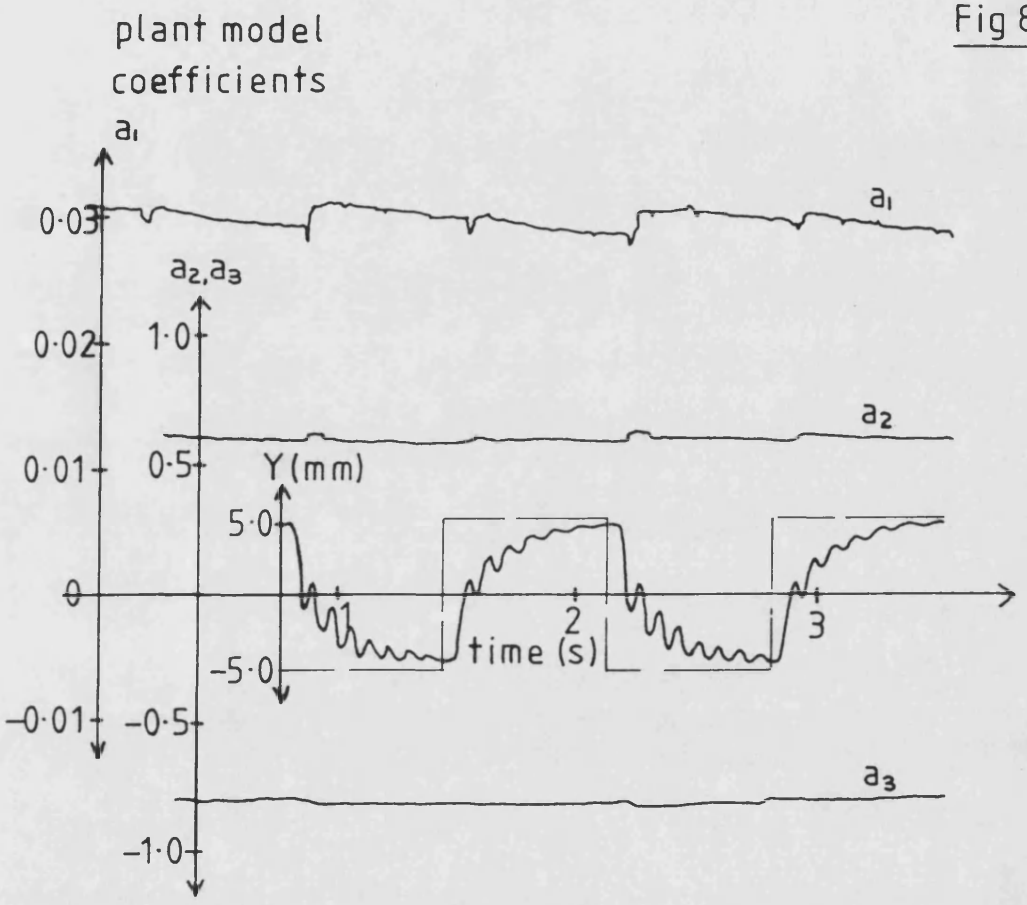

8·12 PARAMETER ESTIMATE FLUCTUATION AT 0·99 FORGETTING FACTOR

Fig 8·13

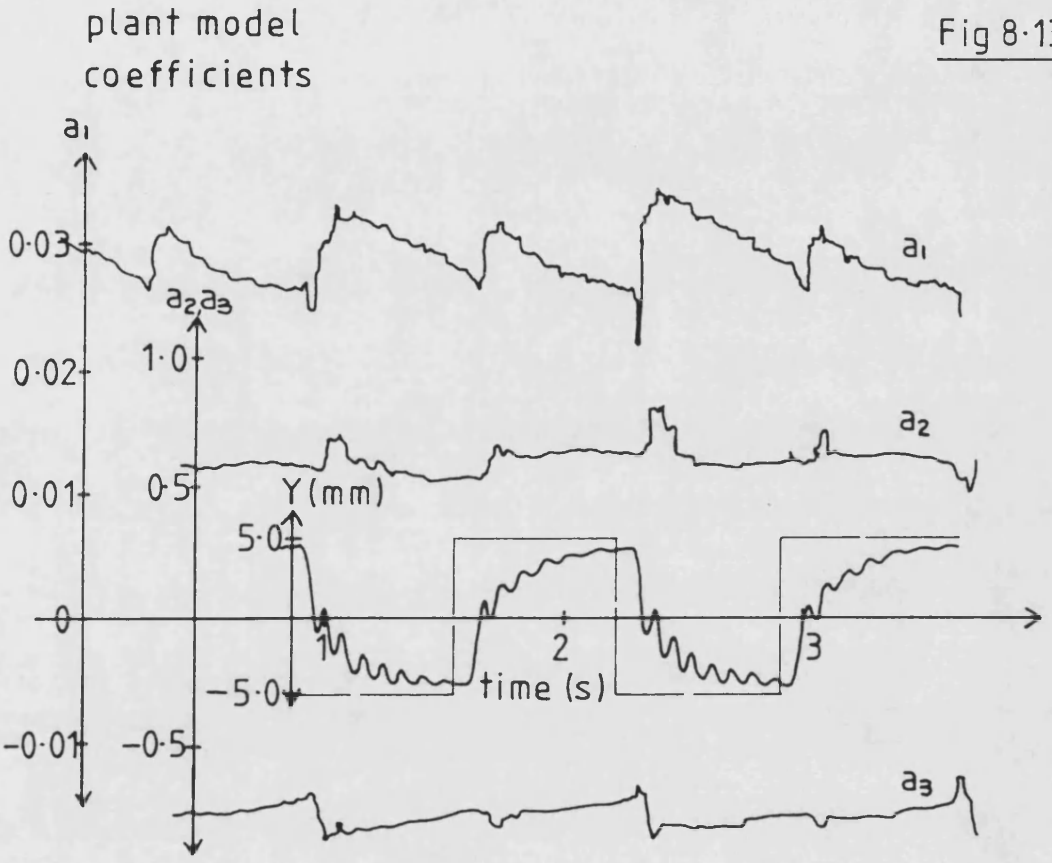

8·13 PARAMETER ESTIMATE FLUCTUATION AT 0·96 FORGETTING FACTOR

Fig 8·14

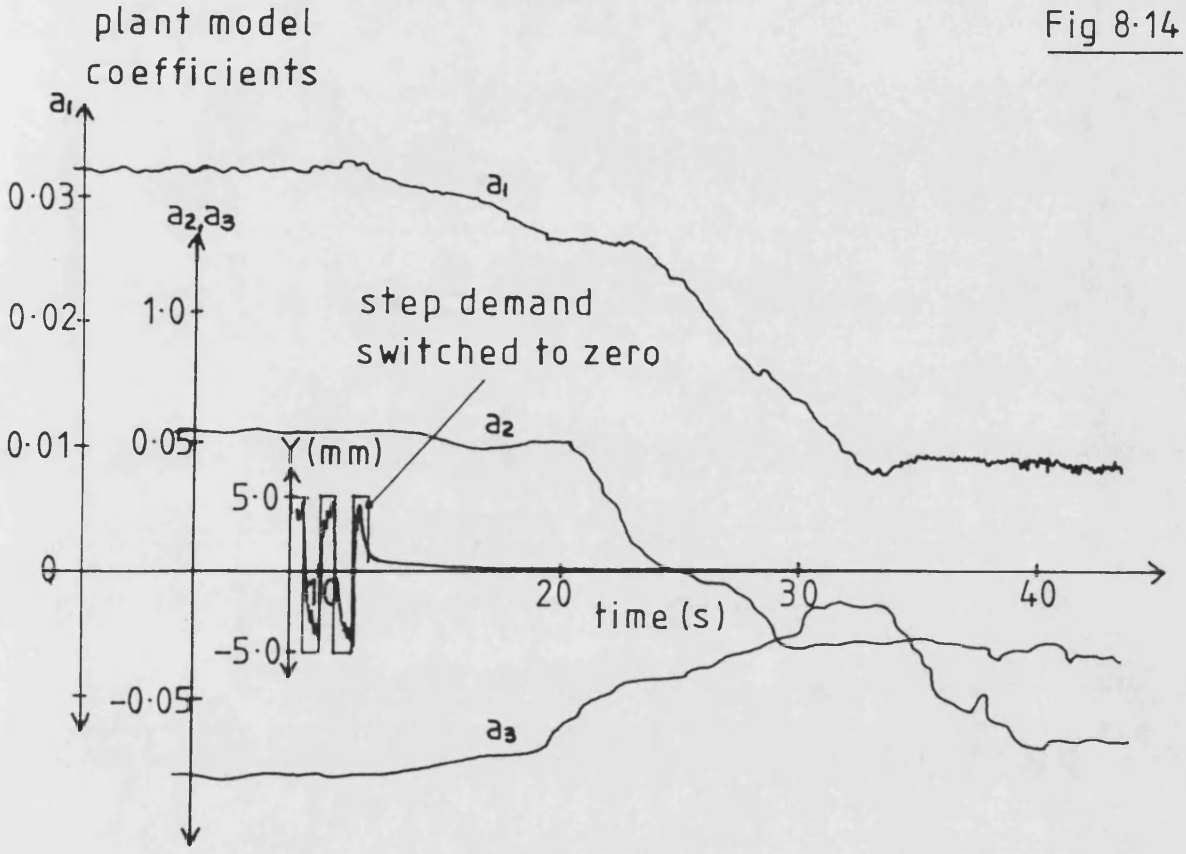

8·14 PARAMETER ESTIMATE DECAY AT 0·996 FORGETTING FACTOR

Fig 8·15

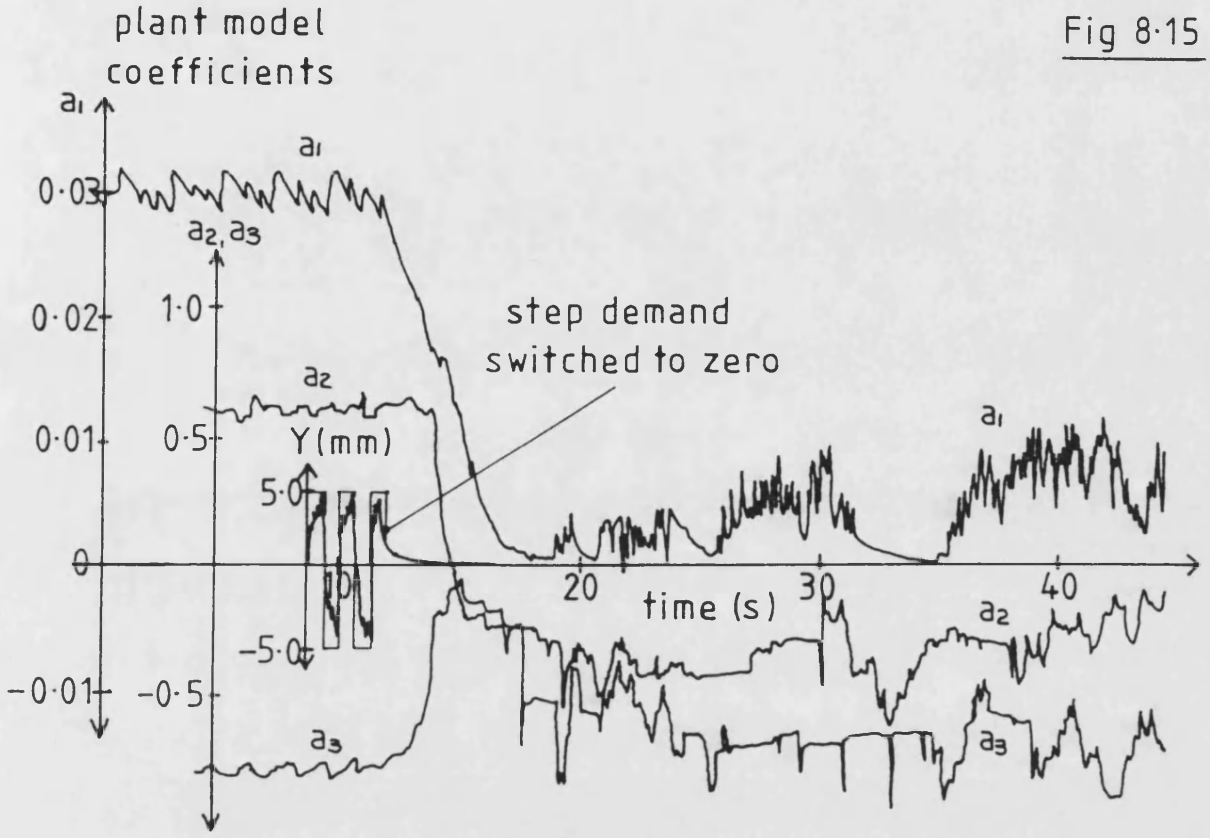

8·15 PARAMETER ESTIMATE DECAY AT 0·98 FORGETTING FACTOR

Fig 8·16

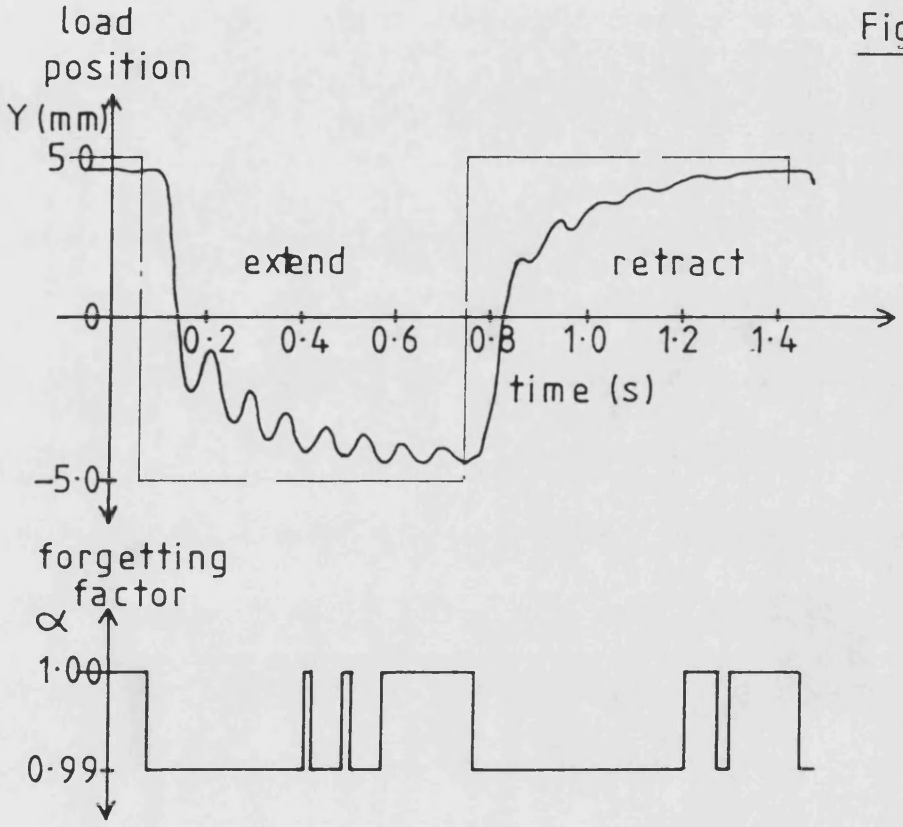

8·16 ACTION OF FORGETTING FACTOR SWITCHING STRATEGY

Fig 8·17

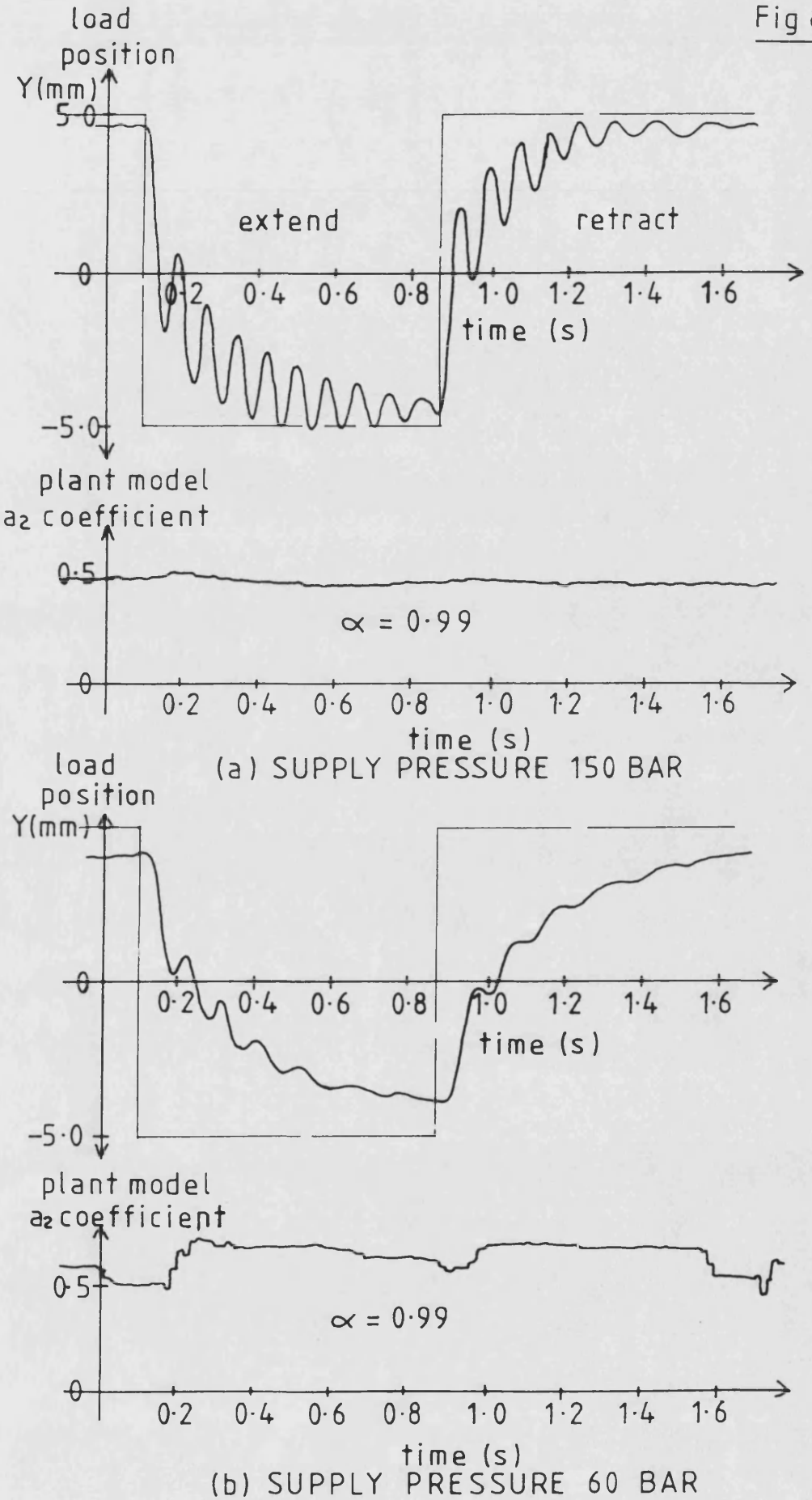

8·17 PARAMETER ESTIMATION ~ EFFECT OF SIGNAL DYNAMICS

Fig 8·18

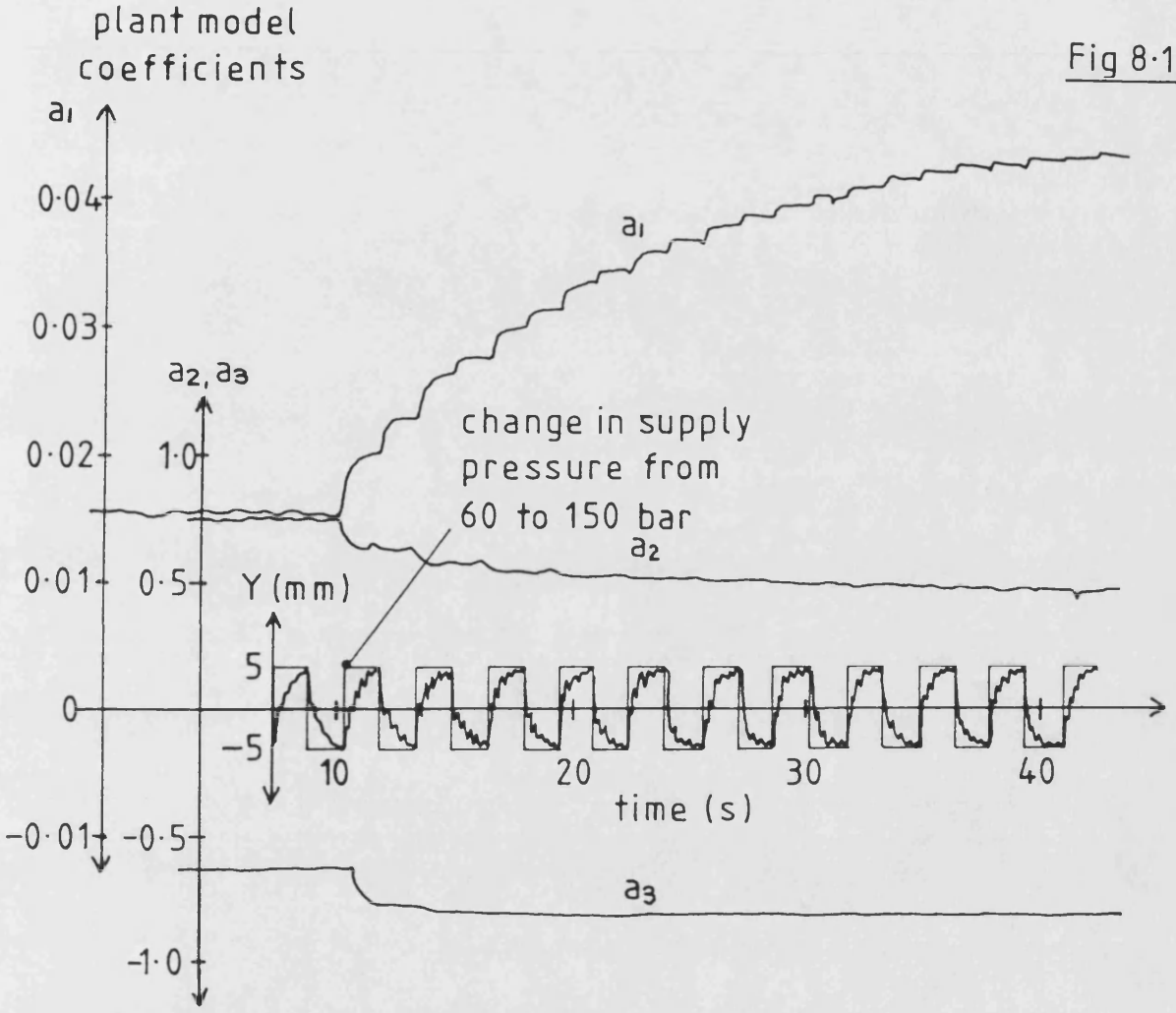

8·18 PARAMETER ESTIMATE CONVERGENCE AT 0·996 FORGETTING FACTOR

Fig 8·19

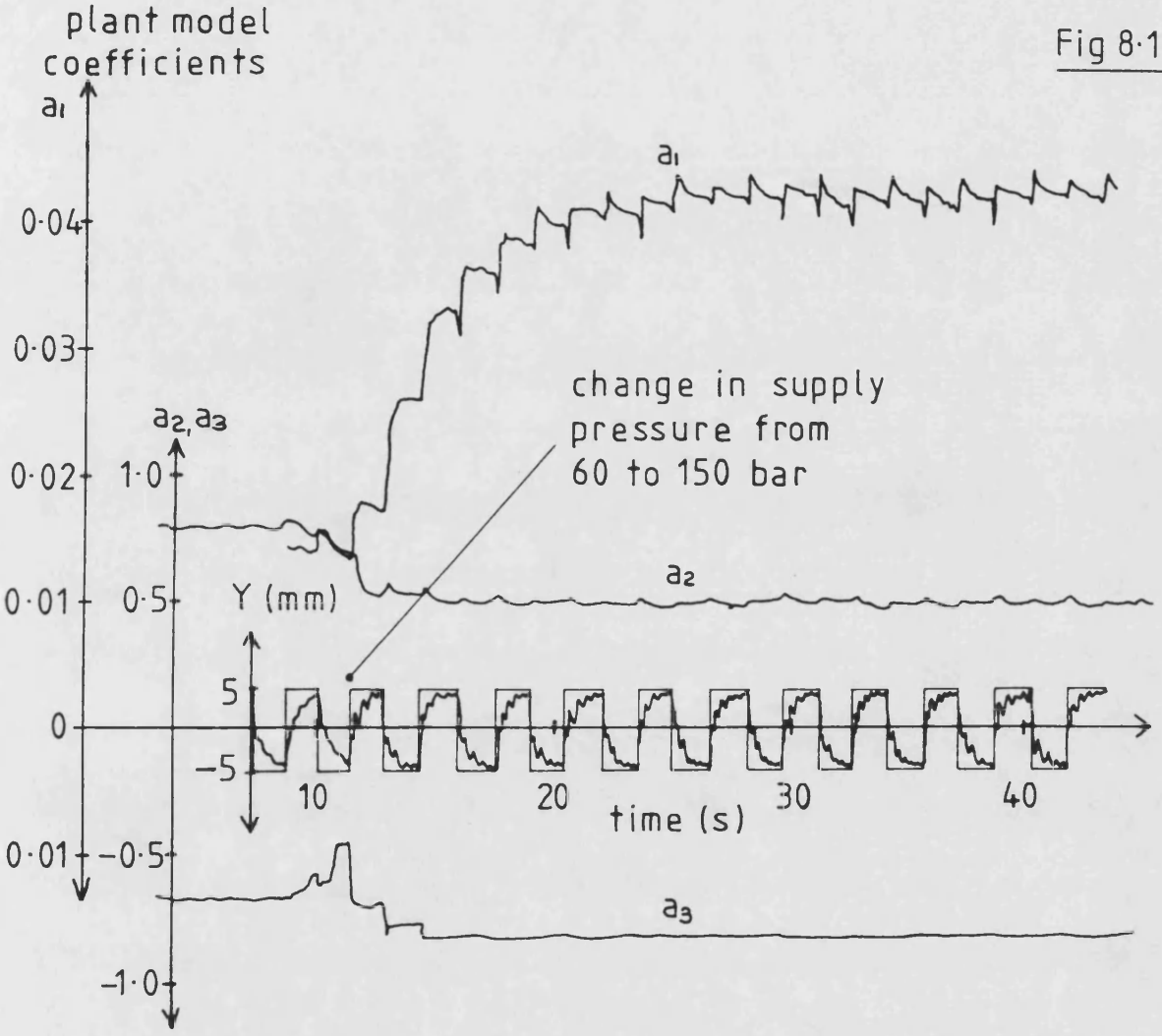

8·19 PARAMETER ESTIMATE CONVERGENCE AT 0·98 FORGETTING FACTOR

9. SERVOSYSTEM AUTOMATIC CONTROLLER DESIGN AND SELF-TUNING CONTROL

9.1 Introduction

901 The identification method described in the previous chapter was shown to be sensitive to the inherent and external time variable nonlinearities of the servosystem, producing linearised transfer functions which appeared to be consistent with theory. However the ultimate test of the method is in its use for controller design. In section 9.2 of this chapter a controller design algorithm is presented which combines the RLS identification and Pole Placement algorithms previously discussed, and which can be used either for automatic controller design or for adaptive control.

902 The algorithm structure is based on Self-Tuning Control (STC) concepts, and thus throughout the chapter is termed the 'STC algorithm'. The concept of STC is discussed and compared with other adaptive methods in section 9.3. The implementation of the STC algorithm requires a large amount of auxiliary processing time, thus in section 9.4 methods of reducing the algorithm processing time are discussed. The important problem of STC algorithm robustness is discussed in section 9.5, and various mechanisms for algorithm failure presented, these being due mostly to poor plant identification.

903 Having presented an algorithm and discussed generally the problems which may occur, application of the algorithm to the servosystem is demonstrated. In section 9.6 use of the algorithm for automatic controller design is discussed, leading to implementation of a full STC controller in section 9.7. The robustness of the STC algorithm applied to the servosystem is demonstrated in section 9.8, and finally some conclusions are drawn in section 9.9.

9.2 Automatic Controller Design and Self-Tuning Control Algorithm

904 Plant identification for controller design is one of the most powerful and demanding uses of an identification method. In this section, the Pole Placement controller design algorithm and the RLS identification algorithm are combined to

enable complete automation of the controller design process. There are several ways in which the two algorithms can be implemented. If both are implemented off-line, ie processing prerecorded batches of sampled data points, then a fixed coefficient controller can be designed. In this way automatic controller design can be carried out with no use of auxiliary processing time, thus even the fastest of digital servosystem controllers can be designed. In the other extreme both of the algorithms can be implemented on-line. Here, a substantial amount of auxiliary processing time is required to recursively update the plant model 'a' coefficients and the controller F and G polynomial coefficients. However implemented on-line, the algorithm can be used in its fullest capacity, either for automatic controller design or for STC adaptive control.

905 The large amount of processing required every sample period restricts the application of adaptive control to low bandwidth systems. To overcome this problem hybrid system configurations have been tried, where the identification and controller design is done semi on-line by processing periodic batches of samples [11]. However the less frequent update of the controller makes it less responsive to plant dynamic changes. In the work presented in this thesis, a relatively low bandwidth servosystem was chosen so that the full STC adaptive control scheme could be implemented and investigated. The basic algorithm has been augmented in several ways for use as a tool in automatic controller design.

906 A STC scheme is shown in Fig 9.1. The conventional closed loop control system with the dynamic filters F and G is implemented. The auxiliary software is used to identify the plant model 'a' coefficients, and this information is passed to the Pole Placement control law design algorithm. Here the controller 'f' and 'g' coefficients are calculated and implemented in the closed loop system. The structure of a third order STC algorithm for servosystem controller design is shown in Fig 9.2, where the various functional parts are illustrated, and the times taken to implement each part indicated. In each sample period the first millisecond is spent inputing the next demand and feedback signal and calculating the current control output from the known 'f' and 'g' coefficients. The calculated control signal is then modified by the inverse filter prior to output to the plant.

907 At the absolute minimum the inverse filter must be designed to include saturation limits to prevent excessive error signals being output. In the

identification algorithm it is important that the saturation limit adjusted signal e, is used in the information vector (see Fig 9.1), giving a true representation of the output drive signal. If the rest of the inverse filter is being used to correct for plant nonlinearities, as in the case of the servosystem, then this should occur downstream of the signal e, as shown in Fig 9.1. This ensures that the identification is of the linearised transfer function from e to y. The inverse filter which linearises the forward path transfer function is thus assumed to be an integral part of the plant.

908 After calculation of the inverse filter, then as shown in Fig 9.2, the current drive signal is output, delayed by 2 ms from the input of the demand and feedback signals. This delay is small compared with the overall 15 ms sample period, and is not taken into account in the algorithm. The remaining 13 ms of the sample period is devoted to identification and controller design. Update of the covariance matrix takes 6 ms to implement and the 'a' coefficients of the parameter vector a further 3 ms. Finally the information vector is updated and this completes the identification calculation. The updated 'a' coefficients are used directly in the control law design to calculate the 'f' and 'g' coefficients, and this process takes a further 4 ms.

909 The execution times quoted were obtained using BCPL as the programming language and a mixture of fixed and floating point arithmetic. Fixed point arithmetic was used in all cases except for the identification algorithm, where the very large numerical range of the covariance matrix elements made the accurate implementation of fixed point arithmetic difficult.

910 The basic algorithm was augmented by a number of additional features useful for controller design, these being invoked by the designer sending a keyboard interrupt to the microcomputer as shown in Fig 9.2. The signaling of an interrupt causes the algorithm to send a zero drive signal to be output, and to await further instructions. While in this state the designer can choose new desired closed loop root positions, and a number of aids to help in the choice of roots can be called if required. For example a full read out of the 'a', 'f' and 'g' coefficients can be selected, and the corresponding closed loop uncompensated root positions calculated and displayed. When chosen, the desired closed loop root positions can be tested by calling the plotting program. This generates plots of the frequency and step responses which can be expected during implementation, thus giving the designer more confidence in the selected root positions. Various other facilities are also shown

in Fig 9.2.

911 When the STC algorithm is started, the plant parameters are unknown and set initially to guessed values. Rapid convergence to the correct values is assured by initially having large diagonal elements in the covariance matrix. During operation, convergence can be tested by observation of an on-line output of one of the 'a' coefficients. At first the trace will be erratic, but very rapidly the coefficient will be seen to converge to a steady value, at this stage identification is complete and the designer can switch from the uncompensated mode to the compensated mode and try some controller designs. The algorithm is designed to operate in the uncompensated mode by default, this ensures that adaptive control is not implemented by accident whilst the identification algorithm is not fully converged.

9.3 Adaptive Control Methods

912 The STC algorithm described in the previous section is one of the most obvious forms of adaptive control, consisting of an on-line implementation of the usual plant identification and controller design stages used in conventional controller design methods. However there are a number of other adaptive control methods, and the purpose of this section is to discuss the alternative techniques, and set the STC method in context.

913 The concept of a control system able to adjust to changes in the plant parameters is very old, but only in recent decades has the theory and the processing power been available to make implementation practical. Adaptive control has been developed from two principal points of view: the Model Reference Adaptive Control (MRAC) approach [91], and the Self-Tuning Control (STC) approach [92,93]. MRAC was originally developed to solve servo problems, and STC for process set point regulation problems. Gain Scheduling is often not considered to be an adaptive control scheme because it can only change the controller in a prespecified manner dependent on external measurements. There is no feedback which compensates for an incorrect schedule.

914 The MRAC schemes are based on matching the closed loop system performance to that of a desired closed loop reference model, from where the technique derives its name. Within this one concept there are a number of variations [94], but all

with the same end result. Fig 9.3 showns a typical scheme configured for the servosystem control loop. The closed loop system follows the same configuration as Fig 9.1, having compensating filters F and G, however a number of other blocks are also seen in the diagram. The overall desired response is specified by the reference model which is operated in parallel with the complete closed loop system. The output from the model is compared with the plant output, and the resulting error signal is used in an adapting mechanism to generate the F and G polynomial coefficients in such a way that the error between the model and plant output is minimised. Thus the F and G polynomials are generated so that the overall closed loop performance is similar to the reference model performance.

915 The particular scheme of Fig 9.3 is termed a 'direct' or 'explicit' MRAC scheme, this is because the control parameters are updated directly as a result of the error between the plant and the explicitly specified reference model in one single stage, ie the adaptation mechanism. There is no obvious identification stage, thus from an STC view point the method uses 'implicit' identification. MRAC schemes can also be implemented using explicit plant identification and controller design stages [94]. Here, the controller design is 'indirect', since two stages are involved, and the overall reference model 'implicitly' specified. This method appears to be similar to STC methods, and it has been shown that both this and many other MRAC schemes are mathematically similar to STC [95,96].

916 There have also been a number of alternative STC schemes developed, the common factor being the presence of some form of plant identification used in the controller design [97]. The method developed in the previous section uses explicit identification of the plant from which the controller is designed, but the problem can be expressed in terms of direct identification of the controller coefficients. In this case the identification and controller design stages merge into one creating a direct scheme, and the identification is then said to be 'implicit'.

917 Other differences in STC schemes have been in the method of controller design implemented. Originally STC was developed using optimal control theory in which the control signal was calculated to minimise a chosen cost function [98]. In these schemes it was natural to formulate the identification problem in terms of the controller parameters rather than the plant parameters. The resulting implicit STC scheme gives the control parameters directly and can often be implemented more

quickly than explicit schemes. This technique is widely used in set point process control problems. For servo problems, the explicit Pole Placement STC scheme has been recommended [87,99,100], since the explicit availability of the model and controller root positions provides valuable information about the system dynamics, and the specification of root positions for the closed loop performance has a meaningful physical interpretation.

918 The wide variety of schemes, and their similarity in function often makes it difficult for the engineer to decide which is the best method to use in a given situation. However, there are a number of clear practical distinctions which can assist in making the correct choice of method. If the system to be controlled is of high bandwidth, and processing speed is a problem, then the direct methods where the identification and controller design stages are lumped together will give some speed advantage. A direct MRAC scheme, designed to control the servosystem test rig was implemented in less than two thirds of the time required for the STC scheme proposed in the previous section [101].

919 Comparing the STC and MRAC schemes of Fig 9.1 and 9.3, it is seen that the direct MRAC approach uses the closed loop control system plant/model error directly to update the controller coefficients, whilst the explicit STC approach uses an open loop plant model error from which a controller transfer function is indirectly derived. Thus in the presence of modelling errors, the STC scheme produces differences between the actual and the expected closed loop response and no direct attempt is made to correct for them. In the MRAC scheme however, the plant/model output error is driven towards zero directly, irrespective of modelling errors. Thus it is likely that there will be significant differences in the behaviour of the two approaches when handling modelling errors. The comparison of the STC and MRAC adaptive schemes in practice must be the subject of further research.

920 In the last twenty years there has been a deluge of papers on adaptive control [8]. Most of these have been the reporting of new algorithms and/or simulation work demonstrating the success (or lack of success), of a particular adaptive scheme. However recently there have been a number of cases reported of the practical use of adaptive control in electrohydraulic servosystems [11,12,102,103,104].

9.4 STC Implementation Speed Improvements

921 The biggest burden on the auxiliary processing time when implementing an STC scheme is the update of the the covariance matrix $\underline{P}(k)$. The first step in reducing the processing time is to reduce the number of plant model 'a' coefficients, and hence the number of elements in the covariance matrix. For the servosystem model this was discussed in section 8.4, and it was found that on conversion from s to z the minimal number of coefficients was given by the the Pole/ Zero Mapping method. In addition to this a number of other possibilities for reducing execution speed were attempted, which although not all were successful in the case of the servosystem, are included in this discussion because of their potential value in other situations.

922 One possibility for improving the processing speed is to use the so called 'fast' algorithms [105,106]. Here advantage is taken of the shift property of the information vector, for example, in equation 8.13, x_2 of the present time instant, becomes x_3 of the next time instant. This causes some duplication of calculation from one sample period to the next. However reformulation of the recursive equations to exploit the shift effect was only found to pay dividends for large numbers of model coefficients. The break even point is reached when the identification algorithm is processing seven coefficients. Ten coefficients yields a 25 % saving in time, but three coefficients turned out to take 50 % longer to implement.

923 A significant increase in speed can be obtained using fixed point arithmetic. On the Darkstar microcomputer 32-bit two's complement integer arithmetic took about half of the speed of the floating point software routines. Fixed point arithmetic was implemented in the control signal calculation and the control law design using a single number base shift, designed such that unity corresponded to the middle of a 32-bit register, ie a shift of 16 binary places was executed. This gave plenty of scope for large numbers, and an adequate degree of precision. Integer arithmetic proved to be more difficult in the identification algorithm due to the large range of numbers encountered. This is particularly true of the covariance matrix where the values of the elements can change by more than ten orders of magnitude from start up to settling. If fixed point arithmetic is used then proper scaling techniques are required to give good results [107]. The covariance matrix does have a tendency to become ill conditioned. This can be seen from equation 8.3, where for large

numbers of sample points the elements of the denominator matrix become very large, thus corresponding to small $\underline{P}(k)$ elements. In the recursive form the forgetting factor prevents these values becoming too small. In the worst cases the covariance matrix is no longer positive definite and the numerical values increase until overflow occurs.

924 In the application of RLS identification to the servosystem the ill conditioning problem did not occur. However if there is a problem, for example due to the use of integer arithmetic or from implementing floating point arithmetic on a low precision machine, this can often be overcome using square root factorisation of the covariance matrix [108]. For example in one scheme [109] the covariance matrix is factorised into $\underline{U}\underline{D}\underline{U}^T$ where $\underline{U}$ is an upper triangular matrix, and $\underline{D}$ is a diagonal matrix. This has the effect of halving the dynamic range of the matrix elements, giving better accuracy and maintaining the stability of the covariance matrix. The square root algorithm was found to take 30 % longer to implement than the standard RLS algorithm.

925 Another potential way of speeding up the algorithm is to use less complicated gains, $\underline{P}(k)\underline{X}(k)$, in the parameter update equation 8.5. Equation 8.5 is just one of a whole class of equations of the form:

$$\underline{A}(k) = \underline{A}(k-1) - \underline{\mu}(k)[\underline{X}^T(k)\underline{A}(k-1) - y(k)] \qquad (9.1)$$

Where $\underline{\mu}(k)$ is the update gain vector. The speed advantage is obtained by using more easily calculated approximate values for the update gains. For example, it has been suggested that the trace of the covariance matrix be used, thus replacing the entire covariance matrix by a single element [110]. This simplification was found to reduce the STC algorithm processing time to less than half of its original value. However, although the plant model followed the plant output well, it was found that the estimated 'a' coefficients did not take up their correct values and led to incorrect controller designs. In direct adaptive schemes based on controller coefficient updates derived from the plant/reference model error, this approach may give more satisfactory results. In fact the MRAC literature shows a large variety of schemes for calculating the update gains for equation 9.1, many of which lead to faster algorithms [111].

9.5 STC Robustness

926 The important question of the robustness of adaptive algorithms is currently the subject of many papers on adaptive control and a source of disagreement amongst theoreticians [112,113,114]. It has been shown that under the right conditions both explicit and implicit adaptive control schemes are stable and convergent [115,116,117]. However these proofs do little to improve the confidence with which adaptive control schemes can be applied in practice. In the final analysis the success of a scheme is only found by application.

927 In the explicit algorithm of section 9.2, lack of robustness can arise from two sources, the controller design algorithm and the RLS identification algorithm. The robustness of the Pole Placement controller design algorithm in the presence of nonlinearities was demonstrated in Chapter 7 by application to the servosystem, and the sensitivity to plant parameter changes was observed. Generally it was found that by careful choice of the closed loop root positions, away from the negative real half of the root locus plot, robust controllers could be designed, the response only becoming unacceptable for very large nonlinear changes in the plant.

928 A much more likely source of lack of robustness arises in the identification algorithm where poor 'a' coefficient estimates can give incorrect controller designs. Identification algorithms are particularly prone to robustness problems when the quality of the plant signals is poor or the signal to noise ratio is low, for example when the system is at rest or slowly moving. In the literature the terminology, 'persistency of excitation' and 'sufficient richness' is often used to describe the qualities of the plant signals from which the parameter estimates are made [118].

929 The concept of persistency of excitation can be understood by considering the recursive plant model equation 8.12 rewritten below:

$$y_d(k) = a_1[e(k-1)+2e(k-2)+e(k-3)]+a_2y_d(k-1)+a_3y_d(k-2) \qquad (9.2)$$

Now suppose the input to the plant is a sinusoidal signal:

$$e(k) = e^{j\omega k\tau} \qquad (9.3)$$

and the output is:

$$y(k) = Re^{j(\omega k\tau-\phi)} \tag{9.4}$$

ie a sinusoid of amplitude R and phase lag ϕ. If these signals are used in the identification algorithm the identified 'a' coefficient estimates can be found by substituting 9.3 and 9.4 into equation 9.2. By comparing the real and complex terms on each side of the equation the 'a' coefficients can be found in terms of the amplitude ratio and phase. The resulting two equations are:

$$a_1 = -\frac{R[1-\cos(\omega\tau)](1+a_3)}{\cos(\phi-\omega\tau)+\cos\phi} \tag{9.5}$$

and:

$$a_2 = 2\cos(\omega\tau)-\frac{\cos\phi+\cos(\phi+\omega\tau)}{\cos(\phi-\omega\tau)+\cos\phi}(1+a_3) \tag{9.6}$$

Thus since a_1 and a_2 are a function of a_3, then there is no unique solution and an infinite number of combinations of the 'a' coefficient values will give the same amplitude ratio and phase difference. In theory this means that the 'a' coefficient values can move around unbounded, and in practice this is exactly what happens, often with drastic consequences for the control system.

930 The equations show that the maximum number of coefficients which can satisfactorily be identified using a sinusoidal signal is two, corresponding to two pieces of data, ie amplitude ratio and phase. Thus a sinusoidal signal is said to be persistently exciting of order two. To be correctly identified the third order model of the plant requires a signal having an excitation persistency of three, corresponding to the number of model coefficients. Thus it can be seen that demands on the type of signal from which identification can take place increase with the order of the model. Even with only three coefficients, some of the most widely used signals are out of the question. In addition to sinusoidal signals, ramp signals, which are only persistently exciting of order one, are also inadequate.

931 In the case of there being no dynamic information, ie when the system is at rest, identification cannot take place. In this situation it is easy to recognise that the

system is at rest and maintain old information by setting the forgetting factor to unity. However, there is no easy way of knowing when the signals are not persistently exciting as even large amplitude signals can be inadequate. In practice the amount of drift in the 'a' coefficients during periods of inadequate signal quality depends on unmodelled quantities such as offset disturbances and noise. A square wave demand signal applied to the closed loop system has good excitation properties, and is thus ideal for identification purposes.

932 Even if the persistency of excitation requirements are met, the plant signals may not be sufficiently rich, that is to say, the signal power spectrum may show insufficient energy levels at the desired frequencies. Generally the parameters should be derived from signals rich in frequencies around the cross over frequency of the open loop frequency plot. In the case of the servosystem, the resonant frequency quite clearly needs to be excited, since it is this effect which is to be controlled. In this case such a requirement is not difficult to achieve because of the very low damping and the closeness of the resonant frequency to the cross over frequency.

933 Recent work [112] has shown that the order of model chosen is also an important factor in determining the robustness of the system. The temptation to use reduced order models can create problems if the plant signals are such as to excite the neglected order dynamics. Using such signals the convergence of the model to incorrect coefficient values can result in an unstable controller design [114]. In a similar manner if the control signal is not of sufficient richness, the unmodelled effects of noise and offset disturbances can swamp out the correct part of the signal, resulting in an unstable controller design.

934 The signal richness criterion is really to do with the changes in the signals from one sample period to the next, and thus is a function of the length of sample period used rather than rates of change in absolute terms. Thus a signal sampled slowly appears to be richer than the same signal sampled very rapidly, and this is a good reason for sampling slowly in adaptive control schemes. Although there is an optimum sampling frequency for the identification algorithm, the choice of frequency is usually made from control system bandwidth criteria, (see section 3.8), however the rule of thumb given in par 333 was found to give good identification results also.

935 The secret of robust adaptive controller design is to ensure the signal richness and persistency of excitation for as much of the time as possible, and to know when the signal quality is poor so that identification can be turned off.

9.6 Servosystem Automatic Controller Design

936 The STC algorithm presented in section 9.2 has been applied to the servosystem to test the suitability of the identification algorithm for use in automatic controller design. The results of Chapter 8 showed that the RLS identification algorithm is sensitive to the nonlinearities of the servosystem, and the '*a*' coefficient parameter changes appeared to agree well with the theory. Although this is encouraging, it does not prove whether or not the much simplified linear model of the plant can give a sufficiently accurate representation to enable a linear controller to be designed. This is the ultimate test of the identification algorithm and is the subject of the following sections.

937 The STC algorithm (see Fig 9.2), was set up in the automatic controller design mode of operation, ie whereby identification of the plant is achieved using a summing junction closed loop controller and a square wave demand signal. This being followed by the calculation of a fixed coefficient controller based on the identified '*a*' coefficients, and designed to meet a desired closed loop performance. This procedure was carried out using the desired root positions: $z = 0.6$ and $z = 0.6 +/- j0.2$. The plant model was identified and the resulting '*a*' coefficients gave the frequency plot shown by the dashed lines in Fig 9.4. However when the designed controller was implemented, the resulting performance was unexpectedly unstable, contrary to the desired root positions. Stable control was only achieved when a very sluggish set of root positions was demanded for the characteristic equation. This undesirable result was a consequence of the nonlinearities of the plant which gave different '*a*' coefficient values depending on the nature of the signals used. This is the same problem as occurred when unrepresentative sinusoidal signals were used to obtain a frequency response of the plant (see section 7.4). In the case in question the uncompensated closed loop step response was highly oscillatory and of slow rise time, whereas the desired performance root positions corresponded to a fast overdamped response. Thus when the control law was implemented, the alteration in plant operating signals were such that the plant input/output relationship was best described by different linear model coefficients, thus making the control law

incorrect for the new plant conditions. Obtaining the correct control law thus becomes a circular problem: the desired response must be achieved prior to controller design so that the correct identification can take place and the controller which gives the desired response be designed and implemented.

938 This unsatisfactory situation was overcome by using the full STC form of the algorithm for controller design, even though at this stage only a fixed coefficient controller was required. The procedure was as follows: first, the identification algorithm was allowed to converge using the uncompensated step response, the control law being calculated but not implemented. Secondly, the designed controller was implemented, leaving the identification and controller design algorithms running. At this point a transient occurred in the system as the identification algorithm and the designed controller reconverged to new values. Finally when the coefficients had settled, the controller coefficients were fixed in memory. A typical controller switching in transient is shown in Fig 9.5. Immediately after switching, the uncompensated plant identification parameters give a highly oscillatory response, however the identification algorithm quickly responds, and a satisfactory step response is achieved corresponding more closely to the demanded root positions.

939 The identified plant model frequency response with the controller implemented is shown in Fig 9.4 by the continuous lines, and considerable difference is seen between the models before and after controller implementation. Most marked is the observed reduction in damping ratio and the increase in forward path gain. The latter observation helps to explain why the instability occurred using uncompensated plant data. The desired performance requirement demanded that during a step response, the valve be left in the high gain region for a longer proportion of time than was the case for the uncompensated response. This is shown experimentally in Fig 9.6 from the step response error signal traces. Thus the mean gain in the uncompensated case was less than for the compensated case and this is reflected in the identified 'a' coefficients. The underestimation of the plant gain caused an excessive controller forward path gain to be implemented which resulted in instability.

940 The valve dual gain characteristic which causes the forward path gain nonlinearity, is a particularly severe test of the STC algorithm. With a linear valve

characteristic the changes in the plant dynamics are less pronounced and the switching transient less severe. However, conceivably there are even more troublesome nonlinearities in which even the STC algorithm would not converge satisfactorily. Suppose for example that the valve gain characteristic had decreased with drive signal, as occurs in the case of saturation. For large input signals the identification would then yield a low forward path gain estimate, the corresponding controller producing an unstable control system around the null point.

941 The problem of saturation, dual gain characteristics, and many other types of nonlinearity can be adequately corrected for by modelling of the nonlinearity in the controller. This requires a detailed knowledge of the nonlinearity, but as in the case of the inverse filter designed for the servosystem, this information is often easily obtained. With the inverse filter implemented it was possible to design an adequate controller for the system based on identification using the uncompensated step response, but the best results were still achieved using the fully adaptive STC algorithm.

9.7 Servosystem Self-Tuning Control

942 In section 7.5 and 7.6 the tolerance of the fixed coefficient controller to changes in the plant dynamics was investigated and it was shown that for large changes in the plant parameters the resulting closed loop response was inadequate. Using the STC algorithm in the fully adaptive mode, ie leaving the identification and controller calculation and update algorithms running all of the time, these problems can be overcome. The test results which follow show how the STC algorithm corrected for the nonlinear plant parameter changes. The inverse filter was not implemented except for the directional gain adjustment and saturation limiting parts, unless otherwise stated. The test results shown in this section were obtained with a forgetting factor of 0.99, and desired characteristic equation root positions at $z = 0.6$ and $z = 0.4 +/- j\ 0.2$. First the time variable nonlinearities, ie supply pressure and load inertia variations are considered.

943 The step response during a step change in supply pressure from 60 to 150 bar is shown in Fig 9.7. The large increase in forward path gain is not immediately identified and initially large overshoots occur. After about 5 s the identification algorithm has converged sufficiently so that the desired response is restored.

944 A similar correction was observed when the extra dead volume was switched in, ie a simulated increase in load inertia. In Fig 9.8(a), it is seen that immediately after the dead volumes are switched in, the step response is oscillatory as in the fixed controller case shown in Fig 7.20. However with the STC algorithm implemented, the reduction in the plant natural frequency is eventually identified, and after about 5 s the original step response restored. The second part of the figure shows that when the dead volume is switched out again, higher frequency oscillations corresponding to a reduced inertia load occur. The original step response is recovered in only 2 s, the faster recovery of the correct response being a result of the higher levels of dynamic information available during the switching out transient.

945 The time variable nonlinearities so far discussed were deliberately changed rapidly so that the convergence response could be observed, but the changes also occurred infrequently enough so that the identification algorithm had a chance to converge to the new plant conditions. The inherent nonlinearities which are a function of the drive signal behave differently, and here as shown by figs 8.6 and 8.11, a mean position is taken up by the identification algorithm. Fortunately the resulting simple linear model is adequate to enable a satisfactory controller design. However as soon as the mean amplitude of the drive signal square wave changes, the mean identified coefficient values must reconverge. This is shown in Fig 9.9 where the step amplitude was suddenly changed from 0.6 to 1.5 cm. The undesirable overshoot due to the effective increase in forward path gain is seen to be eventually reduced so that the original response is maintained.

946 Although as shown, STC can give good results even when rapidly changing nonlinearities are occurring, this is not generally the case. The good result shown in Fig 9.9 is obtained because of the regularity of the demand signal and because there was effectively a single step change in the mean plant parameters. In general where the mean values are moving about in a less regular way, a satisfactory response may not be achieved.

947 The success of the STC algorithm in any given situation depends on the type of nonlinearities and how much those nonlinearities are excited by the control signals. Although the STC algorithm is designed to be general in nature requiring no previous information about the plant, some tailoring may be necessary to get the

best performance. For example in the case of the servosystem test rig, the full inverse filter was an easily implemented piece of tailoring which removes all of the troublesome inherent nonlinearities whilst being very efficient in implementation.

9.8 Servosystem STC Robustness

948 The related problems of the convergence speed and the robustness of the identification algorithm were discussed in section 9.5 and demonstrated in sections 8.7 and 8.9. When full STC adaptive control is implemented the identification errors are reflected in the controller design and hence the system response. For example, Fig 9.10 shows that for a forgetting factor of 0.96 excessively inconsistent step responses result due to the fluctuations in the identified 'a' coefficients under these conditions (see Fig 8.13). Poor step response consistency was also caused by having sluggish control signals. For example, Fig 9.11 shows the typical errors which occurred when the sluggish root positions z = 0.8 and z = 0.6 +/- j0.1 were chosen. The diminished dynamic content in the signal is insufficient to give good 'a' coefficient estimates, and a wide range of variation in the compensated step response is seen to occur.

949 As discussed in section 9.5, signals of a lower order of excitation than required by the plant model can cause coefficient estimate deterioration due to the lack of uniqueness of the model input/output relationship. When the full STC algorithm was implemented using say a sinusoidal demand signal, interaction between the identification and controller design algorithms had some dramatic consequencies. For example, Fig 9.12 shows the closed loop system tracking of a low frequency sinusoidal demand signal. Whilst the tracking error is seen to be small, some undesirable oscillations occur, and it is this spurious superimposed signal caused by poor identification which maintains identification and control on the brink of instability.

950 At higher frequencies even more dramatic results can be obtained. For example Fig 9.13 shows what occurred when a 4 Hz sinusoidal response was demanded. As with most problems caused by poor signal quality, the model numerator coefficient a_1 is seen to be most affected. In Fig 9.13 it is seen that the use of sinusoidal signals causes the numerator coefficient to drift to a low value, the controller forward path gain increasing all the time. Eventually the point of instability is reached and the

plant oscillation amplitude increases. The resulting flurry of nonsinusoidal dynamic information is sufficient to pull the numerator coefficient value up towards its correct level. For a while stability is restored and a good sinusoidal output results. However very soon the process is repeated over again and a limit cycle type instability is set up.

9.9 Concluding Remarks and Recommendations

951 In view of the convergence and robustness problems discussed and demonstrated in this chapter, the practicality and advantages of adaptive controllers compared with more conventional schemes must be questioned. As a means of automatic controller design the usefulness of the STC algorithm is indisputable, since the method is fully automated and requires very little, if any, previous knowledge about the plant to be controlled. The use of suitably rich signals can easily be arranged thus presenting no robustness problems.

952 However for full STC control the story is different, both the type of nonlinearities encountered, and the type of control signals used must be considered. If the nonlinearity is control signal dependent, then it is likely to occur too rapidly to enable useful adaptive correction, and an inverse filter as proposed in section 7.5 is a much better solution. For time variable nonlinearities, unless they are slowly changing effects, then convergence speed can be a problem. For example in the case of a robot arm picking up a large inertia load, the transient oscillation which occurs whilst the identification algorithm is converging to the new plant conditions may not be acceptable. An undesirable dynamic response is useful in order to identify the new plant conditions and implement the correct control law, yet this is the very thing which adaptive control is designed to eliminate.

953 The duty cycle of the control system (if there is one), must be considered to ensure that the signals will always be sufficient to enable good identification. If this cannot be achieved then a strategy must be developed to turn off the identification algorithm during poor signal periods. Sufficient confidence in the use of adaptive controllers in real situations demands the use of some kind of jacketing strategy to ensure that if failure of the adaptive algorithm occurs, a safe back-up controller can take over.

954 All of these restrictions plus the large amounts of processing time required for implementation has put adaptive control out of favour with many systems engineers, however its use as an aid to controller design should not be overlooked.

Fig 9·1

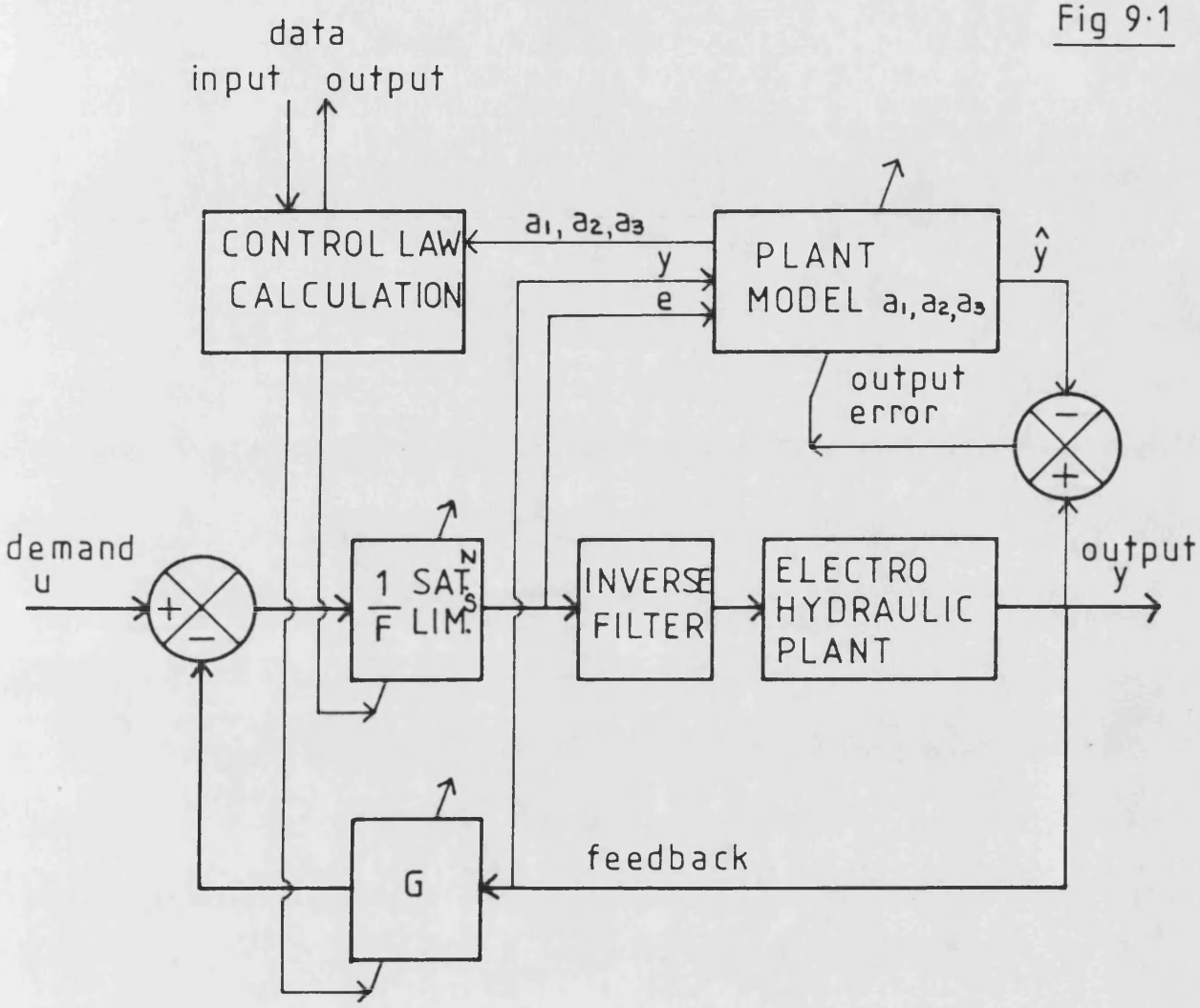

9·1 SELF-TUNING CONTROL SCHEMATIC

Fig 9·2

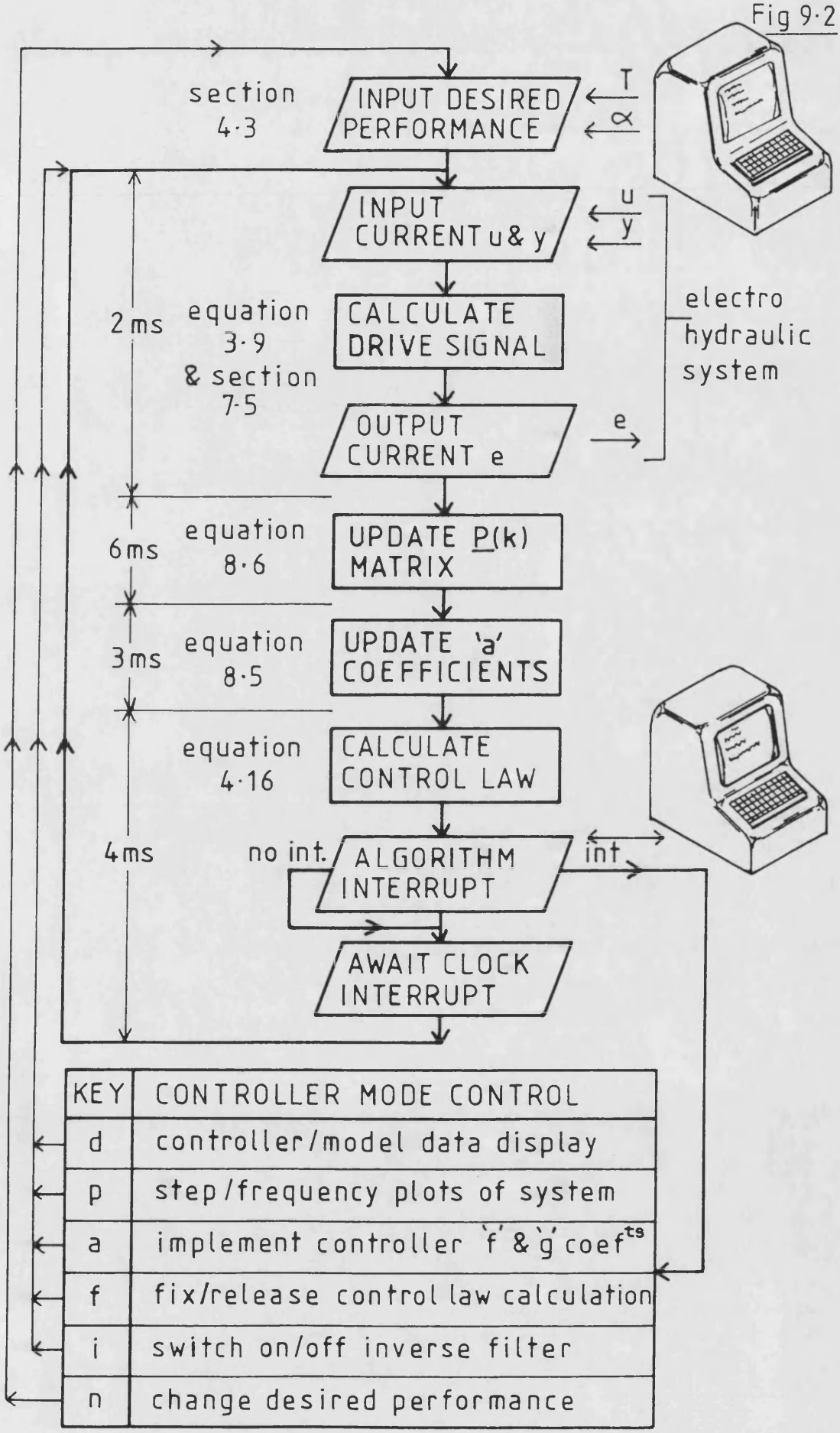

KEY	CONTROLLER MODE CONTROL
d	controller/model data display
p	step/frequency plots of system
a	implement controller 'f' & 'g' coef^{ts}
f	fix/release control law calculation
i	switch on/off inverse filter
n	change desired performance

9·2 STC ALGORITHM IMPLEMENTATION

Fig 9·3

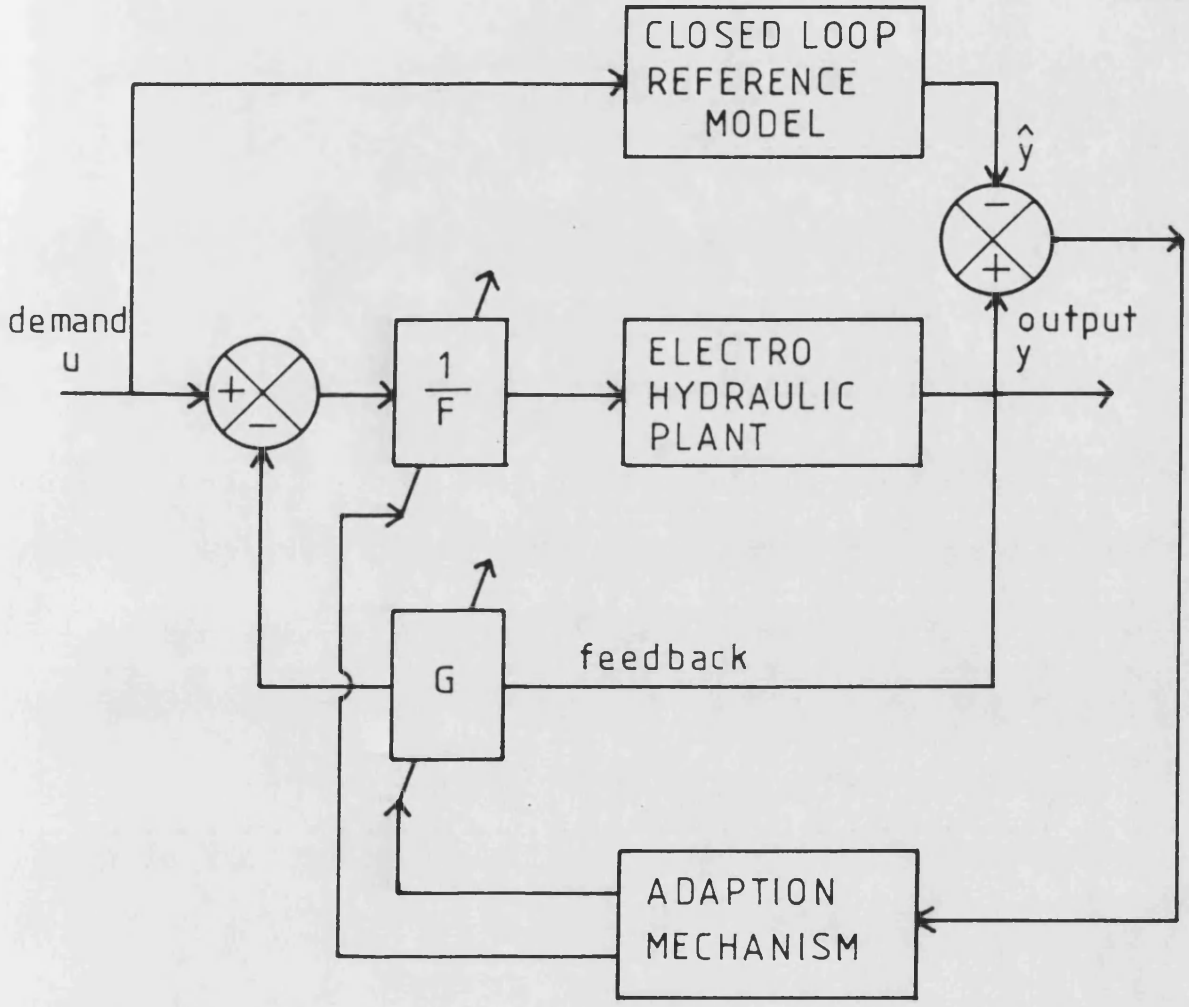

9·3 MODEL REFERENCE ADAPTIVE CONTROL SCHEMATIC

Fig 9·4

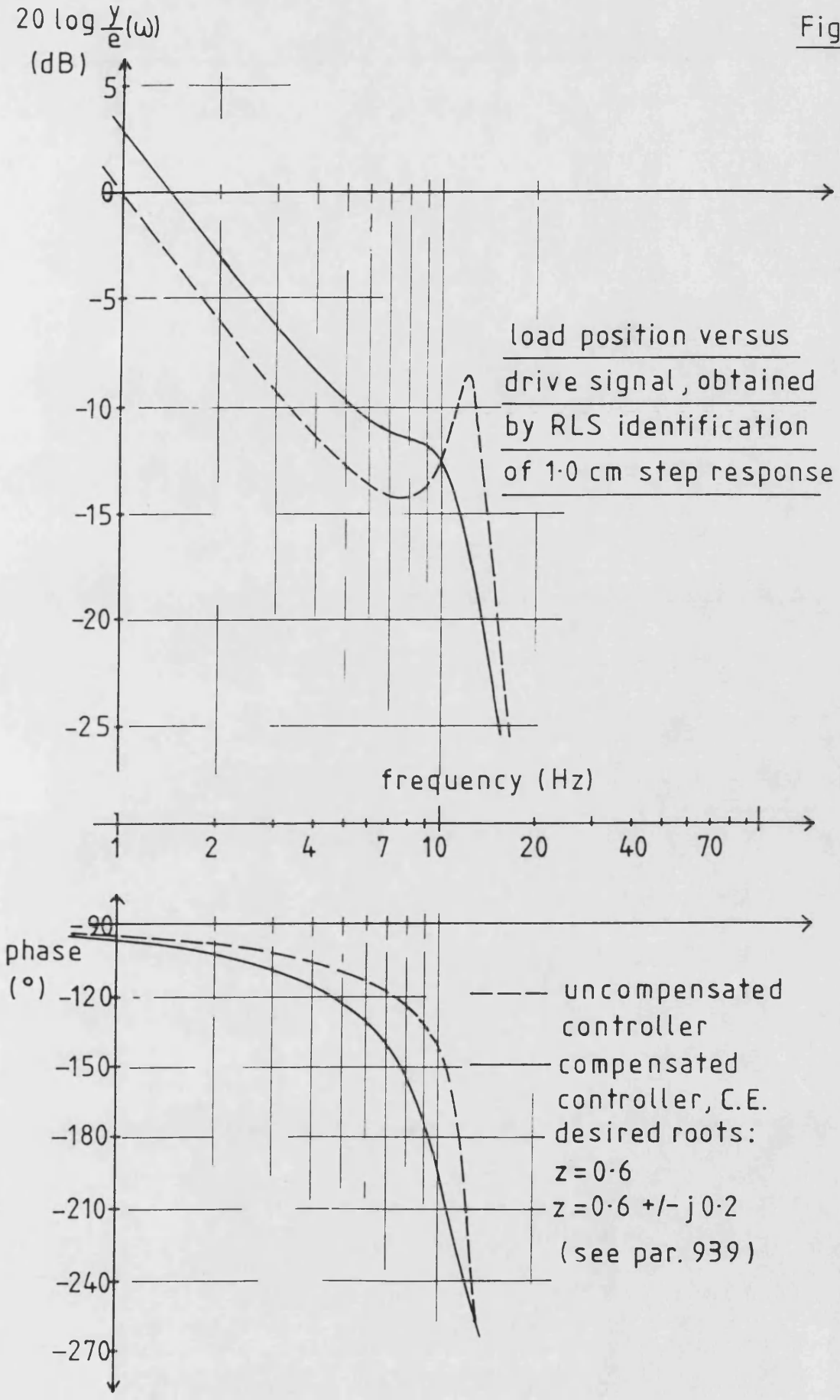

9·4 RLS IDENTIFICATION BEFORE AND AFTER CONTROLLER IMPLEMENTATION

Fig 9·5

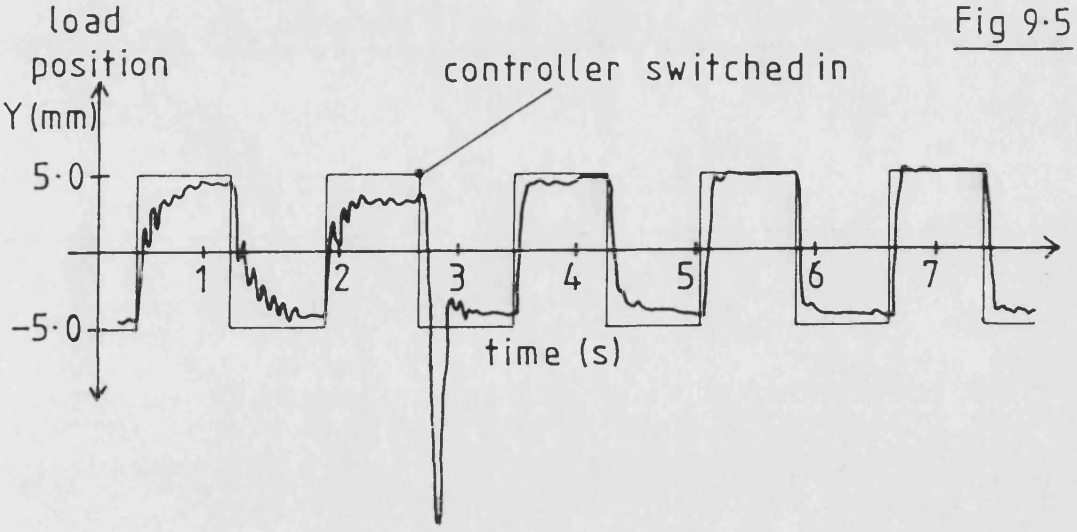

9·5 CONTROLLER SWITCHING IN TRANSIENT

Fig 9·6

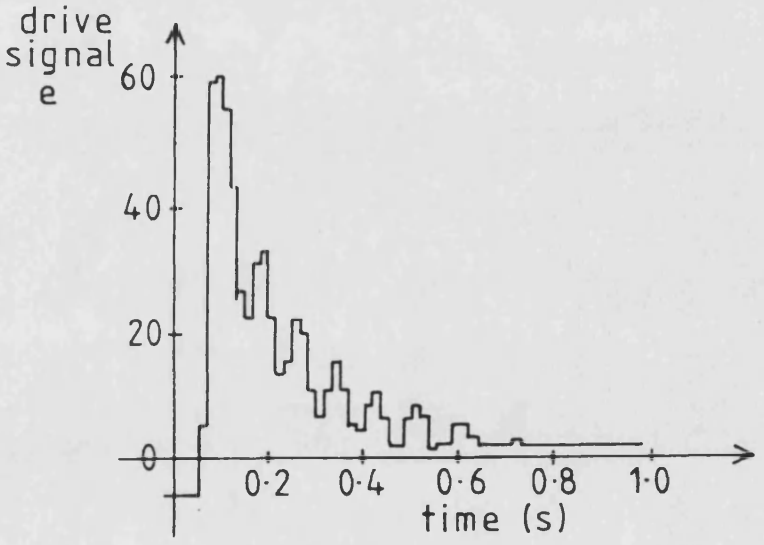

(a) UNCOMPENSATED STEP RESPONSE

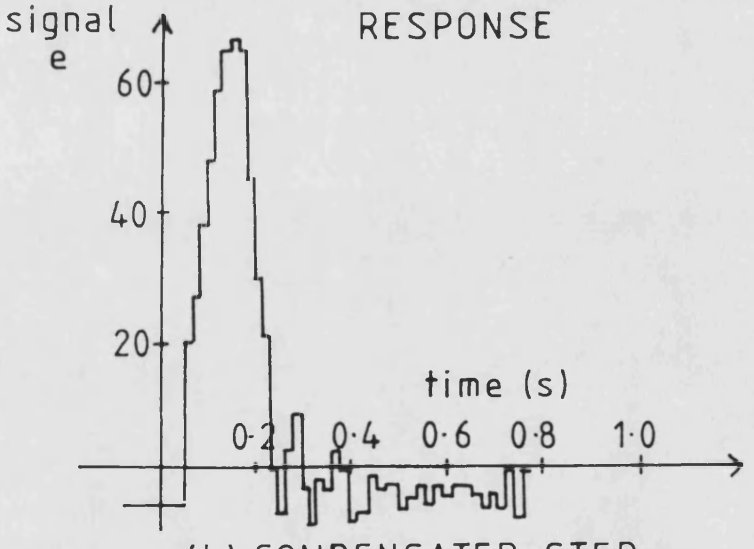

(b) COMPENSATED STEP RESPONSE

9·6 ERROR SIGNAL BEFORE AND AFTER CONTROLLER COMPENSATION

Fig 9·7

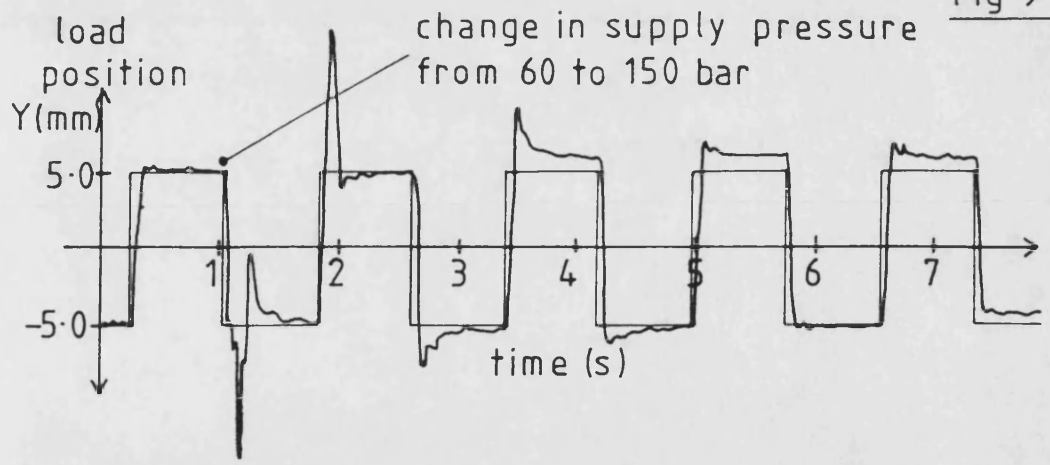

9·7 STC DURING A STEP CHANGE IN SUPPLY PRESSURE

Fig 9·8

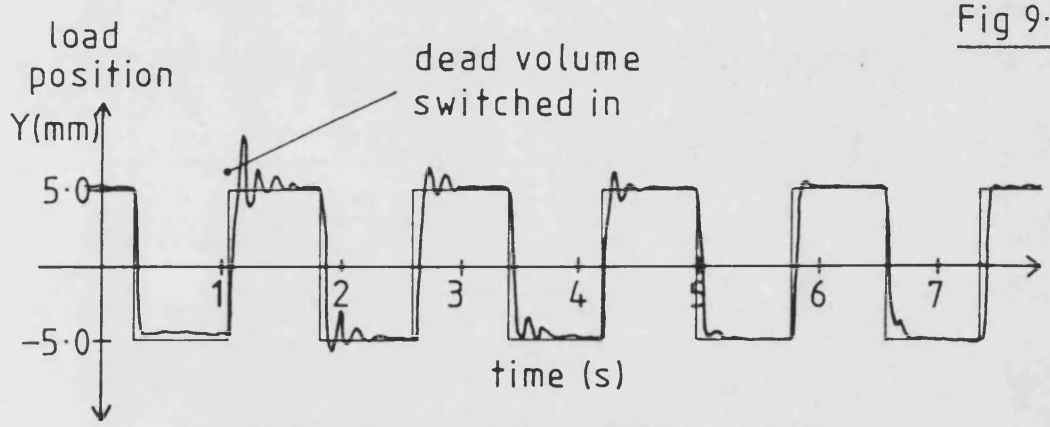

(a) SIMULATED INCREASE IN LOAD

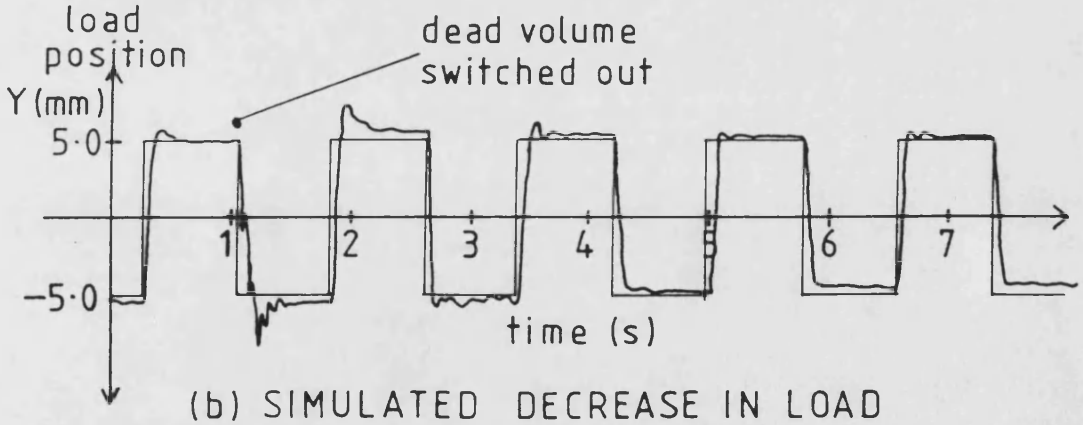

(b) SIMULATED DECREASE IN LOAD

9·8 STC DURING A SIMULATED STEP CHANGE IN LOAD INERTIA

Fig 9·9

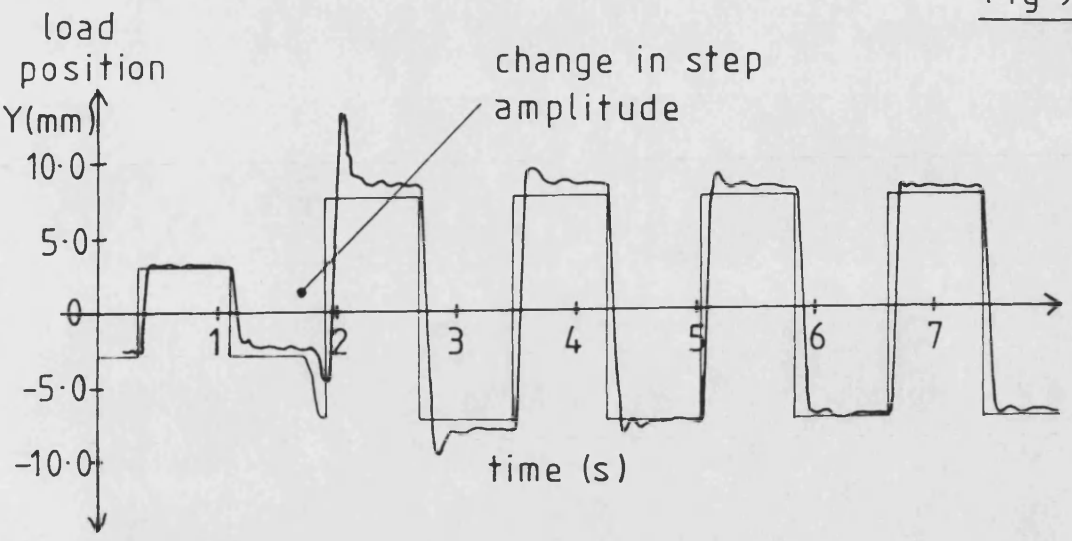

9·9 STC DURING AN INCREASE IN DEMANDED STEP AMPLITUDE

Fig 9·10

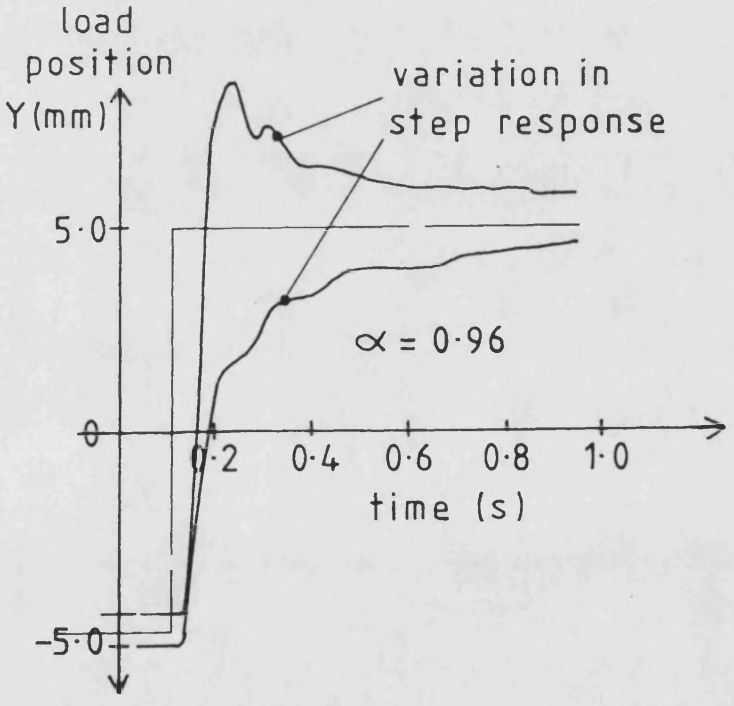

9·10 EFFECT OF LOW FORGETTING FACTOR ON STC STEP RESPONSE

Fig 9·11

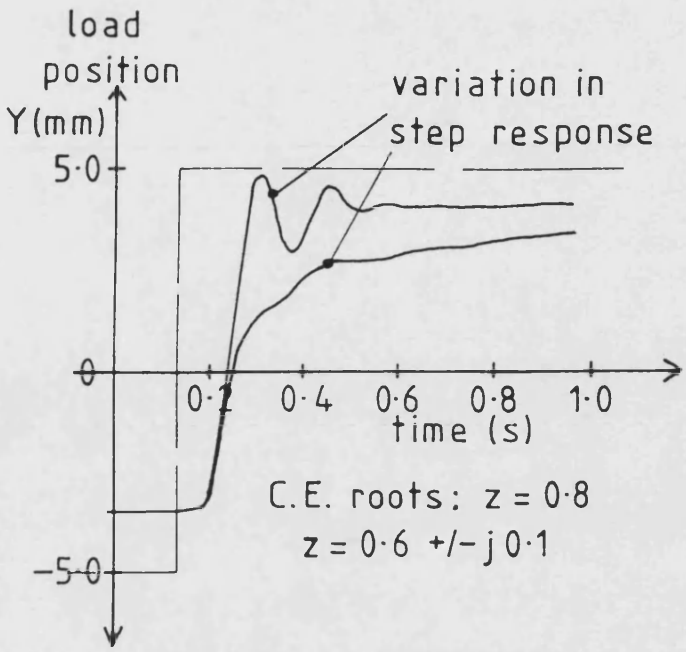

9·11 STC WHEN SLUGGISH ROOT POSITIONS ARE SELECTED

Fig 9·12

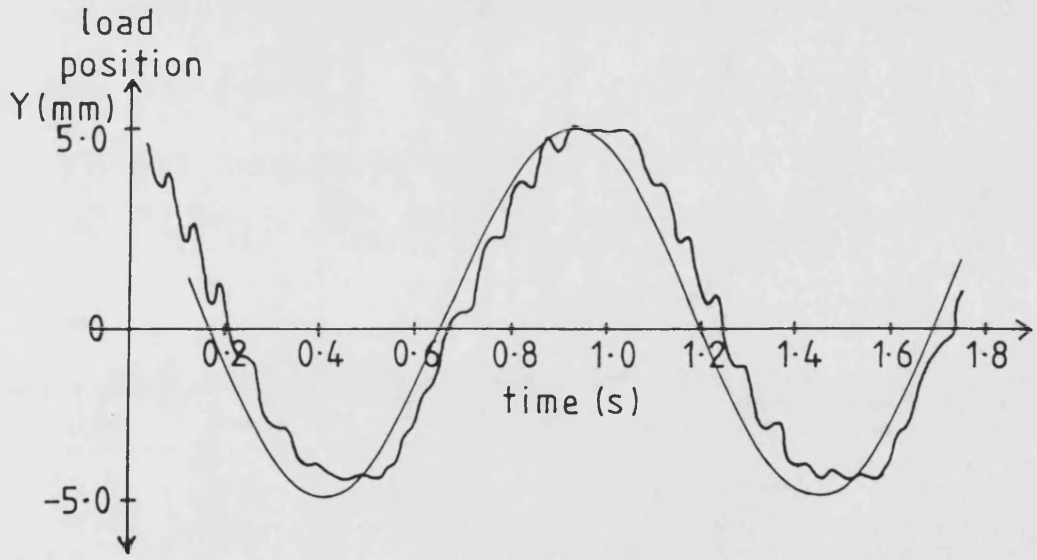

9·12 STC DURING A LOW FREQUENCY SINUSOIDAL DEMAND SIGNAL

Fig 9·13

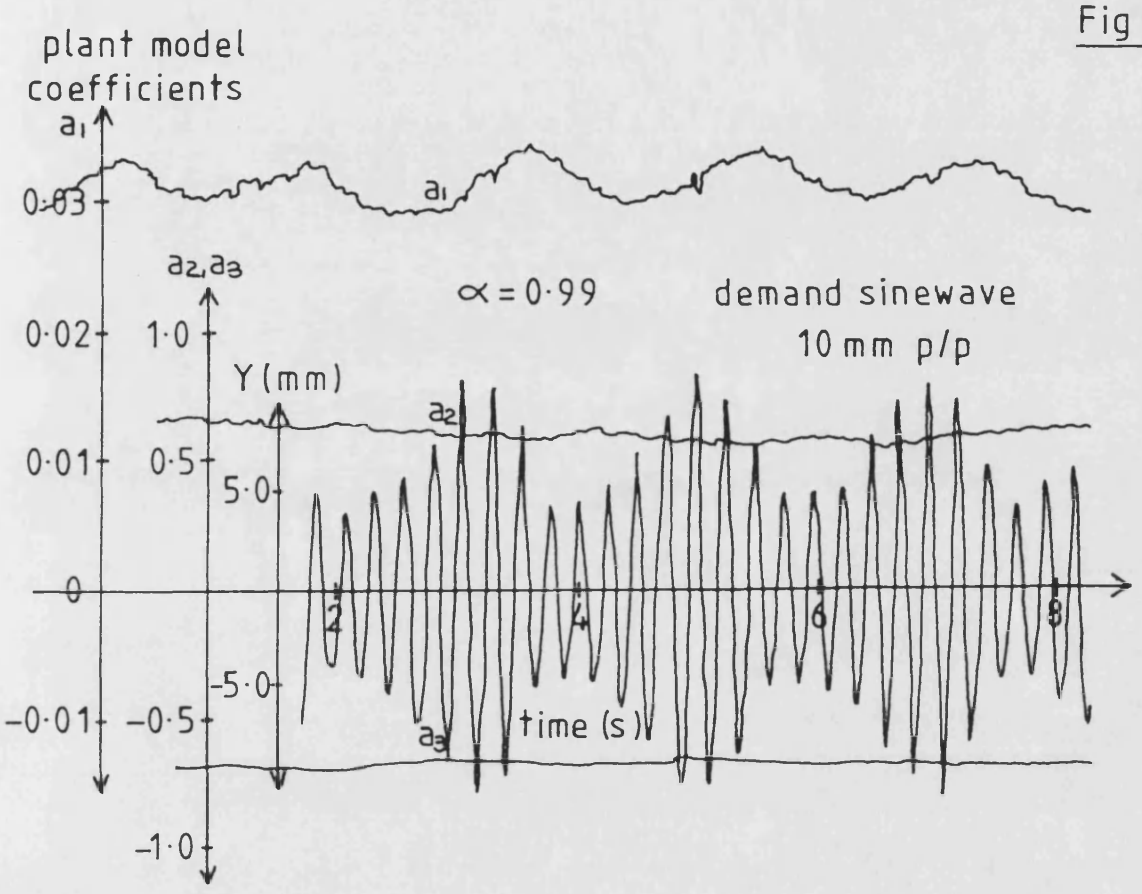

9·13 STC DURING A HIGH FREQUENCY SINUSOIDAL DEMAND SIGNAL

10. CONCLUSIONS

10.1 General Closed Loop Digital Control

1001 The benefits of integrating microprocessor technology into closed loop electrohydraulic systems have been demonstrated by the application of specially developed algorithms to two systems. First the techniques were applied in the design of a new electrohydraulic flow control valve concept; and secondly, in an electrohydraulic position control servosystem. In both cases the electrohydraulic components employed have been conventional devices, and the improvements in performance and simplification in design have resulted entirely from the flexibility and control capability of the microprocessor. In each case the microprocessor was used as a closed loop controller, enhanced by an on-line model of the plant being controlled.

1002 In each case both the plant model and the controller have been represented by discrete transfer functions, and this has resulted in efficient controller implementation and good model accuracy, even for slow sample periods. The Pole/Zero Mapping method of transforming continuous s domain plant models to the z domain, though based on a set of heuristic rules, was found to give sufficiently accurate models for use in controller design, and was thus used throughout the research. This choice was made principally because compared with other methods it yields less complicated discrete transfer functions.

1003 In both of the applications studied, the availability of auxiliary processing time necessary for on-line modelling has been crucial, and has been the motivation for the development of slow sampling techniques and the use of simplified linear models. During the research a rule of thumb for slow sampling was established. Typically the slowest sample frequencies which gave good consistent closed loop step responses were about 5 to 10 times the closed loop system bandwidth.

1004 A Pole Placement controller design method has been developed for electrohydraulic servosystem controllers. The method is based on a Pole/Zero Mapping model of the plant, and a root locus specification of the desired closed loop pole positions, from which the appropriate control law can be calculated. The method proved to be easy to use and yielded good control results.

10.2 Application to New Valve Concept

1005 A survey of electrohydraulic flow control devices showed that a principal area where advances in flow control valve design could be made was in the methods of controlling existing hydromechanical devices rather than in the invention of new ones. Two related areas of work were identified from this observation: first, the development of a valve based on conventional electrohydraulic devices but which could use the benefits offered by closed loop microprocessor control to full advantage; and secondly, the further simplification of the same valve by the use of PWM on/off drive signals.

1006 The microprocessor was successfully used to implement a Pole Placement closed loop controller to give the correct closed loop valve dynamics. However, of principal interest in the research was the on-line modelling of the steady state equations governing the valve internal pressures and flows. Estimation of the valve servo pressure, poppet main flow pressure and poppet flow rate, in addition to the measured poppet feedback signal, meant that any one of these parameters could be controlled by simply selecting them for feedback. The research demonstrated this multi-mode control concept, showing that it can be achieved with an accuracy comparable with conventional proportional control valves.

1007 The generation of four feedback control modes using only one feedback transducer, constitutes a considerable cost saving in the valve design and an increase in flexibility and application. A poppet main stage was used principally for simplicity in design, however the same technique could in principle be used to control the pressures and flows through a four way flow control valve. This remains the subject of further investigation.

1008 Further reductions in the valve cost were obtained by replacing the proportional pilot valve by a simple PWM driven solenoid operated ball valve, and a demodulating restrictor. Fast switching was obtained using an overdriving amplifier, and was essential in minimising the amount of fluctuation passed to the main stage, and in obtaining a good bandwidth. It was found that the PWM frequency needed to be at least ten times the required bandwidth of the pilot valve. The research presented in this thesis demonstrates the basic principle of a PWM driven valve and shows that it could provide a viable alternative to conventionally

driven valves. However the problems of noise and wear in the high frequency switching components require further investigation.

10.3 Application to Servosystem

1009 Microprocessor closed loop control was applied to the servosystem test rig to demonstrate how on-line modelling principles can be used to improve servosystem dynamic performance and to simplify the controller design process. Closing the loop using a microprocessor proved to be an attractive alternative to analogue control since the need for derivative signal feedback transducers was eliminated. It was found that using the Pole Placement method good control could be obtained whilst requiring no additional transducers.

1010 The microprocessor controller was also useful for the correction of undesirable nonlinearities. Two types of nonlinearity were observed in the servosystem test rig: inherent nonlinearities caused by the cylinder drive which were a function of the control signals; and external time variable nonlinearities which were independent of the control signals. In the former category, it was found that the signal dependent nonlinear changes occurred too rapidly to be corrected effectively using adaptive control. A much simpler solution was provided by use of the so called 'inverse filter' technique, whereby the servosystem directional nonlinearity, valve dual gain characteristic and null point dead band effects, were eliminated.

1011 STC adaptive control proved more useful for correcting the effects of external time variable nonlinearities. Normally these nonlinear effects, ie load and supply pressure changes can only be corrected for by direct measurement of their variations (ie, Gain Scheduling). Using STC control the on-line model was made to follow parameter changes, and the correct compensating controller was designed and implemented whilst having no direct measurement of the nonlinear changes which occurred.

1012 Apart from being far quicker than the usual experimental methods of response testing, the RLS identification technique was also found to provide a better linear plant model from which the controller could be designed. The test results have shown that even in the presence of severe nonlinearities the identification algorithm, though based on a linear model, was able to produce a robust controller design. The

STC algorithm was found to be an invaluable tool for automatic controller design, as the technique required no quantitative prior information about the plant being controlled and gave an implementable controller in a matter of a few seconds.

1013 In theory the greatest potential use of an RLS identification algorithm is when it is left on-line and used for adaptive control, however in practice there was a number of constraints which limited its usefulness. The RLS algorithm speed of convergence to step changes in plant parameters was found to take a matter of seconds. During this convergence period inadequate control laws were implemented, which at times gave an unacceptable response. Also in the event of poor signal quality, ie when the system was at rest or when ramp or sinusoidal signals were used, correct identification could not place, and in extreme cases drift in the model coefficient estimates led to instability. All of these problems very much limit the use of fully adaptive control schemes. Unless they can be overcome it is likely that the application of adaptive control techniques to electrohydraulic servosystems will be limited principally to automatic controller design.

REFERENCES

1. I Mech E Conference Publications.
   Microprocessors in Fluid Power Engineering.
   University of Bath, England, Sept 1984.

2. ICFP Conference Publications.
   Zhejiang University, Hangzhou, China, Sept 1985.

3. Huckvale S.A., Chambers P.G., Jones N..
   A Review of the Application of Microprocessors to
   Electrohydraulic Control Systems.
   I Mech E Conference Publications [1], pp 1 -10, Sept 1984.

4. El-Ibiary Y.M..
   Observer Technology Applied to Hydraulic Servosystems.
   Fluid Power Symposium, Aachen, West Germany, March 1986.

5. Chan R.K., Burton R.T., Schoenau G.J., Ukrainetz P.R..
   Utilising a Microprocessor to Achieve Indirect Feedback
   Control in Hostile Environments.
   Proceedings of the 37th NCFP, Vol 35, Oct 1981.

6. Backe W., Anders P., Saffe P..
   Improvement of the Behaviour of Servohydraulic and
   Servopneumatic Drives by Modern Control Conceptions.
   I Mech E Conference Publications.
   Electrics Versus Hydraulics Versus Pneumatics, Oct 1985.

7. Luo H.X., Yan C.P., Xu L..
   The Application of the State Observer to an
   Electrohydraulic Vibrator System.
   ICFP Conference Publications [2], pp 225 - 239, Sept 1985.

8. Jacobs O.L.R..
   When is Adaptive Control Useful?

3rd IMA Conference on Control Theory.
Academic Press, 1981.

9. Cegrell T., Hedqvist T..
Successful Adaptive Control of Paper Machines.
Automatica, Vol 11, pp 53 - 59, 1975.

10. Borisson U., Syding R..
Self-Tuning Control of an Ore Crusher.
Automatica, Vol 12, pp 1 - 7, 1976.

11. Finney J.M., de Pennington A., Bloor M.S., Gill G.S..
A Pole-Assignment Controller for an Electrohydraulic
Cylinder Drive.
Trans. ASME Journal of Dynamic Systems Measurement and Control,
Vol 107, pp 145 - 150, June 1985.

12. Chen J.S., Li Y.P., Ou Y.L., Lu Z.M..
The Further Study of a High Performance Adaptive
Controller for Hydraulic Servosystems.
ICFP Conference Publications [2], pp 163 - 175, Sept 1985.

13. Kinney W., Weiss P..
What You Can Get in Electrohydraulic Servovalves.
Hydraulics and Pneumatics, pp 67 - 78, Feb 1959.

14. Bell R., de Pennington A..
Active Compensation of Lightly Damped Electrohydraulic
Cylinder Drives using Derivative Signals.
I Mech E Proceedings, Vol 184, Pt 1, No 4, pp 83 - 98, 1969/70.

15. I Mech E Conference Publications.
Electrics Versus Hydraulics Versus Pneumatics.
European Conference, Oct 1985.

16. Inoue R..

Contaminant Effects: Look What Happens to Proportional Valves.
Hydraulics and Pneumatics, pp 156 - 159, Nov 1984.

17. Royston D.L..
Proportional Solenoid Valves.
Machine Design, pp 69 - 72, Feb 1983.

18. Xu X..
A Study on the Electrohydraulic Digital Valve.
ICFP Conference Publications [2], pp 374 - 383, Sept 1985.

19. Tsai S.C., Ukrainetz P.R..
Response Characteristics of a Pulse Width Modulated
Electrohydraulic Servo.
Trans. ASME, Journal of Basic Engineering, pp 204 - 214, June 1970.

20. Mansfield G..
Fast Switching Ball Valves as Digital Control Elements
for an Electrohydraulic Servo Actuator.
BHRA 6th International Fluid Power Symposium, Paper G3,
pp 335 - 348, April 1981.

21. Robinson R..
Recent Developments in Electrohydraulic Switching Valves.
Design Engineering, pp 72 - 77, Oct 1981.

22. Brooks D.A..
Electrorheological Effect Adds Muscle.
Control and Instrumentation, pp 58 - 59, Oct 1982.

23. Gorodkin R.G., Korobko Y.V., Blokh G.M., Gleb V.K.,
Sidorova G.I., Ragotner M.M..
Applications of the Electrorheological Effect in Engineering Practice.
Fluid Mechanics - Soviet Research, Vol 8, No 4, pp 48 -61, Aug 1979.

24. Bullough W.A., Stringer J.D..

The Utilisation of the Electroviscous Effect in a Fluid
Power System.
BHRA 3rd International Fluid Power Symposium, Paper F3,
pp 37 - 52, May 1973.

25. O'Neil, Randall, Smiley.
Applying Piezomotors - Electromechanical Muscle.
Design Engineering, pp 28 - 34, Jan 1982.

26. Ikebe Y., Nakada T..
On a Piezoelectric Flapper Type Servovalve Operated by a
Pulse Width Modulated Signal.
Trans. ASME, Journal of Dynamic Systems Measurement and Control,
pp 88 - 94, March 1974.

27. Lee C., Song C..
Analysis of the Solenoid of a Hydraulic
Proportional Compound Valve.
Proceedings of the 35th NCFP, vol 33, pp 21 - 30, Nov 1979.

28. Editorial.
Developments in Solenoids.
Engineering Materials and Design.
Sept 1983.

29. Editorial.
Directional Control Valves for Profit-Making Design.
Hydraulics and Pneumatics, April 1985.

30. Abex Denison Ltd.
Lighting the Way - The Fully Integrated Electrohydraulic
Proportional Directional Valve - D1P 01,
Sales Brochure, 1985.

31. Mc Cloy P., Martin H.R..
Control of Fluid Power - Analysis and Design.

Ellis Horwood Ltd 1980.

32. Ezekiel F.D..
Electromagnetic Actuators.
F.D. Ezekiel Company, Lexington,
Massachusetts, 1966.

33. Moog Inc.
The Deflector Jet Servovalve.
Technical Bulletin 121.

34. Blackburn J.F., Reethof G., Shearer J.L..
Fluid Power Control.
Wiley and MIT Press 1960.

35. Chuen C.W., Jones G.A., Knight J.H..
Microprocessor Based Positional Control of a
Mining Boom Ripper.
I Mech E Conference Publications [1], pp 26 -36, Sept 1984.

36. Holmes R.L..
Two Port Poppet Valve Concept.
Proceedings of the 40th NCFP,
Vol 38, pp 21 - 26 , Dec 1984.

37. Shelley R.T..
The Rego Hydraulic Valve.
Hydraulic and Air Engineering,
pp 19 - 21, Aug 1984.

38. Vaughan N.D..
A Review of Electrohydraulic Modulating Valves
for Microprocessor Control.
I Mech E Conference Publications [1], pp 57 - 69, Sept 1984.

39. Yosuke O..

Operational Performance of Two-Way Flow Control
Valves with Different Design Principles.
O+P, No 8, pp 612 - 616, Aug 1985.

40. Lu Y..
Advanced Achievements of Cartridge Proportional
Valves in Recent Research.
ICFP Conference Publications [2], pp 1 - 20, Sept 1985.

41. Usman A., Parker G.A..
An Electrohydraulic Floating Double Disc Valve.
Proceedings of the 40th NCFP, Vol 38, pp 33 - 41, Dec 1984.

42. Boulden L.L..
Valves That Take Orders from Computers.
Machine Design, pp 70 - 74, June 1974.

43. El-Ibiary Y.M., Dodds D.E., Nikiforuk P.N..
Design and Performance of a Self-Learning Microprocessor
Based Electrohydraulic Position Control System.
Proceedings of the 35th NCFP, Vol 33, pp 215 - 218, Nov 1979.

44. El-Ibiary Y.M., Wilson J.N..
Design and Evaluation of a Rotary Electrohydraulic Valve
for Agricultural Machinery.
Proceedings of the 34th NCFP, Vol 32, pp 71 - 74, Nov 1978.

45. El-Ibiary Y.M., Wilson J.N., Nikiforuk P.N..
Design and Performance of a Microprocessor
Based Digital Flow Control Valve.
Proceedings of the 35th NCFP, Vol 33, pp 199 - 201, Nov 1979.

46. Editorial.
Applying the Microprocessor to Electrohydraulics.
Design Engineering, pp 73 - 81, Oct 1982.

47. Hughes M.L., Dewhirst S., Heron R.A..
A Low-Cost Microprocessor to Fluid Power Interface Valve.
I Mech E Conference Publications [1], Sept 1984.

48. Ramachandran S., Ukrainetz P.R., Nikiforuk P.N..
Digital Flow Control Valve - an Evaluation.
ICFP Conference Publications, pp 310 - 320, Sept 1985.

49. Post K.H..
Electrohydraulic Valves with Fluidic Ball Elements.
Proceedings 1st National Fluid Power Systems and
Controls Conference.
University of Wisconsin, Milwaukee, May 1973.

50. Brown F.T..
The Use of Fluid Inertia for D/A Conversion in
Hydraulic PWM Circuits with Seating Valves, Part I: Concepts.
ASME paper 84-WA/DSC-4, 1984.

51. Brown F.T., Koseoglu A.S..
The Use of Fluid Inertia for D/A Conversion in
Hydraulic PWM Circuits with Seating Valves, Part II: Results.
ASME paper 84-WA/DSC-5, 1984.

52. King T..
Tripos User Guide.
School of Mathematics, University of Bath, March 1983.

53. Richards M., Whitby-Strevens C..
BCPL - The Language and its Compiler.
Cambridge University Press, 1980.

54. Forsythe W., Sherit K.L., Self A.W..
Digital Compensation: a Comparison of Methods.
Trans Inst M C, Vol 7, No 3, pp 117 - 126, April 1985.

55. Franklin G.F., Powell J.D..
Digital Control of Dynamic Systems.
Addison Wesley Pub. Co. Ltd., 1980.

56. Maskery R.H..
The Role of Microprocessors in Closed Loop
Electrohydraulic Control Systems.
Proceedings of the 34th NCFP, Vol 32, pp 145 - 153, Nov 1978.

57. de Pennington A., Marsland D.W., Bell R..
The Improvement of the Accuracy of Electrohydraulic Cylinder Drives
for NC Machine Tools by the Use of Active Feedback Compensation.
Proceedings of 12th Int. Mach. Tool Des. and Res. Conference.
pp 199 - 204, Sept 1971.

58. Astrom K.J., Wittenmark B..
Computer Controlled Systems - Theory and Design.
Prentice-Hall Inc. 1984.

59. Zhiqiang H..
Optimal Selection of Design Parameters for High Frequency
Electrohydraulic Servo System with Large Inertia Load.
ICFP Conference Publications [2], pp 260 - 272, Sept 1985.

60. Forsythe W..
Algorithms for Digital Control.
Trans Inst M C, Vol 5, No 3, July 1983.

61. Astrom K.J., Hagander P., Sternby J..
Zeros of Sampled Systems.
Automatica, Vol 20, No 1, pp 31 - 38, 1984.

62. Phillips C.L..
A Note on Noise Transmission in Digital Control Systems.
IEEE Trans. Automatic Control, Vol AC-23, No 5, pp 956 - 957, Oct 1978.

63. Ashworth M.J..
Robust Design of Sampled Data Systems.
The Radio and Electronic Engineer, No 9, pp 377 - 385, Sept 1984.

64. Finney J.M..
A Study of Self-Tuning Controllers and
Electrohydraulic Cylinder Drives.
Ph.D. Thesis, University of Leeds, 1982.

65. Zafiriou E., Morari M..
Digital Controllers for SISO systems: a Review and a New Algorithm.
Int. J. Control, Vol 42, No 4, pp 855 - 876, 1985.

66. Vickers Catalogue GB-C-2005, Section B.
Proportional Pressure Relief Valves.
ECG-02-7-U-32.

67. Vickers Catalogue GB-C-2005, Section F.
Cartridge Valves to DIN 24342.
Size NG16, 1:2 Area Ratio.

68. Stone J.A..
Discharge Coefficients and Steady-State Flow Forces
for Hydraulic Poppet Valves.
Trans. ASME, Journal of Basic Engineering, pp 144 - 154, March 1960.

69. Emessem Solenoid Co. Ltd..
Technical Data, Linear Inductive Stroke Transducer.
Product AWEX 004 A01.

70. Hewlett G., Brickwood G.S..
Four Poppet Flow Control Valve.
School of Engineering, University of Bath,
Project Report No 784, June 1986.

71. Lisk Catalogue 10a,

Wet Pin Solenoids A/C and D/C,
Solenoid D08, 12V nom.

72. Priest P.H., Vaughan N.D..
Drive Circuits for Pulse Width Modulated Valves.
International Conference on Fluid Power,
Tampere University of Technology, Finland, March 1987.

73. AMI Advanced Product Description, S6840.
Programmable Timer, April 1978.

74. Engelsdorf K..
Damping Networks for Hydraulic Drives and Control Loops.
O+P 29, No 12, pp 916 - 921, 1985.

75. Parker G.A., Desjardins Y.C..
A Comparison of Transfer Function Identification Methods for an
Electrohydraulic Speed Control System.
BHRA 3rd International Fluid Power Symposium, Paper E2, May 1973.

76. Lin W.P..
A Fitting Method to Identify Electrohydraulic Systems from
Frequency Response Characteristics.
ICFP Conference Publications [2], pp 1019 - 1037, Sept 1985.

77. Lynn P.A..
The Analysis and Processing of Signals.
Macmillan Press 1973.

78. Shu N., Changde Y., Weixiang S..
Study of Identification of Hydraulic System by Using
Pseudo-Random Signals.
ICFP Conference Publications [2], pp 999 - 1018, Sept 1985.

79. Williams B.J., Clarke D.W..

Plant Modelling from PRBS Experiments: Part One.
Control pp 856 - 860, Oct 1968.

80. Williams B.J., Clarke D.W..
Plant Modelling from PRBS Experiments: Part Two.
Control pp 947 - 950, Nov 1968.

81. Automatica, Vol 17, No 1, 1981.

82. Astrom K.J., Eykhoff P..
System Identification - A Survey.
Automatica, Vol 7, pp 123 - 162, 1971.

83. Strejc V..
Trends in Identification.
Automatica, Vol 17, No 1, pp 7 - 21, 1981.

84. Kailath T..
A View of Three Decades of Linear Filtering Theory.
IEEE Trans. Information Theory, Vol IT-20, No 2,
pp 146 - 181, March 1974.

85. Young P.C..
Applying Parameter Estimation to Dynamic Systems - Part 1.
Control Engineering, pp 119 - 125, Oct 1969.

86. Young P.C..
Applying Parameter Estimation to Dynamic Systems - Part 2.
Control Engineering, pp 118 - 124, Nov 1969.

87. Wellstead P.E., Sanoff S.P..
Extended Self-Tuning Algorithm.
Int. J. Control, Vol 34, No 3, pp 433 - 455, 1981.

88. Lozano R.L..
Convergence Analysis of Recursive Identification

Algorithms with Forgetting Factor.
Automatica, Vol 19, No 1, pp 95 - 97, 1973.

89. Wittenmark B., Astrom K.J..
Practical Issues in the Implementation of Self-Tuning Control.
Automatica, Vol 20, No 5, pp 595 - 605, 1984.

90. Fortescue T.R., Kershenbaum L.S., Ydstie B.E..
Implementation of Self-Tuning Regulators with
Variable Forgetting Factors.
Automatica, Vol 17, No 6, pp 831 - 835, 1981.

91. Landau I.D..
Adaptive Control - The Model Reference Approach.
Dekker 1979.

92. Harris C.J., Billings S.A..
Self-Tuning and Adaptive Control Theory and Applcations.
IEE Publications, Peter Peregrinus Ltd, 1981.

93. Astrom K.J..
Theory and Applications of Adaptive Control - A Survey.
Automatica, Vol 19, No 5, pp 471 - 486, 1983.

94. Landau I.D..
Model Reference Adaptive Systems - A Survey
(MRAS) - What is Possible and Why?
Trans. ASME, Journal of Dynamic Systems Measurement
and Control, pp 119 - 132, June 1972.

95. Landau I.D..
Model Reference Adaptive Controllers and Stochastic
Self-Tuning Regulators - A Unified Approach.
Trans. ASME, Journal of Dynamic Systems Measurement
and Control, pp 404 - 416, Dec 1981.

96. Egardt B..
Unification of Some Discrete-Time Adaptive Control Schemes.
IEEE trans. Automatic Control, Vol AC-25, No 4 pp 693 - 697, Aug 1980.

97. Astrom K.J., Borisson U., Ljung L., Wittenmark B..
Theory and Application of Self-Tuning Regulators.
Automatica, Vol 13, pp 457 - 476, 1977.

98. Clarke D.W., Gawthrop P.J..
Self-Tuning Controller.
IEE Proceedings, Vol 122, No 9, pp 929 - 934, Sept 1975.

99. Astrom K.J., Wittenmark B..
Self-Tuning Controllers Based on Pole/Zero Placement.
IEE Proceedings, Vol 127, Pt D, No 3, pp 120 - 130, May 1980.

100. Wellstead P.E., Edmunds J.M., Prager D., Zanker P..
Self-Tuning Pole/Zero Assignment Regulators.
Int. J. Control, Vol 30, No 1, pp 1 - 26, 1979.

101. Edge K.A., Figueredo K.R.A..
An Adaptively Controlled Electrohydraulic Servomechanism,
Part 1: Adaptive Controller Design, Part 2: Implementation.
Submitted for publication in I Mech E Proceedings, 1987.

102. Jiashi C., Keller R.B..
The Adaptive Control of Hydraulic Systems
Using Filtered Input and Output Signals.
ASME paper 83-WA/DSC-19, 1983.

103. Vaughan N.D., Whiting I.M..
Self-Tuning Microprocessor Control of Closed
Loop Time-Variable Hydraulic Systems.
Proceedings of the 40th NCFP, Vol 38, Dec 1984.

104. Vaughan N.D., Whiting I.M..

Microprocessor Control Applied to a Nonlinear
Electrohydraulic Position Servosystem.
BHRA 7th International Fluid Power Symposium, Sept 1986.

105. Ljung L., Morf M., Falconer D..
Fast Calculation of Gain Matrices for
Recursive Estimation Schemes.
Int. J. Control, Vol 27, No 1, pp 1 - 19, 1978.

106. Robins A.J., Wellstead P.E..
Recursive System Identification using Fast Algorithms.
Int. J. Control, Vol 33, No 3, pp 455 - 480, 1981.

107. Belanger P.R., Gonheim Y..
Fixed Point Arithmetic Microprocessor Implementation
of Self-Tuning Regulators.
IEEE Proceedings, Joint Automatic Control Conference,
San Fransisco, Aug 1980.

108. Morf M., Kailath T..
Square-Root Algorithms for Least-Squares Estimation.
IEEE Trans. Automatic Control, Vol AC-20,
pp 487 - 497, Aug 1975.

109. Bierman G.J..
Measurement Updating Using the U-D Factorisation.
Automatica, Vol 12, pp 375 - 382, 1976.

110. Dexter A.L..
Self-Tuning Control Algorithm for Single-Chip
Microcomputer Implementation.
IEE Proceedings, Vol 130, Pt D, No 5, pp 255 - 260, Sept 1983.

111. Dasgupta S., Johnson C.R..
Some Comments on the Behaviour of Sign-Sign Adaptive Identifiers.
Systems and Control Letters, Vol 7, No 2, pp 75 - 82, April 1986.

112. Rohrs C.E., Valavani L., Athans M., Stein G..
Robustness of Continuous-Time Adaptive Control Algorithms
in the Presence of Unmodelled Dynamics.
IEEE Trans. Automatic Control, Vol AC-30, No 9,
pp 81 - 889, Sept 1985.

113. Rohrs C.E..
How the Paper 'Robustness of Model-Reference Adaptive Control
Systems with Unmodelled Dynamics' Misrepresents the Results of
Rohrs and his coworkers.
Int. J. Control, Vol 41, No 2, pp 575 - 580, 1985.

114. Astrom K.J..
Analysis of Rohrs Counterexamples to Adaptive Control.
IEEE Conference Decision and Control, paper TP8.4:30,
pp 982 - 987, 1983.

115. Elliot H., Cristi R., Das M..
Global Stability of Adaptive Pole Placement Algorithms.
IEEE Trans. Automatic Control, Vol AC-30, No 4,
pp 348 - 356, April 1985.

116. Gawthrop P.J..
On the Stability and Convergence of a Self-Tuning Controller.
Int. J. Control, Vol 31, No 5, pp 973 - 998, 1980.

117. Egart B.O..
Stability Analysis of Discrete-Time Adaptive Control Schemes.
IEEE Trans. Automatic Control, Vol AC-25, No 4,
pp 710 - 716, Aug 1980.

118. Bai E.W., Sastry S.S..
Persistency of Excitation, Sufficient Richness and Parameter
Convergence in Discrete-Time Adaptive Control.
Systems and Control Letters, Vol 6, No 3, pp 153 - 163, Aug 1985.

APPENDIX 1 - ELECTROHYDRAULIC SERVOSYSTEM SMALL PERTURBATION MODEL

A1.1 Equation Development

The derivation of a dynamic transfer function for an electrohydraulic cylinder drive is presented, and is based on small perturbation theory using the nomenclature shown in Fig A1.1. The small perturbation equations are written down directly for each part of the cylinder drive:

SERVOVALVE DYNAMICS:

The dynamic characteristics of the servovalve are assumed negligible compared to the other cylinder drive components, and a linear relationship is assumed between the drive current I, and the spool position X:

$$x = (K_i)i \tag{A1.1}$$

CYLINDER VOLUME FLOW:

Flow out of the piston side chamber Q_p, gives:

$$q_p = (A_p)sy - \frac{V_p}{\beta}sp_p \tag{A1.2}$$

and in to the annulus side gives:

$$q_a = (A_a)sy + \frac{V_a}{\beta}sp_a \tag{A1.3}$$

SPOOL FLOW:

The orifice equation applied to each of the spool flow areas, for small perturbations gives:

$$q_p = (C_{xp})x + (C_{pp})p_p \tag{A1.4}$$

$$q_a = (C_{xa})x - (C_{pa})p_a \qquad \text{(A1.5)}$$

where the C coefficients are the pressure and spool position dependent flow gains.

CYLINDER FORCES:

The load inertia and cylinder rod and piston is assumed to be a rigid body, and equating the static and dynamic forces acting on the body gives:

$$Ms^2y + Csy = (A_a)p_a - (A_p)p_p + f \qquad \text{(A1.6)}$$

Substituting equations A1.1 to A1.5 into A1.6 gives:

$$(Ms^2 + Cs)y + \frac{(A_a)^2 sy}{C_{pa} + \frac{V_a}{\beta}s} + \frac{(A_p)^2 sy}{C_{pp} + \frac{V_p}{\beta}s}$$

$$= \frac{(A_a C_{xa} K_i)i}{C_{pa} + \frac{V_a}{\beta}s} + \frac{(A_p C_{xp} K_i)i}{C_{pp} + \frac{V_p}{\beta}s} + f \qquad \text{(A1.7)}$$

The compressibility lag terms for volumes V_a and V_p are of different time constants for all except one cylinder piston position, this is when the time constant is :

$$T = \frac{V_a}{\beta C_{pa}} = \frac{V_p}{\beta C_{pp}} = \frac{V}{\beta C_p} \qquad \text{(A1.8)}$$

Making this assumption reduces the equation A1.7 to:

$$y(s) = \frac{(K_i K_g)i(s) + (1+Ts)f(s)}{s(MTs^2 + (M+TC)s + C + \frac{A_a^2}{C_{pa}} + \frac{A_p^2}{C_{pp}})} \qquad \text{(A1.9)}$$

where: $K_g = \frac{A_a C_{xa}}{C_{pa}} + \frac{A_p C_{xp}}{C_{pp}}$

This equation gives transfer functions of the form:

$$\frac{y}{i}(s) = \frac{K\omega_n^2}{s(s^2+2\zeta\omega_n s+\omega_n^2)} \qquad \text{(A1.10)}$$

and

$$\frac{y}{f}(s) = \frac{(1+Ts)K_f\omega_n^2}{s(s^2+2\zeta\omega_n s+\omega_n^2)} \qquad \text{(A1.11)}$$

These equations are represented in block diagram form in Fig A1.2. At other cylinder positions when equation A1.8 is not true, the system should really be represented by a forth order model. However in practice the transfer function equations A1.10 and A 1.11 give a good representation of the electrohydraulic system, and thus are used as the general plant models.

A1.2 Damping and Natural Frequency

NATURAL FREQUENCY:

The natural frequency arises because of the inertia of the load and the stiffness of the oil in the cylinder. Assuming the spool to be closed (ie at the null position), the stiffness can easily be found from equation A1.7. The dynamic terms are neglected, and if the flow gains C_{pa} and C_{pp} are assumed zero at the null point, the load stiffness is:

$$\frac{f}{y} = \beta\left(\frac{A_a^2}{V_a}+\frac{A_p^2}{V_p}\right) \qquad \text{(A1.12)}$$

Thus the natural frequency is:

$$\omega_n = \sqrt{\frac{\beta}{M}\left(\frac{A_a^2}{V_a}+\frac{A_p^2}{V_p}\right)}$$

or using the dimensions of Fig A1.1:

$$\omega_n = \sqrt{\frac{\beta}{M}\left(\frac{A_a}{L_a}+\frac{A_p}{L_p}\right)} \qquad \text{(A1.13)}$$

In this equation the natural frequency is seen to change as the piston is moved. The lowest frequencies occur towards the middle of the stroke, and the highest at each end.

DAMPING:

From equations A1.8, A1.9 and A1.10, the damping ratio is:

$$\zeta = \frac{\frac{1}{2}(\frac{C}{M}+\frac{\beta C_p}{V})}{\omega_n} \qquad \text{(A1.14)}$$

where C_p, and V are mean values.

Thus the damping ratio is seen to be dependent on the natural load damping C, and the valve flow versus pressure gain C_p. The value of C_p depends on the opening of the spool, and the pressure drop across each orifice. About the null point the valve damping is very dependent on the spool lap, however in any case the valve damping is generally very low.

A1.3 Steady State Valve Drive Signal

Ideally when the cylinder piston is at rest, the valve spool should be closed off at $X=0$, requiring zero drive signal. However in the case of a single ended cylinder or if external loads are applied, the differential in pressure required on the piston to maintain equilibrium demands that the valve be cracked open. The amount of opening depending on the pressure gain of the valve. Generally it is best to have a high pressure gain so that only a small drive signal is required to sustain large loads. The factors influencing the required spool offset can be seen from equation A1.7 by setting all of the dynamic terms to zero. This gives:

$$\frac{f}{x} = -(\frac{A_a C_{xa}}{C_{pa}}+\frac{A_p C_{xp}}{C_{pp}}) \qquad \text{(A1.15)}$$

A1.4 Directional Forward Path Gain Nonlinearity

In the case of a single ended cylinder the differential piston areas cause a directional

nonlinearity in the system which affects the closed loop response. The change in forward path gain when the valve spool position is reversed can be seen by considering the piston velocity in each direction.

If the spool is considered to open a positive amount X^+, giving a velocity V^+, the orifice equation applied to each of the spool orifices yields:

$$V^+ = \frac{K_s X^+ \sqrt{P_c - P_a^+}}{A_a} = \frac{K_s X^+ \sqrt{P_p^+}}{A_p} \qquad \text{(A1.16)}$$

Where K_s is the orifice flow gain. Now for $F=0$ and neglecting the load damping C, then for a steady piston velocity:

$$A_a P_a = A_p P_p \qquad \text{(A1.17)}$$

Substituting into equation A1.16 gives the retract stroke piston pressure:

$$P_p^+ = \frac{P_c}{\frac{A_p}{A_a}(1+(\frac{A_a}{A_p})^3)} \qquad \text{(A1.18)}$$

The retract stroke gain is:

$$\frac{V^+}{X^+} = \frac{K_s}{A_p}\sqrt{P_p^+} \qquad \text{(A1.19)}$$

Similarly, for a negative opening X^-, and corresponding velocity V^-, applying the orifice equation gives:

$$V^- = \frac{K_s X^- \sqrt{P_c - P_p^-}}{A_p} = \frac{K_s X^- \sqrt{P_a^-}}{A_a} \qquad \text{(A1.20)}$$

Substituting from equation A1.17 gives:

$$P_a^- = \frac{P_c}{\frac{A_a}{A_p}(1+(\frac{A_p}{A_a})^3)} \qquad \text{(A1.21)}$$

The extend stroke gain is:

$$\frac{V^-}{X^-} = \frac{K_s}{A_a}\sqrt{P_a^-} \qquad \text{(A1.22)}$$

The ratio of the extend and retract stroke gains is found by dividing equations A1.22 by A1.19 and substituting from equations A1.18 and A1.21, giving the gain ratio:

$$R_G = \frac{V^-}{V^+} = \sqrt{\frac{A_p}{A_a}} \qquad \text{(A1.23)}$$

Thus the extend stroke gain is faster than the retract stroke gain by a factor equal to the square root of the ratio of the piston side and the annulus side cylinder areas.

A1.5 The Effect of the Directional Nonlinearity on the Valve Damping.

Equation A1.14 shows that the damping ratio in equation A1.11 is affected by the valve flow versus pressure gains C_{pa} and C_{pp}. These gains are a function of both the spool position and the pressure drop across the spool. In this part of the appendix the change in C_p caused by reversing the spool direction is considered.

The valve gains C_{pa} and C_{pp} are found by differentiating the orifice equation with respect to the pressure drop across the orifice, and it is found that for a constant spool Position X that:

$$C_p \propto \frac{1}{\sqrt{\Delta P}} \qquad \text{(A1.24)}$$

Where ΔP is the orifice pressure drop. Equation A1.24 can be used to find the change in C_p when the spool direction is changed. Considering the piston side spool orifices, define the ratio between the extend and retract stroke gains as:

$$R_P = \frac{C_{pp}^-}{C_{pp}^+} \qquad \text{(A1.25)}$$

From equation A1.24:

$$R_p = \sqrt{\frac{P_p^+}{P_c - P_p^-}} \qquad \text{(A1.26)}$$

P_p^+ was derived in equation A1.18, and P_p^- is derived from equation A1.17 and A1.21 to give:

$$P_p^- = \frac{P_c}{1+\left(\frac{A_p}{A_a}\right)^3} \qquad \text{(A1.27)}$$

Thus substituting A1.18 and A1.27 into A1.26 yields the result:

$$R_P = \sqrt{\frac{A_a}{A_p}} \qquad \text{(A1.28)}$$

An identical equation can be derived for the annulus port orifices. The equation shows that the extend stroke damping ratio is less than the retract stroke damping ratio by a factor equal to the square root of the ratio between the annulus side area and the piston side area of the cylinder.

Fig A1·1

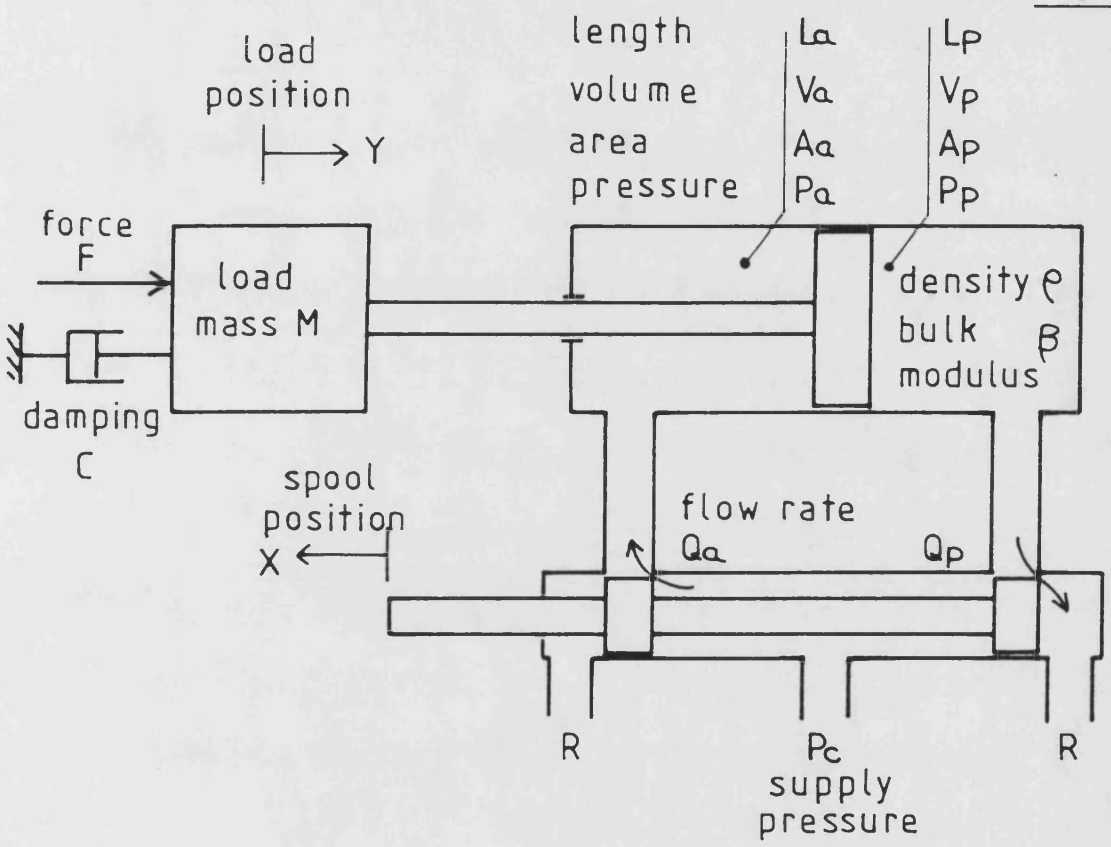

A1·1 ELECTROHYDRAULIC SERVOSYSTEM PLANT MODEL

Fig A1·2

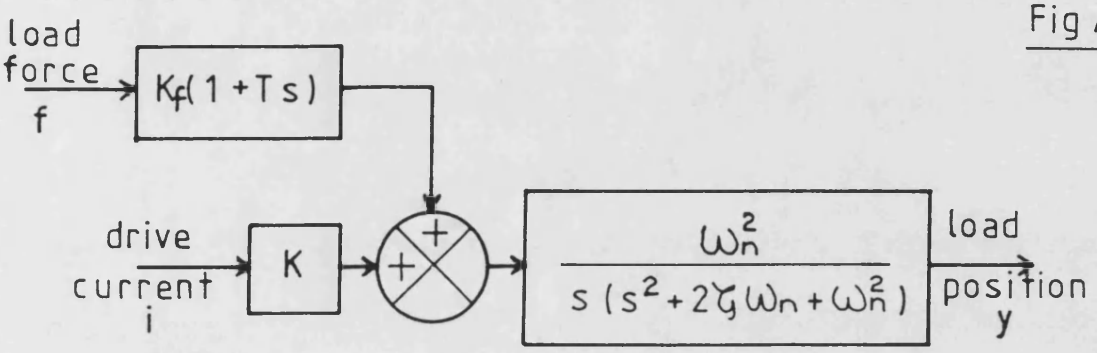

A1·2 BLOCK DIAGRAM REPRESENTATION

APPENDIX 2 - POLE/ZERO MAPPING RULES

The poles of a discrete transfer function can be related to a continuous transfer function according to the equation:

$$z = e^{\tau s} \qquad \text{(A2.1)}$$

The Pole/Zero Mapping method is based on the idea that this equation can also be applied to the zeros of the transfer function. The technique consists of a set of heuristic rules for determining the zeros and gain of a discrete transfer function which approximates the continuous transfer function. The rules for changing the continuous transfer function $H(s)$, to a discrete transfer function $H(z)$, are as follows:

(a) All of the poles of $H(s)$ are mapped according to equation A2.1, thus an s plane pole at $s=-b$ becomes a z plane pole at $z=e^{-\tau b}$. Second order oscillatory polynomials are first factorised into complex pairs of roots. These can then be mapped to a discrete complex pair and expanded out into a real second order polynomial in the z plane.

(b) All finite zeros are mapped in exactly the same way as the poles, ie as described in rule (a).

(c) If there are infinite zeros present in the continuous transfer function then all except one are mapped to the point $z=-1$. For example a continuous transfer function such as equation A1.10 would have two roots at $z=-1$ in the numerator polynomial.

(d) Finally the gain of the discrete transfer function is found by matching its frequency response amplitude ratio to that of the continuous transfer function at any desired frequency. Generally the transfer functions are matched at low frequencies, forcing any mismatch due to the approximate nature of the method to occur at high frequencies.

APPENDIX 3 - STEADY STATE GAIN THEOREM

The steady state gain of a discrete transfer function can be found using the final value theorem. If a unity step input is applied to the transfer function, then the converged value of output (if it converges at all), is also the steady state gain of the system. If the system transfer function is $H(z)$ and the input z transform $u(z)$, then the z transform of the output sequence is:

$$y(z) = H(z)u(z) \tag{A3.1}$$

The final value theorem states that provided the poles of $(1-z^{-1})y(z)$ are inside the unit circle, the converged value of the output is:

$$\lim_{k\to\infty} y(k) = \lim_{z\to 1}(1-z^{-1})y(z) \tag{A3.2}$$

Assuming the system block diagram structure of Fig A3.1, the closed loop transfer function is:

$$H(z) = \frac{A_N(z)}{F(z)A_D(z)+G(z)A_N(z)} \tag{A3.3}$$

Now for a unit step:

$$u(z) = \frac{z^{-1}}{1-z^{-1}} \tag{A3.4}$$

thus substituting equations A3.3 and A3.4 into equation A3.1 to obtain $y(z)$, and then $y(z)$ into A3.2, the steady state value of $y(k)$ is:

$$\lim_{k\to\infty} y(k) = \lim_{z\to 1}\frac{A_N(z)}{F(z)A_D(z)+G(z)A_N(z)} \tag{A3.5}$$

If the plant being controlled has integral action then:

$$A_D(z)_{z\to 1} = 0 \tag{A3.6}$$

and the steady state output value $y(\infty)$, ie the transfer function steady state gain.

is:

$$G_{ss} = \lim_{k \to \infty} y(k) = \frac{1}{G(1)} \qquad \text{(A3.7)}$$

Thus the steady state gain is determined by the sum of the terms in the controller feedback filter, since from equation A3.7:

$$G_{ss} = \frac{1}{g_1 + g_2 + g_3 + \ldots\ldots} \qquad \text{(A3.8)}$$

Fig A3·1

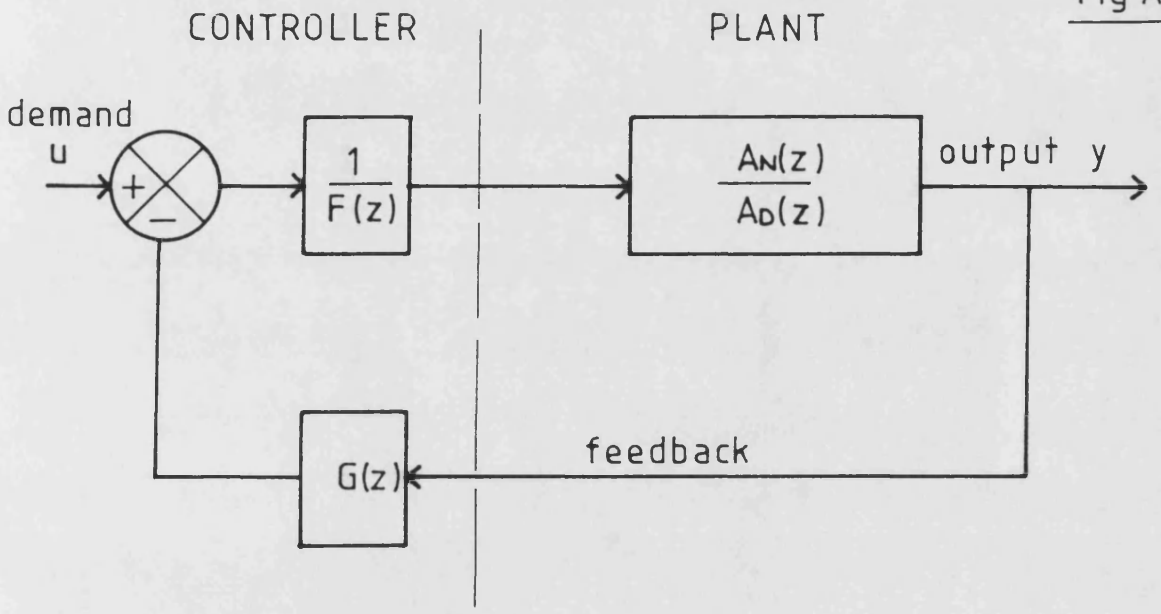

A3·1 DIGITAL CONTROLLER BLOCK DIAGRAM

APPENDIX 4 - PROPORTIONAL FLOW CONTROL VALVE SMALL PERTURBATION MODEL

A4.1 Equation Development

The dynamic equations for the valve hardware of the new flow control valve are derived using small perturbation theory, the equations being derived for each part of the valve based on the nomenclature of Fig A4.1. The small perturbation equations are written down directly.

ELECTROMAGNETIC INTERFACE:

The dynamic effects of the solenoid electrical and magnetic circuits are neglected and a linear relationship is assumed, the magnetic force F_m, being related to the drive current by the equation:

$$f_m = (K_a)i \qquad \text{(A4.1)}$$

ARMATURE FORCE BALANCE

Considering the solenoid armature in Fig A4.1 as a rigid free body, equating the static and dynamic forces gives the equation:

$$M_a s^2 x + C_a s x = f_s - f_m$$

which rearranged gives:

$$-x = \frac{f_m - f_s}{s(C_a + M_a s)} \qquad \text{(A4.2)}$$

The change in flow force f_s, is a function of the servo pressure P_s, and the flapper lift X, given by the equation [31]:

$$F_s = \frac{\pi}{4} D_n^2 P_s \left(1 + \left(\frac{4C_q X}{D_n}\right)^2\right) \qquad \text{(A4.3)}$$

The lift dependent term inside the brackets can be shown to have a minor effect on

the nozzle flow force, and thus the simplified equation:

$$f_s = (K_s)p_s \tag{A4.4}$$

is used in this analysis.

SERVO FLOW EQUATIONS:

Equating the flows into and out of the chambers, including the effects of oil compressibility gives:

$$q_c = q_n + q_d + \frac{V_s}{\beta} s p_s \tag{A4.5}$$

$$q_d = -(A_p)sy + \frac{V_d}{\beta} s p_d \tag{A4.6}$$

and applying the orifice equation to the restrictors gives:

$$q_n = (C_{na})x + (C_{ns})p_s \tag{A4.7}$$

$$q_d = (C_d)p_s - (C_d)p_d \tag{A4.8}$$

$$q_c = -(C_{cs})p_s \tag{A4.9}$$

The C coefficients are derivative flow gains, assumed constant for small perturbations about the valve operating point. Substituting these equations into equation A4.5 gives:

$$p_s = \frac{(C_d)p_d - (C_{na})x}{C_t + \frac{V_s}{\beta} s} \tag{A4.10}$$

Where:

$$C_t = C_{cs} + C_{ns} + C_d$$

Similarly, substituting into equation A4.6 gives:

$$p_d = \frac{(C_d)p_s + (A_p)sy}{C_d + \frac{V_d}{\beta}s} \qquad \text{(A4.11)}$$

POPPET FORCE BALANCE:

The return line of the poppet is assumed to be closed off so that the upstream pressure P, is acting over the full poppet area (see Fig A4.1). The poppet preload spring has a very low rate and can be neglected. Equating the poppet static and dynamic forces gives:

$$M_p s^2 y + C_p sy = A_p (p - p_d)$$

which rearranged gives:

$$-y = \frac{A_p (p_d - p)}{s(C_p + M_p s)} \qquad \text{(A4.12)}$$

Equations A4.1, A4.2, A4.4 and equations A4.10 to A4.12 can now be arranged in block diagram form as shown in Fig A4.2. The pilot valve and poppet valve form two separate closed loop systems, where both of the loops are closed by hydromechanical feedback mechanisms. The dynamics of the two devices however interact, due to a third feedback loop caused by flow between the two devices via the damping restrictor. The overall transfer function of Fig A4.2 is of sixth order, and is too complex for use as a model for Pole Placement controller design. A simplified model can be achieved by neglecting some of the dynamic terms.

A4.2 Simplified Transfer function

Simplification of the block diagram of Fig A4.2 can be made by neglecting the poppet inertia and damping forces which can be considered small compared to the pressure forces. Also the compressibility terms that occur in the equations can be neglected, ie assume that:

$$V_s = V_d = 0 \quad C_p = 0, \text{ and } M_p = 0 \qquad \text{(A4.13)}$$

By making these assumptions, the pressure on the back face of the poppet becomes

equal to the main flow pressure P, which can be considered as an external disturbance. The poppet dynamics are reduced to integral action. The simplified block diagram is shown in Fig A4.3. Further reduction to a second order transfer function is achieved if the pressure control valve armature inertia is neglected. The resulting transfer function is:

$$\frac{y}{i}(s) = -\frac{K}{s(1+Ts)} \qquad \text{(A4.14)}$$

where:

$$K = \frac{K_a C_d}{K_s A_p}, \quad T = \frac{C_a C_t}{K_s C_{na}} \qquad \text{(A4.15)}$$

In this equation the poppet is modelled as an integrator and the pressure control valve as a first order lag.

Fig A4·1

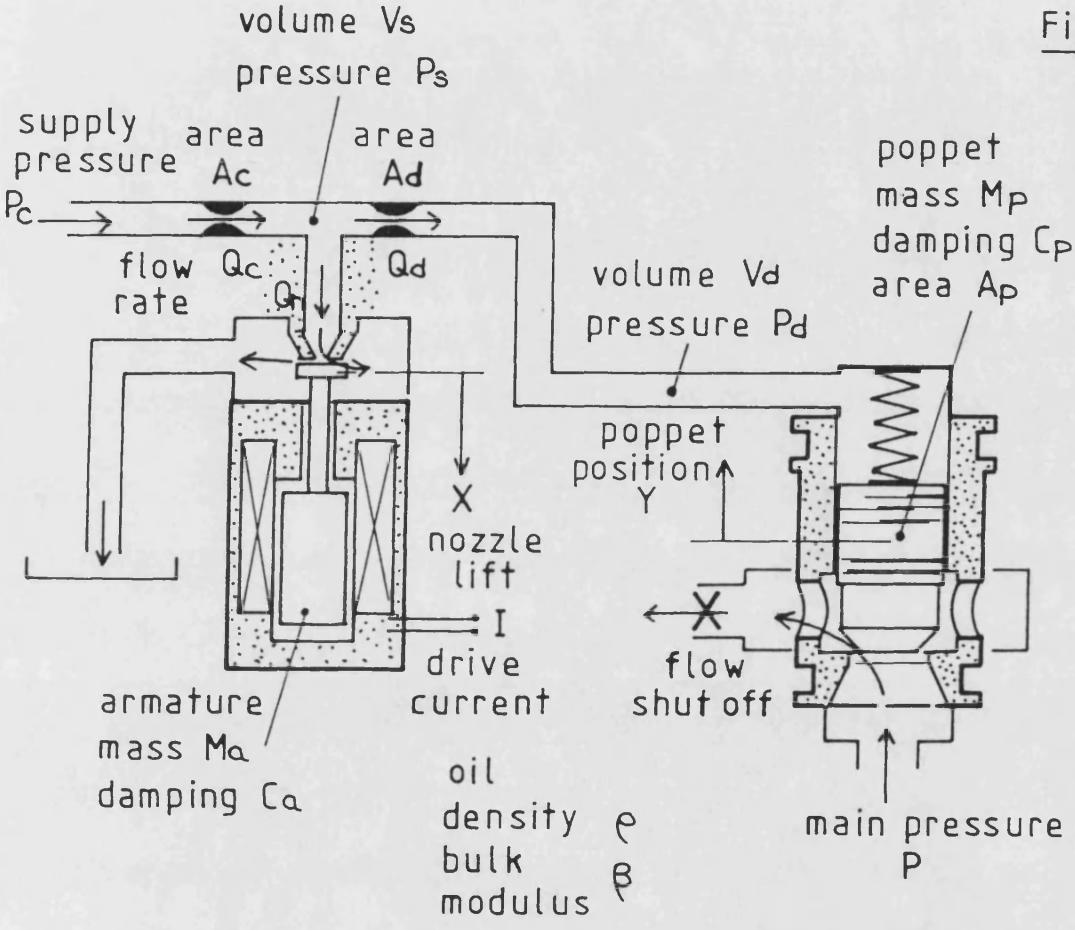

A4·1 FLOW CONTROL VALVE PLANT MODEL

Fig A4·2

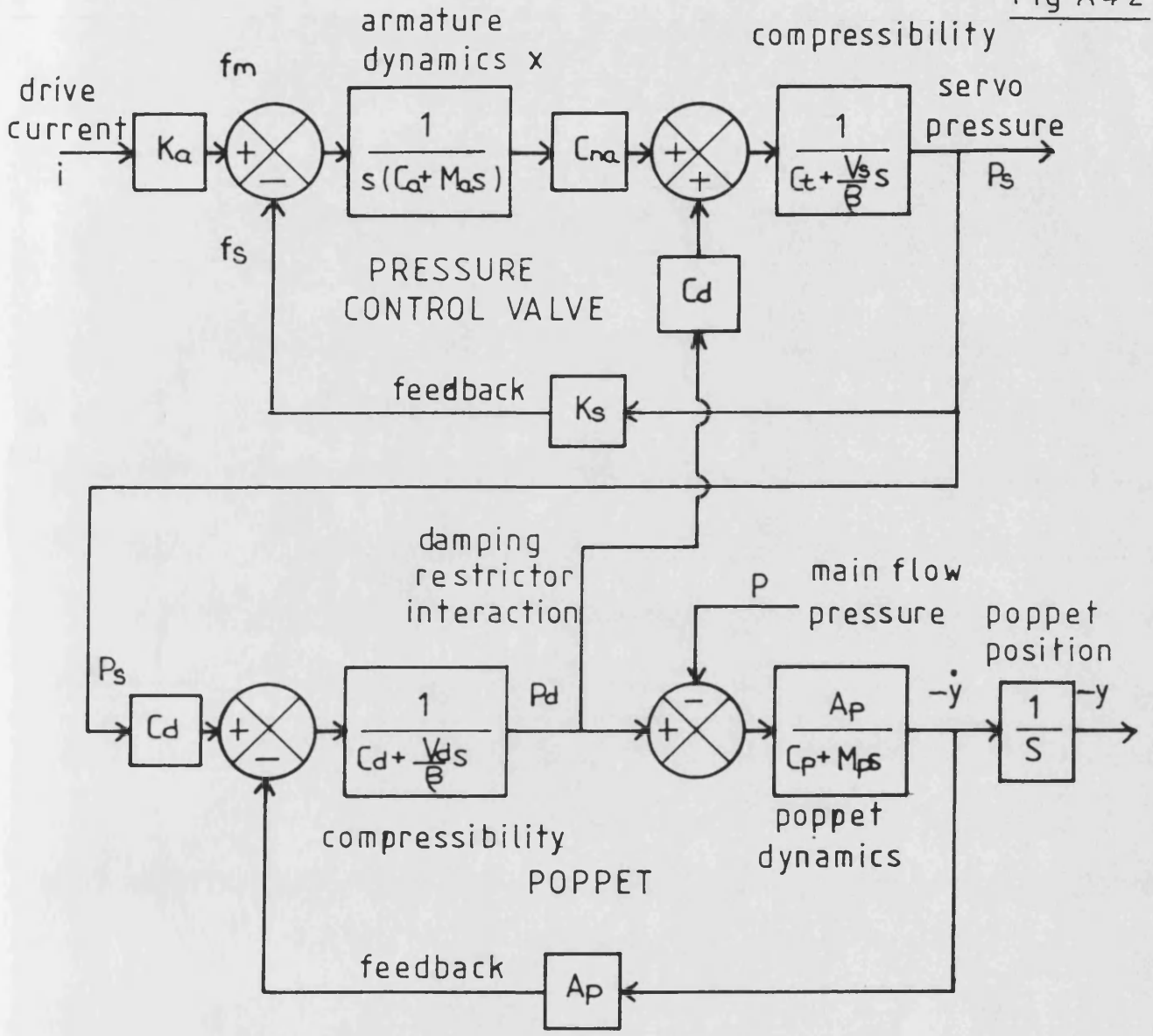

A4·2 DETAILED BLOCK DIAGRAM

Fig A4·3

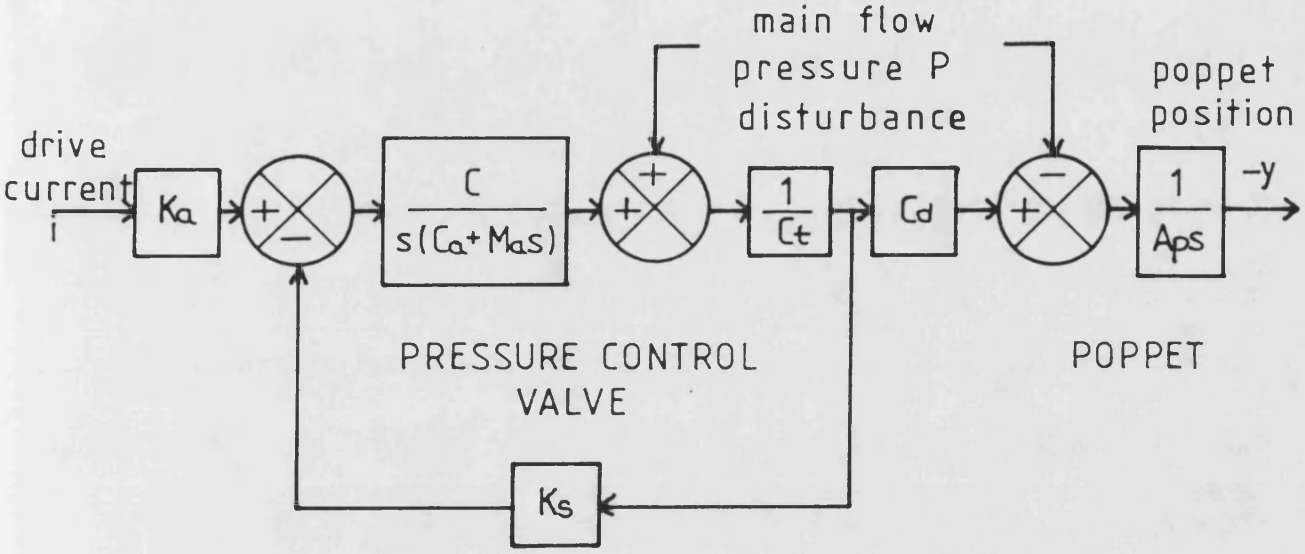

A4·3 REDUCED ORDER BLOCK DIAGRAM

APPENDIX 5 - RLS IDENTIFICATION EQUATIONS

The full derivation of the least squares and recursive least squares equations can be found in the control literature [85,86]. Here the principal equations are presented to enhance discussion of the technique within the main text of the thesis, thus much of the tedious algebraic manipulation in achieving the final equations is left out.

PLANT MODEL STRUCTURE:

The plant to be identified is assumed to be represented by a linear discrete parametric model of the form:

$$\frac{y}{e}(z) = \frac{a_{N1}z^{-1}+a_{N2}z^{-2}+a_{N3}z^{-3}+ \ldots\ldots}{1-a_{D1}z^{-1}-a_{D2}z^{-2}-a_{D3}z^{-3}- \ldots\ldots} \qquad \text{(A5.1)}$$

which expressed recursively becomes:

$$\hat{y}(k) = a_{N1}e(k-1)+a_{N2}e(k-2)+a_{N3}e(k-3) \ldots\ldots$$
$$a_{D1}y(k-1)+a_{D2}y(k-2)+a_{D3}y(k-3) \ldots\ldots \qquad \text{(A5.2)}$$

Where $\hat{y}(k)$ is the present estimated output value derived from the previous measured plant input and output values. Equation A5.2 can be rewritten more generally as:

$$\hat{y}(k) = a_1x_1+a_2x_2+a_3x_3+ \ldots\ldots +a_n x_n \qquad \text{(A5.3)}$$

Where $a_1, a_2, a_3 \ldots\ldots$ are the model parameters, and $x_1, x_2, x_3 \ldots\ldots$ are previous input/output information values. In matrix notation the equation can be written:

$$\hat{y}(k) = \underline{X}^T(k)\underline{A}(k) \qquad \text{(A5.4)}$$

Where $\underline{X}(k)$ is the current information vector, and $\underline{A}(k)$ is the current parameter vector.

LEAST SQUARES CRITERION:

The parameters are estimated such that the sum of the squares of the errors between the plant output $y(i)$ and the model output $\hat{y}(i)$ are minimised over a large number of samples, ie:

$$\frac{\partial}{\partial \underline{A}(k)} \sum_{i=1}^{k} [\hat{y}(i) - y(i)]^2 \alpha^{k-i} = 0 \qquad \text{(A5.5)}$$

The forgetting factor α is set to slightly less than unity and has the effect of reducing the value of previous errors. The consequent discounting of old data allows the identification algorithm to converge only to the most recent information, and provides a mechanism whereby the parameter estimates can be adapted to follow changes in the plant parameters. Carrying out the differentiation in equation A5.5 yields the result:

$$\underline{A}(k) = \frac{\sum_{i=1}^{k} \underline{X}(i) y(i) \alpha^{k-i}}{\sum_{i=1}^{k} \underline{X}(i) \underline{X}^T(i) \alpha^{k-i}} \qquad \text{(A5.6)}$$

Thus for a batch of samples, an $n \times 1$ vector:

$$\underline{B}(k) = \sum_{i=1}^{k} \underline{X}(i) y(i) \alpha^{k-i} \qquad \text{(A5.7)}$$

and an $n \times n$ square matrix:

$$\underline{P}^{-1}(k) = \sum_{i=1}^{k} \underline{X}(i) \underline{X}^T(i) \alpha^{k-i} \qquad \text{(A5.8)}$$

must be calculated. The parameter estimates are then found by inverting the square matrix and multiplying by the vector $\underline{B}(k)$, ie:

$$\underline{A}(k) = \underline{P}(k) \underline{B}(k) \qquad \text{(A5.9)}$$

The matrix $\underline{P}(k)$ is known as the 'Covariance Matrix'.

RECURSIVE LEAST SQUARES:

The previous equations are suitable for fitting a linear model to a batch of plant data points, however for use in on-line identification the data at each sampling instant must handled as it occurs and the batch processing format is unsuitable. Thus for on-line purposes the equations are rearranged into recursive form. The $\underline{P}(k)$ matrix can be updated on-line without any need for inversion using the recursive equation:

$$\underline{P}(k) = \frac{\underline{P}(k-1)}{\alpha} - \frac{\underline{P}(k-1)\underline{X}(k)\underline{X}^T(k-1)\underline{P}(k-1)}{\alpha[\alpha+\underline{X}^T(k)\underline{P}(k-1)\underline{X}(k)]} \qquad \text{(A5.10)}$$

Having calculated the current covariance matrix the parameter estimates can be updated recursively from the equation:

$$\underline{A}(k) = \underline{A}(k-1) - \underline{P}(k)\underline{X}(k)[\underline{X}^T(k)\underline{A}(k-1) - y(k)] \qquad \text{(A5.11)}$$